Assessment and Benchmarking of Proposed Exchange-Correlation Approximations in Density Functional Theory

By

SUBRATA JANA

Enrolment No: PHYS11201304012

National Institute of Science Education and Research, Bhubaneswar

A thesis submitted to the

Board of Studies in Physical Sciences

In partial fulfillment of requirements
for the Degree of

DOCTOR OF PHILOSOPHY

of

HOMI BHABHA NATIONAL INSTITUTE

December, 2019

Homi Bhabha National Institute

Recommendations of the Viva Voce Committee

As members of the Viva Voce Committee, we certify that we have read the dissertation prepared by Subrata Jana entitled "Assessment and Benchmarking of Proposed Exchange-Correlation Approximations in Density Functional Theory" and recommend that it may be accepted as fulfilling the thesis requirement for the award of Degree of Doctor of Philosophy

Chairman - Prof. Bedangadas Mohanty   **Date**

Guide/Convener - Dr. Prasanjit Samal   **Date**

Examiner - Prof. Indra Dasgupta   **Date**:

Member 1- Dr. Joydeep Bhattacharjee   **Date**

Member 2- Dr. A. V. Anil Kumar   **Date**

Member 3- Prof. Suresh Kumar Patra   **Date**

Final approval and acceptance of this thesis is contingent upon the candidates submission of the final copies of the thesis to HBNI.

I/We hereby certify that I/we have read this thesis prepared under my/our direction and recommend that it may be accepted as fulfilling the thesis requirement.

Date:

Place: Signature   Signature

                                     Co-guide(if any)   Guide

STATEMENT BY AUTHOR

This dissertation has been submitted in partial fulfillment of requirements for an advanced degree at Homi Bhabha National Institute (HBNI) and is deposited in the Library to be made available to borrowers under rules of the HBNI.

Brief quotations from this dissertation are allowable without special permission, provided that accurate acknowledgement of source is made. Requests for permission for extended quotation from or reproduction of this manuscript in whole or in part may be granted by the Competent Authority of HBNI when in his or her judgment the proposed use of the material is in the interests of scholarship. In all other instances, however, permission must be obtained from the author.

<div align="right">

Signature

SUBRATA JANA

</div>

DECLARATION

I, hereby declare that the investigation presented in the thesis has been carried out by me. The work is original and has not been submitted earlier as a whole or in part for a degree / diploma at this or any other Institution / University.

Signature

SUBRATA JANA

List of Publications arising from the thesis

Published:

1. *Semilocal Exchange Energy Functional for Two-Dimensional Quantum Systems: A Step Beyond Generalized Gradient Approximations, **Subrata Jana** and Prasanjit Samal, J. Phys. Chem. A 121, 4804 (2017).

2. *Gradient approximated exchange energy functionals with improved performances for two-dimensional quantum dot systems, **Subrata Jana**, Abhilash Patra and Prasanjit Samal, Physica E 97, 268-276 (2018).

3. *Exploration of near the origin and the asymptotic behaviors of the Kohn-Sham kinetic energy density for two-dimensional quantum dot systems with parabolic confinement, **Subrata Jana** and Prasanjit Samal, J. Chem. Phys. 148, 024111 (2018).

4. *A meta-GGA level screened range-separated hybrid functional by employing short range Hartree- Fock with a long range semilocal functional, **Subrata Jana** and Prasanjit Samal, Phys. Chem. Chem. Phys., 20, 8999-9005 (2018).

5. *Assessing the performance of the Tao-Mo semilocal density functional in the projector-augmented- wave method, **Subrata Jana**, Abhilash Patra and Prasanjit Samal, J. Chem. Phys. 149, 044120 (2018).

6. *Efficient lattice constants and energy band gaps for condensed systems from a meta-GGA level screened range-separated hybrid functional, **Subrata Jana**, Abhilash Patra and Prasanjit Samal, J. Chem. Phys. 149, 094105 (2018).

7. *On the Many-Electron Self-Interaction Error of the Semilocal Exchange Hole Based meta-GGA Level Range-Separated Hybrid and B88 Hybrids, **Subrata Jana**, Bikash Patra, Hemanadhan Myneni and P. Samal, Chem. Phys. Lett. Vol. 713, Pages 1-9, (2018).

8. *Assessing the performance of the recent meta-GGA density functionals for describing the lattice constants, bulk moduli and cohesive energies of alkali, alkali-earth and transition metals, **Subrata Jana**, Kedar Sharma, and Prasanjit Samal, J. Chem. Phys. 149, 164703 (2018).

Other Publications:

1. Long-range corrected density functional through the density matrix expansion based semilocal exchange hole, Bikash Patra, **Subrata Jana** and Prasanjit Samal, Phys. Chem. Chem. Phys., 20, 8991-8998 (2018).

2. A Parameter-Free Semilocal Exchange Energy Functional for Two-Dimensional Quantum Systems, Abhilash Patra, **Subrata Jana** and Prasanjit Samal, J. Phys. Chem. A 122(13), 3455-3461 (2018).

3. Inhomogeneity induced and appropriately parameterized semilocal exchange and correlation energy functionals in two-dimensions, Abhilash Patra, **Subrata Jana** and Prasanjit Samal, J. Chem. Phys. 148, 134117 (2018).

*: Publications related to the thesis

Signature

SUBRATA JANA

DEDICATIONS

Dedicated to

.....

My Family

.....

.....

My Teacher

ACKNOWLEDGEMENTS

Contents

6 Studies of Two-Dimensional Quantum Systems 119

7 Conclusions and Outlook 149

A Supplementary Materials for Chapter 4 153

SUMMARY

In density functional theory (DFT), there are mainly two classes of approximations of the exchange-correlation (XC) functional that are in wide use: The first one is the semilocal formalism and the other one is the hybrid functional theory. However, higher-order accurate many-body approaches are also possible. Depending on the ingredients used, the XC functionals are classified through Jacob's ladder. Each rung of the ladder adds an extra ingredient starting from the local density approximation (LDA), generalized gradient approximations (GGA) and meta-generalized gradient approximations (meta-GGA). LDA, GGA and meta-GGA are known as semilocal functionals and those are quite accurate in describing several thermochemical properties, bond lengths, equilibrium lattice constants, bulk modulus, cohesive energy, and surface properties. From the construction point of view, the semilocal functionals are developed either by satisfying various exact constraints or from exchange hole or by both. A systematic evaluation of the XC approximations is necessary, especially when a new functional is proposed. The motivation of this thesis is largely inspired by the benchmarking of several recent XC functionals and the necessity to improvise the new functionals for obtaining more accurate results.

The starting point of this thesis is involved on the benchmarking of the Tao-Mo semilocal functional with various approximations. TM functional is designed by designing the exchange hole which is constructed from the density matrix approximation technique. The TM functional is found to be very accurate both for the quantum chemistry and solid-state physics. In this thesis, the performance of several solid-state properties are addressed using the TM functional along with other popularly used GGA and meta-GGA level functionals in the projector-augmented-(plane-)wave (PAW) method. Particularly, the accuracy of TM functional with most advanced strongly constrained and appropriately normed (SCAN) meta-GGA functional is noticeable. It is observed in this thesis

that for several solid-state properties, TM functional works comparatively better than other meta-GGA and GGA functionals. Utilizing the semilocal exchange hole of the TM functional in this thesis we also construct the the range-separated hybrid functional with long-range HF and short-range HF analogous to that of the range-separated hybrid functional Heyd-Scuseria-Ernzerhof (HSE), but in the meta-GGA level. To check the accuracy and performance of the constructed functional, it is applied to determine several properties of the molecular and solid-state test.

Besides of the construction of the 3D functionals, this thesis also focuses on the construction of the functional for the 2D quantum systems. It is well known the the 3D functionals actually breakdown when it is applied to the 2D electronic systems. Though in practice the 2D systems are considered as quasi-2D systems (Q2D), yet the 2D functional can be used to explore the systematic DFT investigations for proper explanations of numerous properties of low-dimensional systems. Beyond the 2D-LDA, and 2D-GGA the first ever meta-GGA functional is proposed and applied to the 2D quantum systems. The motivation of the construction is followed from its 3D counterpart based on the DME technique. Further, the newly constructed functional shows improvement when applied to study a few electrons trapped inside parabolic and Gaussian quantum dots. We also explore the behavior of the Kohn-Sham kinetic energy density by taking the two-dimensional parabolic quantum dots as a model system. Also, an improved version of the existing 2D-GGA functional is proposed by extrapolating between the small and large density-gradient limit of the exchange hole.

List of Figures

List of Tables

Chapter 1

Introduction

The basis constituents of any material that we experience every day are built up from nuclei and electrons. Electrons which are the quantum particles repel each other due to Coulomb interactions. However, the massive nuclei are treated as classical particle compared to the dynamics of electrons. It is partcularlly very difficult to solve the many body interaction exactly.Continuous thought-provoking efforts of bridging the gap between theoretical and experimental aspects of many-electron phenomena led to several successful models during the last couple of decades. Accurate solutions of many-electron Schrödinger equation [1, 2] have been found and successfully implemented in several computational packages. Continuous efforts led to many accurate wavefunction based approaches like configuration interactions (CI), couple clusters (CCSD), many-body perturbation theory (MBPT) and quantum Monte Carlo techniques. But those are wavefunction based methods and becomes very demanding as the system size increases. In the search for the less demanding and accurate solutions of many-electron phenomena lead to density functional theory (DFT) [3–31] which becomes the *de facto* standard for calculating the many-electron phenomena starting from atoms, molecules to clusters of thousands of electrons. The successful implementation of DFT in physics, chemistry, and biological studies brings the Nobel prize in chemistry for Walter Kohn in 1998 [32]. But, its development originally started much earlier through the pioneering work of Thomas [9], Fermi [10], Hartree [3], Dirac [4], Fock [5] and Slater [6–8]. Almost forty years after the

work of Thomas and Fermi, a remarkable theorem and its computational aspects given by Hohenberg, Kohn, and Sham established the firm foundation of DFT [11, 12]. DFT which relies upon the ground state density depends only on the three coordinates no matter how large the system. Therefore, DFT is extremely simple and straight forward compared to the wavefunction based approaches. In Hohenberg-Kohn-Sham DFT all many-body interactions are included in a effective one-electron like potential known as the exchange-correlation (XC) energy functional. Since the exact many-electron behavior is not known exactly, the main research of DFT is to construct the XC energy (or potential) [13–31]. The aim of this thesis is to development of accurate methods through different level of approximations and its application towards atomic, molecular and material sciences.

Next chapter, we will review the different wavefunction based methods such as Hartree, Hartree-Fock level theories and their limitations in the context of many-electron calculations. Following this, the fundamental theorems of density functional theory upon which it is based on and further relevant developments are discussed. However, the computational aspects of DFT, which includes all many-body effects through the approximation of XC functional. Several levels of approximations make Kohn-Sham formalism as a widely used computational method. As this thesis focuses mainly on the assessment and development of different levels of energy functionals, in chapter 2, a summary of the different level of approximate XC functionals are reviewed. Formal properties of exchange-correlation functionals are also discussed. Next, the significance of Kohn-Sham energy eigenvalue and its connections to the fractional occupation number, ionization potential, and band gap problem are also explored. The computational framework and details of various software packages used in this thesis to solve the DFT equation are also described briefly in this chapter.

In chapter 3, the performance of different levels of density functional approximations are assessed based on the plane-wave basis set [33]. In this chapter we study and compare the performance of different density functional approximations for solid-state systems. Such comparison is desirable to test the robustness and accuracy of several recently developed approximations using the plane-wave basis set. Most interesting aspects of this work is that it compares the recent accurate meta-generalized gradient approximations

(meta-GGA) along with others developed approximations proposed during the last couple of decades.

In chapter 4 we assess the performance of density matrix expansion (DME) [35] based long-range corrected (Hartree-Fock in long-range) range-separated hybrid functionalto the properties related to the fractional occupation of atoms and molecules. The performance of the proposed functional is benchmarked against family of popular hybrid functional based on BECKE88 [37] exchange. Though the range-separated parameter of the present functional is fixed to minimize the AE6 atomization energies, still it works well for barrier height. Its performance for barrier heights are accurate compared to the popular BECKE88 family global and range-separated functionals. This work further extended to propose a screened range-separated hybrid functional theory [38].Performance of the screened hybrid functional has been carried with different level of approximations.Further extensions and performance of this scheme for the solid-state systems are also carried in the next chapter.

Motivated by the construction of the range-separated hybrid functionals in chapter 4, we develop a meta-GGA screened hybrid functional to be useful for the solid-state system in chapter 5. The functional is proposed by utilizing short-range Hartree-Fock exchange coupled with the very accurate meta-generalized gradient level semilocal functional. The performance of the proposed functional for various material properties indicate that the present meta-GGA level screened hybrids functional is quite productive beyond the generalized gradient approximation (GGA) level.

Our final investigation in chapter 6 is based on the development of a meta-GGA level theory for two-dimensional quantum dots systems [39]. We first investigate the behavior of Kohn-Sham kinetic energy (KS-KE) density for a perfectly solvable model. Based on these studies, we further construct a meta-GGA functional in two dimensions by appropriately designing the exchange hole model through the density matrix expansion technique. The construction of the two-dimensional functional is analogous to that proposed in three dimensional by Tao et. al. [35]. The performance of constructed functional shows in accuracy for various quantum dot systems. In this chapter, we also construct a generalized-gradient approximation level functional in two dimensions by appropriately

extrapolating the exchange energies between the low and high-density limits of the exchange hole model [41]. Performance of the functional demonstrates that it improves the performance of the previously proposed GGA functionals.

In Chapter 7, we conclude and summarize the research work carried out and reported in this thesis. This chapter also outlines the further directions and improvements that can be carried out based on the research work embedded in this thesis.

Chapter 2

Review of Density Based Theory

This chapter introduces the review of density-based theory. We start from the time-independent Schrödinger equation (TDSE) for the many-electron system and rewrite its equivalent for the density functional theory (DFT). Lastly, a scheme for solving the complex many-body problem is also provided.

2.1 Solving Many Electron Schrödinger Equation

Since the time-independent Schrödinger equation [1] has been introduced, it provides a very useful understanding of the microscopic world. But, the exact solutions of it is limited only for few restricted systems. A complex electronic structure of multi-electron systems are very difficult to solve. It is because of the involvement of a complex many-electron Schrodinger equation that describes a many-electronic system. The time-independent Schrödinger equation is a eigenvalue problem with energy eigenvalue E and energy eigenstate Ψ_T for the Hamiltonian $\hat{H}_T$:

$$\hat{H}_T \Psi_T = E_T \Psi_T \,, \tag{2.1}$$

where the symbol T stands for the total (nuclear and electronic) Hamiltonian, energy eigenvalue and energy eigenstates. However, this Hamiltonian which involves both the

nuclear and electronic motion can be treated separatelybecause of the Born-Oppenheimer approximation [2].This approximation separates the total Hamiltonian, energy eigenvalue and energy eigenstates into independent Hamiltonian of nuclei ($\hat{H}_n$) and electrons ($\hat{H}$) with energy eigenvalues E_n and E and eigenstates Ψ_n and Ψ. The result is:

$$\hat{H}_T = \hat{H} + \hat{H}_n \tag{2.2}$$

$$E_T = E + E_n \tag{2.3}$$

$$\Psi_T = \Psi\Psi_n \tag{2.4}$$

However, in many-body problem the nucleonic part not very complicated to handle. But, the main challenge is to find the solution for the electronic part. The electronic part of the system is described by the many-electron Schrödinger equation with N particles interacting via the Coulomb potential and subject to an external potential v_{ext} as,

$$\underbrace{\left\{ -\frac{1}{2}\nabla_i^2 + \sum_i^N v_{ext}(\mathbf{r}_i) + \frac{1}{2}\sum_{i=1}\sum_{j\neq i}\frac{1}{|\mathbf{r}_i - \mathbf{r}_j|} \right\}}_{\hat{H}=\hat{T}+\hat{v}_{ext}+\hat{V}_{ee}} \Psi(\mathbf{x},...\mathbf{x}_i,...,\mathbf{x}_j....,\mathbf{x}_N) \tag{2.5}$$

$$= E\Psi(\mathbf{x},...\mathbf{x}_i,...,\mathbf{x}_j....,\mathbf{x}_N),$$

where the 1st, 2nd and 3rd terms of Eq.(2.5) correspond to the kinetic energy, external potential and complex electron-electron Coulomb interaction respectively. The electron-electron repulsion operator contains both purely classical Coulomb repulsion and non-classical terms which come from the fermionic nature of the electrons. The simple Eq.(2.5) is quite difficult to solve because of the complex electron-electron interaction. Being fermions, electrons avoid one another due to the charge and spin which are incorporated in the antisymmetric nature of the wavefunction. Also, repulsion forces occur due to the same charge of the electrons. The first one is well known as the Coulomb correlation. Whereas, the later is known as Pauli or Fermi correlation. So, the many-electron

wavefunction is antisymmetric under the exchange of electrons as,

$$\Psi(\mathbf{x}, ...\mathbf{x}_i, ..., \mathbf{x}_j...., \mathbf{x}_N) = -\Psi(\mathbf{x}, ...\mathbf{x}_j, ..., \mathbf{x}_i...., \mathbf{x}_N) ,$$ (2.6)

where $\mathbf{x}_i = (\mathbf{r}_i, \sigma_i)$ are the spin-orbital indices of the ith electron. The square of the defined many-electron wavefunction i.e., $|\Psi(\mathbf{r}\sigma, \mathbf{r}_2\sigma_2.....\mathbf{r}_N\sigma_N)|^2$ is the probability of finding electron 1 at position $\mathbf{r}_1$ and with spin state σ_1,......, electron N at position $\mathbf{r}_N$ and spin state σ_N. Also, the many-electron wavefunction satisfies the normalization condition

$$\sum_{i,\sigma} \int d^3r.....d^3r_N |\Psi(\mathbf{r}\sigma, \mathbf{r}_2\sigma_2.....\mathbf{r}_N\sigma_N)|^2 = 1 .$$ (2.7)

Now, using the above many-electron wavefunction the one-electron spin density is obtained as,

$$\rho_\sigma(\mathbf{r}) = N \sum_{\sigma_2,...,\sigma_N} \int d^3r_2.....d^3r_N |\Psi(\mathbf{r}\sigma, \mathbf{r}_2\sigma_2.....\mathbf{r}_N\sigma_N)|^2 ,$$ (2.8)

where the prefactor N is coming from the permutation of electron positions. As electrons are indistinguishable particles, there are $N!$ distinct possible permutations for which the $|\Psi|^2$ is the same. Now, upon coupling Eq.(2.7) with Eq.(2.8) one can obtain

$$\sum_\sigma \int d^3r \rho_\sigma(\mathbf{r}) = N .$$ (2.9)

Using the many-electron wavefunction the expectation value of the electronic Hamiltonian H_e becomes,

$$\begin{aligned}
&\langle\Psi(\mathbf{x}, ...\mathbf{x}_i, ..., \mathbf{x}_N)|H|\Psi(\mathbf{x}, ...\mathbf{x}_i, ..., \mathbf{x}_N)\rangle \\
=\ &\langle\Psi(\mathbf{x}, ...\mathbf{x}_i, ..., \mathbf{x}_N)|\hat{T} + \hat{v}_{ext} + \hat{U}|\langle\Psi(\mathbf{x}, ..., \mathbf{x}_i...., \mathbf{x}_N)|\rangle \\
=\ &T + V_{ext} + U = E_e ,
\end{aligned}$$ (2.10)

The individual expectation values of the kinetic, external potential and Coulomb operator are given by,

$$
\begin{aligned}
\langle \hat{T} \rangle &= -\frac{1}{2} \sum_{\sigma} \langle \Psi | \sum_{i=1}^{N} \nabla_i^2 | \Psi \rangle \\
\langle \hat{v}_{ext} \rangle &= \langle \Psi | \sum_{i=1}^{N} \hat{v}_{ext}(\mathbf{r}_i) | \Psi \rangle = \int d\mathbf{r} \rho(\mathbf{r}) v_{ext}(\mathbf{r}) \\
\langle \hat{V}_{ee} \rangle &= \frac{1}{2} \sum_{\sigma} \int d^3 r_i \int d^3 r_j \frac{\rho(\mathbf{r}_i)\rho(\mathbf{r}_j)}{|\mathbf{r}_i - \mathbf{r}_j|} \, ,
\end{aligned}
\tag{2.11}
$$

where ρ is the total density.

2.1.1 Wavefunction Variational Principle

The quantum mechanical variational approach is considered as an alternative way to solve the Schrödinger equation by variationally optimized the wavefunction for a given configuration. It is also considered as one of the most important theoretical principle upon which many theoretical and computational approaches rely. In principle, the TDSE can be constructed from the wavefunction variational principle by extremizing the expectation values of Hamiltonian i.e., $\langle \Psi | \hat{H}_e | \Psi \rangle$ subject to the constraint that the variational wavefunction always normalized to 1. This corresponds to

$$
\delta \{ \langle \Psi | \hat{H} | \Psi \rangle - \mu \langle \Psi | \Psi \rangle \} = 0 \, ,
\tag{2.12}
$$

where μ is the Lagrange multiplier. This is the minimization principle which leads to the energy eigenvalue and eigenfunction and it is known as the Rayleigh-Ritz variational principle.

The solution of the above variation corresponds to the time-independent Schrödinger equation which is obtained through the infinitesimal variation of the wavefunction $\delta\Psi$ as,

$$
\langle \delta\Psi | \hat{H} - \mu | \Psi \rangle + c.c = 0 \, .
\tag{2.13}
$$

This implies

$$(\hat{H} - \mu)|\Psi\rangle = 0 \ . \tag{2.14}$$

μ is nothing but ground-state energy for the configuration which is presented by the Hamiltonian. This wavefunction variational principle forms the basis of the wavefunctional (Hartree-Fock, Configuration-Interaction (CI), Hellmann-Feynman theorems) and density functional (the Hohenberg-Kohn density functional variational principle) formalism. While the CI is very accurate methods but it is computationally very demanding.

2.1.2 Hartree-Fock Approximation

The Hartree-Fock (HF) [3–8] approximation relies on the wavefunction variational principle of Eq.(2.12). The variational wavefunction in HF approximation is considered as the antisymmetric product of the N single-particle orbitals or a single Slater determinant defined as,

$$\Psi_{HF} = \frac{1}{\sqrt{N!}} det[\psi_1, ..., \psi_N] \tag{2.15}$$

or more elaborately,

$$\Psi_{HF}(\vec{x}_1, \vec{x}_2, .., \vec{x}_N) = \sqrt{\frac{1}{N!}} \begin{vmatrix} \psi_1(\vec{x}_1) & \psi_1(\vec{x}_2) & .. & \psi_1(\vec{x}_N) \\ \psi_2(\vec{x}_1) & \psi_2(\vec{x}_2) & .. & \psi_2(\vec{x}_N) \\ . & . & . & . \\ . & . & . & . \\ \psi_N(\vec{x}_1) & \psi_N(\vec{x}_2) & .. & \psi_N(\vec{x}_N) , \end{vmatrix} \tag{2.16}$$

where ψ_is are the spin-orbitals. The HF equation is obtained by varying the occupied spin-orbitals $\psi_i(\vec{x}_i)$ and extrimizing $\langle \Psi_{HF}|\hat{H}|\Psi_{HF}\rangle$ subject to the normalization condi-

tion $\langle \psi_i | \psi_i \rangle = \delta_{ij}$. The total energy in the HF approximation as,

$$\langle \Psi_{HF} | \hat{H} | \Psi_{HF} \rangle = \sum_i \int d^3r \, \psi_i^*(\mathbf{r}, \sigma) \left(-\frac{1}{2}\nabla^2 \right) \psi_i(\mathbf{r}, \sigma) + \int \rho(\mathbf{r}) v_{ext}(\mathbf{r}) d^3r$$

$$+\frac{1}{2} \int d^3r \, d^3r' \, \frac{\rho(\mathbf{r})\rho(\mathbf{r})'}{|\mathbf{r} - \mathbf{r}'|} - \frac{1}{2} \sum_{i,j} \sum_{\sigma,\sigma'} \int \int d^3r \, d^3r' \, \frac{\psi_i^*(\mathbf{r}, \sigma)\psi_j(\mathbf{r}, \sigma)\psi_j^*(\mathbf{r}', \sigma')\psi_i(\mathbf{r}', \sigma')}{|\mathbf{r} - \mathbf{r}'|} \, ,$$

$$(2.17)$$

where i and j denotes the space and spin component of ith and j^{th} optimized orbitals. The 1st, 2nd, 3rd and 4th terms are kinetic energy, interaction of the electrons with the external potential, classical Coulomb energy ($J[\rho]$) and the exchange energy respectively. It is noteworthy to mention that for $i = j$, the 4th term exactly cancels with the 3rd term of Eq.(2.17). Therefore, the HF energy equation is self-interaction free. The exchange energy functional in the HF energy equation is orbital-dependent which needs to be calculated self-consistently during each iteration of the variational extremization. The variational minimization of Eq.(2.17) respecting the orbitals leads to HF equation for i^{th} orbital which is given by,

$$\left[-\frac{1}{2}\nabla^2 + v_{ext} + \sum_j \int d^3r' \, \frac{\rho(\mathbf{r}')}{|\mathbf{r} - \mathbf{r}'|} \right] \psi_i(\mathbf{r}'\sigma') - \sum_j \int d^3r' \, \psi_j^*(\mathbf{r}'\sigma')\psi_i(\mathbf{r}'\sigma') \frac{1}{|\mathbf{r} - \mathbf{r}'|} \psi_j(\mathbf{r}\sigma)$$

$$= \epsilon_i \psi_i(\mathbf{r}\sigma) \, ,$$

$$(2.18)$$

where the Lagrange multiplier ϵ_i enters into the HF equation through the normalization condition. The ϵ_i is recognized as the optimized single-particle orbital energy. The HF approximation is exact for systems with no correlation. Higher-order accurate wavefunctional methods like CI are considered to be the most accurate as these are including both the exchange and correlation but highly demanding computationally for large systems.

2.1.3 Hellmann-Feynman Theorem

In quantum many-electron systems, Hellman-Feynman theorem provides a way to calculate forces. To explain elaborately the Hellmann-Feynman Theorem, let's consider a parameter λ as the continuous function of the Hamiltonian. Then the question is how the eigenfunction $\Psi(\lambda)$ and energy $E(\lambda)$ of the Hamiltonian $\hat{H}$ depend on the parameter λ. Lets consider any normalized eigenfunction $\Psi(\lambda)$ be the solution of the Hamiltonian $\hat{H}(\lambda)$.Hence, the energy is given by,

$$E(\lambda) = \langle \Psi(\lambda)|\hat{H}(\lambda)|\Psi(\lambda)\rangle \ . \tag{2.19}$$

Taking derivative of the Eq.(2.19) with respect to λ one can obtain,

$$\frac{dE(\lambda)}{d\lambda} = \frac{d}{d\lambda'}\langle \Psi(\lambda')|\hat{H}(\lambda')|\Psi(\lambda')\rangle|_{\lambda'=\lambda} + \langle \Psi(\lambda')|\frac{\partial \hat{H}(\lambda')}{\partial \lambda'}|\Psi(\lambda)|_{\lambda'=\lambda} \ . \tag{2.20}$$

The 1st term of Eq.(2.20) vanishes due to the normalization condition of $\Psi(\lambda)$. Thus

$$\frac{dE(\lambda)}{d\lambda} = \langle \Psi(\lambda)|\frac{\partial \hat{H}(\lambda)}{\partial \lambda}|\Psi(\lambda)|\rangle \tag{2.21}$$

or

$$E(\lambda_2) = E(\lambda_1) + \int_{\lambda_1}^{\lambda_2} d\lambda \, \langle \Psi(\lambda)|\frac{\partial \hat{H}(\lambda)}{\partial \lambda}|\Psi(\lambda)|\rangle \ . \tag{2.22}$$

These two identities (i.e., Eq.(2.21) and Eq.(2.22)) are the differential and integral form of Hellmann-Feynman theorem. Note that this form is often used to construct the coupling-constant integral, which is the path of obtaining the exact form of exchange and correlation functional which we will elaborately discuss later in this chapter.

2.2 Density Based Theory

In modern electronic structure theory, the density functional theory (DFT) is considered as an efficient way to model the complex many-electron system with sizeable electron numbers. However, before going into the details of the formal computational framework of the DFT, the concept of the functional is important. Therefore, we start this section with the concept of the functional.

2.2.1 Functional and functional derivative

The concept of functional and functional derivatives are very important from the construction of density functionals point of view. In this section, we will elaborately discuss these two concepts. A function $f(x)$ is a mapping from a variable x to a number, whereas, a functional $F[f]$ is a mapping from a function to a number. For example, the expectation value of Hamiltonian $E[\Psi] = \langle \Psi(\lambda)|\hat{H}|\Psi \rangle$ is the functional of the wavefunction Ψ, and gives the number (or eigenvalue) for a well-defined Ψ.

If a functional $F[f(x)]$ is well defined and differentiable, then the functional is Taylor series expandable about $\delta f(x) = 0$ as,

$$F[f(x)+\delta f(x)] = F[f]+\int \, d\mathbf{x} \left(\frac{\delta F}{\delta f(x)}\right) \delta f(x)+\frac{1}{2}\int \, d\mathbf{x}\, d\mathbf{x}'\left(\frac{\delta^2 F}{\delta f(x)\delta f(x')}\delta f(x)\delta f(x')\right)+.... \,.$$

(2.23)

Now, assuming that the variation δf is small and keeping the variation terms upto 1st order in the series expansion of $F[f(x)]$, the difference $F[f(x) + \delta f(x)] - F[f]$ is obtained as,

$$F[f(x) + \delta f(x)] - F[f] = \delta F[f] = \int \, d\mathbf{x} \left(\frac{\delta F}{\delta f(x)}\right) \delta f(x) \,,$$

(2.24)

where $\frac{\delta F}{\delta f(x)}$ is the functional derivative of the functional F with respect to f at x.

To illustrate, let us consider the classical Coulomb energy of Eq.(2.17) is

$$J[\rho] = \frac{1}{2}\int \, d^3r \, d^3r' \frac{\rho(\mathbf{r})\rho(\mathbf{r}')}{|\mathbf{r} - \mathbf{r}'|} \,.$$

(2.25)

So,

$$
\begin{aligned}
J[\rho + \delta\rho] &= \frac{1}{2}\int d^3r\, d^3r' \frac{[\rho(\mathbf{r}) + \delta\rho(\mathbf{r})][\rho(\mathbf{r}') + \delta\rho(\mathbf{r}')]}{|\mathbf{r} - \mathbf{r}'|} \\
&= J[\rho] + \int d^3r \left(\int d^3r' \frac{\rho(\mathbf{r}')}{|\mathbf{r} - \mathbf{r}'|} \right) \delta\rho(\mathbf{r}) \\
&\quad + \frac{1}{2}\int d^3r\, d^3r' \left(\frac{1}{|\mathbf{r} - \mathbf{r}'|} \right) \delta\rho(\mathbf{r})\, \delta\rho(\mathbf{r}') \, ,
\end{aligned}
\tag{2.26}
$$

which upon identifying the functional derivative as done in Eq.(2.24) gives,

$$
\frac{\delta J[\rho]}{\delta\rho(\mathbf{r})} = \int d^3r' \frac{\rho(\mathbf{r}')}{|\mathbf{r} - \mathbf{r}'|} \, .
\tag{2.27}
$$

This is the classical Hartree potential. Therefore, functional derivatives play importance role in DFT.

2.3 History of Density Based Theory

2.3.1 The first density based theory: Thomas-Fermi theory

Along the line of development of density-based theory, Thomas and Fermi [9, 10] proposed the first-ever density-based theory known as "Thomas-Fermi (TF)" theory. In the Hartree-Fock theory, we have noticed that everything is the functional of the density except the kinetic energy and the exchange functional. If one neglects exchange functional and expresses the kinetic energy as the functional of density then everything becomes density-dependent. This is what "Thomas-Fermi" did during the early nineties, earlier than the formalism of density functional theory was proposed by Hohenberg and Kohn. They approximated that the system becomes homogeneous and replace the kinetic energy functional by the homogeneous electron gas. The total electronic energy of the system under TF approximation becomes,

$$
E[\rho] = T_{TF}[\rho] - \int \frac{Z}{r}\rho(\mathbf{r})d^3r + \frac{1}{2}\int d^3r\, d^3r' \frac{\rho(\mathbf{r})\rho(\mathbf{r}')}{|\mathbf{r} - \mathbf{r}'|} \, ,
\tag{2.28}
$$

where

$$T_{TF}[\rho] = \frac{3}{10}(3\pi^2)^{2/3} \int \rho(\mathbf{r})^{5/3} \, d^3r \ . \tag{2.29}$$

Here, $\rho(\mathbf{r})$ is assumed to be the density of the uniform electron gas and it depends at the point $\mathbf{r}$ in space, no longer how the density is varying. In TF theory, the system is assumed to be uniform and the expression of the kinetic energy density still valid for the non-uniform or varying system. The energy is given by Eq.(2.28) always overestimates the actual total energy because a part of energy known as the exchange-correlation energy has not been considered. The TF theory is the simplified conventional way to introduce the kinetic energy in term of density and it is considered as the predecessor of the modern density functional theory. The Coulomb expression present in Eq.(2.28) does not include any self-interaction correction. As a matter of which, the Coulomb interaction always overestimated in Eq.(2.28). This fact is modified and improved further by Fermi and Amaldi. They subtract energy per electron from the classical Coulomb energy as,

$$J_{FA}[\rho] = \frac{1}{2}\left(1 - \frac{1}{N}\right) \int \int d^3r \, d^3r' \frac{\rho(\mathbf{r})\rho(\mathbf{r}')}{|\mathbf{r} - \mathbf{r}'|} \ . \tag{2.30}$$

Further, the missing part of energy i.e., exchange energy is included in the energy expression by Dirac as,

$$E_x = -\frac{3}{4}\left(\frac{3}{\pi}\right)^{1/3} \int \rho(\mathbf{r})^{4/3} \, d^3r \ . \tag{2.31}$$

So, the inclusion of Dirac exchange energy functional, the Thomas-Fermi-Dirac (TFD) energy functional becomes,

$$E_{TFD}[\rho] = T_{TF}[\rho] - \int \frac{Z}{r}\rho(\mathbf{r})d^3r + \frac{1}{2} \int d^3r \, d^3r' \frac{\rho(\mathbf{r})\rho(\mathbf{r}')}{|\mathbf{r} - \mathbf{r}'|} - \frac{3}{4}\left(\frac{3}{\pi}\right)^{1/3} \int \rho(\mathbf{r})^{4/3} \, d^3r \ . \tag{2.32}$$

The main noticeable and appealing feature of the energy expression in Eq.(2.32) is that it is functional of the density and all the ground-state properties can be determined explicitly through the ground state density. It is well known that the equation of density or the Euler-Lagrange equation is obtained by applying the variational principle. Therefore, the TFD "equation for density" is obtained by the minimization of the TFD energy

expression subject to the constraint that the ground state density corresponds to the fixed number particle, which leads to

$$\frac{1}{2}[3\pi^2\rho(\mathbf{r})]^{2/3} - \frac{Z}{r} + \int d^3r' \frac{\rho(\mathbf{r}')}{|\mathbf{r} - \mathbf{r}'|} - \left(\frac{3}{\pi}\right)^{1/3}\rho(\mathbf{r})^{1/3} = \mu_{TFD} , \qquad (2.33)$$

where μ_{TFD} is the Lagrange multiplier obtained by satisfying the constraint of a fixed number of particles i.e., $N = \int \rho(\mathbf{r}) \, d^3r$, and N is the total number of electrons.

Albeit the TFD theory is one of the simplified many-electron density-based approximation, it qualitatively predicts wrong densities. Along the line of improvement of TFD theory, it has been proposed to include the gradient of density, which is well known as "Weizsäcker correction". In spite of several drawbacks, the TFD theory is considered as one of the first steps towards the formal development of density functional theory which was introduced in 1964 through the seminal work of Hohenberg and Kohn (HK). In the next section, we will discuss the HK formalism in details.

2.3.2 Hohenberg-Kohn theorem

The Hohenberg-Kohn (HK) theorem [11] is a phenomenal doorstep of the many-electron quantum physics by considering that only the ground-state electron density legitimizes all the ground state properties. The original proof of the HK theorem is based on two basic theorems:

Theorem 1: *There exists a one-to-one mapping between the ground state density and the external potential. In another way, it can be stated as the external potential of the many-electron systems is determined uniquely up to an additive constant by the ground state density of the system.*

Proof: The proof of the 1st HK theorem is based on the *reductio ad absurdum*. Let us assume that a ground-state density $\rho(\mathbf{r})$ corresponds to two different external potentials $v(\mathbf{r})$ and $v'(\mathbf{r})$ such that $v(\mathbf{r}) \neq v'(\mathbf{r}) + c$, where c is a constant. The ground-state wavefunctions Ψ and Ψ' corresponding to the two potentials can not be identical i.e., $\Psi \neq \Psi'$.

Then the energy variational method suggests that

$$
\begin{aligned}
E &= \langle \Psi | \hat{H}[v] | \Psi \rangle < \langle \Psi' | \hat{H}[v] | \Psi' \rangle, \\
&= \langle \Psi' | \hat{H}[v'] | \Psi' \rangle + \int \{v(\mathbf{r}) - v'(\mathbf{r})\} \rho(\mathbf{r}) d^3r \\
&= E' + \int \{v(\mathbf{r}) - v'(\mathbf{r})\} \rho(\mathbf{r}) d^3r \ ,
\end{aligned}
\tag{2.34}
$$

where Ψ is the ground-state wavefunction of the Hamiltonian H and the Hamiltonian H is the functional of external potential v and total number of particle N. The variational principle is also true for the ground-state E' of $\hat{H}'$ with external potential v', i.e.,

$$
\begin{aligned}
E' &= \langle \Psi' | \hat{H}[v'] | \Psi' \rangle < \langle \Psi | \hat{H}[v'] | \Psi \rangle, \\
&= \langle \Psi | \hat{H}[v'] | \Psi \rangle + \int \{v'(\mathbf{r}) - v(\mathbf{r})\} \rho(\mathbf{r}) d\mathbf{r} \\
&= E + \int \{v'(\mathbf{r}) - v(\mathbf{r})\} \rho(\mathbf{r}) d^3r \ .
\end{aligned}
\tag{2.35}
$$

So, Eq.(2.34) and Eq.(2.35) lead to the inequality $E + E' < E' + E$, which is a contradiction. This implies that our starting assumption " a ground density $\rho(\mathbf{r})$ corresponds to two different external potentials $v(\mathbf{r})$ and $v'(\mathbf{r})$" is invalid. Alternatively, knowing the ground-state density one can determine the unique external potential. In a simple mathematical notation, this can also be expressed as,

$$
\rho(\mathbf{r}) = \rho[v(\mathbf{r})] \iff v(\mathbf{r}) = v[\rho(\mathbf{r}), N] \ .
\tag{2.36}
$$

Now, relating the HK theorem to the Thomas-Fermi energy expression of Eq.(2.28) one can rewrite the total energy as,

$$
\begin{aligned}
E[\rho] &= T[\rho] + V_{ee}[\rho] + \int v_{ext}(\mathbf{r}) \rho(\mathbf{r}) \, d^3r \\
&= F_{HK}[\rho] + \int v_{ext}(\mathbf{r}) \rho(\mathbf{r}) \, d^3r \ ,
\end{aligned}
\tag{2.37}
$$

where $F_{HK}[\rho] = T[\rho] + V_{ee}[\rho]$ is the HK universal functional of density.

Theorem 2: *The second Hohenberg-Kohn theorem redefines the variational principle based on particle density. It states that: For a trial density $\tilde{\rho}(\mathbf{r}) \ni \tilde{\rho}(\mathbf{r}) \geq 0$ and $\tilde{\rho}(\mathbf{r})d\mathbf{r} = N$,*

$$E_0 \leq E[\tilde{\rho}(\mathbf{r})] \,, \tag{2.38}$$

where $E[\tilde{\rho}(\mathbf{r})]$ is the energy functional (like it was defined in Eq.(2.37)).

Proof: Note from the 1st HK theorem establishes that the ground state density $\rho(\mathbf{r})$ determines its own potential $v(\mathbf{r})$, Hamiltonian $\hat{H}$ and wavefunction Ψ. Now by variational method

$$\langle \tilde{\Psi}|\hat{H}|\tilde{\Psi}\rangle = \int \tilde{\rho}(\mathbf{r})v(\mathbf{r})d\mathbf{r} + F_{HK}[\tilde{\rho}(\mathbf{r})] = E[\tilde{\rho}] \geq \langle \Psi|\hat{H}|\Psi\rangle = E[\rho] \,, \tag{2.39}$$

where $\tilde{\rho}$ is the ground state density of the potential $v(\mathbf{r})$ and Ψ is the ground state wavefunction. This is analogous to the quantum mechanical variation principle in density functional theory. In principle, Eq.(2.39) states that the trail density always gives energy higher than or equal to the true ground state energy.

Now, assuming the differentiability of the energy functional $E[\rho]$, the variational principle of theorem 2 satisfies the stationarity principle condition,

$$\delta\{E[\rho] - \mu[\int \rho(\mathbf{r})\,d\mathbf{r} - N]\} = 0 \,, \tag{2.40}$$

which gives the Euler-Lagrange equation as,

$$\mu = \frac{\delta E[\rho]}{\delta\rho(\mathbf{r})} = v(\mathbf{r}) + \frac{\delta F_{HK}[\rho]}{\delta\rho(\mathbf{r})} \,, \tag{2.41}$$

where μ is the Lagrange multiplier that ensures the normalization of the density during the density variation.

2.3.3 $v-$ and $N-$ representability and constraint search formalism

HK theorem is associated with the antisymmetric ground-state wavefunction of the Hamiltonian with external potential $v(\mathbf{r})$. This is known as $v-$ *representable* [22, 42–47] density because the density is obtained from the ground-state wavefunction of the external potential $v(\mathbf{r})$. This is a serious restriction of the HK formalism. Since, a given density may or may not be $v-$ representable [42], an extension of the functional $F_{HK}[\rho]$ to a more general domain is required, where the density becomes $N-$ representable. The $N-$ representability of a density implies that,

$$\rho(\mathbf{r}) \geq 0, \quad \int \rho(\mathbf{r})d^3r = N, \;\; and \;\; \int |\nabla\rho(\mathbf{r})^{1/2}|^2 \, d^3r < \infty \, . \qquad (2.42)$$

Following Levy and Lieb [42], the extension of the HK functional to the domain of $N-$representability is achieved through the constraint search formalism of density functional theory. The Levy-Lieb functional is defined as,

$$F_{LL}[\rho] \equiv min_{\Psi \to \rho}\langle\Psi|\hat{T} + \hat{V}_{ee}|\Psi\rangle \, , \qquad (2.43)$$

where the minimum condition is taken over all possible anti-symmetric wavefunction, not necessarily the ground state solution of an external potential. The HK functional F_{HK} is on the subspace of the more general functional $F_{LL}[\rho]$, where the minimum condition is taken over the $v-$representable wavefunctions.

The constraint search formula of Eq.(2.43) eliminates the $v-$representability problem of the HK variational principle and represents it in a more general domain of the $N-$ representability densities. The energy minimization condition of the $N-$ representability densities can also be represented through the Rayleigh-Ritz variation minimization

procedure as,

$$
\begin{aligned}
E_0 &= min_{\Psi}\langle\Psi|\hat{T} + \hat{V}_{ee} + \sum_i^N v_{ext}(\mathbf{r}_i)|\Psi\rangle \\
&= min_{\rho}\{min_{\Psi\to\rho}\langle\Psi|\hat{T} + \hat{V}_{ee} + \sum_i^N v_{ext}(\mathbf{r}_i)|\Psi\rangle\} \\
&= min_{\rho}\{min_{\Psi\to\rho}[\langle\Psi|\hat{T} + \hat{V}_{ee}|\Psi\rangle + \int v_{ext}(\mathbf{r}\rho(\mathbf{r})d\mathbf{r})]\} \\
&= min_{\rho}\{F_{LL} + \int v_{ext}(\mathbf{r})\rho(\mathbf{r})d^3r\} \ .
\end{aligned}
\tag{2.44}
$$

In the second line, the inner minimization corresponds to the **search** for all the anti-symmetric wavefunctions subject to the **constraint** that the wavefuncton corresponds to the given density. This is why the Levy-Lieb minimization procedure is known as "constraint search" formalism [42].

In summary, it is proved through the constraint search formalism that there exists a universal functional $F[\rho]$ (or Levy-Lieb functional) for any $N-$representable density. Hence, one can perform energy minimization procedure for a broader class of $N-$representable trial densities and the $v-$representability is a subclass of it.

2.4 Effective Single Particle Equation

2.4.1 The Kohn-Sham formalism

Having established the density to potential mapping via the HK theorem, it is now important to construct a computational setup to solve the many-electron problem. In the TF model, a direct approach of construction for the approximation of $T[\rho]$ and V_{ee} has been prescribed. But, unfortunately, there are seemingly insurmountable difficulties in the approximation of kinetic energy density. To circumvent the TF problem of the many-electron systems, Kohn-Sham (KS) invented a method in the year 1964 [12]. KS proposed that the kinetic energy can be treated to good accuracy by introducing the orbitals into the problem leaving only a residual part which can be handled separately. In the KS approach,

the true interacting system is replaced by a fictitious non-interacting system with the same
particle numbers and density. This is the key assumption of KS construction. Under this
assumption, the Hamiltonian of the $N-$ non-interaction electrons reduce to,

$$\hat{H} = \hat{T} + (V_{ee} = 0) + \sum_{i=1}^{N} v(\mathbf{r}_i) . \tag{2.45}$$

Thus, the HK functional of Eq.(2.43) becomes,

$$
\begin{aligned}
F_{non-interacting}[\rho] &= min_{\Psi \to \rho} \langle \Psi | \hat{T} + \hat{V}_{ee} = 0 | \Psi \rangle \\
&= \langle \Phi_{\rho}^{min} | \hat{T} | \Phi_{\rho}^{min} \rangle = T_s[\rho] ,
\end{aligned}
\tag{2.46}
$$

where Φ_{ρ}^{min} is the non-interacting wavefunction or a single Slater determinant ($\Phi = \frac{1}{\sqrt{N!}}[\phi_1 \phi_2 .... \phi_N]$ with ϕ_i is the non-interacting single-particle states or orbitals) that min-
imizes the expectation value of kinetic energy operator subject to the constraint that the
density remains the same as the actual interacting system. This minimization is the
same as HK functional minimization but only in the non-interaction particle framework.
Eq.(2.46) corresponds to the Euler-Lagrange equation analogous to the Eq.(2.41) but in
the non-interaction framework as,

$$
\begin{aligned}
\mu_s &= v_s(\mathbf{r}) + \frac{\delta F_{non-interacting}[\rho]}{\delta \rho(\mathbf{r})} \\
&= v_s(\mathbf{r}) + \frac{\delta T_s[\rho]}{\delta \rho(\mathbf{r})} ,
\end{aligned}
\tag{2.47}
$$

where v_s is the KS potential which we will identify in the following section.

Let us now recall the interacting HK functional of Eq.(2.37) as,

$$F[\rho] = T[\rho] + V_{ee}[\rho] . \tag{2.48}$$

Alternatively, this can also be written as,

$$
\begin{aligned}
F[\rho] &= T[\rho] + V_{ee}[\rho] - T_s[\rho] + T_s[\rho] + J[\rho] - J[\rho] \\
&= T_s[\rho] + J[\rho] + E_{xc}[\rho] \,,
\end{aligned} \tag{2.49}
$$

where $E_{xc}[\rho] \equiv T[\rho] - T_s[\rho] + V_{ee}[\rho] - J[\rho]$ is defined as the exchange-correlation (XC) energy functional. The Euler-Lagrange Eq.(2.47) now becomes,

$$
\mu = v_{KS}(\mathbf{r}) + \frac{\delta T_s[\rho]}{\delta \rho} \,, \tag{2.50}
$$

where the KS *effective potential* ($v_{KS}(\mathbf{r})$) is defined as,

$$
\begin{aligned}
v_{KS}(\mathbf{r}) &= v_{ext}(\mathbf{r}) + \frac{\delta J[\rho]}{\delta \rho(\mathbf{r})} + \frac{\delta E_{xc}[\rho]}{\delta \rho(\mathbf{r})} \\
&= v_{ext}(\mathbf{r}) + \int d^3 r' \frac{\rho(\mathbf{r}')}{|\mathbf{r} - \mathbf{r}'|} + v_{xc}(\mathbf{r}) \,.
\end{aligned} \tag{2.51}
$$

The last term of Eq.(2.51) is known as the exchange-correlation potential,

$$
v_{xc}(\mathbf{r}) = \frac{\delta E_{xc}[\rho]}{\delta \rho(\mathbf{r})} \,. \tag{2.52}
$$

But in practice, one does not attempt to solve the Eq.(2.50) because the $T_s[\rho]$ is not known in terms of the density. Rather one follow Schrödinger like equation for the practical calculations. Eq.(2.51) with the constraint that density $\rho(\mathbf{r})$ integrates to the total number of particle effectively gives a Schrödinger like equation (like Eq.(2.5)), but all the many-electrons phenomena are now embedded into the effective potential $v_{KS}(\mathbf{r})$. This implies following simple canonical form of effective one-electron like equation,

$$
[-\frac{1}{2}\nabla^2 + v_{KS}(\mathbf{r})]\phi_i = \varepsilon_i \phi_i \,. \tag{2.53}
$$

Here, the KS eigenvalues ε_i are assumed to be ordered as,

$$\varepsilon_1 \leq \varepsilon_2 \leq .....\varepsilon_N = \varepsilon_F < \varepsilon_{N+1} \leq .... \tag{2.54}$$

The Fermi energy ε_F is identified as the one with the highest energy eigenvalue at the single-particle level. The physical meaning of the KS eigenvalues will be interpreted in the next section.

2.5 Interpretation of Kohn-Sham Eigenvalues

Since the effective potential or KS potential is a fictitious system, the meaning of the KS energy eigenvalues and KS orbitals are itself a very foremost question in DFT. In the Hartree-Fock theory, the meaning of HF eigenvalues is found from the Koopman's theorem which states that "*the HK eigenvalues are the energy necessary to add or remove an electron from a given orbital*" [48–56]. A similar theorem was suggested by Janak [57]. In this section, we will interpret the meaning of the KS eigenvalues and orbitals through the Janak's theorem, ionization potential and its connection to the bandgaps. These three phenomena are important to understand physically the importance of KS eigenvalues. Also, it will help to do practical calculations by solving KS single-particle equation.

2.5.1 Janak's theorem and fractional particle number prospective

Janak's theorem is analogous of the Koopman's theorem in HF theory. It states that "*the variation of the density functional total energy with respect to the orbital occupation of a state is equal to the eigenvalue of that orbital*" [57]. i.e.,

$$\frac{\delta E}{\delta n_i} = \varepsilon_i \,, \tag{2.55}$$

where n_i be the occupation and ϵ_i is the eigenvalue of the concerned state. If we consider the variation of the frontier orbitals, then the Eq.(2.55) leads to a rigorous connection between the highest occupied molecular orbitals (HOMO) and lowest unoccupied molecular

orbitals (LUMO). During the occupation number variation of the frontier orbital,

$$E(N) - E(N-1) \; = \; \int_0^1 \varepsilon_{HOMO} \partial n_{HOMO} \tag{2.56}$$

and

$$E(N) - E(N+1) \; = \; \int_0^1 \varepsilon_{LUMO} \partial n_{LUMO} \, . \tag{2.57}$$

Instead of the integer particle number, in the case of fractional occupation number, the above two equation is still valid and this is known as the Janak's theorem [57] in fractional particle number perspective. The fractional particle number perspective has special importance in DFT and it is shown by Perdew-Parr-Levy-Balduz [48] that the exact density functional formalism shows piece-wise linear behavior with a discontinuity at the integer number. The detail of the piece-wise linear behavior of the exact and approximate density functional theory will be discussed in chapter 4.

2.5.2   Ionization potential theorem

The ionization potential theorem in DFT connects the eigenvalue of the highest occupied KS level of a system with exponentially decaying density to the ionization potential. It states that "*the eigenvalue of the highest occupied KS orbital is equal to the ionization potential (IP)*". Based on the Janak's theorem [57] Perdew et. al. [49] showed for an atom of nuclear charge Z,

$$\varepsilon_{max} = \begin{cases} \text{-IP} & (Z-1) < N < Z \\ \text{-EA} & (Z) < N < (Z+1) \, , \end{cases} \tag{2.58}$$

where ε_{max} is the highest occupied KS orbital energy. This equation has been interpreted as follows: within the exact KS density functional theory, the highest occupied KS orbital energy of a system with $N-$electrons is negative of the exact ionization potential. Later,

in the subsequent work, Kleinman [53] showed that the HOMO energy should not be exactly equal to the IP. But, as the reply, Perdew and Levy [54] showed that Eq.(2.58) holds without going through the Janak's theorem.

2.5.3 Bandgap in Kohn-Sham formalism

Having established the Janak's theorem and ionization potentials theorem the obvious question is that: "*is there any connection between the KS orbital energies and bandgaps ?*" E_g. In DFT, this has been investigated several times [49, 50, 58–66]. This is an important question for quantum chemist and solid-state physicist. The bandgaps determine many important physical phenomena in molecular crystals and solids. The *fundamental bandgap* (E_g) is defined by taking the difference of the binding energy of the most weekly bound electron in the ground state of a system that of the ground state of the system obtained by addition of one more electron i.e.,

$$E_g = -\{[E_0^N - E_0^{N-1}] - [E_0^{N+1} - E_0^N]\} \,, \tag{2.59}$$

where the name bandgap originates from the removal of an electron from HOMO and addition of an electron in the LUMO level. In the non-interacting systems or the KS scheme, the bandgap is identified as [49],

$$\Delta_g^{KS} = \varepsilon_{N+1} - \varepsilon_N \,. \tag{2.60}$$

This is due to the relationship between the ionization potential and electron affinity of the KS system. Now using the variational equation the fundamental bandgap can be written as [49],

$$\begin{aligned} E_g &= IP - EA \\ &= lim_{\omega \to 0}\{\frac{\delta E[\rho]}{\delta \rho(\mathbf{r})}\Big|_{N+\omega} - \frac{\delta E[\rho]}{\delta \rho(\mathbf{r})}\Big|_{N-\omega}\} \,, \end{aligned} \tag{2.61}$$

where ω is the fraction of electron to be added or removed from the LUMO and HOMO respectively. Finally, the total energy in Eq.(2.61) can be recomposed into $E[\rho] = T[\rho] + E_H + E_{ext} + E_{XC}$ and using the fact that the E_{ext} and E_H depend continuously on the particle number one arrives,

$$
\begin{aligned}
E_g &= lim_{\omega \to 0}\{[\frac{\delta T_s[\rho]}{\delta \rho(\mathbf{r})}\Big|_{N+\omega} - \frac{\delta T_s[\rho]}{\delta \rho(\mathbf{r})}\Big|_{N-\omega}] + [\frac{\delta E_{xc}[\rho]}{\delta \rho(\mathbf{r})}\Big|_{N+\omega} - \frac{\delta E_{xc}[\rho]}{\delta \rho(\mathbf{r})}\Big|_{N-\omega}]\} \\
&= \Delta_g^{KS} + \Delta_{xc} .
\end{aligned}
\tag{2.62}
$$

The second term of Eq.(2.62) is originating from the derivative discontinuity of the exchange-correlation (XC) energy functional. In the exact KS theory, the Δ_{xc} is finite but for approximate XC functionals, Δ_{xc} is often neglected because of the approximate nature of it. The Δ_{xc} includes a prime amount of bandgap value. Though recent developments in advanced Kohn-Sham kinetic energy density-dependent functionals include some amount of Δ_{xc} but still away from accuracy. Several resolutions are also proposed to improve the bandgap performance such as the exact-exchange (EXX) formalism [60, 67–76], which by construction possesses Δ_{xc}. Other resolutions like hybrid functional approach are also proposed to improve the bandgap performance by mixing some amount of HF exact exchange and keeping the accuracy of the semilocal functional. The details of this approach will be discussed in chapter 4 and chapter 5.

2.6   Designing Exchange and Correlation Energy Functionals

2.6.1   Definitions

Due to different properties of the exchange and correlation energies, these can be decomposed into the exchange and correlation as,

$$E_{xc}[\rho] = E_x[\rho] + E_c[\rho] \ . \tag{2.63}$$

The exact definition of the exchange and correlation can be given from the constraint search formalism. In constraint search, the exchange is defined as,

$$E_x[\rho] = \langle \phi_\rho^{min} | \hat{V}_{ee} | \phi_\rho^{min} \rangle - J[\rho] \ , \tag{2.64}$$

where $J[\rho]$ is the Coulomb energy defined in Eq.(2.27). Here, ϕ_ρ^{min} is the single Slater determinant obtained by minimization of the Kinetic energy operator only, subject to the constraint that the wavefunction gives the same density as the fully interacting system. Note that

$$\langle \phi_\rho^{min} | \hat{T} + \hat{V}_{ee} | \phi_\rho^{min} \rangle = T_s[\rho] + J[\rho] + E_x[\rho] \ , \tag{2.65}$$

which in $\hat{V}_{ee} = 0$ limit becomes,

$$\begin{aligned} T_s &= T_s[\rho] + J[\rho] + E_x[\rho] \\ E_x[\rho] &= -J[\rho] \ . \end{aligned} \tag{2.66}$$

Thus for one-electron, the exchange energy cancels the Hartree electrostatic self-repulsion energy exactly. In the same line of analysis, the correlation energy is defined as,

$$
\begin{aligned}
E_c[\rho] &= F[\rho] - T_s[\rho] + J[\rho] + E_x[\rho] \\
&= \langle \Psi_\rho^{min} | \hat{T} + \hat{V}_{ee} | \Psi_\rho^{min} \rangle - \langle \phi_\rho^{min} | \hat{T} + \hat{V}_{ee} | \phi_\rho^{min} \rangle \\
&= [\langle \Psi_\rho^{min} | \hat{T} | \Psi_\rho^{min} \rangle - \langle \phi_\rho^{min} | \hat{T} | \phi_\rho^{min} \rangle] + [\langle \Psi_\rho^{min} | \hat{V}_{ee} | \Psi_\rho^{min} \rangle - \langle \phi_\rho^{min} | \hat{V}_{ee} | \phi_\rho^{min} \rangle] \\
&= T_c + V_c \, .
\end{aligned}
\tag{2.67}
$$

T_c is the correlation energy arising due to the difference between the exact kinetic energy and KS kinetic energy. The motion of the electron is modified due to the correlated wavefunction of the real and KS system. Similarly, due to the difference between the expectation value of the electron-electron repulsion with respect to the real and KS wavefunction give rise the correlation energy from the electron-electron repulsion integral.

2.6.2 Exchange-Correlation and coupling-constant integration

From the discussions above, it is quite evident that the calculation of exchange and correlation energy requires the real and non-interacting wavefunction. But, it is impracticable to construct the real interacting system wavefunction. Therefore, it is always necessary to construct the exchange and correlation differently. Two ways of obtaining the expressions for the exchange-correlation are
(a) Kohn-Sham Perturbation theory, and
(b) adiabatic connection or the coupling constraint integral approach.
In both methods, the exact form of exchange and correlation energy are obtained to be the same. In this section, we will describe the coupling constraint integral formula for the exchange and correlation energy. The basic assumption is that the ground state density ρ of the interacting system is $v-$representable for any arbitrary interaction strength λV_{ee}, where $\lambda \in [0, 1]$, i.e.,

$$
\rho_\lambda(\mathbf{r}) = \langle \Psi_0^\lambda | \hat{\rho}(\mathbf{r}) | \Psi_0^\lambda \rangle \equiv \rho(\mathbf{r}) \quad \textit{for all} \ \ 0 \leq \lambda \leq 1 \, .
\tag{2.68}
$$

The external potential is denoted by u_λ has three different forms,

$$
u_\lambda = \begin{cases} v_{KS}(\mathbf{r}) & \text{for } \lambda = 0 \\ \text{unknown} & \text{for } 0 \leq \lambda \leq 1 \\ v_{ext}(\mathbf{r}) & \text{for } \lambda = 1 \,. \end{cases} \tag{2.69}
$$

With this external potential, the λ dependent Hamiltonian becomes,

$$
\hat{H}(\lambda) = \hat{T} + \int d^3r \, u_\lambda(\mathbf{r})\hat{\rho}(\mathbf{r}) + \lambda V_{ee} \,. \tag{2.70}
$$

For $\lambda = 0$, the Hamiltonian becomes KS Hamiltonian and $\lambda = 1$ leads to the fully interacting Hamiltonian. Using this coupling constant Hamiltonian, the λ dependent Schrödinger equation becomes,

$$
E_0(\lambda) = \langle \Psi_0^\lambda | \hat{H}(\lambda) | \Psi_0^\lambda \rangle \,. \tag{2.71}
$$

Differentiation of $E_0(\lambda)$ with respect to λ and using the Hellman-Feynman theorem, Eq.(2.71) becomes,

$$
E_0(\lambda = 1) - E_0(\lambda = 0) = \int_{\lambda=0}^{\lambda=1} d\lambda \Big\langle \Psi_0^\lambda \Big| \int d^3r \hat{\rho}(\mathbf{r})\frac{du_\lambda(\mathbf{r})}{d\lambda} + V_{ee} \Big| \Psi_0^\lambda \Big\rangle \,. \tag{2.72}
$$

After evaluation of the integral formula and applying the definition of the response function, the compact form of the exchange-correlation energy functional in terms of the response function (χ_λ) and electron-electron repulsion potential v_{ee} is obtained to be,

$$
E_{xc}[\rho] = \frac{1}{2} \int d^3r \int d^3r' v_{ee}(\mathbf{r}, \mathbf{r}') \int_{\lambda=0}^{\lambda=1} d\lambda [i\chi_\lambda(\mathbf{r}0, \mathbf{r}'0) - \rho(\mathbf{r})\delta^3(\mathbf{r} - \mathbf{r}')] \,. \tag{2.73}
$$

This is the exact formulation of exchange-correlation functional in terms of the coupling constant integral. Upon applying the Fourier representation, this can be further divided into the exchange and correlation parts. This results in the decomposition of the exact formulation of the exchange and correlation energy functional. The exchange part is

given as,

$$E_x = \frac{1}{2} \int d^3r \int d^3r' \frac{1}{|\mathbf{r} - \mathbf{r}'|} \left[i \int_0^\infty \frac{d\omega}{\pi} \chi_s(\mathbf{r}, \mathbf{r}', \omega) - \rho(\mathbf{r}) \delta^3(\mathbf{r} - \mathbf{r}') \right], \qquad (2.74)$$

where χ_s is the time-ordered response function obtained from the KS orbital and ω is obtained from the Fourier transform of time. Subtracting the exchange energy functional from the total exchange-correlation energy of Eq.(2.73) the correlation energy functional becomes,

$$E_c = -\frac{1}{2} \int d^3r \int d^3r' \frac{1}{|\mathbf{r} - \mathbf{r}'|} \int d\lambda \int_0^\infty \frac{d\omega}{\pi} \left[\chi_\lambda(\mathbf{r}, \mathbf{r}', i\omega) - \chi_s(\mathbf{r}, \mathbf{r}', i\omega) \right]. \quad (2.75)$$

The expression of the E_x and E_c as obtained from the response function is particularly important in deriving the exchange and correlation energy functional. It is well known that the second-order and fourth-order slowly varying gradient approximation derived from the coupling constant integral formula of exchange and correlation is the main framework for the construction of the modern GGA and meta-GGA functionals. We will discuss the construction of GGA and meta-GGA later in this chapter and chapter 3.

2.6.3   Reduced density matrices

The concept of Density matrices is very important in DFT, in particular when designing the exchange energy functional from the Taylor series expansion of the exchange-hole or using density matrix expansion technique. We start from the $N-$elctron wavefunction ,$\Psi_N(\mathbf{x}, \mathbf{x}_2....\mathbf{x}_N)$ in co-ordinate space. The Nth order density matrix is defined as,

$$\gamma_N(\mathbf{x}', \mathbf{x}_2' \cdots \mathbf{x}_N', \mathbf{x}_1, \mathbf{x}_2 \cdots \mathbf{x}_N) \equiv \Psi_N(\mathbf{x}', \mathbf{x}_2' \cdots \mathbf{x}_N') \Psi_N^*(\mathbf{x}_1, \mathbf{x}_2 \cdots \mathbf{x}_N). \qquad (2.76)$$

Using the above definition, the pth order reduced density matrix is obtained as,

$$\gamma_p(\mathbf{x}', \mathbf{x}_2' \cdots \mathbf{x}_p', \mathbf{x}_1, \mathbf{x}_2 \cdots \mathbf{x}_p)$$

$$= \binom{N}{p} \int \cdots \int \gamma_N(\mathbf{x}', \mathbf{x}'_2 \cdots \mathbf{x}'_p, \mathbf{x}'_{p+1} \cdots \mathbf{x}'_N, \mathbf{x}_1, \mathbf{x}_2 \cdots \mathbf{x}_p, \mathbf{x}_{p+1} \cdots \mathbf{x}_N) d^3 x_{p+1} \cdots d^3 x_N \,,$$

$$(2.77)$$

where $\binom{N}{p}$ is the binomial coefficient arising from the permutations of the coordinates

of the identical particles (Fermions). If $p = 2$ we obtain the 2nd order reduced density

matrix,

$$\gamma_2(\mathbf{x}', \mathbf{x}'_2, \mathbf{x}, \mathbf{x}_2) = \frac{N(N-1)}{2} \int \cdots \int \Psi(\mathbf{x}', \mathbf{x}'_2 \cdots \mathbf{x}'_N) \Psi^*(\mathbf{x}, \mathbf{x}_2 \cdots \mathbf{x}_N) \, d^3 x_3 \cdots d^3 x_N$$

$$(2.78)$$

and for $p = 1$ the 1st order reduced density matrix is obtained as,

$$\gamma_1(\mathbf{x}', \mathbf{x}) = N \int \cdots \int \Psi(\mathbf{x}', \mathbf{x}_2 \cdots \mathbf{x}'_N) \Psi^*(\mathbf{x}, \mathbf{x}_2 \cdots \mathbf{x}_N) \, d^3 x_2 \cdots d^3 x_N \,. \qquad (2.79)$$

Here the spin-coordinate $\mathbf{x} \equiv (\mathbf{r}, \sigma)$ involves both the space and spin coordinates. But,

the spin coordinated can be reduced by doing summation over all the spin coordinated.

Therefore, the 1st and 2nd order *spinless density matrices* are given by,

$$\Gamma_1(\mathbf{r}', \mathbf{r}) \;=\; \sum_{\sigma} \gamma_1(\mathbf{r}', \sigma, \mathbf{r}, \sigma) \qquad\qquad (2.80)$$

and

$$\Gamma_2(\mathbf{r}', \mathbf{r}'_2, \mathbf{r}, \mathbf{r}_2) \;=\; \sum_{\sigma, \sigma_2} \gamma_2(\mathbf{r}', \sigma, \mathbf{r}'_2, \sigma_2, \mathbf{r}, \sigma, \mathbf{r}_2, \sigma_2) \,. \qquad\qquad (2.81)$$

Note that, the diagonal element of the 1st order reduced matrix is just the electron density,

$$\rho(\mathbf{r}) = \Gamma_1(\mathbf{r}', \mathbf{r})|_{\mathbf{r}'=\mathbf{r}} \,. \qquad\qquad (2.82)$$

and the shorthand notation of the diagonal element of $\Gamma_2(\mathbf{r}', \mathbf{r}_2', \mathbf{r}, \mathbf{r}_2)$ is

$$\Gamma_2(\mathbf{r}', \mathbf{r}_2) = \Gamma_2(\mathbf{r}, \mathbf{r}_2, \mathbf{r}, \mathbf{r}_2)|_{\mathbf{r}'=\mathbf{r}, \mathbf{r}_2'=\mathbf{r}_2} = \frac{N(N-1)}{2} \sum_{\sigma_1 \cdots \sigma_N} \int \cdots \int |\Psi|^2 \, d^3r_3 \cdots d^3r_N \, . \tag{2.83}$$

The expectation value of kinetic energy operator and the two body operators can also be expressed in terms of 1st order and 2nd order reduced density matrices as,

$$\langle \hat{T} \rangle = -\frac{1}{2} \int d\mathbf{r} \frac{\partial}{\partial \mathbf{r}} \cdot \frac{\partial}{\partial \mathbf{r}} \Gamma_1(\mathbf{r}', \mathbf{r})|_{\mathbf{r}'=\mathbf{r}} \, . \tag{2.84}$$

and

$$\langle \hat{V}_{ee} \rangle = \int d^3r' d^3r \frac{\Gamma_2(\mathbf{r}', \mathbf{r})}{|\mathbf{r} - \mathbf{r}'|} \, . \tag{2.85}$$

Note that in Eq.(2.85), we denote the $\Gamma_2(\mathbf{r}', \mathbf{r}_2)$ as $\Gamma_2(\mathbf{r}', \mathbf{r})$ i.e., we change the variable $\mathbf{r}_2$ to $\mathbf{r}$. This is done to make it conventional to the notational representation of the other operators.

Now, noting that the $\langle \hat{V}_{ee} \rangle$ can be expressed in terms of the $J[\rho]$+non-classical terms i.e.,

$$\int d^3r' d^3r \frac{\Gamma_2(\mathbf{r}', \mathbf{r})}{|\mathbf{r} - \mathbf{r}'|} = \frac{1}{2} \int d^3r' d^3r \frac{\rho(\mathbf{r}')\rho(\mathbf{r})}{|\mathbf{r} - \mathbf{r}'|} + \textit{non-classical term} \, . \tag{2.86}$$

Using this fact, lets define the non-classical term as,

$$\frac{1}{2} \int d^3r' d^3r \frac{\rho(\mathbf{r}')\rho(\mathbf{r})h(\mathbf{r}', \mathbf{r})}{|\mathbf{r} - \mathbf{r}'|} \, , \tag{2.87}$$

where $h(\mathbf{r}', \mathbf{r})$ contains all the non-classical effects. It is best known as *pair correlation function*. Physically, it is defined as *the probability function − for an electron located at* $\mathbf{r}$, *the probability of finding another electron at the point* $\mathbf{r}'$. From Eq.(2.85) and Eq.(2.87), $h(\mathbf{r}', \mathbf{r})$ is defined as,

$$h(\mathbf{r}', \mathbf{r}) = \frac{2\Gamma_2(\mathbf{r}', \mathbf{r}) - \rho(\mathbf{r}')\rho(\mathbf{r})}{\rho(\mathbf{r}')\rho(\mathbf{r})} \, . \tag{2.88}$$

The two-particle density matrix $\Gamma_2(\mathbf{r}', \mathbf{r})$ becomes uncorrelated whenever the two coordi-

nates are very far apart implying,

$$\Gamma_2(\mathbf{r}', \mathbf{r}) \approx \rho(\mathbf{r}')\rho(\mathbf{r}), \tag{2.89}$$

which makes

$$h(\mathbf{r}', \mathbf{r}) = 1 . \tag{2.90}$$

For small distances, $h(\mathbf{r}', \mathbf{r})$ is smaller than 1 because of both the repulsion effects originating from the Pauli exclusion principle and electron-electron repulsion. Defining $\Gamma_2(\mathbf{r}', \mathbf{r})$ from Eq.(2.88) and integrating with respect to $d\mathbf{r}'$ one can obtain,

$$
\begin{aligned}
\int \Gamma_2(\mathbf{r}', \mathbf{r}) \, d^3r' &= \frac{1}{2}\rho(\mathbf{r}) \int \rho(\mathbf{r}') \, d^3r' + \int \rho(\mathbf{r}')h(\mathbf{r}', \mathbf{r}) \, d^3r' \\
\frac{N-1}{2}\rho(\mathbf{r}) &= \frac{1}{2}\rho(\mathbf{r})[N + \int \rho(\mathbf{r}')h(\mathbf{r}', \mathbf{r}) \, d^3r'] .
\end{aligned} \tag{2.91}
$$

This implies that

$$\int \rho(\mathbf{r}')h(\mathbf{r}', \mathbf{r}) \, d^3r' = -1 . \tag{2.92}$$

Here, the term $\rho(\mathbf{r}')h(\mathbf{r}', \mathbf{r})$ has special importance in DFT, and it is known as the exchange-correlation hole ($\rho_{xc}(\mathbf{r}', \mathbf{r})$). The constraint of presented in Eq.(2.92) is known as the normalization condition of the exchange-correlation hole. The exchange-correlation hole is one of the main constituents of constructing the exchange-correlation functional. Now, using the exchange-correlation hole the $\langle V_{ee} \rangle$ is defined as,

$$\langle V_{ee} \rangle = J[\rho] + \frac{1}{2} \int d^3r' d^3r \frac{\rho(\mathbf{r})\rho_{xc}(\mathbf{r}', \mathbf{r})}{|\mathbf{r} - \mathbf{r}'|} \tag{2.93}$$

2.6.4 Exchange-correlation hole

As mentioned above the concept of the density matrix is very useful in describing the exchange-correlation hole and related models. In this thesis, the exchange hole will be used further to construct the exchange energy functionals. But, before that the knowledge of the physical contents of the exchange-correlation hole is very important. To do so, we

start with the coupling constraint integral formula of the constraint search formalism. Let us define a functional $F_\lambda[\rho]$ as,

$$F_\lambda[\rho] = min_{\Psi^\lambda \to \rho} \langle \Psi^\lambda | \hat{T} + \lambda \hat{V}_{ee} | \Psi^\lambda \rangle = \langle \Psi_\rho^{min,\lambda} | \hat{T} + \lambda \hat{V}_{ee} | \Psi_\rho^{min,\lambda} \rangle \,, \qquad (2.94)$$

where $\Psi_\rho^{min,\lambda}$ yields the same density ρ and minimize the expectation value of $\hat{T} + \lambda \hat{V}_{ee}$ for each values of λ, where λ varies from $0 \to 1$. The $\lambda = 0$ corresponds to the KS system, whereas, $\lambda = 1$ corresponds to the true interacting many-electron systems. Using the above coupling constant functional, the exchange-correlation energy functional becomes,

$$
\begin{aligned}
E_{xc}[\rho] &= \langle \Psi^\lambda | \hat{T} + \lambda \hat{V}_{ee} | \Psi^\lambda \rangle |_{\lambda=1} - \langle \Psi^\lambda | \hat{T} + \lambda \hat{V}_{ee} | \Psi^\lambda \rangle |_{\lambda=0} - J[\rho] \\
&= \int_{\lambda=0}^{\lambda=1} d\lambda \frac{d}{d\lambda} \langle \Psi^\lambda | \hat{T} + \lambda \hat{V}_{ee} | \Psi^\lambda \rangle - J[\rho] \,, \\
&= \int_{\lambda=0}^{\lambda=1} d\lambda \langle \Psi^\lambda | \hat{V}_{ee} | \Psi^\lambda \rangle - J[\rho] \,, \qquad (2.95)
\end{aligned}
$$

where the last line of the Eq.(2.95) is due to the Hellman-Feynman theorem. Here, the Eq.(2.95) is obtained by rewriting Eq.(2.70), Eq.(2.71) and Eq.(2.72).

Now, using Eq.(2.85), the coupling-constant integral $\int_{\lambda=0}^{\lambda=1} d\lambda \langle \Psi^\lambda | \hat{V}_{ee} | \Psi^\lambda \rangle$ becomes,

$$
\begin{aligned}
\int_{\lambda=0}^{\lambda=1} d\lambda \langle \Psi^\lambda | \hat{V}_{ee} | \Psi^\lambda \rangle &= \int d\lambda \int d\mathbf{r}' d\mathbf{r} \frac{\Gamma_2^\lambda(\mathbf{r}', \mathbf{r})}{|\mathbf{r} - \mathbf{r}'|} \\
&= \int d^3r' d^3r \frac{\langle \Gamma_2^\lambda(\mathbf{r}', \mathbf{r}) \rangle}{|\mathbf{r} - \mathbf{r}'|} \,, \qquad (2.96)
\end{aligned}
$$

where $\langle \Gamma_2^\lambda(\mathbf{r}', \mathbf{r}) \rangle = \int d\lambda \Gamma_2^\lambda(\mathbf{r}', \mathbf{r})$. Using Eq.(2.96), density matrix and exchange hole, Eq.(2.95) becomes,

$$E_{xc}[\rho] = \frac{1}{2} \int d^3r' d^3r \frac{\rho(\mathbf{r}) \langle \rho_{xc}(\mathbf{r}', \mathbf{r}) \rangle}{|\mathbf{r} - \mathbf{r}'|} \,, \qquad (2.97)$$

where $\langle \rho_{xc}(\mathbf{r}', \mathbf{r}) \rangle = \int_{\lambda=0}^{\lambda=1} d\lambda \rho_{xc}(\mathbf{r}', \mathbf{r})$. However, due to different properties, the exchange-correlation hole can be decomposed into exchange and correlation hole as, $\rho_{xc}(\mathbf{r}', \mathbf{r}) = \rho_x(\mathbf{r}', \mathbf{r}) + \rho_c(\mathbf{r}', \mathbf{r})$. Now, using the fact that for $\lambda = 0$, i.e., in the non-interacting particle

framework, the many-electron system can be expressed as the product of single-particle systems, which give a direct connection between the HF exchange with the exchange hole. Therefore, the HF 1st order reduced density matrix is expressed as,

$$E_x = -\frac{1}{2} \int d^3r' d^3r \frac{|\Gamma_1(\mathbf{r}', \mathbf{r})|^2}{|\mathbf{r} - \mathbf{r}'|} , \tag{2.98}$$

where $\Gamma_1(\mathbf{r}', \mathbf{r}) = \sum_i \Psi_i(\mathbf{r}')\Psi_i(\mathbf{r})$. This is obtained by rewritting the HF exchange in term of the 1st order reduced density matrix. Now, using the exchange only notation of Eq.(2.97) and $\lambda = 0$ formalism of the HF exchange as given in Eq.(2.98) one can obtain,

$$\rho_x(\mathbf{r}', \mathbf{r}) = -\frac{|\Gamma_1(\mathbf{r}', \mathbf{r})|^2}{\rho(\mathbf{r})} . \tag{2.99}$$

This equation is very important in the sense that knowing the density matrix one can design the exchange hole and from the exchange hole, the exchange energy functional can be derived. The density matrix expansion based functionals are developed in this line by explicitly constructing the density matrix. We will discuss this construction later in this thesis.

2.7   Formal Properties of Functionals

2.7.1   Uniform coordinate scaling

Let consider for any scaling parameter $\gamma > 0$ (with $\mathbf{r} \to \gamma\mathbf{r}$), the wavefunction in 3D scaled as,

$$\Psi_\gamma(\mathbf{r}_1, \cdots, \mathbf{r}_N) = \gamma^{3N/2}\Psi_\gamma(\gamma\mathbf{r}_1, \cdots, \gamma\mathbf{r}_N) , \tag{2.100}$$

because it satisfies the normalization condition as,

$$\langle \Psi_\gamma | \Psi_\gamma \rangle = \langle \Psi | \Psi \rangle = 1 . \tag{2.101}$$

The corresponding density of the scaled wavefunctions becomes,

$$\rho_\gamma(\mathbf{r}) = \gamma^3 \rho(\gamma \mathbf{r}) , \tag{2.102}$$

which also conserve the total particle number constraint as,

$$\int d^3r \rho_\gamma(\mathbf{r}) = \int d^3(\gamma r)\rho(\gamma \mathbf{r}) = N . \tag{2.103}$$

Under the scaling relation, the Hartree electrostatic potential becomes,

$$J[\rho_\gamma] = \gamma \frac{1}{2} \int d^3(\gamma r) \, d^3(\gamma r') \frac{\rho(\gamma \mathbf{r})\rho(\gamma \mathbf{r}')}{|\gamma \mathbf{r} - \gamma \mathbf{r}'|} = \gamma J[\rho] . \tag{2.104}$$

Due to the second-order derivative $\sum_{i=1,2,3} \frac{d^2}{dx_i^2}$, the scaling relation of the expectation value of kinetic energy is straight forward,

$$\langle \Psi_\gamma | \hat{T} | \Psi_\gamma \rangle = \gamma^2 \langle \Psi | \hat{T} | \Psi \rangle . \tag{2.105}$$

Now, for the non-interacting N-electron system, the KS orbitals also obey the same scaling rule of the real interacting system which results to,

$$T_s[\rho_\gamma] = \gamma^2 T_s[\rho] . \tag{2.106}$$

The scaling relation of the exchange energy functional is derived from the constraint search formalism by using the definition of exchange energy as given by Eq.(2.64) i.e.,

$$E_x[\rho] = \langle \phi_\rho^{min} | \hat{V}_{ee} | \phi_\rho^{min} \rangle - J[\rho] . \tag{2.107}$$

which under the uniform density scaling can be written as,

$$E_x[\rho_\gamma] = \langle \phi_{\rho_\gamma}^{min} | \hat{V}_{ee} | \phi_{\rho_\gamma}^{min} \rangle - J[\rho_\gamma] . \tag{2.108}$$

Upon applying the scaling relation of J and also using the fact that the electron-electron interaction potential is a homogeneous function of first degree we obtain the scaling relation of the exchange energy functional as,

$$E_x[\rho_\gamma] = \gamma E_x[\rho] \ . \tag{2.109}$$

However, for correlation energy there exist no straight forward scaling relation.

2.7.2 Non-uniform coordinate scaling

The non-uniform coordinate scaling relation is important for the dimensional crossover from three dimensions to two dimensions or one dimensional. Under one-dimensional coordinate scaling the density scales as,

$$\rho_\gamma = \gamma \rho(\gamma x, y, z) \ . \tag{2.110}$$

The electron number conservation of the scale density gets satisfied as,

$$\int dx\, dy\, dz\, \rho_\gamma(x, y, z) = \int d(\gamma x) dy\, dz\, \gamma \rho(\gamma x, y, z) = N \ . \tag{2.111}$$

However, the scaling relation of KS kinetic energy, exchange energy, and correlation energy also exist only in the $\gamma \to \infty$ as,

$$T_s[\rho_\gamma] \to T_w[\rho_\gamma] \ , \tag{2.112}$$

$$E_x[\rho_\gamma] \to constant \ , \tag{2.113}$$

$$E_c[\rho_\gamma] \to constant \tag{2.114}$$

2.7.3 Spin scaling relations

Spin scaling relation is important because, through it, any spin-unpolarized energy functional can be transformed into the spin-polarized form. The density can be expressed as

the sum of the spin-up ($\rho_\uparrow$) and spin-down ($\rho_\downarrow$) densities i.e.,

$$\rho(\mathbf{r}) = \rho_\uparrow(\mathbf{r}) + \rho_\downarrow(\mathbf{r}) \ . \tag{2.115}$$

Using this density scaling relation the exchange energy scaling relation becomes,

$$E_x[\rho_\uparrow, \rho_\downarrow] = \frac{1}{2}(E_x[2\rho_\uparrow] + E_x[2\rho_\downarrow]) \ . \tag{2.116}$$

Analogously the spin-scaling relation of kinetic energy becomes,

$$T_s[\rho] = \frac{1}{2}(T_s[2\rho_\uparrow] + T_s[2\rho_\downarrow]) \ . \tag{2.117}$$

Similarly, the spin scaling relation of the exchange hole can also be written as,

$$\rho_x[\rho](\mathbf{r}, \mathbf{r} + \mathbf{u}) = \frac{\rho_\uparrow(\mathbf{r})}{\rho(\mathbf{r})}\rho_x[2\rho_\uparrow](\mathbf{r}, \mathbf{r} + \mathbf{u}) + \frac{\rho_\downarrow(\mathbf{r})}{\rho(\mathbf{r})}\rho_x[2\rho_\downarrow](\mathbf{r}, \mathbf{r} + \mathbf{u}) \ . \tag{2.118}$$

However, like coordinate scaling, there is no simple spin scaling relation for correlation energy functional.

2.7.4   Other miscellaneous properties

Exchange energy for one and two electron system: For the one-electron system, the exchange energy must be equal to the Hartree energy as

$$E_x[\rho] = -J[\rho] \tag{2.119}$$

and correlation should vanish i.e.,

$$E_c[\rho] = 0 \tag{2.120}$$

For two electron system it becomes,

$$E_x[\rho] = -\frac{1}{2}J[\rho] \ . \tag{2.121}$$

Exact conditions on exchange-correlation hole: As discussed earlier, the exchange-correlation hole is an important concept for the development of functionals. The exchange-correlation energy is nothing but the electrostatic interaction between the electron located at $\vec{r}$ and the exchange-correlation hole at $\vec{r} + \vec{u}$ surrounding it, where $\vec{u}$ is the relative separation of the two electrons with the same spin. The exchange-correlation hole obeys important normalization condition: $\int \rho_{xc}(\vec{r}, \vec{r} + \vec{u}) \, d^3u = -1$. The exact properties of exchange-correlation hole along with the exact small $-u$ expansion will be discussed in details in chapter 3.

2.8   Hierarchy of Different Levels of Exchange-Correlation Approximations

2.8.1   Local (spin-)density approximation

The first-ever approximation which has been used vastly during the initial years of development and applications of the density functional formalism is the local density approximation (LDA). The LDA is one of the simplest and easily implementable approximations of the DFT. The LDA exchange functional is based on the homogeneous electron gas (HEG). The HEG model is a model system where the electrons are uniformly distributed over the space and the positive background charges are assumed to be distributed uniformly to neutralize the electron charge. To understand the construction and mathematical formulation of the LDA, we first recall the kinetic energy approximation in the Thomas-Fermi approximation. In this approximation, the homogeneous electron gas-based kinetic energy density becomes,

$$t_s^{hom} = \frac{3}{10}(3\pi^2)^{2/3}\rho(\mathbf{r})^{5/3} \ . \tag{2.122}$$

This method has been formulated using the uniform electron gas in a cubical volume $V = l^3$ and considering the KS orbitals as plane-waves $\exp(i\mathbf{k}.\mathbf{r})/\sqrt{V}$, where $\mathbf{k}$ is the

Thomas-Fermi wave vector. Similarly, the exchange energy density is obtained to be

$$\epsilon_x^{LDA}[\rho] = -\frac{3}{4}(\frac{3}{\pi})^{1/3}\rho(\mathbf{r})^{4/3} \,, \tag{2.123}$$

which leads to the LDA exchange energy functional,

$$E_x^{LDA}[\rho] = \int \rho(\mathbf{r})\epsilon_x^{LDA}[\rho] \, d^3r \,. \tag{2.124}$$

However, deriving the correlation energy is quite difficult because in the correlation energy, only two extreme limits are known exactly: The high-density limit ($r_s \rightarrow 0$) and the low density limit ($r_s \rightarrow \infty$), where $r_s = \left(\frac{3}{4\pi\rho(\mathbf{r})}\right)^{1/3}$ is the Wigner-Seitz radius. The parametrized form of the correlation energy is obtained by extrapolating between these two limits. In high density or $r_s \rightarrow 0$ limit, the correlation energy per electron becomes,

$$\epsilon_c^{unif}[\rho] \rightarrow c_0 \ln(r_s) - c_1 + \cdots \quad (r_s \rightarrow 0) \tag{2.125}$$

and in the low density or $r_s \rightarrow \infty$ limit it becomes,

$$\epsilon_c^{unif}[\rho] \rightarrow -\frac{d_0}{r_s} + \frac{d_1}{r_s^{3/2}} + \cdots \quad (r_s \rightarrow \infty) \,, \tag{2.126}$$

where c_0, c_1, d_0, and d_1 are given in reference [77]. An extrapolation of these two limits and parametrization with the accurate quantum Monte-Carlo results, the correlation energy per electron for the LDA exchange as,

$$\epsilon_c^{unif}[\rho] = -2c_0(1 + \alpha_1 r_s)ln\left[1 + \frac{1}{2c_0(\beta_1 r_s^{1/2} + \beta_2 r_s + \beta_3 r_s^{3/2} + \beta_4 r_s^2)}\right], \tag{2.127}$$

where

$$\beta_1 = \frac{1}{2c_0}exp(\frac{c_1}{2c_0}) \tag{2.128}$$

and

$$\beta_2 = 2c_0\beta_1^2 \tag{2.129}$$

are two non-empirical parameters. The parameters α_1, β_3, and β_4 are obtained from the accurate quantum Monte-Carlo results.

The LDA exchange energy of Eq.(2.124) together with correlation energy is given by Eq.(2.127) results the local spin density approximation (LSDA) as,

$$E_{xc}^{LSDA}[\rho_\uparrow, \rho_\downarrow] = \int d^3r \rho(\mathbf{r}) \epsilon_{xc}^{unif}[\rho_\uparrow, \rho_\downarrow] \,, \tag{2.130}$$

where $\rho(\mathbf{r}) = \rho_\uparrow(\mathbf{r}) + \rho_\downarrow(\mathbf{r})$ is the sum of spin densities. $\epsilon_{xc}^{unif}[\rho_\uparrow, \rho_\downarrow]$ is the exchange-correlation energy per electron in the homogeneous electron gas limit.

For the spin-polarized system, one can define a non-vanishing spin-polarization parameter,

$$\zeta = \frac{\rho_\uparrow - \rho_\downarrow}{\rho_\uparrow + \rho_\downarrow} \neq 0, \tag{2.131}$$

and using it the exchange energy per electron is further defined as,

$$\epsilon_x^{unif}[\rho_\uparrow, \rho_\downarrow] = \epsilon_x^{unif}[\rho] \frac{[(1+\zeta)^{4/3} + (1-\zeta)^{4/3}]}{2} \,. \tag{2.132}$$

2.8.2   Gradient approximations

The L(S)DA is a good approximation for the solid-state lattice constants for a while but shows large errors in predicting the bulk moduli, cohesive energies and atomization energies of molecules. All these properties are greatly improved by the inclusion of the gradient terms in the functional form. The relevance of slowly varying or non-uniform density limit is included in the functional form through the dimensionless quantities,

$$s = \frac{|\nabla \rho(\mathbf{r})|}{2k_F \rho(\mathbf{r})}; \; p = \frac{|\nabla \rho(\mathbf{r})|^2}{2(3\pi^2)^{1/3}\rho(\mathbf{r})^{4/3}} \,, \tag{2.133}$$

and reduced Laplacian of density

$$q = \frac{\nabla^2 \rho(\mathbf{r})}{4(3\pi^2)^{2/3}\rho^{5/3}} \,. \tag{2.134}$$

The reduced density gradient s measures how fast and how much density varies in the scale of local Fermi momentum $2\pi/k_F$. However, the region $0 < s < 3$ is important for atoms, molecules, and solids, whereas, $0 < s < 1$ is important for solids than molecules. The $s > 3$ region is unimportant.

In modern density functional exchange approximations, the higher-order terms of density gradient expansion is obtained from the linear response theory of Eq.(2.74) as,

$$E_x[\rho] = \int d^3r\rho(\mathbf{r})\epsilon_x[\rho(\mathbf{r})][1 + \frac{10}{81}p + \frac{146}{2025}q^2 - \frac{73}{146}qp + Dp^2] \,. \tag{2.135}$$

This is best known as the fourth-order gradient approximation (GE4) of exchange. The Perdew-Burke-Ernzerhof (PBE) [78] generalized-gradient approximation (GGA) is developed by truncating the series up to 2nd terms and using the series re-summation technique. The details of the PBE functional construction is discussed in chapter 3. However, in PBE functional different coefficient of p has been used than Eq.(2.135) to better the performance for the atomic and molecular systems. Though the PBE functional improves the atomization energies compared to L(S)DA but the performance of PBE for solid-state lattice constants is not so impressive as compared to L(S)DA. However, in the modified version of PBE for solids (known as PBEsol) the coefficient of p i.e., $10/81$ is restored [79].

Regarding the generalized gradient approximation based correlation energy, it is constructed from the second-order gradient expansion approximation (GEA) as,

$$E_c[\rho] = \int d^3r\rho(\mathbf{r})[\epsilon_c^{unif}[\rho_\uparrow, \rho_\downarrow] + C_c[\rho_\uparrow, \rho_\downarrow]\frac{|\nabla\rho(\mathbf{r})|^2}{\rho(\mathbf{r})^{4/3}} + \dots\dots] \,, \tag{2.136}$$

where the coefficient C_c is obtained from the high-density limit and found to be

$$C_c[\rho_\uparrow, \rho_\downarrow] = \frac{0.066725}{16\phi(\zeta)^2}(\frac{\pi}{3})^{1/3} \,, \tag{2.137}$$

The spin scaling factor $\phi(\zeta)$ is defined as,

$$\phi(\zeta) = \frac{1}{2}[(1+\zeta)^{2/3} + (1-\zeta)^{2/3}] \tag{2.138}$$

However, Langreth and Perdew [80, 81] showed that the GEA correlation with the exchange of Eq.(2.135) does not improve the performance of solids and an improved version of GGA correlation has been proposed by Wang and Perdew in 1991 [82]. Later, it is used in the PBE functional by incorporating more easily. The general form of GGA exchange-correlation functional can be written in terms of the enhancement factor as,

$$E_{xc}^{GGA}[\rho] = \int d^3r\rho(\mathbf{r})\epsilon_{xc}^{unif}[\rho]F_{xc}[\rho_\uparrow, \rho_\downarrow, \nabla\rho_\uparrow, \nabla\rho_\downarrow] \tag{2.139}$$

2.8.3   Meta-generalized gradient approximations

On the next level of approximation, the meta-generalized gradient approximations (meta-GGA) are proposed by making use of the Laplacian of density of Eq.(2.135) or the kinetic energy density τ_σ,

$$E_{xc}^{meta-GGA}[\rho] = \int d^3r\rho(\mathbf{r})\epsilon_{xc}^{unif}[\rho]F_{xc}^{meta-GGA}[\rho_\uparrow, \rho_\downarrow, \nabla\rho_\uparrow, \nabla\rho_\downarrow, \nabla^2\rho_\uparrow, \nabla^2\rho_\downarrow, \tau_\uparrow, \tau_\downarrow] , \tag{2.140}$$

with $\tau_\sigma = \sum_\sigma \frac{1}{2}|\nabla\Psi_\sigma(\mathbf{r})|^2$ is the kinetic energy density. The Perdew-Kurth-Zupan-Blaha (PKZB) [83] meta-GGA functional is proposed by replacing the Laplacian of Eq.(2.135) by the gradient expansion of the kinetic energy density. The motivation behind the replacement of the Laplacian of density follows from the divergence nature of the Laplacian of density near the nucleus. The PKZB correlation in one electron self-interaction free and it yields the correct correlation energy in the low-density or strongly interacting limit. While PKZB functional is quite accurate than GGA in predicting the atomization energies, surface energies of metals and lattice constants of solids but predicts the bond lengths of molecules less accurately than GGA. This problem has been eliminated in the Tao-Perdew-Staroverov-Scuseria (TPSS) [84] meta-GGA functional by including

the one-electron iso-orbital information into the meta-GGA functionals. The TPSS functional improves the performance of PZKB but predicts too-long lattice constants which have been improved in the same line as it had been done in the case of PBEsol functional [79]. The 'revised TPSS' (revTPSS) [85] meta-GGA yields very accurate lattice constants, surface energies, and atomization energies.

Beyond all these non-empirical meta-GGA functionals, recently major improvement in meta-GGA level functionals come through the Strongly Constrained and Appropriately Normed (SCAN) [86] and Tao-Mo (TM) [35] functionals. Both functionals are proposed to better the accuracy of both the molecular, and solid-state systems. The SCAN meta-GGA functional is proposed by satisfying seventeen known exact constraints, whereas, the TM functional is proposed from the exchange hole based on the density matrix expansion technique. The performance of SCAN and TM functionals along with other GGA and meta-GGA functionals are extensively studied in this thesis. The novel techniques of the construction of TM functional is very important to construct next level of meta-GGA hybrids and extension of the functional in the two-dimensional limit. We will discuss details construction of the TM functional in chapter 3.

Several other parametrized meta-GGA functional are also proposed. These functionals are very popular in the molecular systems but not so efficient in the solid-state systems. One such functional is the. Minnesota 2006 local functional (M06L) [87]. In this thesis, we also have taken into account the performance of this functional for solid-state test cases. It is noteworthy to mention that before the advent of SCAN meta-GGA, several meta-GGAs functionals are also proposed by Sun et. al. [88, 89] which are commonly known as meta-GGA Made Simple (MS) functionals. In this thesis, we also have taken into account the performance of those functionals in several solid-state test cases.

2.8.4   Beyond semilocal approximations: hybrid functionals

So far, the functional forms we discussed are semilocal. Though the semilocal functionals enjoy early successes, yet the role of the exact HF exchange is always desirable in several molecular and solids cases. Especially, for the properties related to the fractional particle

number, the exact exchange plays an important role (see chapter 4 and chapter 5 for detail discussion). Therefore, the idea of mixing the HF exchange with the semilocal functionals arises from the computationally cheap way to correct the problem related to the density functional approximation (DFA). The functionals which mix the HF with the DFA are known as the hybrid functional. The hybrid functionals are placed on the 4th rung of the Jacob ladder. The idea of the hybrid functionals has originated by A. D. Becke in early 1988 [90]. The concept of hybrid functional can be understood starting from the coupling-constant integral formula of Eq.(2.95) as,

$$E_{xc}[\rho] = \int_{\lambda=0}^{\lambda=1} d\lambda \langle \Psi^\lambda | \hat{V}_{ee} | \Psi^\lambda \rangle - J[\rho] = \int_{\lambda=0}^{\lambda=1} d\lambda \, E_{xc}^\lambda \, . \qquad (2.141)$$

Using the simple trapezoidal quadrature rule the Eq.(2.141) becomes,

$$E_{xc}[\rho] \approx \frac{1}{2} E_{xc}^0[\rho] + \frac{1}{2} E_{xc}^1[\rho] = \frac{1}{2} E_x^{HF}[\rho] + \frac{1}{2} E_{xc}^1[\rho] \, . \qquad (2.142)$$

Becke [90] argued that $E_{xc}^0[\rho]$ is the exact HF exchange (because of Eq.(2.95)) and $E_{xc}^1[\rho]$ is the exchange-correlation of the fully interacting systems that can be approximated by density functionals exchange-correlation. Becke's decomposition of this kind is known as "half-and-half theory". The half-and-half theory followed by another three-parameter hybrid functional scheme which popularly known as the B3LYP functional [91], proposed using BECKE98 (B88) [37], LDA exchange, Lee-Yang-Parr [36] and LDA correlation energy as,

$$E_{xc} = a_0(E_x^{HF} - E_x^{LDA}) + E_x^{LDA} + a_x(E_x^{GGA} - E_x^{LDA}) + a_c(E_c^{GGA} - E_c^{LDA}) \, , \quad (2.143)$$

where a_0, a_x and a_c are the empirical parameters fitted to obtain good atomization energies. Though the B3LYP is less connected with the Becke's half-and-half theory but till now it is a popular hybrid functional in the quantum chemistry community.

Following Becke's strategies, several hybrid functionals are proposed based on several semilocal functional forms. The hybrid functionals based on Perdew-Burke-Ernzerhof (PBE0) [92], Tao-Perdew-Staroverov-Scuseria (TPSS0) [93, 94], Minnesota functionals

are of these kinds and quite popular in quantum chemistry. It is noteworthy to mention that any semilocal functional has its hybrid form by mixing HF exchange. In this thesis, the PBE0 and TPSS0 hybrid functionals are used to access the performance of the developed hybrid functionals. The general form of a hybrid functional can be expressed as,

$$E_{xc}^{hyd} = \alpha E_x^{HF} + (1 - \alpha) E_x^{GGA/meta-GGA} + E_c^{GGA/meta-GGA} . \qquad (2.144)$$

The hybrid functionals proposed in this way use the HF exact exchange overall. Beyond this, other strategies of developing the hybrid functionals are also proposed by splitting the Coulomb operator into the short-range and long-range part and utilizing the model exchange hole. The hybrid functionals proposed in this way are known as the range-separated hybrid functionals and it improves several drawbacks that are not achievable within the global hybrid functionals. If HF exchange is used in the long-range part of the exchange functional that is known as the long-range corrected (LC) hybrid functionals. These functionals reduce the many-electron self-interaction error and improve the performance of several quantum chemistry problems. Details of the construction and performance of the selected range-separated hybrid functionals will be provided in chapter 4.

Though the long-range corrected functionals are popular in quantum chemistry, those are far from accuracy in case of solid-state systems. In solids state systems, it is important to preserve the accuracy of semilocal functionals because of the error cancellation of exchange and correlation. Therefore, a strategy of designing a hybrid functional using short-range HF exchange is proposed by Heyd-Scuseria-Ernzerhof (HSE) [95, 96]. The HSE functional is proposed based on the PBE semilocal functional and instead of the full HF exchange as used in the PBE0 functional, it uses the HF only in its short-range part. The HSE06 is very popular in the solid-state community for its improved bandgap performance. The detail construction of HSE functional along with a newly proposed meta-GGA level hybrid functional will be provided elaborately in chapter 5.

2.8.5 The generalized Kohn-Sham scheme

The implementation of the orbital-dependent functionals (meta-GGA or hybrid functionals) into the molecular and solid-state codes are known as Kohn-Sham-Hartree-Fock scheme or the generalized Kohn-Sham (gKS) Scheme [58–62, 97]. In the gKS scheme, the most common way to rewrite the KS equation (Eq.(2.53)),

$$\underbrace{[-\frac{1}{2}\nabla^2 + v_{ext}(\mathbf{r}) + \int d^3r' \frac{\rho(\mathbf{r}')}{|\mathbf{r}-\mathbf{r}'|} + v_{xc}^{DFA}]\phi_i(\mathbf{r}) - \int d^3r' v_x^{NL}(\mathbf{r},\mathbf{r}')\phi_i(\mathbf{r}')}_{v_{gKS}=semilocal\ exchange\text{-}correlation\ +\ HF\ exchange} = \varepsilon_i\phi_i(\mathbf{r}) \ ,$$

(2.145)

where v_{xc}^{DFA} is the exchange-correlation potential in the LDA, GGA or meta-GGA approximations which is given by,

$$v_x^{DFA}(\mathbf{r})\phi_i(\mathbf{r}) = \underbrace{\left[\frac{\partial(\rho(\mathbf{r})\epsilon_x^{DFA}(\mathbf{r}))}{\partial\rho(\mathbf{r})} - \nabla\frac{\partial(\rho(\mathbf{r})\epsilon_x^{DFA}(\mathbf{r}))}{\partial\nabla\rho(\mathbf{r})}\right]}_{v_x^{GGA}}\phi_i(\mathbf{r})$$

$$\underbrace{-\frac{1}{2}\nabla\left(\frac{\partial(\rho\epsilon_x^{DFA}(\mathbf{r}))}{\partial\tau(\mathbf{r})}\right)\nabla\phi_i(\mathbf{r}) - \frac{1}{2}\frac{\partial(\rho(\mathbf{r})\epsilon_x^{DFA}(\mathbf{r}))}{\partial\tau(\mathbf{r})}\vec{\nabla}^2\phi_i(\mathbf{r})}_{v_x^\tau=extra\ for\ meta\text{-}GGA} \ .$$

(2.146)

The 1st two terms come from LDA and GGA exchange and the last two-term are the Kohn-Sham kinetic energy dependent terms originate from kinetic energy dependence of the meta-GGA exchange functional. The non-local (NL) exchange potential v_x^{NL} is given by,

$$v_x^{NL} = -\sum_{j=1}^{N}\frac{\phi_j(\mathbf{r})\phi_j^*(\mathbf{r}')}{|\mathbf{r}-\mathbf{r}'|} \ .$$

(2.147)

The Eq.(2.145) is the most general representation of the exchange-correlation functional in the Kohn-Sham-Hartree-Fock scheme. In this thesis, this scheme has been used to implement the meta-GGA level hybrid and screened hybrid functionals.

2.9   Beyond Density Functional Approximations: RPA, GW, BSE

Beyond the hybrid functionals, the highest rung of Jacob ladder [98] is constructed with the methods which use unoccupied Kohn-Sham orbitals. The random-phase-approximation (RPA), quasi-particle green function (GW) and Bethe-Salpeter Equation (BSE) are examples of this kind. Due to a large number of empty states, all these methods are computationally very expensive compared to the density functional approximations. The RPA includes very accurate correlation effects. On the other-hand GW and BSE treats the excitonic effects accurately. It is shown that using RPA long-range correlation coupled with the hybrid density functional improves various molecular properties. Regarding the GW method, it improves the bandgaps on the top of the LDA or GGA functionals.

2.10   Overview of the Actual Calculation

The practical computational calculations of density functional theory are done based on the Kohn-Sham scheme implemented on several platforms with different basis sets. The KS equation is the most simplified form of many-electron Schrödinger equation. There are different classes of codes freely or commercially available which uses a basis set or pseudo-potential approach to solve the Schrödinger equation. The qualitative concept basis set and pseudo-potential are important as these are used throughout this thesis. In this section, we will focus on the practical implementation and computational framework of the KS equation.

2.10.1   Kohn-Sham equation in pseudo-potential and basis set framework

Lets recall the KS equation,

$$(-\frac{1}{2}\nabla^2 + v_{ext}(\mathbf{r}) + \int d^3r' \frac{\rho(\mathbf{r}')}{|\mathbf{r} - \mathbf{r}'|} + v_{xc,\sigma}[\rho])\phi_{i,\sigma} = \varepsilon_{i,\sigma}\phi_{i,\sigma} \ , \qquad (2.148)$$

where $\psi_{i,\sigma}$ is the single particle spin-orbital and the density $\rho(\mathbf{r})$ is given by,

$$\rho(\mathbf{r}) = \sum_\sigma \sum_{i=1}^{N} f_i|\psi_{i,\sigma}(\mathbf{r})|^2 \qquad (2.149)$$

with f_i be the occupation of the state. Now, the question is how to solve numerically this single-particle equation. Like solving the HF equation, the KS orbitals are also solved starting from an initial basis set. The 1st and the foremost choice is the Gaussian basis set, which is the basis of several quantum chemistry codes. In this thesis the Gaussian basis set dependent code NWChem [99] is used to calculation purpose. It is noteworthy to mention that the Gaussian basis consists of localized functions which are centered at the atomic position or center of two bonded atom. Therefore, this class of basis set is usually more suitable to describe the localized system such as atoms and molecules. In some codes, this basis set also used to solid-state calculations. Next classes of basis set which are widely used in the solid-state calculation are the plane-wave basis. The plane wave basis consists of delocalize functions. Therefore, it is independent of the atomic positions. Due to the delocalization, this type of basis set is very useful in treating the solid-state systems. All the popularly used solid-state codes use a plane-wave basis. Another class of basis set which are implemented in several codes are the augmented basis set. The augmented basis set keeps all the good properties of all-electron calculations and more flexible to treat both the molecular and solid-state systems.

The simulations and benchmarking calculation presented in this thesis are carried out with Gaussian-type basis as implemented in NWChem code, projector-augmented-plane-wave basis set as implemented in VASP [100–104], and real space grid-based (localized-)

basis set code as implemented in OCTOPUS code [105].

2.10.2 Pseudo potential approach

The pseudo-potential approach is one of the efficient ways of calculating solid-state properties. The main motivation of the pseudo-potential approach comes from the nature of the atomic orbitals which take part in the chemical reaction. There are three classes or region of the orbitals: firstly, core electrons which are tightly bound to the nuclei, valence electrons which take part in the chemical reaction and the semi-core states which are sufficiently close to the valence states but do not actively take part in the chemical bonding. Since the effect of the core electrons is removed, the effective nuclei contribution can be written as $Z_{eff} = Z_{tot} - Z_{core}$. In this way, one removes the contribution of the core electrons and represents the potential by an effective or pseudopotential. Since the core electrons contribution is removed from the calculations, the basis set size also decrease effectively. However, there are several ways one can implement the basis set within the solid-state codes.

2.10.3 Basis overview of density functional theory applied to solid-state physics

A crystalline solid is the ordered arrangement of the atoms or group of atoms. Therefore, the structural knowledge of the smallest unit cell is sufficient to treat the whole solid. There are two distinct types of unit-cell which are used in the periodic calculations: primitive and non-primitive. Primitive unit cell consists of a single lattice point, whereas, the non-primitive unit cell contains more than one lattice points. Since solids are symmetric, they remain invariant upon translation of the unit cell. To describe a solid, knowledge of three-unit cell lattice vectors a, b, c and the angle between these vectors α, β, γ are necessary. The three lattice vectors are described along with three crystallographic axes x, y, z. Based on the lattice vectors, angle between the lattice vectors and position of the lattice points within the cell, the lattice system is classified as primitive, body-centered,

face-centered, base-centered and rhombohedral. In total, there are seven types of crystalline structures: triclinic, monoclinic, orthorhombic, tetragonal, trigonal, hexagonal, and cubic. All these crystal structures are used in this thesis to perform the benchmark calculations of different functionals. In this thesis, we recognize the crystalline solids according to the space group as bcc, $diamond$, fcc, and hcp. The atomic coordinates and primitive transnational vectors a_1, a_2, a_3 of different crystalline structures are given in the Table (2.1).

Table 2.1: Atomic coordinates and lattice vectors for different space groups.

Space group	Atomic coordinates			Lattice vectors		
fcc	0	0	0	0	a/2	a/2
				a/2	0	a/2
				a/2	a/2	0
diamond	0	0	0	0	a/2	a/2
	a/4	a/4	a/4	a/2	0	a/2
				a/2	a/2	0
bcc	0	0	0	-a/2	a/2	a/2
				a/2	-a/2	a/2
				a/2	a/2	-a/2
hcp	0	0	0	a/2	$-a/\sqrt{3}/2$	0
	0	$-a/\sqrt{3}$	c/2	a/2	$a/\sqrt{3}/2$	0
				0	0	c
fcc anti-ferromagnetic	0	0	0	a/2	-a/2	0
	a/2	0	a/2	a/2	a/2	0
				0	0	a

Every periodic vector is associated with direct and reciprocal lattice vectors. The reciprocal lattice vectors are defined as $\mathbf{a}_1^*$, $\mathbf{a}_2^*$, and $\mathbf{a}_3^*$ which are connected to the real

lattice vectors as,

$$
\begin{aligned}
\mathbf{a}_1^* &= \frac{2\pi(\mathbf{a}_2 \times \mathbf{a}_3)}{|\mathbf{a}_1.(\mathbf{a}_2 \times \mathbf{a}_3)|} \\
\mathbf{a}_2^* &= \frac{2\pi(\mathbf{a}_3 \times \mathbf{a}_1)}{|\mathbf{a}_1.(\mathbf{a}_2 \times \mathbf{a}_3)|} \\
\mathbf{a}_3^* &= \frac{2\pi(\mathbf{a}_1 \times \mathbf{a}_3)}{|\mathbf{a}_1.(\mathbf{a}_2 \times \mathbf{a}_3)|} \ .
\end{aligned}
\tag{2.150}
$$

If position of any atom in real lattice is defined as,

$$
\mathbf{R} = u\mathbf{a}_1 + v\mathbf{a}_2 + w\mathbf{a}_3 \ ,
\tag{2.151}
$$

then the corresponding position in reciprocal space is defined as,

$$
\mathbf{G} = h\mathbf{a}_1^* + k\mathbf{a}_2^* + l\mathbf{a}_3^* \ ,
\tag{2.152}
$$

where u, v, w and h, k, l are integers and $\mathbf{R}$ and $\mathbf{G}$ are connected by

$$
\mathbf{G}.\mathbf{R} = 2\pi n, \qquad n = \pm 1, \pm 2, ... \ .
\tag{2.153}
$$

Regarding the KS equation for the periodic system, it comes from the time-independent electronic Schrödinger equation in a periodic potential $U(\mathbf{r})$ as,

$$
[-\frac{1}{2}\nabla^2 + U(\mathbf{r})]\psi_n(\mathbf{r}) = \varepsilon_n \psi_n(\mathbf{r}) \ .
\tag{2.154}
$$

The solution of the above equation is the Bloch states or the Bloch wavefunction which is defined as,

$$
\psi_{n,\mathbf{k}}(\mathbf{r}) = exp(i\mathbf{k}.\mathbf{r})f_n(\mathbf{r}) \ .
\tag{2.155}
$$

The first part is the plane-wave part and the second part is related to the cell periodicity of the wavefunction. Now, f_i can be expressed in terms of the reciprocal lattice vector of

the crystal as

$$f_n(\mathbf{r}) = \sum_{\mathbf{G}} c_{n,\mathbf{G}} exp(i\mathbf{G}.\mathbf{r}) \ . \tag{2.156}$$

Upon using this in the Bloch states of Eq.(2.155), it becomes

$$\psi_{n,\mathbf{k}}(\mathbf{r}) = \sum_{\mathbf{G}} c_{n,\mathbf{k}+\mathbf{G}} \ exp\{i(\mathbf{k}+\mathbf{G}).\mathbf{r}\} \ . \tag{2.157}$$

Thus, each electron in the reciprocal space is now connected with the periodicity of the system. Therefore, the knowledge of the first Brillouin zone is sufficient to know the infinite periodic solid. Now, substituting Eq.(2.157) into the Kohn-Sham Eq.(2.154), it takes into simpler form as,

$$\sum_{G'}\{\frac{1}{2}|\mathbf{k}+\mathbf{G}|\delta_{\mathbf{G},\mathbf{G}'}+v_{ext}(\mathbf{G}-\mathbf{G}')+v_{ee}(\mathbf{G}-\mathbf{G}')+v_{xc}(\mathbf{G}-\mathbf{G}')\}c_{n,\mathbf{k}+\mathbf{G}'} = \varepsilon_n c_{n,\mathbf{k}+\mathbf{G}'} \ .$$

$$\tag{2.158}$$

This is a simple matrix equation which can be solved by using conventional matrix diagonalization techniques.

Chapter 3

Performance of Semilocal Functionals For Condensed Systems

In the previous chapter, the theoretical and computational framework of the density functional theory (DFT) is discussed. It is shown that the most difficult task is to construct the exchange-correlation energy and the corresponding potential of the Kohn-Sham equation. Relevant exchange-correlation approximations with increasing accuracy are also discussed in the previous chapter. In this chapter, we focus on the assessment of the different levels of approximation for the solid-state systems. This chapter is based on the following research outcomes

(i) Subrata Jana, Abhilash Patra and Prasanjit Samal, J. Chem. Phys. 149, 044120 (2018).

(ii) Subrata Jana, Kedar Sharma, and Prasanjit Samal, J. Chem. Phys. 149, 164703 (2018).

3.1   Introduction

The solid-state electronic structure calculations within the Density functional theory (DFT) are mostly done within the framework of the semilocal exchange-correlation (XC) functionals. In general, these type of XC functionals is constructed employing the semilocal

quantities such as density, the gradient of density, Laplacian of density or Kohn-Sham (KS) kinetic energy density. Semilocal approximations [4, 35–37, 65, 78, 79, 83–89, 106–170] with different level of accuracy and broad applicability for solids and surfaces [33, 171–210] are proposed from time to time and still continuing to be an active research field with promisingly new prospects. Semilocal functionals for solids are mainly developed by satisfying the exact constraints [86]. Whereas, part of the parameters is fitted with experimentally measurable quantities. Functionals constructed in this manner are either semiempirical or empirical by nature. To perform satisfactorily for most of the properties of solids, a semilocal functional should respect the slowly varying density gradient approximation. As a matter, several (highly-)parametrized functionals plunge precipitously when applied to the solid-state systems in spite of its accuracy for molecular systems [195]. Such types of non-empirical functionals perform well only for targeted molecular and solid-state properties [87, 133].

Based on the slowly varying density approximations, ingredients, and constraint satisfaction, semilocal functionals are arranged in different rungs of Jacob ladder [98]. The lowest rung is recognized as local density approximation (LDA) [4, 142], whereas, rungs higher to it are categorized as generalized gradient approximation (GGA) [65, 78, 79, 106–119, 122, 123, 126–131, 148, 150, 158], meta-generalized gradient approximation (meta-GGA) [35, 83–89, 133–137, 139–141, 157, 160, 161, 163–167] and so on. The research related work in this chapter is motivated by the alluring properties of the developed semilocal density functionals in recent times where the accuracy of the semilocal functionals are improved by satisfying as much as quantum mechanical constraints in its functional form. Two such functionals are Strongly Constrained and Appropriately Normed (SCAN) [86] and Tao-Mo (TM) [35] semilocal density functionals. The first one is proposed by satisfying seventeen exact constraints in its functional form. Whereas, the later is proposed from semilocal exchange hole together with the slowly varying gradient approximation of exchange. This chapter mainly focuses on the transferability, robustness, and universality of semilocal functionals for different solid-state systems. Also, to measure the accuracy of these functionals, we compare the results to that of other popular XC functionals.

To do so, we devide this chapter into three parts. In the first part, a brief description of the construction and implementation of the TM [35] functional is provided within the plane wave suite code Vienna Ab initio simulation package (VASP) [100–104]. Following it, the application of the most popular and recent semilocal XC functionals for the properties related to the solids are given. Lastly, the focus is given on the properties of the simple and transition metals.

3.2 Relevance of the Slowly Varying Density in (meta-)GGA Approximation

The simplest approximation for the XC functional is the local (spin-)density approximation (LSDA):

$$E_{xc}^{L(S)DA}[\rho_\uparrow, \rho_\downarrow] = \int d^3 r \rho(\mathbf{r}) \epsilon_{xc}^{unif}[\rho_\uparrow, \rho_\downarrow] , \qquad (3.1)$$

where $\epsilon_x = \frac{3k_f}{4\pi}$ is the energy density of exchange within homogeneous electron gas. Fermi vector k_f in 3D is defined as $k_f = (3\pi^2 \rho)^{\frac{1}{3}}$, where the total electronic density is sum of up and down spin-densities ($\rho = \rho_\uparrow + \rho_\downarrow$). In case of solids, the electron density of the system varies slowly over the space. Therefore, the L(S)DA makes useful predictions of the equilibrium geometries of solids and molecules but overestimates the other properties of for solids (e.g. bulk moduli, cohesive energies) and atomization energies of molecules. The noteworthy success of L(S)DA in predicting the solid-state properties are because of the exchange hole satisfies the sum rule [211]. However, the performance of L(S)DA in predicting solid-state properties and atomization energies of molecules is greatly improved by the generalized gradient approximations (GGA).

3.2.1 Generalized gradient approximations: PBE and PBEsol

In general, to study a wide range of quantum systems consistently, the generalized gradient approximations (GGA) has been proposed by including the gradient of density in the functional and by satisfying other constraints in its functional form. As the name

suggest, the GGA functionals for solids are proposed incorporating the (generalized) gradient approximation of 2nd order [212–222]. The general way of expressing the GGA XC functional is,

$$E_{xc}[\rho_\uparrow, \rho_\downarrow] = \int d^3r \rho(\mathbf{r}) \epsilon_{xc}^{GGA}[\rho_\uparrow, \rho_\downarrow, \nabla\rho_\uparrow, \nabla\rho_\downarrow] , \qquad (3.2)$$

where $\nabla\rho_\uparrow, \nabla\rho_\downarrow$ are two extra ingredients included in the construction of it in addition to density. The initial attempt of constructing the GGA follows from the generalized expansion approximation (GEA), which is expressed as,

$$E_{xc}^{GEA}[\rho_\uparrow, \rho_\downarrow] = \int d^3r [\rho(\mathbf{r})\epsilon_{xc}^{unif} + \sum_{\sigma,\sigma'} C_{xc}^{\sigma,\sigma'} \frac{\nabla\rho_\sigma . \nabla\rho_{\sigma'}}{\rho_\sigma^{2/3} \rho_{\sigma'}^{2/3}}] . \qquad (3.3)$$

The coefficients related to density gradient expansion $C_{xc}^{\sigma,\sigma'}$ is derived to improve the results over L(S)DA. But, the attempt remained a disappointment and later on further studies and investigations are followed by Langreth and Perdew [80, 81]. As an attempt, new functionals are proposed by the satisfaction of the exact or nearly exact constraints which are the root of the development of the present-day semilocal functionals [86].

The first-ever successful attempt to construct a GGA functional by satisfying exact constraints is done in the Perdew-Burke- Ernzerhof (PBE) GGA [78]. The PBE GGA is derived by satisfying the constraint related to the XC hole and XC energy. PBE functional removes several issues related to Perdew-Wang (PW91) functional [126–130, 223] and presents in a simplified form.

Regarding the construction of the correlation part, it is expressed as,

$$E_c^{PBE}[\rho_\uparrow, \rho_\downarrow] = \int d^3r \underbrace{\left[\epsilon_c^{unif}(r_s, \zeta) + H(r_s, \zeta, t)\right]}_{\epsilon_c^{PBE}} , \qquad (3.4)$$

where $r_s = (\frac{3}{4\pi\rho})^{1/3}$ is the local Seitz radius, $\zeta = \frac{\rho_\uparrow - \rho_\downarrow}{\rho}$ is the relative spin polarization and $t = \frac{|\nabla\rho|}{[(1+\zeta)^{2/3} + (1-\zeta)^{2/3}]k_s\rho}$ is the dimensionless density gradient with $k_s = (\frac{4k_f}{\pi a_0})$ is the Thomas-Fermi screening vector. The parameter H in PBE correlation functional is constructed by satisfying the (i) second-order gradient expansion, (ii) rapidly varying limit, and (ii) uniform scaling in the high-density limit of the correlation energy functional [77,

80, 224–227]. This results in the non-empirical form of H,

$$H = (e^2/a_0)\gamma[(1+\zeta)^{2/3} + (1-\zeta)^{2/3}]^3 \ln\{1 + \frac{\beta}{\gamma}t^2[\frac{1+At^2}{1+At^2+a^2t^4}]\} \,, \tag{3.5}$$

where

$$A = \frac{\beta}{\gamma \exp\{-\epsilon_c^{unif}/(\gamma[(1+\zeta)^{2/3} + (1-\zeta)^{2/3}]^3)/a_0)\} - 1} \tag{3.6}$$

with the parameter $\beta \approx 0.066725$ obtained from the high-density limit ($r_s \to 0$) of the gradient expansion of the correlation [80, 224, 225] and $\gamma = 0.025$.

Regarding its the construction, the PBE exchange functional is constructed by satisfying the (i) uniform density scaling [228], (ii) spin-scaling relationship [229], (iii) slowly varying density gradient expansion [230] , and (iv) Lieb-Oxford bound [231, 232]. The PBE exchange functional is given by,

$$E_x^{PBE} = \int d^3r\rho(\mathbf{r})\epsilon_x^{unif} F_x[s] \,, \tag{3.7}$$

where the PBE exchange enhancement factor is given by,

$$F_x[s] = 1 + \kappa - \frac{\kappa}{1 + \frac{\mu s^2}{\kappa}} \,, \tag{3.8}$$

with $s = \frac{|\nabla\rho|}{2k_f\rho}$. The $\kappa = 0.804$ parameter is determined by satisfying the bound (Lieb-Oxford bound) of the exchange energy functional. $\mu = \beta(\pi^2/3) = 0.21951$ is the gradient coefficient for exchange.

Since the advent of PBE GGA functional, the acceptance of density functional formalism becomes more versatility and popular in physics and chemistry. PBE performs reasonably well for solid-state properties compared to LSDA.

While the PBE functional is the most popular functional since its advent but latter it has been observed that PBE overestimates the lattice constants by about 1%. Though several modifications have been carried over the PBE functional to improve its performance for solids [107–111] but simultaneously criticized for worsening its performance for the atomization energies [192]. On the next level of major modifications over the

PBE functional for solids came through the PBEsol functional [79] by satisfying correct second-order gradient expansion for exchange. The PBEsol shows its accurate performance for the lattice constants and surface energies of solids. Regarding the correlation energy functional of the PBEsol, it takes the same form as PBE but replaces the β with $\beta = 0.046$ which improves the surface energy of large jellium cluster [79] and remains considerably closer to that of the local density linear response criterion. Other modifications based on the reduced density gradient dependence μ values and fitted β parameter from the jellium surface energies are also proposed to balance the performance of the functional for atomic, molecular and solid-state systems [112–119].

3.2.2   The Meta-generalized gradient approximations

One of the natural way to improve both the quantum chemical and material properties together came through the meta-generalized gradient approximations (meta-GGA). The meta-GGA functionals depend on the Laplacian of the density or Kohn-Sham (KS) kinetic energy density. The general form of meta-GGA functionals is given as:

$$E_{xc}^{meta-GGA}[\rho] = \int \, d^3r \epsilon_{xc}^{unif} F_{xc}[\rho_\uparrow, \rho_\downarrow, \nabla\rho_\uparrow, \nabla\rho_\downarrow, \nabla^2\rho_\uparrow, \nabla^2\rho_\downarrow, \tau_\uparrow, \tau_\downarrow] \,, \qquad (3.9)$$

where $\tau_\sigma = \sum_i^{occ} \frac{1}{2}|\nabla\psi_{i,\sigma}(\mathbf{r})|^2$ is the KS kinetic energy density and $\nabla^2\rho$ is Laplacian of density. Several meta-GGA functionals are proposed during last couple of decades or so. But, in our solid-state calculations we use Tao-Perdew-Staroverov-Scuseria (TPSS) [84], revised TPSS (revTPSS) [85], strongly constrained and appropriately normed (SCAN) [86] and Tao-Mo (TM) [35] functionals which are the mainstream meta-GGA functionals in Jacob's ladder.

    Regarding the performance of TPSS meta-GGA, it predicts solid-state lattice constants quite similar to PBE but improves the atomization energies for molecules than PBE. The performance of the TPSS functional has been improved on further modification by taking the insights from the PBEsol which is known as revised TPSS (revTPSS).

The revTPSS not only showing improvement of the lattice constants of solids compared to its TPSS counterpart but also retains the atomization accuracy of TPSS. The revTPSS shows improved performance due to changing of (i) the enhancement factor such that it recovers forth order gradient approximation (GE4) over wide range of s values (≤ 0.3) which improves the accuracy of revTPSS for bulk solids, and (ii) the β parameter fitted from the parametrization of the of the Hu and Langreth [233]. This modification improves the functional performances for the surface energies keeping the atomization energy accuracy. Based on these modifications, several other constructions are also proposed in recent times [116, 135, 148]. We do not discuss those modifications in details in this thesis.

On next level, the SCAN [86] and TM [35] functionals are proposed. From construction point of view, the SCAN functional is designed through constraint satisfaction while the TM functional is proposed by using the semilocal exchange hole and the slowly varying fourth-order gradient expansion. This chapter is assessed the performance of several semilocal approximations for the solid-state structural and energetic properties. But, before comparing the performances, a discussion on the construction of TM semilocal functional is required. It is important because it will be used further in this thesis to construct range-separated hybrid functional and two-dimensional counterpart of the functional.

In the construction of the TM functional [35] the density matrix expansion (DME) technique is applied which makes the exchange hole localized under a general coordinate transformation. Also, the slowly varying gradient approximation is introduced into the DME by properly interpolating with fourth-order density gradient expansion. Let's first discuss the generalized coordinate transformation based DME exchange hole. The details of the generalized coordinate transformation can be found in references [234, 235]. Under generalized coordinate transformation, the exchange energy functional becomes,

$$E_x = \frac{1}{2} \int d^3 r_\lambda \rho(\vec{r}^\lambda) \int \frac{\rho_x^t(\vec{r}_\lambda, u)}{u} \, d^3 u \,, \qquad (3.10)$$

where the transformed exchange hole ρ_x^t can be defined using the Kohn-Sham first-order

reduced density matrix $\Gamma_{1t}(\vec{r}^\lambda - (1-\lambda)\vec{u}, \vec{r}^\lambda + \lambda\vec{u})$ as,

$$\rho_x^t = -\frac{|\Gamma_{1t}(\vec{r}^\lambda - (1-\lambda)\vec{u}, \vec{r}^\lambda + \lambda\vec{u})|^2}{2\rho(\vec{r})} \ . \tag{3.11}$$

The real parameter, λ varies from $1/2 \to 1$ (or, $0 \to 1/2$). Using the Kohn-Sham single particle orbital the Taylor series expansion of the coordinate transformed first order reduced density matrix around $u = 0$ becomes,

$$\Gamma_{1t}(\vec{r}, \vec{u}) = e^{\vec{u}.[-(1-\lambda)\vec{\nabla}_1 + \lambda\vec{\nabla}_2]}\Gamma_{1t}(\vec{r}, \vec{u})|_{\vec{u}=0} = e^{\vec{u}.[-(1-\lambda)\vec{\nabla}_1 + \lambda\vec{\nabla}_2]}\sum_i^{occ}\psi_i^*(\vec{r}^\lambda - (1-\lambda)\vec{u})$$

$$\times \psi_i(\vec{r}^\lambda + \lambda\vec{u})|_{\vec{u}=0} \ . \tag{3.12}$$

The exchange energy, E_x is evaluated from the spherical average of the exchange hole as [211],

$$\langle\rho_x(\vec{r}, \vec{r} + \vec{u})\rangle_{spherical} = \int \rho_x(\vec{r}, \vec{r} + \vec{u}) \frac{d\Omega_u}{4\pi} \ . \tag{3.13}$$

Therefore, spherical average of Eq.(3.12) yields,

$$\langle\rho_x^t\rangle = -\frac{\rho(\vec{r})}{2} - \frac{1}{6}\left[\left(\lambda^2 - \lambda + \frac{1}{2}\right)\nabla^2\rho(\vec{r}) - 2\tau + \frac{1}{4}\left(2\lambda - 1\right)^2\frac{|\vec{\nabla}\rho(\vec{r})|^2}{\rho(\vec{r})}\right]u^2 \ . \tag{3.14}$$

The expression in Eq.(3.14) is originally proposed in [122, 140, 236] for the conventional exchange hole model i.e, $\lambda = 1$. But, it failed to recover the uniform density limit and one can't directly use this expansion in the exchange energy expression because the large $u-$ limit diverges. To recover the LDA exchange hole and remove the divergence nature of the hole in the large u limit, the whole expression needs to be multiplied by the uniform electron gas exchange hole [122, 236]. In TM [35] functional satisfies the uniform exchange hole limit automatically through DME.

The TM exchange hole [35] correctly recovers (i) uniform electron gas limit, (ii) small-u behavior i.e. Eq.(3.14), and (iii) large $-u$ limit. To achieve this goal, TM ex-

press $e^{xcos\phi y}$ in three terms using spherical Bessel and Legendre polynomial as,

$$e^{xcos\phi y} = \frac{1}{x}\sum_{l=0}^{\infty}(-1)^l(4l+3)j_{2l+1}(x)Q_{2l+1}(i\cos\theta y) + \frac{1}{x}\sum_{l=0}^{\infty}(-1)^l(4l+3)j_{2l+1}(x)$$
$$y\frac{d}{dy}Q_{2l+1}(i\cos\theta y) + \frac{1}{x^2}\sum_{l=0}^{\infty}(-1)^l(4l+3)j_{2l+1}(x)\frac{1}{\cos\theta}\frac{d^2}{dy^2}Q_{2l+1}(i\cos\theta y)\,,$$

$$(3.15)$$

where $Q_{2l+1}(z) = P_{2l+1}(z)/z$, $x = ku$ and $y = [-(1-\lambda)\vec{\nabla}_1 + \lambda\vec{\nabla}_2]/k$. The Eq.(3.15) obtained by using series resummation technique to fulfill above three essential criterion $((i) - (iii))$. This leads to the transformed first-order reduced density matrix (i.e., DME expansion) expression

$$\Gamma_{1t}(\vec{r},\vec{u}) = 3\rho\frac{j_1(ku)}{ku} + \frac{35j_3(ku)}{2k^3u}G + \frac{105j_3(ku)}{2k^3u^2}H\,, \qquad (3.16)$$

where $G = \{3\cos^2\theta[(\lambda^2 - \lambda + 1/2)\nabla^2\rho - 2\tau] + 3k^2\rho/5\}$, and $H = \cos\theta\,(2\lambda - 1)\nabla\rho$. Using this density matrix form, the coordinate transformed spherically-averaged TM exchange hole becomes,

$$\rho_x^t = -\frac{9\rho}{2}\frac{j_1^2(ku)}{k^2u^2} - \frac{105j_1(ku)j_3(ku)}{k^4u^2}L - \frac{3675j_3^2(ku)}{8k^6u^4}M\,, \qquad (3.17)$$

where $L = [3(\lambda^2 - \lambda + 1/2)(\tau - \tau^{\text{unif}} - |\nabla\rho|^2/72\rho) - \tau + 3k^2\rho/10]$, and $M = (2\lambda - 1)^2|\nabla\rho|^2/\rho$. Here, the inhomegeneity parameter f is obtained as,

$$f = [1 + 10(70y/27) + \beta y^2]^{1/10}\,. \qquad (3.18)$$

To make the exchange hole and exchange energy finite everywhere, the Laplacian of density is substituted by semiclassical approximation $\tau = \tau^{\text{unif}} + |\nabla\rho|^2/(72\rho) + \nabla^2\rho/6$.Hemce, the DME exchange energy part becomes [35],

$$E_x[\rho] = \int d^3r\,\rho\epsilon_x^{\text{unif}}(\rho)F_x^{\text{DME}}(p,\tau)\,, \qquad (3.19)$$

with $F_x^{\mathrm{DME}} = 1/f^2 + 7R/(9f^4)$ and $R = 1 + 595(2\lambda - 1)^2 p/54 - [\tau - 3(\lambda^2 - \lambda + 1/2)(\tau - \tau^{\mathrm{unif}} - |\nabla\rho|^2/72\rho)]/\tau^{\mathrm{unif}}$. The DME expansion is accurate for the compact density. However, to perform in a better way for solids the slowly varying density gradient correction (sc) is included in the functional form as [35],

$$F_x^{TM} = wF_x^{DME} + (1 - w)F_x^{sc}, \tag{3.20}$$

where the fourth-order gradient correction given by $F_x^{sc} = \{1 + 10[(10/81 + 50p/729)p + 146\tilde{q}^2/2025 - (73\tilde{q}/405)[3\tau_W/(5\tau)](1 - \tau_W/\tau)]\}^{1/10}$, and $\tilde{q} = (9/20)(\alpha - 1) + 2p/3$ with $w = [(\tau_W/\tau)^2 + 3(\tau_W/\tau)^3]/[1 + (\tau_W/\tau)^3]^2$ being the weight factor.

Regarding correlation, it is constructed from the TPSS correlation by obeying more exact constraint as [35]

$$E_c^{meta-GGA}[\rho_\uparrow, \rho_\downarrow] = \int d^3r\rho\epsilon_c^{\mathrm{revPKZB}} \times [1 + d\epsilon_c^{revPKZB}(\tau^W/\tau)^3], \tag{3.21}$$

where

$$
\begin{aligned}
\epsilon_c^{revPKZB} &= \epsilon_c^{PBE}(\rho_\uparrow, \rho_\downarrow, \nabla\rho_\uparrow, \nabla\rho_\downarrow)[1 + C^{TM/TPSS}(\zeta, \xi)(\tau^W/\tau)^2] \\
&\quad - [1 + C(\zeta, \xi)](\tau^W/\tau)^2 \sum_\sigma \frac{n_\sigma}{n}\tilde{\epsilon}_c .
\end{aligned}
\tag{3.22}
$$

Here,

$$C^{TM}(\zeta, \xi) = \frac{0.1\zeta^2 + 0.32\zeta^4}{\{1 + \xi^2[(1 + \zeta)^{-4/3} + (1 - \zeta)^{-4/3}]/2\}^4}, \tag{3.23}$$

and

$$C^{TPSS}(\zeta, \xi) = \frac{0.53 + 0.87\zeta^2 + 0.50\zeta^4 + 2.26\zeta^6}{\{1 + \xi^2[(1 + \zeta)^{-4/3} + (1 - \zeta)^{-4/3}]/2\}^4}, \tag{3.24}$$

where $\zeta = (\rho_\uparrow - \rho_\downarrow)/n$, and $\xi = |\nabla\zeta|/2(3\pi^2\rho)^{1/3}$. The parameter $d = 2.8$ Hartree^{-1} is

chosen for good reference value of the jellium surface energies [84]. This leads to the two functionals: (i) TMTPSS (TMx+TPSSc) and (ii) TM (TMx+TMc).

3.3   Implementation of Tao-Mo Functional in PAW Environment

We implement the TM functional in VASP [100–104] to assess its performance. It is well known that the accuracy of the PAW method is same as the all-electron calculation with less computational cost. Note that the meta-GGA functionals are implemented in VASP using generalized KS (gKS) framework, where the XC potential is defined as,

$$
v_{xc}^{meta-GGA}\psi_i = \underbrace{\left[\frac{\partial(\rho\epsilon_{xc})}{\partial\rho} - \vec{\nabla}\frac{\partial(\rho\epsilon_{xc})}{\partial\vec{\nabla}\rho}\right]}_{v_{xc}^{GGA}}\psi_i \underbrace{-\frac{1}{2}\vec{\nabla}\left(\frac{\partial(\rho\epsilon_{xc})}{\partial\tau}\right)\vec{\nabla}\psi_i - \frac{1}{2}\frac{\partial(\rho\epsilon_{xc})}{\partial\tau}\vec{\nabla}^2\psi_i}_{v_{xc}^{\tau}} \ ,
$$

(3.25)

where v_{xc}^{GGA} is the XC potential in GGA and the additional term we encounter here is the non-multiplicative $\tau-$ dependent part $\{v_{xc}^{\tau}\}$. In DFT the XC are treated differently and implemented separately because of the physically differing nature of the same. Therefore, one can separate both the derivatives of the exchange and correlation energy part separately. Regarding the exchange potential, partial derivatives i.e., $\frac{\partial(\rho\epsilon_x)}{\partial\rho}$, $\frac{\partial(\rho\epsilon_x)}{\partial\vec{\nabla}\rho}$ and $\frac{\partial(\rho\epsilon_x)}{\partial\tau}$ are need o be calculated. Here, we denote the potentials with respect to ρ, $|\nabla\rho|$ and τ as v_x^1, v_x^2, v_x^3 i.e, $v_x^1 = \epsilon_x^{TM} + \rho\frac{\partial\epsilon_x^{TM}}{\partial\rho}$, $v_x^2 = \rho\frac{\partial\epsilon_x^{TM}}{\partial|\nabla\rho|}$ and $v_x^3 = \rho\frac{\partial\epsilon_x^{TM}}{\partial\tau}$. The term ϵ_x^{TM} corresponds to $\epsilon_x^{unif}F_x^{TM}$. This completes the exchange functional implementation. Concerning the correlation, it is implemented in VASP beforehand and the details of the implementation of the TPSS correlation and its corresponding potential is given in reference [178].

3.4 Results and Discussions

3.4.1 General definitions and computational setup

We test the TM functional implemented in PAW environment along with other popularly used and contemporary functionals for calculating the basic properties of solids like lattice constants, bulk-moduli, and cohesive energies. All these are fundamental ground-state properties. The accuracy of obtaining the lattice constants is one of the fundamental test that predicts the accuracy level of XC functional.

In VASP code, lattice constants are measured by relaxing the system geometry. The relaxed structure is used to calculate the lattice constants of each solid. The ISIF = 3 algorithm is used to relax both the volume and atomic coordinates.

The bulk modulus (B_0) is defined as,

$$B_0 = -V_0 \Big(\frac{\partial P}{\partial V} \Big)_{a=a_0} , \tag{3.26}$$

where a_0 and V_0 are the equilibrium lattice constant and volume of the system. Note that in practice equations of state (EOS) [237–241] are applied to fit the energy versus volume curve as obtained from the DFT calculation to determine the bulk moduli. Here, we want to mention that within different EOS the most popular is the Birch-Murnaghan equation of state [237] which is used in this thesis to obtain the bulk moduli of several solid-state systems.

The cohesive energies of the bulk solids is defined as the,

$$E_{coh} = E_{atom} - \frac{E_{bulk}}{N} , \tag{3.27}$$

where the atomic energy (E_{atom}) and bulk energy (E_{bulk}) is required to obtain the cohesive energies and N is the number of atoms in the bulk solids.

3.4.2   Lattice constants

For benchmark calculations of various approximations we consider 47 crystalline structures which includes (i) semiconductors , (ii) ionic solids, and (iv) metal structures. Table 3.1 presents the benchmark calculations of TMTPSS and TM along with other popular semilocal functionals. In Fig 3.1, we also plot the MRE (in percentage) of all the functionals. From these, it is evident that LSDA underestimates the lattice constants, whereas, PBE overestimates it. It is not surprising because, in LSDA, the gradient terms are missing. The overestimation in the lattice constants of the PBE functional improves upon using the solid-state version of the PBE i.e., PBEsol. It is shown in Table 3.1 that the PBEsol dramatically improves the performance of PBE for solids. The improvement of the PBEsol functional can be understood from the satisfaction of the exact second-order gradient approximation (GE2). Within the meta-GGAs, the TPSS functional also shows the PBE like overestimation, which again rectified by its improved version i.e., revTPSS. Note that revTPSS functional is designed by taking insights from the obtained outcomes of the PBEsol functional. Regarding SCAN, TMTPSS and TM, the SCAN and TM perform accurately but TMTPSS overestimates the TM values. This is due to the change in correlation in TM functional.

3.4.3   Bulk moduli

Our second test case consists of the bulk moduli of 20 solids. The results are given in Table 3.2. As mentioned before, to obtain the bulk moduli energy (E)-volume (V) curve is fitted with the Murnaghan equation of state [237] by employing the post-processing code VASPKIT [242].

Form the results presented in Table 3.2 and Fig. 3.2, it is evident that LSDA overestimates the bulk moduli, whereas, PBE underestimates it. It is quite predictable because the lattice constants of LSDA are underestimated and PBE is overestimated. In all the functionals, we obtain the same tendency as observed in the performance of lattice constants. The performance of bulk moduli is improved from that of PBEsol. However, the TPSS functional performs better compared to the revTPSS in this regard. Concerning all

Table 3.1: Calculated lattice constant a_0 (in Å) of bulk solids. The zero point anharmonic expansion (ZPAE) uncorrected experimental values are taken from [179, 245]. Last column reports the errors. Best/worst MAE result is shown in bold/underline style.

Solids	LSDA	PBE	PBEsol	TPSS	revTPSS	SCAN	TMTPSS	TM	Expt.
Li	3.368	3.441	3.444	3.458	3.452	3.474	3.400	3.402	3.477
K	5.029	5.300	5.222	5.394	5.349	5.262	5.186	5.167	5.225
Al	3.987	4.043	4.081	4.014	4.009	4.009	3.984	3.982	4.032
Cu	3.520	3.634	3.566	3.568	3.538	3.555	3.528	3.528	3.603
Pd	3.844	3.949	3.878	3.912	3.884	3.906	3.908	3.894	3.881
Ag	4.001	4.148	4.052	4.092	4.059	4.084	4.082	4.067	4.069
C	3.536	3.573	3.557	3.572	3.563	3.555	3.560	3.554	3.567
Si	5.400	5.467	5.433	5.450	5.436	5.425	5.423	5.411	5.430
Ge	5.648	5.785	5.704	5.754	5.710	5.687	5.691	5.672	5.652
SiC	4.332	4.379	4.359	4.365	4.357	4.352	4.351	4.344	4.358
BN	3.583	3.625	3.607	3.624	3.618	3.605	3.615	3.608	3.607
BP	4.490	4.546	4.521	4.545	4.531	4.521	4.522	4.510	4.538
BAs	4.742	4.817	4.778	4.810	4.787	4.779	4.775	4.763	4.777
BSb	5.198	5.280	5.234	5.270	5.242	5.257	5.227	5.212	n/a
AlP	5.433	5.504	5.470	5.489	5.480	5.478	5.463	5.450	5.460
AlAs	5.637	5.732	5.681	5.707	5.685	5.670	5.669	5.656	5.658
AlSb	6.120	6.232	6.168	6.208	6.180	6.173	6.161	6.143	6.136
$\beta-$GaN	4.503	4.588	4.547	4.581	4.569	4.524	4.559	4.549	4.531
GaP	5.425	5.533	5.474	5.523	5.499	5.457	5.482	5.464	5.448
GaAs	5.627	5.763	5.684	5.737	5.699	5.664	5.681	5.664	5.648
GaSb	6.067	6.226	6.130	6.190	6.144	6.117	6.126	6.102	6.096
InP	5.878	6.001	5.932	5.989	5.965	5.938	5.945	5.923	5.866
InAs	6.061	6.211	6.122	6.182	6.144	6.122	6.126	6.104	6.054
InSb	6.472	6.651	6.543	6.611	6.565	6.545	6.546	6.521	6.479
ZnS	5.403	5.440	5.355	5.401	5.358	5.370	5.388	5.364	5.409
ZnSe	5.570	5.734	5.634	5.681	5.625	5.652	5.658	5.633	5.668
ZnTe	5.995	6.178	6.064	6.115	6.048	6.077	6.082	6.056	6.089
CdS	5.758	5.926	5.824	5.933	5.926	5.856	5.889	5.857	5.818
CdSe	6.009	6.195	6.080	6.192	6.195	6.100	6.133	6.102	6.052
CdTe	6.405	6.610	6.291	6.604	6.610	6.521	6.532	6.497	6.480
MgS	5.580	5.684	5.642	5.681	5.673	5.634	5.643	5.629	5.202
MgTe	6.365	6.506	6.439	6.500	6.478	6.452	6.444	6.422	6.420
LiCl	4.977	5.148	5.071	5.123	5.104	5.097	5.071	5.047	5.106
LiF	3.940	4.059	4.006	4.022	4.005	3.975	3.974	3.969	4.010
NaCl	5.432	5.648	5.558	5.648	5.616	5.526	5.415	5.496	5.595
NaF	4.437	4.621	4.548	4.599	4.569	4.475	4.498	4.492	4.609
MgO	4.145	4.242	4.206	4.224	4.222	4.184	4.209	4.202	4.207
MgSe	5.382	5.501	5.445	5.491	5.476	5.454	5.456	5.435	5.400
CaS	5.570	5.710	5.632	5.698	5.694	5.683	5.681	5.657	5.689
CaSe	5.798	5.955	5.869	5.947	5.932	5.921	5.919	5.894	5.916
CaTe	6.215	6.389	6.291	6.386	6.366	6.375	6.350	6.317	6.348
SrS	5.910	6.056	5.973	6.047	6.040	6.031	6.035	6.007	5.990
SrSe	6.129	6.297	6.203	6.286	6.270	6.264	6.264	6.234	6.234
SrTe	6.531	6.714	6.609	6.708	6.685	6.693	6.677	6.641	6.640
BaS	6.289	6.433	6.362	6.448	6.440	6.441	6.423	6.390	6.389
BaSe	6.510	6.681	6.577	6.670	6.657	6.659	6.659	6.622	6.595
BaTe	6.890	7.080	6.964	7.075	7.054	7.071	7.056	7.012	7.007
ME(Å)	-0.055	0.076	0.002	0.061	0.039	0.020	0.019	0.000	—
MAE(Å)	0.072	<u>0.078</u>	0.041	0.065	0.053	0.041	0.045	**0.038**	—
MRE(%)	-1.045	1.361	0.027	1.059	0.657	0.310	0.274	-0.065	—
MARE(%)	1.375	1.406	0.738	1.157	0.961	0.753	0.854	0.753	—
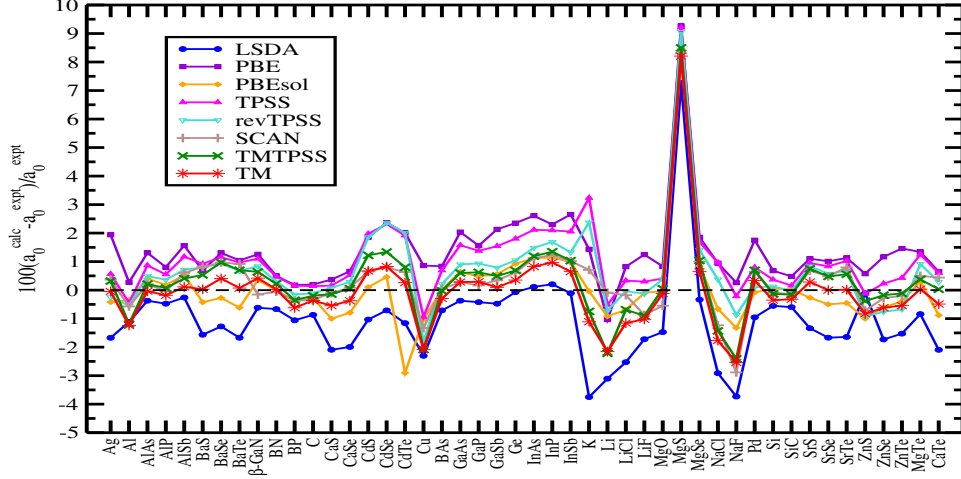
Figure 3.1: Percentage deviation of lattice constants as obtained from different functionals presented in Table 3.1.

Table 3.2: Shown is the bulk moduli (B_0) (in GPa) of 20 solids. The reference experimental values are taken from [179, 246, 247].

Solids	LSDA	PBE	PBEsol	TPSS	revTPSS	SCAN	TMTPSS	TM	Expt.
Ag	138.5	90.9	118.9	110.0	120.5	111.0	111.0	115.4	109.0
Al	83.7	77.3	81.9	85.6	85.7	69.8	76.8	74.7	79.4
AlAs	74.5	67.4	71.6	70.3	72.2	75.5	75.7	76.4	82.0
AlP	89.0	82.0	85.9	84.9	86.1	90.7	89.4	90.7	86.0
BP	168.0	156.2	162.5	155.7	158.3	166.5	164.4	165.8	173.0
C	465.8	433.2	450.2	430.3	439.5	458.9	446.0	452.4	443.0
Cu	181.6	138.2	161.5	155.0	168.1	156.8	166.2	169.1	142.0
GaAs	75.1	60.5	69.9	64.8	66.8	73.3	71.7	74.1	75.6
GaN	209.8	183.5	197.1	188.9	191.2	210.2	197.3	200.5	190.0
GaP	90.7	78.0	85.3	79.6	82.5	90.7	87.5	90.1	88.0
Ge	70.5	59.4	65.8	60.2	65.0	71.2	60.5	60.5	75.8
K	5.2	3.7	3.9	3.4	3.4	3.8	4.2	4.1	3.7
Li	15.1	13.8	13.7	13.3	13.4	12.9	14.2	14.2	13.0
LiCl	41.5	31.7	35.4	33.4	34.0	35.8	36.2	36.7	35.4
LiF	86.7	66.9	72.2	66.2	68.9	81.2	79.6	80.2	69.8
NaF	61.5	45.2	48.8	42.9	44.0	61.9	59.5	59.9	51.4
Pd	226.3	169.4	205.2	195.4	209.7	190.6	186.8	195.0	195.0
Rh	315.6	256.4	295.0	281.9	296.1	284.5	277.2	284.5	269.0
Si	93.7	85.5	90.5	88.9	90.8	96.6	94.3	96.6	99.2
SiC	221.5	205.1	213.7	217.7	221.3	225.7	217.8	221.1	225.0
ME (GPa)	9.3	-11.2	0.1	-5.0	-0.5	2.0	-0.6	1.7	—
MAE (GPa)	<u>14.1</u>	11.2	8.4	8.3	9.2	7.9	**7.3**	7.9	—
MRE(%)	6.7	-12.0	-3.4	-8.1	-4.9	-1.0	-1.9	-0.5	—
MARE(%)	15.1	12.0	8.9	10.4	10.4	9.1	9.5	9.8	—
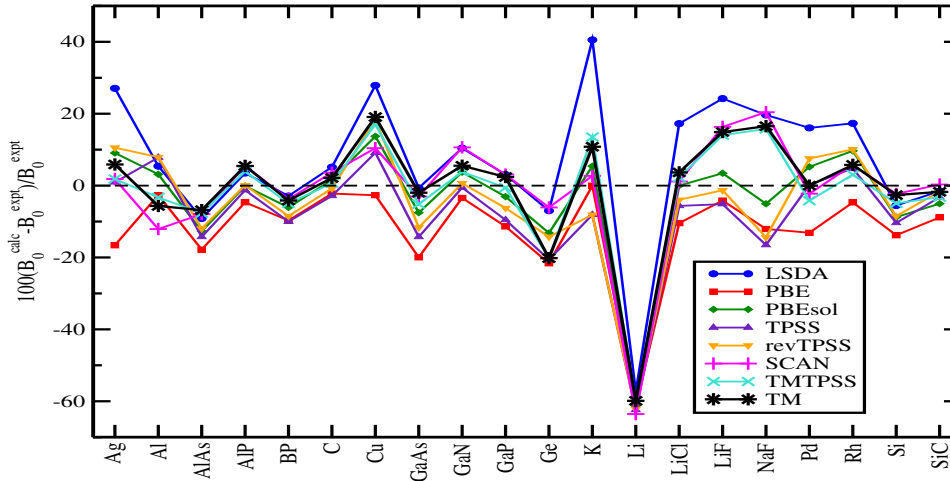
Figure 3.2: Percentage deviation of bulk moduli of different functional presented in Table 3.2.

the advanced meta-GGA, all perform quite similarly.

3.4.4 Bandgaps

The meta-GGA functional implemented in the gKS scheme shows improvement for the band gap compared to the GGA functional due to the inclusion of the some amount of derivative discontinuity. In Table 3.3 we calculate band gap of the 37 semiconductors.

We observe from Table 3.3 that all the semilocal density functionals underestimate the band gap. Improvement in bandgaps from GGA to the meta-GGA functional is observed. However, the SCAN functional shows impressive improvement for the band gap. This is because the SCAN functional obeys more exact constraints than other semilocal functionals. An interesting observation is that the bandgap values of Ge and InSb are predicted to be non-zero with the SCAN, TMTPSS and TM functionals. These are the most interesting features of the SCAN and TM based functional.

Table 3.3: Bandgaps using different functionals as obtained from different approximations.

Solids	LSDA	PBE	PBEsol	TPSS	revTPSS	SCAN	TMTPSS	TM	Expt. [245]
C	4.17	4.13	4.03	4.17	4.04	4.56	4.15	4.09	5.48
Si	0.46	0.64	0.48	0.67	0.57	0.85	0.65	0.56	1.17
Ge	0.00	0.00	0.00	0.00	0.00	0.06	0.23	0.29	0.74
SiC	1.38	1.47	1.34	1.42	1.30	1.82	1.47	1.38	2.42
BN	4.48	4.52	4.36	4.52	4.38	5.04	4.59	4.49	6.22
BP	1.17	1.28	1.14	1.29	1.15	1.55	1.28	1.19	2.4
BAs	1.14	1.22	1.10	1.21	1.10	1.44	1.19	1.13	1.46
BSb	0.70	0.75	0.65	0.65	0.54	0.88	0.61	0.57	n/a
AlP	1.47	1.68	1.50	1.73	1.64	1.95	1.75	1.63	2.51
AlAs	1.36	1.54	1.38	1.59	1.51	1.79	1.59	1.49	2.23
AlSb	1.11	1.24	1.13	1.32	1.23	1.39	1.25	1.16	1.68
$\beta-$GaN	1.82	1.41	1.54	1.31	1.28	2.05	1.47	1.48	3.30
GaP	1.45	1.51	1.52	1.72	1.60	1.89	1.46	1.56	2.35
GaAs	0.50	0.15	0.39	0.38	0.57	0.80	0.80	0.84	1.52
GaSb	0.11	0.00	0.00	0.00	0.17	0.12	0.39	0.46	0.73
InP	0.52	0.37	0.48	0.54	0.59	0.87	0.71	0.73	1.42
InAs	0.00	0.00	0.00	0.00	0.00	0.00	0.00	0.00	0.41
InSb	0.00	0.00	0.00	0.00	0.00	0.00	0.00	0.05	0.23
ZnS	1.89	2.02	2.09	2.29	2.33	2.71	2.32	2.31	3.66
ZnSe	1.28	1.15	1.24	1.45	1.51	1.80	1.60	1.59	2.70
ZnTe	1.31	1.07	1.24	1.42	1.58	1.62	1.63	1.64	2.38
CdS	0.97	1.04	1.01	1.23	1.18	1.47	1.23	1.21	2.55
CdSe	0.43	0.49	0.48	0.71	0.70	0.94	0.81	0.79	1.90
CdTe	0.66	0.59	0.93	0.82	0.82	0.97	1.01	1.00	1.92
MgO	5.13	4.53	4.68	4.77	4.72	5.77	4.96	4.88	7.22
MgS	3.14	3.34	3.35	3.63	3.64	4.19	3.80	3.70	5.4
MgSe	1.80	1.84	1.85	2.14	2.16	2.51	2.23	2.15	2.47
MgTe	2.41	2.32	2.35	2.66	2.72	3.03	2.89	2.74	3.6
CaS	2.00	2.40	2.18	2.47	2.46	2.84	2.54	2.43	n/a
CaSe	1.73	2.10	1.90	2.18	2.18	2.55	2.26	2.15	n/a
CaTe	1.33	1.57	1.37	1.64	1.63	2.14	1.71	1.80	n/a
SrS	2.14	2.52	2.30	2.59	2.54	2.92	2.57	2.47	n/a
SrSe	1.91	2.25	2.05	2.32	2.29	2.67	2.33	2.23	n/a
SrTe	1.43	2.09	2.12	2.31	2.38	2.74	2.51	2.44	n/a
BaS	1.14	2.17	1.98	2.26	2.19	2.52	2.16	2.08	3.88
BaSe	1.67	1.97	1.79	2.05	2.01	2.33	2.01	1.92	3.58
BaTe	1.30	1.61	1.41	1.67	1.63	1.94	1.66	1.56	3.08
MAE (eV)	1.158	1.154	<u>1.173</u>	1.033	1.055	**0.736**	0.949	0.996	–

3.4.5   Cohesive energies

The cohesive energy performance of the functionals is assessed using a set of 14 crystalline solids which includes (transition) metals, semiconductors, and ionic solids. The atomic calculations for the cohesive energies are performed using the spin-polarized calculation within the $10 \times 10 \times 10$ Å^3 simulation box.

Table 3.4: Shown is the cohesive energies of 14 solids (in eV/atom).

Solids	LSDA	PBE	PBEsol	TPSS	revTPSS	SCAN	TMTPSS	TM	Expt. [178]
Li	1.786	1.583	1.653	1.738	1.625	1.545	1.664	1.662	1.658
C	8.867	7.714	8.215	7.420	7.504	7.899	7.624	7.845	7.545
SiC	7.305	6.356	6.779	6.298	6.380	6.689	6.478	6.652	6.478
Si	5.194	4.464	4.810	4.444	4.531	4.811	4.628	4.788	4.685
LiF	4.867	4.411	4.515	4.469	4.389	4.784	4.565	4.554	4.457
LiCl	3.739	3.332	3.467	6.442	3.430	3.632	3.551	3.536	3.586
NaF	4.396	3.962	4.061	4.272	3.944	4.394	4.163	4.147	3.970
NaCl	3.438	3.085	3.197	6.389	3.199	3.438	3.349	3.326	3.337
MgO	5.982	5.152	5.441	5.271	5.295	5.654	5.439	5.496	5.203
Al	3.904	3.397	3.741	3.545	3.672	3.739	3.770	3.961	3.431
Pd	5.053	3.738	4.464	4.004	4.392	4.384	4.620	4.717	3.938
Cu	4.523	3.490	4.038	3.749	4.087	3.887	4.327	4.385	3.524
Ag	3.627	2.514	3.072	2.724	3.030	2.883	3.296	3.357	2.985
GaAs	4.024	3.126	3.518	3.126	3.273	3.422	3.422	3.518	3.337
ME(eV/atom)	0.569	-0.173	0.159	-0.056	-0.010	0.173	0.154	0.229	–
MAE(eV/atom)	<u>0.569</u>	0.197	0.214	**0.161**	0.178	0.203	0.185	0.229	–
MRE(%)	13.563	-4.778	3.519	-0.875	0.112	3.669	4.409	6.033	–
MARE(%)	13.563	5.100	4.953	4.136	4.507	5.123	5.034	6.033	–

From Table 3.4 and Fig. 3.3, we observe that TPSS functional performs better than other functionals.Here, performance of revTPSS and TMTPSS report almost similar MAE. We observe that the TMTPSS performs slightly better compared to the TM functional. It is also indicative from Table 3.4 that the performance of TMTPSS is even better than the SCAN functional. From Fig. 3.3, it is noticeable that the performance of the TMTPSS is quite well for ionic solids and semiconductors but overestimates the cohesive energies for the transition metals.

3.5   Extensive Study of Simple and Transition metals

This section assess the benchmark calculations of the various semilocal functionals for the different bulk properties of simple and Transition metals. It is well known that though describing the bulk properties of transition metals quite difficult within different levels of approximations, still, outcomes of DFT quite accurate [194].
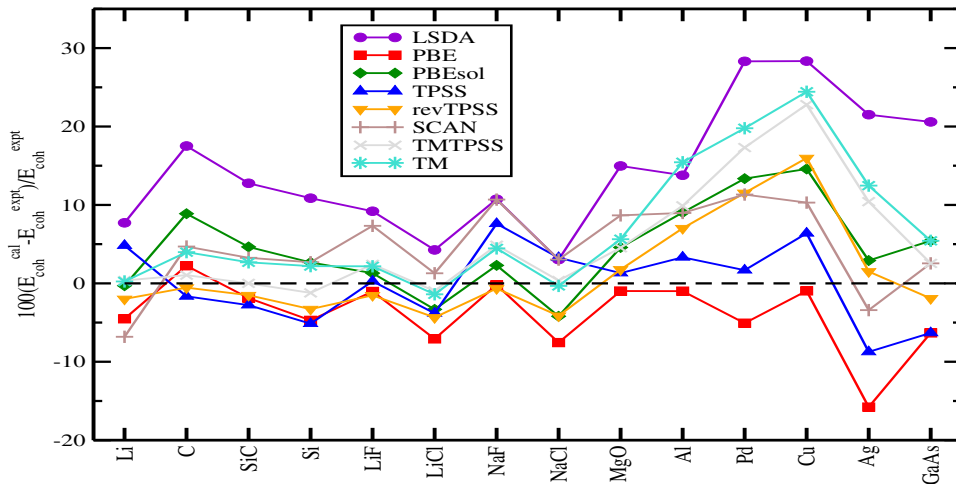
Figure 3.3: Percentage error of cohesive energies from different functionals.

Regarding the earlier attempt studies has been done in several literature [171–173, 176, 186, 191, 209, 210]. within different level of XC approximations. In this section, our considered meta-GGA functionals includes: Tao-Perdew-Staroverov-Scuseria (TPSS) [84], revised TPSS (revTPSS) [85], Minnesota 2006 local functional (M06L) [87], optimized TPSS (oTPSS) [137], modified TPSS (modTPSS) [136], regularized TPSS (regTPSS) [141], meta-GGA made simple (MS0, MS1, and MS2) [88, 89], Strongly Constrained and Appropriately Normed (SCAN) [86], and Tao-Mo [35] meta-GGA functional (TMTPSS and TM). The TPSS, revTPSS, SCAN, TMTPSS and TM functionals are already introduced in our previous study. In this section, we include more meta-GGA functionals − M06L, oTPSS, modTPSS, regTPSS, MS0, MS1, and MS2. M06L local functional is proposed by parametrizing for wide set of test set [87, 133], oTPSS is the optimized TPSS functional for molecular test set [137], modTPSS is the one parametric modification of the TPSS functional [136], regTPSS is proposed by eliminating the order of limit problem of the TPSS and revTPSS functionals [141], and MS0, MS1, and MS2 are the different levels of meta-GGA functionals with simpler in form compared to earlier meta-GGA functionals [88, 89]. Not only that to put our comparison in broader prospects
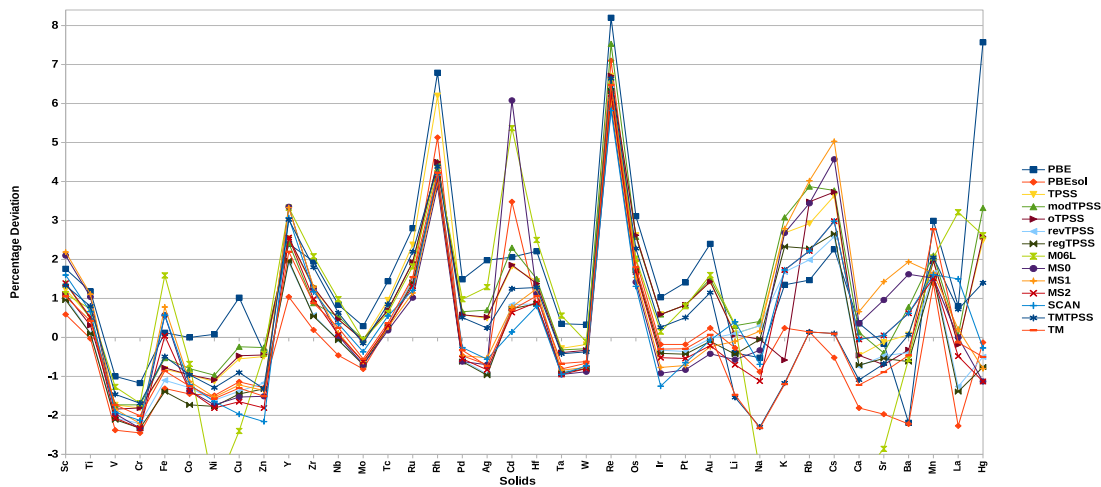
Figure 3.4: Relative error in lattice constants of various solids as presented in Table 3.5.

we also consider popular GGA based functionals PBE and PBEsol.

In ref. [209] it is shown that the canonical PBE functional performs not satisfactorily for all properties of metals because of different types of bonding [188, 209]. Due to these difficulties, the transition metals are often excluded in the benchmark calculations. However, in ref. [209] it is also shown that improvement is achieved by going into the higher rungs of approximation i.e., meta-GGA level. Note that due to one-electron free correlation and more conveniently separating the important regions, the meta-GGA functionals are one of the most preferred choice for different solids having different interaction. The motivation of this section follows those facts. Also, it is believed that SCAN and TM functionals include intermediate dispersion interaction [86, 180, 257] which assumed to improve the transition metals performance.

3.5.1 Benchmark calculations

3.5.1.1 Atomic pair distances

The performance of different functional is presented in Table 3.5. The error statistics (mean relative percentage error (MRPE) (in %)) of the individual solids are plotted in Fig. (3.4). In Table 3.5, the calculated values are compared with the zero-point vibrational effects (ZPVE) corrected experimental values.

Table 3.5: Shown is the calculated inter-atomic distances (δ) (in Picometer (pm)) as obtained from different density functional approximations. The ZPVE corrected reference values are collected from [171, 209, 210]. For Mn, La and Hg the ZPVE un-corrected values are taken from [210]. The best and most deviating values values are in bold and underline format.

Solids	CS	GGA							meta-GGA							Expt.
		PBE	PBEsol	TPSS	modTPSS	oTPSS	revTPSS	regTPSS	M06L	MS0	MS1	MS2	SCAN	TMTPSS	TM	
Sc	hcp	330.1	**326.3**	328.4	328.9	328.0	327.7	327.5	328.0	<u>331.2</u>	331.5	328.9	329.6	328.7	327.8	324.4
Ti	hcp	**292.3**	288.8	290.4	290.3	289.8	289.2	289.2	291.0	291.9	292.1	290.4	290.8	291.2	290.1	288.9
V	bcc	**258.0**	<u>254.4</u>	256.1	256.1	255.8	255.2	255.1	257.3	255.5	255.8	255.2	255.6	256.8	256.1	260.6
Cr	bcc	**245.6**	<u>242.4</u>	244.0	244.2	244.0	243.0	242.7	244.3	242.7	243.0	242.7	243.2	244.3	243.5	248.5
Fe	bcc	245.3	241.8	243.0	243.7	243.1	242.3	241.6	<u>248.9</u>	246.4	246.9	**245.1**	246.4	243.8	242.9	245.0
Co	hcp	**248.8**	245.2	246.4	246.8	246.4	245.6	<u>244.5</u>	247.1	245.4	246.0	245.4	245.8	246.4	245.7	248.8
Ni	fcc	**248.6**	244.7	245.6	246.0	245.7	244.4	244.0	<u>238.6</u>	244.1	244.6	243.9	244.3	245.2	244.5	248.4
Cu	fcc	257.0	251.5	253.0	**253.8**	253.2	250.9	250.7	<u>248.3</u>	250.5	251.3	250.2	249.4	252.1	251.1	254.4
Zn	hcp	263.5	261.1	263.2	**263.8**	263.3	261.4	261.0	263.4	260.5	260.9	259.7	<u>258.8</u>	261.0	260.5	264.5
ME		**0.6**	<u>-3.0</u>	-1.5	-1.1	-1.6	-2.6	<u>-3.0</u>	-1.8	-1.7	-1.3	-2.4	-2.2	-1.6	-2.4	
MAE		**2.1**	3.5	2.7	2.4	2.6	3.4	3.8	4.0	<u>4.2</u>	4.0	3.8	4.1	3.0	3.4	
MRPE		**0.2**	<u>-1.2</u>	-0.6	-0.5	-0.7	-1.1	<u>-1.2</u>	-0.8	-0.7	-0.6	-1.0	-0.9	-0.7	-1.0	
AMRPE		**0.7**	1.3	1.0	0.9	1.0	1.3	1.5	1.5	<u>1.6</u>	1.4	1.5	1.4	1.1	1.3	
Y	hcp	363.3	**358.5**	363.8	363.4	363.9	361.6	361.8	366.6	<u>366.7</u>	366.6	363.9	365.7	365.5	362.6	354.8
Zr	hcp	323.6	**318.0**	321.4	320.2	321.5	319.2	319.1	<u>324.0</u>	321.4	321.5	320.5	321.1	323.1	320.2	317.4
Nb	bcc	287.8	284.1	286.7	286.9	286.7	285.2	**285.2**	<u>288.2</u>	285.5	285.7	285.6	286.4	287.2	286.1	285.4
Mo	bcc	272.9	<u>269.9</u>	271.9	**272.0**	271.9	270.3	270.2	271.9	270.2	270.4	271.1	271.7	271.7	270.6	272.1
Tc	hcp	**274.4**	271.2	273.1	272.4	272.4	271.3	271.2	272.2	**271.0**	271.2	271.3	272.0	272.8	271.5	270.5
Ru	hcp	<u>271.6</u>	268.1	270.5	269.3	269.3	268.1	267.9	269.0	**266.9**	267.2	267.7	267.4	270.0	268.3	264.2
Rh	fcc	<u>270.4</u>	266.2	268.9	264.6	264.6	263.6	263.5	264.2	**263.0**	263.3	263.5	263.8	264.3	263.9	253.2
Pd	fcc	<u>278.6</u>	273.2	276.1	276.3	276.1	272.9	272.8	277.2	272.8	273.2	273.0	**273.8**	275.9	273.6	274.5
Ag	fcc	<u>293.4</u>	285.7	289.1	289.7	289.2	285.0	284.9	291.4	285.7	286.2	285.3	286.1	**288.4**	285.6	287.7
Cd	hcp	302.0	306.2	301.3	302.7	301.4	298.4	298.1	311.8	<u>313.9</u>	298.2	297.8	**296.3**	299.6	298.0	295.9
ME		<u>6.2</u>	2.5	4.7	4.2	4.1	2.0	**1.9**	6.1	4.1	2.8	2.3	2.8	4.3	2.5	
MAE		<u>6.2</u>	3.9	4.8	4.2	4.2	3.3	**3.2**	6.1	5.3	3.7	3.5	3.5	4.4	3.4	
MPE		<u>2.2</u>	0.9	1.7	1.5	1.4	**0.7**	**0.7**	2.1	1.4	0.9	0.8	0.9	1.5	0.9	
MAPE		<u>2.2</u>	1.4	1.7	1.5	1.4	**1.1**	**1.1**	2.1	1.8	1.3	1.2	1.2	1.5	1.2	
Hf	hcp	319.5	315.2	317.1	317.3	316.9	315.3	315.3	<u>320.4</u>	316.1	316.5	315.4	**315.1**	316.6	315.9	312.6
Ta	bcc	286.6	283.3	**284.8**	284.7	284.5	283.1	283.0	287.2	<u>282.9</u>	283.2	<u>282.9</u>	<u>282.9</u>	284.4	283.7	285.6
W	bcc	274.7	272.0	273.3	273.0	272.9	271.6	271.6	**273.5**	<u>271.4</u>	271.7	271.6	271.8	272.8	272.1	273.8
Re	hcp	<u>277.2</u>	274.4	273.4	275.5	273.4	272.5	272.4	273.0	271.4	271.8	272.2	**271.1**	273.2	272.8	256.2
Os	hcp	<u>275.4</u>	272.4	274.1	274.0	274.1	271.8	271.7	272.5	270.9	271.2	271.6	**270.6**	273.2	271.9	267.1
Ir	fcc	273.8	270.5	272.6	272.6	272.6	270.1	269.9	**271.4**	268.5	268.9	269.6	<u>267.6</u>	271.7	270.2	271.0
Pt	fcc	<u>280.5</u>	**276.1**	278.9	278.9	278.9	275.6	275.4	278.8	274.3	274.6	275.1	274.8	278.0	275.8	276.6
Au	fcc	<u>293.9</u>	287.7	291.1	291.3	291.1	**286.9**	286.7	291.6	285.8	286.3	286.4	286.8	290.3	287.2	287.0
ME		<u>6.5</u>	2.7	4.4	4.7	4.3	2.1	2.0	4.8	**1.4**	1.8	1.9	**1.4**	3.8	2.5	
MAE		<u>6.5</u>	4.0	4.8	5.1	4.8	**3.8**	3.9	4.9	4.2	4.1	4.0	3.9	4.3	**3.8**	
MPE		<u>2.4</u>	1.0	1.6	1.7	1.6	0.8	0.8	1.8	0.6	0.7	0.7	**0.5**	1.4	0.9	
MAPE		<u>2.4</u>	1.5	1.8	1.9	1.8	**1.4**	**1.4**	1.8	1.6	1.5	1.5	**1.4**	1.6	**1.4**	
Li	bcc	297.7	298.1	299.2	299.8	**299.1**	299.2	297.6	299.9	297.2	298.6	296.8	300.1	<u>294.3</u>	294.5	298.9
Na	bcc	362.6	361.3	365.6	366.0	**364.3**	365.6	364.3	<u>352.0</u>	363.3	365.1	360.4	362.0	356.1	356.0	364.3
K	bcc	457.5	**452.5**	463.5	465.3	448.8	459.0	461.9	<u>427.8</u>	463.5	464.0	459.2	459.2	446.1	446.0	451.4
Rb	bcc	490.1	**483.7**	497.1	501.7	499.8	492.6	494.0	<u>451.6</u>	499.6	502.4	493.7	493.7	**483.7**	**483.7**	483.0
Cs	bcc	534.8	520.3	542.0	542.7	542.5	536.5	536.9	<u>482.2</u>	546.9	549.3	538.6	538.6	**523.5**	**523.5**	523.0
ME		4.4	**-1.0**	9.3	10.9	6.7	6.4	6.8	<u>-21.5</u>	9.9	11.7	5.6	6.6	-3.4	-3.4	
MAE		5.6	**1.7**	9.3	10.9	7.9	6.4	7.4	<u>21.9</u>	11.1	11.8	8.1	7.6	3.9	3.9	
MPE		0.8	**-0.3**	1.9	2.3	1.3	1.3	1.4	<u>-4.5</u>	2.0	2.4	1.0	1.3	-1.0	-1.0	
MAPE		1.2	**0.4**	1.9	2.3	1.6	1.3	1.6	<u>4.7</u>	2.3	2.4	1.8	1.6	1.1	1.0	
Ca	fcc	394.3	385.8	391.1	393.4	391.1	390.0	390.1	<u>378.7</u>	394.3	395.5	**392.7**	**392.7**	388.6	388.1	392.9
Sr	fcc	426.4	418.7	426.6	425.4	424.1	425.1	424.8	<u>414.9</u>	431.2	433.2	**427.3**	**427.3**	424.2	423.3	427.1
Ba	bcc	423.7	<u>423.6</u>	**433.5**	436.6	431.8	431.5	430.5	430.8	440.2	441.6	435.9	435.9	**433.5**	431.2	433.2
ME		-2.9	-8.4	**-0.7**	0.7	-2.1	-2.2	-2.6	<u>-9.6</u>	4.2	5.7	0.9	0.9	-2.3	-3.5	
MAE		3.9	8.4	**0.9**	2.0	2.0	2.2	2.6	<u>9.6</u>	4.2	5.7	1.0	1.0	2.5	3.5	
MPE		-0.7	-2.0	**-0.2**	0.2	-0.5	-0.5	-0.6	<u>-2.3</u>	1.0	1.3	0.2	0.2	-0.6	-0.9	
MAPE		0.9	2.0	**0.2**	0.4	0.5	0.5	0.6	<u>2.3</u>	1.0	1.3	0.2	0.2	0.6	0.9	
Mn	c	<u>230.7</u>	**227.1**	228.4	228.7	228.4	227.7	227.5	228.6	227.4	227.7	227.4	227.6	228.6	230.2	224.0
La	h	376.9	365.4	373.3	374.1	373.2	369.2	368.7	<u>385.9</u>	373.9	374.7	372.1	379.5	376.6	373.4	373.9
Hg	r	<u>323.8</u>	**300.6**	308.5	311.0	308.8	299.5	298.7	308.9	297.6	298.6	297.6	300.2	305.2	299.5	301.0
ME		<u>10.8</u>	-1.9	3.8	5.0	3.8	-0.8	-1.3	8.2	**0.0**	0.7	-0.6	2.8	3.8	1.4	
MAE		<u>10.8</u>	4.0	4.2	5.0	4.3	3.3	3.7	8.2	**2.3**	**2.3**	2.9	3.3	3.8	2.7	
MPE		<u>3.8</u>	-0.3	1.4	1.8	1.5	**0.0**	-0.2	2.6	0.1	0.4	**0.0**	0.9	1.4	0.7	
MAPE		<u>3.8</u>	1.3	1.5	1.8	1.6	1.1	1.2	2.6	**0.9**	**0.9**	1.0	1.1	1.4	1.1	
TME		<u>4.4</u>	-0.4	3.3	3.7	2.6	1.0	0.8	-0.8	2.6	2.9	1.2	1.7	1.2	**0.0**	
TMAE		5.4	3.9	4.5	4.7	4.3	3.7	4.0	<u>7.9</u>	5.2	5.0	4.0	4.0	3.8	**3.5**	
TMRPE		<u>1.5</u>	**0.0**	1.0	1.1	0.8	0.2	0.2	0.2	0.6	0.7	0.3	0.4	0.5	0.1	
TAMRPE		1.8	1.3	1.4	1.5	1.4	**1.2**	1.3	<u>2.3</u>	1.6	1.5	1.3	1.3	1.3	**1.2**	

Regarding the results presented in Table 3.5, it follows a clear trend throughout. The GGA PBE functional yields the least error for the $3d$ group elements while shows overestimation for $4d$ and $5d$ group metals. Unlike PBE functional, the PBEsol shows underestimation in predicting the lattice constants of $3d$ transition metals. While it shows improved performance for for $4d$ and $5d$ transition metals compared to its $3d$ counterpart. It is also observed that more than half-filled d bands of each block, the PBE functional shows overestimation because of the self-interaction error of the d shell [171]. Regarding the ferromagnetic Fe, Co, and Ni, the PBE functional performs quite satisfactorily.

Now turn into the meta-GGA functionals, we observe that the TPSS meta-GGA functional shows PBE like performance $3d$ block transition metals. The underestimation in the inter-atomic distances are observed from the revTPSS functional. Note that the revTPSS performs closely that of the PBEsol with the d band filling [171].

Regarding the performance of modified TPSS (modTPSS) and optimized TPSS (oTPSS) functionals [136, 137], both parametrized functionals improve the performance of TPSS for both the $3d$ and $4d$ block metals. While for $5d$ block metals, we observe similar performance from TPSS, and its different modified versions.

Beyond TPSS and revTPSS, Ruzsinszky et. al. [141] proposed a new kind of functionality by eliminating the order of limit anomaly of meta-GGA functionals (regTPSS) functional. In Table 3.5, we also enlist the performance of regTPSS. The main motivation of the regTPSS functional is to remove the order of limit problem by keeping the accuracy of revTPSS functional. We observe similar performance as obtained form revTPSS in the case of the regTPSS functional.

Concerning Minnesota local functional (M06L), this functional can not be recommended for the inter-atomic distances because of its error statistics. Now considering the different variant of simple meta-GGA functionals (MS0, MS1, and MS2) [88, 89], we obtain the error order as order MS0 > MS1 > MS2 for inter-atomic lattice constants. Note that "MS" functionals performs differently based on the construction of their exchange enhancement factor. The MS2 exchange enhancement factor is less steep than that of MS0 and MS1 functionals in the region $s < 1$ which is important for solids [171, 191]. The error as obtained from "MS" functionals is in the order MS0 > MS1 > MS2.

Most advanced density functional SCAN does not show much improvement for $3d$ block metals. But showing improvement for other block metals. However, regarding the performance of the TM functional it is quite impressive for $3d$ block metals.

In Table 3.5, we listed the the inter-atomic distances of Li, Na, K, Rb, and Cs. Note that a sizable interaction nature of these solids originated from van-der-Waals bonding [171, 188]. Concerning the PBE functional, we observe deviation in its performance due to the lack of the short-range van-der-Waals interactions. However, the improvement is observed from PBEsol functional which yields the least MAE in this case. Considering the meta-GGA, except TMTPSS and TM, all functionals show overestimation nature in its performance. Note that TMTPSS and TM include some amount of short-range van-der-Waals interactions which assume to be improve the lattice constants of those solids. Here also M06L shows underestimation in its performance due to lack of uniform density limit in its form. However, the trends of PBE functional does not follow for alkaline-earth metals and it performs reasonably well, while the PBEsol functional underestimates the same. Within meta-GGAs, we observe quite a good performance from TPSS and MS2 while MS0, MS1 and SCAN show overestimation.

Here we will discuss about Mn, La, and Hg separately because of their complicated structures. The PBE functional shows massive overestimation in this case, while, PBEsol performs well. Regarding meta-GGAs, all (except M06L) perform reasonably well and show a similar kind of tendency. A sizable overestimation is observed in the performance of M06L.

3.5.1.2   Performance in Bulk moduli

Obtaining the bulk moduli from the semilocal functional is a challenging task [210]. In Table 3.6 the performances of simple and transition metals are listed and the MRPE is plotted in Fig. 3.5. However, the semilocal functionals do not follow the trend of the the inter-atomic distances in case of bulk moduli.

Inspecting the performance of PBE functional from Table 3.6, we observe that for the $3d$, $4d$ and $5d$ block metals it performs quite well. However, PBEsol does not perform according to its merit for $3d$ block metals and deviates more compared to PBE. However,

Table 3.6: Shown is the Bulk moduli (B_0) (in GPa) using different functionals. The finite thermal effect corrected reference values are taken from [171, 209, 210]. The finite thermal effect uncorrected reference values of Mn, La and Hg are taken from [210]. We also report the error statistics. The bold and underline style is used for indicating least and most deviating values.

Solids	CS	GGA							meta-GGA							Expt.
		PBE	PBEsol	TPSS	modTPSS	oTPSS	revTPSS	regTPSS	M06L	MS0	MS1	MS2	SCAN	TMTPSS	TM	
Sc	hcp	52.6	55.4	54.6	59.8	59.8	**55.6**	59.4	<u>62.6</u>	54.2	53.6	56.0	59.8	61.8	57.4	55.6
Ti	hcp	**116.8**	125.6	123.2	121.4	122.6	125.8	126.8	<u>128.6</u>	124.0	122.4	127.6	125.2	125.8	127.0	108.3
V	bcc	187.8	204.0	201.8	198.8	200.2	205.6	205.0	198.0	200.8	199.6	<u>207.0</u>	203.8	201.8	**181.8**	158.9
Cr	bcc	**263.6**	288.2	283.2	281.2	282.5	291.8	<u>292.4</u>	276.8	284.8	281.2	292.0	280.2	283.6	286.8	174.5
Fe	bcc	161.1	<u>271.4</u>	163.6	161.1	161.8	232.5	**174.8**	145.3	154.3	150.4	161.7	144.7	267.3	272.5	169.8
Co	hcp	287.0	<u>287.2</u>	257.2	224.6	228.4	239.7	242.0	**223.3**	239.7	230.6	245.8	239.4	239.6	242.9	193.0
Ni	fcc	208.6	231.9	228.7	208.6	218.7	244.7	225.6	<u>262.0</u>	240.5	235.3	243.5	241.5	**199.9**	238.2	185.5
Cu	fcc	**137.1**	163.3	156.5	152.7	160.8	170.5	<u>171.1</u>	151.9	158.9	146.9	155.9	152.4	161.2	164.2	140.3
Zn	hcp	**74.0**	91.8	86.0	84.0	88.0	97.8	100.4	74.2	99.4	82.8	102.0	105.2	96.8	<u>105.6</u>	69.7
ME		**25.9**	<u>51.5</u>	33.2	26.3	29.7	45.4	38.1	29.7	33.4	27.5	37.3	33.0	42.5	46.8	
MAE		29.2	<u>51.5</u>	34.8	**28.2**	31.5	45.4	38.1	35.1	37.2	32.2	39.1	38.5	42.5	46.8	
MPE		**14.6**	<u>32.3</u>	21.0	17.7	20.1	29.7	26.3	19.1	22.5	17.2	25.3	23.4	28.9	31.4	
MAPE		**17.5**	<u>32.4</u>	22.2	18.8	21.2	29.7	26.3	22.3	25.0	20.5	26.3	26.7	28.9	31.4	
Y	hcp	39.6	**42.0**	40.2	39.3	37.9	40.2	<u>37.8</u>	44.4	37.4	37.2	36.6	36.4	38.4	**41.4**	41.7
Zr	hcp	92.8	98.8	96.4	94.7	95.0	97.0	97.4	95.4	92.8	<u>92.2</u>	95.6	**95.8**	96.2	97.0	95.9
Nb	bcc	**172.0**	186.8	183.4	181.7	181.7	<u>187.6</u>	<u>187.6</u>	169.0	181.6	180.4	183.4	180.8	181.2	183.2	172.0
Mo	bcc	266.4	289.0	278.6	277.3	278.4	286.2	<u>290.4</u>	260.2	287.0	285.2	287.4	284.0	278.6	283.6	264.7
Tc	hcp	301.4	330.6	317.0	315.6	317.5	329.0	331.2	292.2	<u>334.6</u>	331.2	331.2	324.2	319.0	325.2	303.1
Ru	hcp	316.4	353.8	334.4	332.9	335.2	350.4	353.4	302.0	<u>365.4</u>	361.4	356.8	342.2	337.0	345.8	317.7
Rh	fcc	254.8	295.8	276.7	274.1	292.4	292.4	295.5	<u>235.0</u>	298.4	294.7	292.9	**290.3**	275.9	284.0	288.7
Pd	fcc	165.3	201.8	187.9	184.0	186.5	201.1	203.1	<u>148.3</u>	199.5	**195.3**	200.1	193.5	189.5	**195.3**	195.4
Ag	fcc	<u>86.1</u>	112.3	102.3	98.9	102.5	113.0	113.9	89.1	**103.7**	100.9	110.7	105.4	109.3	113.0	103.8
Cd	hcp	<u>40.8</u>	59.4	**54.4**	51.6	56.3	62.2	63.4	58.6	59.6	56.0	63.4	57.4	64.8	50.2	53.8
ME		-10.1	13.4	3.5	**1.3**	4.7	12.2	13.7	<u>-14.3</u>	12.3	9.8	12.1	7.3	5.3	8.2	
MAE		10.5	13.4	8.0	8.7	**7.6**	12.5	14.5	<u>15.8</u>	13.8	12.0	13.2	8.8	9.7	9.9	
MPE		<u>-7.7</u>	6.6	1.0	**-0.7**	1.1	6.2	6.5	-5.4	4.2	2.4	5.3	2.2	3.3	3.1	
MAPE		7.8	6.6	**3.6**	4.6	4.3	6.9	8.4	<u>8.5</u>	6.9	5.9	7.8	5.0	6.3	4.9	
Hf	hcp	**110.0**	116.6	114.2	113.0	114.8	116.4	116.6	114.2	113.8	112.8	117.0	116.6	117.4	<u>118.2</u>	109.7
Ta	bcc	199.0	199.0	207.8	206.6	207.4	213.0	<u>214.6</u>	**196.8**	210.4	208.8	213.4	212.0	210.8	212.6	193.7
W	bcc	309.6	309.6	324.6	323.8	309.6	336.0	336.8	**310.6**	<u>338.8</u>	332.2	336.0	331.4	330.2	334.4	312.3
Re	hcp	**370.6**	399.6	390.8	390.3	396.3	406.8	407.8	392.8	<u>417.8</u>	410.2	408.4	412.6	398.8	404.8	368.8
Os	hcp	405.6	443.6	**426.8**	427.1	434.3	450.8	453.4	409.0	<u>466.6</u>	461.0	455.6	459.6	440.6	449.4	424.6
Ir	fcc	350.5	391.0	369.9	**369.6**	376.9	394.2	396.9	343.8	<u>416.6</u>	409.8	402.0	415.9	382.7	392.8	365.2
Pt	fcc	245.0	285.8	264.6	262.9	266.2	**284.1**	287.7	<u>224.2</u>	305.9	298.8	294.4	244.1	271.2	280.4	284.2
Au	fcc	131.1	164.1	157.6	147.2	149.9	162.7	165.3	<u>127.7</u>	168.2	**172.5**	167.8	158.2	153.1	159.5	174.8
ME		-14.0	9.5	2.9	**0.9**	2.8	16.3	18.2	-14.3	<u>25.6</u>	21.6	20.2	14.6	8.9	14.9	
MAE		15.8	12.9	**12.1**	13.1	14.2	19.4	20.6	22.2	27.3	22.2	22.1	<u>28.8</u>	17.6	19.6	
MPE		-5.6	2.8	0.8	**-0.3**	0.4	5.1	5.8	-5.7	<u>7.7</u>	6.6	6.5	4.0	2.7	4.7	
MAPE		6.5	**4.6**	5.0	5.5	5.8	6.9	7.2	8.8	8.7	6.9	7.5	<u>9.9</u>	6.9	7.2	
Li	bcc	14.1	13.8	13.6	**13.0**	**13.0**	13.6	**13.0**	14.1	14.1	13.9	14.2	13.3	<u>14.8</u>	14.7	13.1
Na	bcc	8.0	**7.9**	7.4	7.3	7.4	7.5	7.4	7.6	**7.9**	7.7	8.0	**7.9**	8.5	<u>8.9</u>	7.9
K	bcc	3.5	3.5	3.3	3.3	3.3	3.3	3.3	3.2	3.1	<u>3.0</u>	3.2	3.2	**3.8**	**3.8**	3.7
Rb	bcc	2.8	**2.9**	3.7	3.8	3.7	3.5	3.5	<u>4.7</u>	3.6	2.8	3.3	3.1	3.1	3.1	2.9
Cs	bcc	2.0	2.0	1.8	1.9	1.8	1.9	1.8	<u>4.1</u>	2.0	2.0	2.0	2.0	**2.1**	**2.1**	2.1
ME		0.1	0.1	**0.0**	-0.1	-0.1	**0.0**	-0.1	<u>0.8</u>	0.2	-0.1	0.2	-0.1	0.5	0.6	
MAE		0.3	**0.2**	0.5	0.4	0.4	0.4	0.4	<u>1.1</u>	0.5	0.4	0.4	**0.2**	0.5	0.6	
MPE		-1.0	-0.9	**0.0**	0.5	-0.9	-0.2	-2.3	<u>29.5</u>	2.1	-4.9	0.9	-2.1	6.1	6.8	
MAPE		4.4	**3.2**	12.7	11.9	12.0	10.0	10.6	<u>36.4</u>	10.7	7.2	8.2	5.4	6.1	6.8	
Ca	fcc	16.8	17.2	16.8	16.7	16.8	17.1	16.9	<u>20.9</u>	18.2	17.5	17.7	17.6	**18.4**	18.5	18.4
Sr	fcc	11.5	**12.3**	11.4	11.2	11.4	11.7	11.6	<u>17.1</u>	11.4	11.4	11.9	11.1	12.5	12.6	12.4
Ba	bcc	8.7	**9.3**	8.4	8.1	8.4	8.7	8.6	<u>11.8</u>	7.7	7.6	8.3	8.1	9.2	9.2	9.3
ME		-1.0	-0.4	-1.2	-1.4	-1.2	-0.9	-1.0	<u>3.2</u>	-0.8	-1.2	-0.7	-1.1	**0.0**	0.1	
MAE		1.0	0.4	1.2	1.4	1.2	0.9	1.0	<u>3.2</u>	0.8	1.2	0.7	1.1	**0.1**	**0.1**	
MPE		-7.5	-2.4	-8.8	-10.6	-8.8	-6.4	-7.4	<u>26.1</u>	-7.7	-10.4	-6.2	-9.2	**-0.1**	0.4	
MAPE		7.5	2.4	8.8	10.6	8.8	6.4	7.4	<u>26.1</u>	7.7	10.4	6.2	9.2	**0.6**	1.1	
Mn	c	183.2	305.4	299.4	**145.3**	298.4	309.1	311.7	298.0	311.0	306.6	312.6	<u>315.3</u>	302.6	306.5	90.4
La	h	24.2	**26.4**	25.8	25.0	24.7	25.4	25.4	28.0	22.8	<u>22.6</u>	23.6	24.2	25.6	24.2	26.6
Hg	r	<u>9.6</u>	36.0	22.4	18.3	21.1	32.4	34.8	19.6	**24.4**	21.6	24.0	21.2	33.6	38.8	28.2
ME		23.9	74.2	67.5	**14.5**	66.3	73.9	<u>75.6</u>	66.8	71.0	68.5	71.7	71.8	72.2	74.8	
MAE		37.9	74.3	71.9	**22.1**	72.3	74.7	76.4	72.5	76.1	75.6	76.5	<u>78.1</u>	72.9	76.4	
MPE		9.2	88.2	69.2	**6.5**	65.9	84.1	87.9	68.1	72.1	66.9	73.2	71.6	83.4	<u>89.2</u>	
MAPE		59.2	88.7	84.9	**34.0**	87.5	87.1	90.9	88.5	90.6	92.5	90.7	94.2	85.9	<u>95.2</u>	
TME		**2.3**	<u>23.5</u>	14.6	7.8	14.0	23.2	22.3	5.9	22.1	18.9	21.9	18.4	19.1	22.3	
TMAE		16.1	<u>24.3</u>	18.7	**13.6**	18.3	24.1	23.3	23.3	<u>24.3</u>	21.6	23.5	23.8	22.1	23.9	
TMPE		**0.3**	16.7	10.2	3.7	9.5	15.9	15.2	13.2	13.4	9.9	14.2	11.6	15.6	<u>17.2</u>	
TMAPE		13.4	18.0	16.3	**11.9**	16.5	19.0	19.1	<u>23.2</u>	18.8	17.0	18.6	18.6	17.6	18.7	
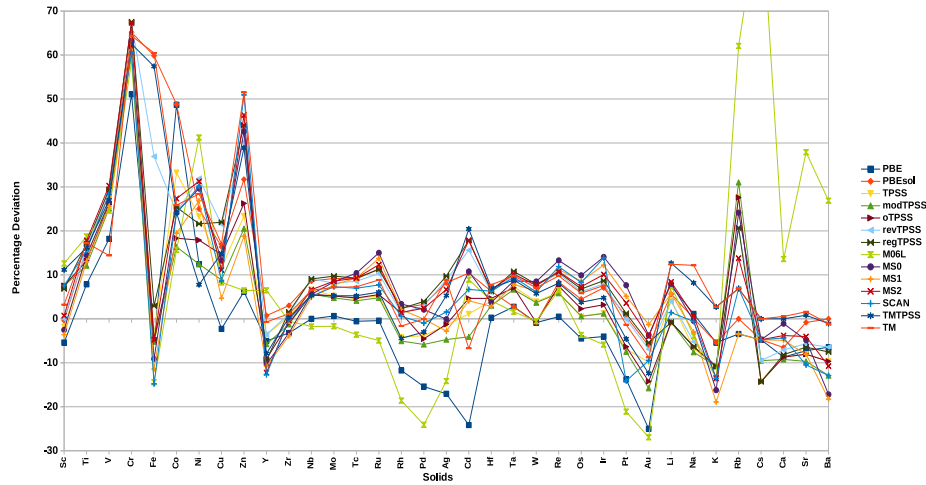
Figure 3.5: Shown is the percentage error of bulk-moduli using different functionals.

the performance of PBEsol quite similar for $4d$ and $5d$ transition metals.

Considering the meta-GGA functionals, except M06L overestimation in observed in all functional performance in determining the bulk moduli for $3d$, $4d$ and $5d$ block transition metals. As the electrons in the d block filling increases the overestimating tendency of meta-GGA functionals become more intense. We observe modTPSS improves over TPSS while oTPSS shows similar performance as TPSS. Regarding the most recent and advanced meta-GGAs like TM, deviation in its performance is observed for the $3d$ transition metals while it shows improved performance for $4d$ and $5d$ transition metals.

Due to the smaller extend of the bulk moduli values the alkali metals are considered as a "soft-matter". For these solids a sizable performance is originated from the short or intermediate range van der Waals interaction. Therefore, we observe in the performance for both the TMTPSS and TM functional.

3.5.1.3 Cohesive energies

The "strong" correlation of transition metals creates a challenge for obtaining cohesive energy of transition metals. We list the all the functional performance in Table 3.7 and plotted the relative error in Fig. 3.6.

As it is observed from Table 3.7, the PBE functional as usual quite a good candidate for the cohesive energies of all the metals. Whereas, PBEsol overestimates it. The differ-

Table 3.7: Shown is the cohesive energies (in eV/atom) as obtained from different functionals. The finite temperature corrected reference values are taken from [209, 210]. The finite temperature un-corrected reference values of Mn, La and Hg are taken from [210]. We use the similar style as indicated for Table 3.5.

Solids	CS	GGA							meta-GGA							Expt.
		PBE	PBEsol	TPSS	modTPSS	oTPSS	revTPSS	regTPSS	M06L	MS0	MS1	MS2	SCAN	TMTPSS	TM	
Sc	hcp	**4.20**	4.58	4.47	4.41	4.47	4.58	4.61	<u>5.08</u>	4.39	4.31	4.49	4.37	4.69	4.81	3.93
Ti	hcp	5.40	5.87	5.56	5.55	5.62	5.77	5.72	<u>6.22</u>	5.29	**5.23**	5.48	5.30	6.01	6.04	4.88
V	bcc	**5.25**	5.83	5.51	5.43	5.51	5.76	5.62	<u>6.28</u>	5.09	5.01	**5.43**	4.96	5.89	5.93	5.34
Cr	bcc	4.05	4.71	4.24	**4.14**	4.24	4.47	4.31	4.50	3.49	3.44	3.96	<u>3.26</u>	4.62	4.66	4.15
Fe	bcc	**4.81**	5.58	5.29	5.17	5.28	5.55	5.52	5.03	5.08	5.00	5.38	4.88	5.58	<u>5.70</u>	4.32
Co	hcp	**5.09**	5.85	5.74	5.63	5.74	6.09	5.99	5.84	5.88	5.77	6.13	5.92	6.25	<u>6.37</u>	4.47
Ni	fcc	**4.67**	5.34	5.07	4.96	5.06	5.44	5.41	<u>5.81</u>	5.20	5.09	5.46	5.25	5.61	5.69	4.48
Cu	fcc	3.48	4.03	3.75	3.66	3.75	4.09	4.08	3.06	3.80	3.71	4.09	3.87	4.32	<u>4.38</u>	3.51
Zn	hcp	1.10	1.57	**1.34**	1.28	1.34	1.61	1.67	1.54	1.55	1.46	1.74	1.52	1.71	<u>1.89</u>	1.38
ME		**0.20**	0.86	0.56	0.47	0.57	0.86	0.81	0.86	0.41	0.32	0.71	0.36	1.03	<u>1.13</u>	
MAE		**0.32**	0.86	0.57	0.50	0.58	0.86	0.81	0.98	0.64	0.58	0.76	0.68	1.03	<u>1.13</u>	
MPE		**2.7**	20.9	12.6	10.1	12.7	21.2	20.4	19.8	10.7	7.90	15.7	9.3	25.7	<u>29.1</u>	
MAPE		**9.0**	20.9	13.4	12.0	13.5	21.2	20.4	23.0	15.8	13.8	19.9	16.4	25.7	<u>29.1</u>	
Y	hcp	4.21	4.60	4.43	4.22	4.28	4.57	4.32	<u>5.06</u>	4.36	4.30	4.49	**4.42**	4.70	4.81	4.42
Zr	hcp	6.27	6.78	6.35	**6.31**	6.39	6.55	**6.28**	6.80	5.83	5.83	6.04	6.12	6.82	<u>6.84</u>	6.32
Nb	bcc	6.79	**7.47**	7.14	7.00	7.09	7.40	7.13	<u>8.63</u>	6.85	6.75	7.07	6.56	7.45	7.49	7.47
Mo	bcc	6.35	7.18	6.63	6.53	6.63	6.95	6.79	**6.85**	6.34	6.23	6.61	<u>5.81</u>	6.96	7.03	6.84
Tc	hcp	6.90	<u>7.85</u>	**7.17**	7.03	7.14	7.59	7.50	6.53	7.28	7.16	7.57	6.72	7.61	7.78	7.17
Ru	hcp	6.88	<u>7.87</u>	7.21	6.99	7.10	7.66	7.65	**6.78**	7.69	7.54	7.79	7.53	7.70	7.85	6.80
Rh	fcc	5.86	<u>6.73</u>	6.00	6.08	6.20	6.40	6.67	5.40	5.90	**5.81**	6.17	5.58	6.41	6.55	5.76
Pd	fcc	3.74	4.47	4.00	**3.88**	4.00	4.39	4.39	4.17	4.24	4.13	4.46	4.38	4.61	<u>4.71</u>	3.93
Ag	fcc	<u>2.52</u>	3.08	2.73	2.63	2.73	3.03	**3.00**	3.24	2.79	2.70	3.10	2.88	3.29	3.35	2.96
Cd	hcp	<u>0.73</u>	1.16	0.95	0.87	0.95	1.20	**1.24**	1.33	1.08	1.01	1.34	1.03	1.39	1.49	1.18
ME		-0.26	0.43	**-0.02**	-0.13	-0.03	0.29	0.21	0.19	-0.05	-0.14	0.18	-0.18	0.41	<u>0.51</u>	
MAE		0.30	0.44	**0.18**	0.23	0.21	0.30	0.32	0.40	0.34	0.34	0.36	0.42	0.41	<u>0.51</u>	
MPE		-8.1	7.5	-2.2	-4.8	-2.4	5.3	4.3	5.1	**-1.4**	-3.6	4.8	-3.3	9.3	<u>11.7</u>	
MAPE		8.6	7.8	**4.7**	6.5	5.4	5.5	5.9	8.2	6.4	6.9	7.4	7.7	9.3	<u>11.7</u>	
Hf	hcp	**6.48**	7.14	6.77	6.70	6.77	7.08	7.09	<u>7.40</u>	6.82	6.73	7.03	6.35	7.05	7.22	6.44
Ta	bcc	**8.25**	9.00	8.67	8.57	8.67	9.03	9.13	9.00	9.18	8.85	9.15	8.80	9.04	<u>9.23</u>	8.11
W	bcc	8.47	9.27	**8.83**	8.72	**8.83**	9.22	9.01	<u>9.77</u>	9.31	9.12	9.46	9.09	9.41	9.45	8.83
Re	hcp	7.79	8.77	8.22	**8.09**	8.20	8.65	8.67	7.74	8.89	8.68	<u>8.95</u>	8.51	8.71	8.91	8.06
Os	hcp	8.30	9.36	8.80	8.62	8.73	9.10	9.37	**8.23**	9.53	9.34	<u>9.53</u>	9.08	9.26	9.49	8.22
Ir	fcc	7.19	8.27	7.56	7.45	7.56	8.10	8.19	**6.97**	<u>8.51</u>	8.31	8.43	8.37	8.07	8.27	6.96
Pt	fcc	5.42	6.27	5.74	5.65	5.76	6.18	6.17	**5.81**	6.31	6.15	6.42	6.17	<u>6.46</u>	6.87	5.87
Au	fcc	<u>3.03</u>	3.72	3.27	3.16	3.27	3.60	3.61	3.57	3.59	3.45	3.81	3.55	**3.83**	3.93	3.83
ME		-0.17	0.69	0.19	**0.08**	0.18	0.58	0.62	0.27	0.73	0.54	0.81	0.45	0.67	<u>0.83</u>	
MAE		**0.30**	0.71	0.37	0.33	0.35	0.64	0.67	0.43	0.79	0.63	0.81	0.54	0.67	<u>0.83</u>	
MPE		-3.7	9.3	1.6	**-0.1**	1.5	7.4	7.9	3.1	9.3	6.6	10.8	5.5	9.0	<u>11.3</u>	
MAPE		**5.3**	9.8	5.8	5.6	5.6	8.9	9.4	6.1	10.9	9.0	10.9	7.7	9.0	<u>11.3</u>	
Li	bcc	1.60	**1.67**	1.63	1.63	1.62	1.64	1.53	<u>1.83</u>	1.54	1.52	1.54	1.56	1.68	1.68	1.67
Na	bcc	1.08	1.15	**1.14**	**1.14**	**1.14**	1.16	1.08	<u>1.49</u>	1.07	1.05	1.09	**1.10**	1.22	1.21	1.12
K	bcc	0.86	0.92	0.92	0.95	0.91	**0.94**	0.88	<u>0.66</u>	0.86	0.84	0.88	0.84	0.99	0.99	0.94
Rb	bcc	0.78	**0.84**	0.81	0.80	0.81	0.83	0.79	<u>1.30</u>	0.78	0.76	0.80	0.76	0.93	0.92	0.86
Cs	bcc	0.72	**0.78**	0.74	0.73	0.74	0.77	0.74	<u>1.35</u>	0.73	0.71	0.76	0.70	0.88	0.88	0.81
ME		-0.07	**-0.01**	-0.03	-0.03	-0.04	**-0.01**	-0.08	<u>0.25</u>	-0.08	-0.10	-0.07	-0.09	0.06	0.06	
MAE		0.07	**0.02**	0.04	0.04	0.04	0.03	0.08	<u>0.36</u>	0.08	0.10	0.07	0.09	0.06	0.06	
MPE		-7.3	**-1.1**	-3.4	-3.3	-3.8	-1.3	-7.0	<u>26.1</u>	-8.0	-10.0	-6.0	-8.8	5.9	5.9	
MAPE		7.3	**2.2**	4.2	4.4	4.5	2.8	7.0	<u>38.1</u>	8.0	10.0	6.0	8.8	6.3	5.9	
Ca	fcc	**1.91**	2.11	2.02	1.99	2.02	2.08	2.08	<u>2.50</u>	2.00	1.96	2.03	2.08	2.17	2.29	1.86
Sr	fcc	1.61	1.81	1.76	**1.72**	1.76	1.83	1.85	<u>2.27</u>	1.79	**1.74**	1.84	1.82	1.96	2.06	1.73
Ba	bcc	**1.88**	2.12	2.03	1.98	2.03	2.11	2.14	<u>2.51</u>	2.00	1.95	2.10	2.04	2.24	2.34	1.91
ME		**-0.03**	0.18	0.10	0.06	0.10	0.17	0.19	<u>0.59</u>	0.10	0.05	0.16	0.15	0.29	0.40	
MAE		0.07	0.18	0.10	0.07	0.10	0.17	0.19	<u>0.59</u>	0.10	**0.05**	0.16	0.15	0.29	0.40	
MPE		**-1.9**	9.7	5.5	3.4	5.5	9.4	10.3	<u>32.4</u>	5.2	2.7	8.5	8.0	15.8	21.6	
MAPE		3.7	9.7	5.5	3.7	5.5	9.4	10.3	<u>32.4</u>	5.2	**2.7**	8.5	8.0	15.8	21.6	
Mn	c	3.80	<u>4.55</u>	3.95	3.82	3.96	4.06	4.03	2.81	3.04	3.01	3.54	**2.90**	4.13	4.28	2.92
La	h	4.30	4.79	4.51	4.31	4.39	4.56	**4.40**	5.03	3.83	3.82	4.06	<u>3.72</u>	4.58	4.61	4.47
Hg	r	0.15	0.54	0.22	**0.14**	0.22	0.43	0.47	0.55	0.43	0.32	<u>0.64</u>	0.39	0.67	0.75	0.62
ME		**0.08**	<u>0.62</u>	0.22	0.09	0.19	0.35	0.30	0.13	-0.24	-0.29	**0.08**	-0.33	0.46	0.54	
MAE		0.51	<u>0.68</u>	0.49	0.51	0.51	0.47	0.44	**0.25**	0.32	0.35	0.35	0.33	0.46	0.54	
MPE		-16.5	16.7	-9.5	-16.7	-10.2	3.5	4.1	**-0.8**	-13.6	-20.0	5.1	-18.2	17.3	<u>23.6</u>	
MAPE		36.6	25.3	33.6	<u>37.3</u>	34.0	23.9	21.3	**9.2**	16.4	22.0	11.2	18.2	17.3	23.6	
TME		**-0.07**	0.50	0.17	0.09	0.17	0.42	0.38	0.38	0.21	0.11	0.38	0.10	0.53	<u>0.63</u>	
TMAE		**0.26**	0.52	0.30	0.29	0.31	0.45	0.47	0.51	0.43	0.39	0.47	0.42	0.53	<u>0.63</u>	
TMPE		-4.7	10.2	1.7	-0.6	1.5	8.3	7.3	12.1	2.1	-0.6	7.7	**0.3**	13.2	<u>15.9</u>	
TMAPE		9.4	11.6	**8.9**	9.2	9.2	10.8	11.2	<u>16.6</u>	10.1	9.9	10.8	10.3	13.2	15.9	
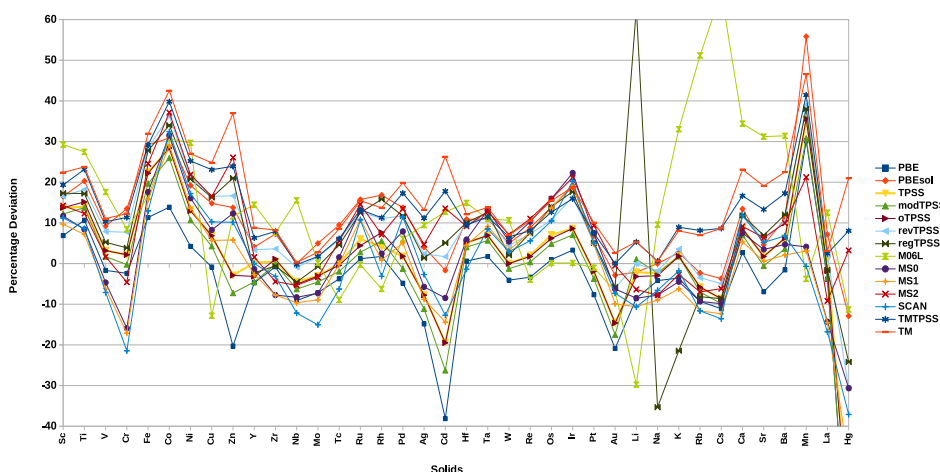
Figure 3.6: Histograms of relative error in cohesive energies (in %) are presented. The numbering of the figures are as the order of the solids presented in Table 3.7.

ence in the performance of PBE and PBEsol indicates that PBE is better functional than PBEsol for the atomization energies.

Concerning the next level of approximation and overall consideration, we observe more deviation from TM functional than the SCAN. The SCAN functional quite closely follows the "MS" functionals. While we observe that initially developed meta-GGA like different variant of TPSS functional works better in this case.
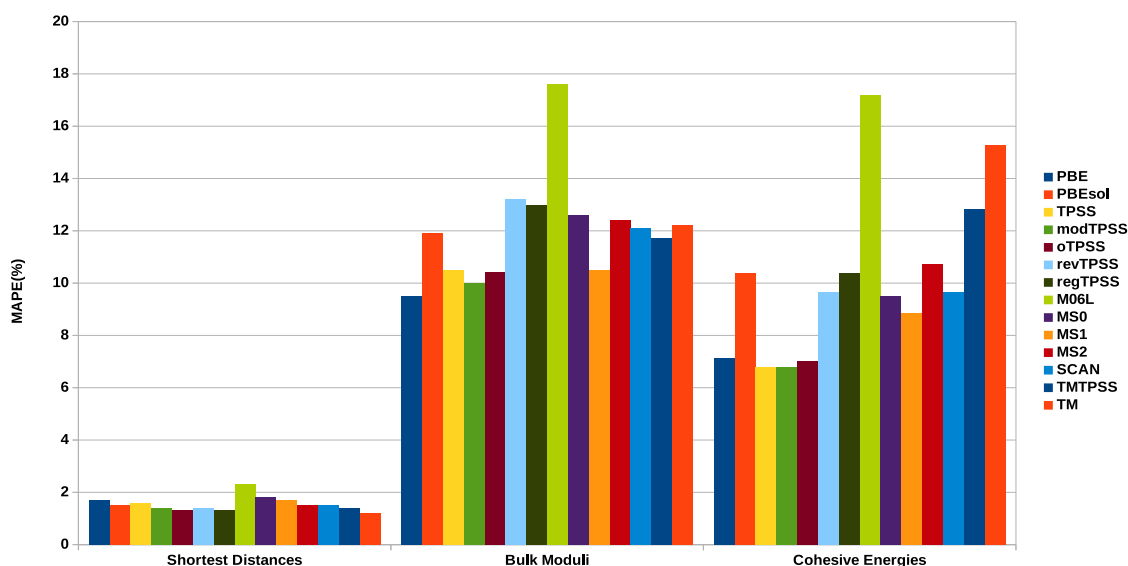
Figure 3.7: Overall statistics and conformal ranking of different methods for the structural and energetic properties of the considered solids (excluding Mn, La and Hg).

Table 3.8: Shown in the tabular form of the overall statistics and conformal ranking of different methods for the structural and energetic properties of the considered solids (excluding Mn, La and Hg).

		PBE	PBEsol	TPSS	modTPSS	oTPSS	revTPSS	regTPSS	M06L	MS0	MS1	MS2	SCAN	TMTPSS	TM
Inter-atomic distances	ME	3.5	-0.6	3.0	<u>3.6</u>	2.5	0.8	1.0	-1.9	2.4	2.6	0.9	1.1	0.7	**-0.1**
	MAE	5.2	4.2	4.8	4.7	4.3	4.1	4.1	<u>8.0</u>	5.9	5.6	4.5	4.5	4.1	**3.6**
	MPE	<u>1.2</u>	-0.2	0.8	1.0	0.8	0.1	0.2	-0.2	0.5	0.5	0.1	0.2	0.3	**0.0**
	MAPE	1.7	1.5	1.6	1.4	1.3	1.4	1.3	2.3	<u>1.8</u>	1.7	1.5	1.5	1.4	**1.2**
	rank	6	4	5	3	2	3	2	<u>8</u>	7	6	4	4	3	1
Bulk moduli	ME	**0.5**	<u>19.2</u>	10.1	7.2	9.5	18.8	17.8	0.7	17.9	14.7	17.6	13.8	14.6	17.8
	MAE	14.2	<u>20.1</u>	14.2	**12.9**	13.7	19.8	18.8	19.0	19.9	16.9	19.0	19.1	17.8	19.4
	MPE	**-0.5**	10.5	5.1	3.4	4.7	10.0	9.0	8.5	8.4	5.0	9.1	6.5	9.8	<u>11.0</u>
	MAPE	**9.5**	11.9	10.5	10.0	10.4	13.2	13.0	<u>17.6</u>	12.6	10.5	12.4	12.1	11.7	12.2
	rank	**1**	6	4	2	3	12	11	<u>13</u>	10	4	9	7	5	8
Cohesive energies	ME	**-0.08**	0.49	0.17	0.09	0.17	0.43	0.39	0.40	0.24	0.15	0.40	0.13	0.54	<u>0.63</u>
	MAE	**0.24**	0.50	0.28	0.27	0.29	0.45	0.46	0.54	0.44	0.39	0.49	0.42	0.54	<u>0.63</u>
	MPE	-3.73	9.65	2.61	0.75	2.50	8.67	7.58	13.19	3.47	**1.10**	7.97	1.86	12.81	<u>15.27</u>
	MAPE	7.12	10.37	**6.80**	**6.80**	7.02	9.65	10.38	<u>17.18</u>	9.51	8.84	10.72	9.67	12.83	15.27
	rank	3	8	**1**	**1**	2	6	9	<u>13</u>	5	4	10	7	11	12
	ave rank	3.3	6.0	3.3	**2.0**	2.3	7.0	7.3	<u>11.3</u>	7.3	4.7	7.7	6.0	6.3	7.0

To encapsulate the overall performance of the different methods and overall statistical we analysis our results in Table 3.8 and plotted it in Fig. 3.7. Regarding the recent popular functionals like SCAN and TM, those improves over the GGA functional over the inter-atomic lattice constants but remain difficult for other properties. Whereas, overall PBE is a good functional for metals.

3.6   Conclusions

This chapter assess the performance of various proposed semilocal XC functionals for the solid-state structural and energetic properties. Let summarize the contents of this chapter.

In the first part of this chapter, solid-state performance of the TM and TMTPSS functionals are assessed by implementing those in the the VASP code. The TMTPSS and TM functionals perform quite accurately for various solid-state properties and both are as accurate as the popular functional like SCAN. However, the SCAN performs well than TM based functional in predicting bandgaps. This improved behavior of the SCAN is due to the satisfaction of the several quantum mechanical constants.

Next, the semilocal functional performance are assessed for the structural and energetic properties of simple and transition metals. From the performance of several semilocal functional one can conclude that though the recent meta-GGAs like SCAN and TM improve the performance of the lattice constants of those solids, the PBE is quite a good

functional for overall performance.

Chapter 4

Range-Separated Hybrid Functional from Semilocal Exchange Hole

This chapter will focus on the construct and benchmark of screened hybrid functional for the molecular systems using the exchange hole of the Tao-Mo exchange-correlation functional. This chapter is based on the following research outcomes

(i) Subrata Jana, Bikash Patra, Hemanadhan Myneni and Prasanjit Samal, Chem. Phys. Lett. Vol. 713, Pages 1-9, (2018).

(ii) Subrata Jana and Prasanjit Samal, Phys. Chem. Chem. Phys., 20, 8999-9005 (2018).

4.1 Introduction

As discussed in chapter 3, the semilocal functionals are quite accurate in describing several molecular and solid-state physics. In spite of the success, the semilocal functionals often fail to predict the excited state properties of molecules and solids. This is due to the absence of non-locality in the construction of semilocal exchange-correction (XC) functionals [48, 144, 259–271]. Later on, the non-locality information are included through the Hartree-Fock (HF) exact exchange into the density functional approximations (i) either globally (global hybrid functional) [90–94, 149, 154, 169, 272–298] or (ii) in the

short or long-range scheme (SR or LR) (range-separated hybrid functional) [34, 38, 262, 268, 299–321]. Though another class of hybrid, local hybrid functionals [322–331] are also proposed but these are not so popular in describing molecular properties. Range-separated hybrids are particularly interesting in DFT because of lesser (many-electron) self-interaction ((ME)SI) error which is also known as delocalization error. Functional with less MESI works better for molecular excitation energies, reaction barrier heights, Rydberg excitation, and solid-state bandgaps. In all these cases, the performance of range-separated hybrid functionals is particularly very appealing. Though the global hybrid functionals improved the performance of semilocal functionals for the atomization energies but not so appealing for other properties like: the dissociation curve, reaction barriers height, and properties associated with the fractional occupation numbers. In particular, the global hybrid functionals show $\sim a/\mathbf{r}$ behavior.Whereas, the range-separated hybrid functionals show correct asymptotic behavior.

Concerning the underlying construction of the range-separated (RS) hybrid functionals, it relies on the construction of the exchange hole (details will be provided later in this chapter). Concept of the exchange hole already discussed in the previous two chapters. The exchange hole coupled with the error function separates the Coulomb operator into the long- and SR parts. Therefore, it is important to know the construction of the exchange hole. The exchange hole can be constructed in several ways. It can be constructed from the Taylor series expansion technique [140], or reverse engineered way [306, 314, 332, 333], or density matrix expansion (DME) technique [35]. The reverse-engineered technique is proposed by reversing the exchange energy expression to construct the exchange hole. Note that the popular LR corrected LC-ωPBE [334] is proposed based on the reverse-engineered based exchange hole, . This technique has also been used to construct the screened hybrid functional for solids [95, 96]. Beyond all these propositions, the advanced DME technique is also proposed to construct the exchange hole and the exchange energy functional [35]. The construction of the DME based exchange hole is described in chapter 3. Based on this exchange hole, a meta-generalized gradient approximation (meta-GGA) level LR corrected hybrid functional is proposed [34]. This chapter focuses on the behavior of the proposed LR corrected functional in the context of problems re-

lating to the many-electron self-interaction (MESI) error [48, 144, 260–271]. Not only that, a screened hybrid functionals is also constructed using HF in the SR and semilocal functional in the LR.

In the first part of this chapter, we assess the performance of the LR corrected functional for studying the fractional occupation number, dissociation curve, its connection to fractional occupation number as well as thermodynamic properties. A comparison of the DME based RS functional with other popular functionals can be found in ref. [34], which is not the main focus of this thesis. Regarding the second part of this chapter, a screened RS hybrid functional is proposed for solids. The proposed functional is analogous to that of the popular RS hybrid functional as proposed by Heyd-Scuseria-Ernzerhof (HSE) [335].

4.2   Long-range Corrected Hybrid Functional Schemes

The electronic ground state in the density functional theory is given by,

$$E^{DFT}[\rho] = \sum_i n_i \langle \psi_i | -\frac{1}{2}\nabla^2 | \psi_i \rangle + \int \rho(\mathbf{r}) v_{ext}(\mathbf{r}) d\mathbf{r} + J[\rho] + E_{xc}[\rho], \qquad (4.1)$$

where

$$J[\rho] = \frac{1}{2} \int \int \frac{\rho(\mathbf{r})\rho(\mathbf{r}')}{|\mathbf{r}-\mathbf{r}'|} d\mathbf{r} d\mathbf{r}' \qquad (4.2)$$

is the Hartree, $E_{xc}[\rho]$ is the exchange-correlation (XC) energy functional and n_i is the occupation of the ith Kohn-Sham (KS) orbital. The main challenge of KS DFT is to construct the XC functional because all the terms in Eq.(4.16) except XC are known exactly. As shown in the previous chapter, the exchange energy can be formulated from the exchange hole as,

$$E_x[\rho] = \frac{1}{2} \int d^3r \, \rho(\mathbf{r}) \int d^3u \frac{\rho_x(\mathbf{r}, \mathbf{r}+\mathbf{u})}{u} \; . \qquad (4.3)$$

This equation is the starting point to understand the construction of the RS hybrid functionals in DFT. Utilizing the local density approximation (LDA) based exchange hole,

Savin [336, 337] suggested a LR exchange correction scheme as,

$$\frac{1}{u} = \underbrace{\frac{\alpha + \beta erf(\mu u)}{u}}_{LR} + \underbrace{\frac{1 - [\alpha + \beta erf(\mu u)]}{u}}_{SR} , \tag{4.4}$$

where the parameters μ, α and β control the amount of SR part of the density functional approximations (DFA) and LR part of the HF exchange. Here, μ is the RS parameter that controls the amount of (LR/SR) HF to be mixed with the (SR/LR) semilocal approximation. Using the above decomposition, the short and LR parts of exchange functional become,

$$E_x^{SR} = -\frac{1}{2} \int d^3r \rho(\mathbf{r}) \int \frac{1 - erf(\mu u)}{u} \rho_x(\mathbf{r}, \mathbf{r} + \mathbf{u}) \, d^3u, \tag{4.5}$$

and

$$E_x^{LR} = -\frac{1}{2} \int d^3r \rho(\mathbf{r}) \int \frac{erf(\mu u)}{u} \rho_x(\mathbf{r}, \mathbf{r} + \mathbf{u}) \, d^3u \tag{4.6}$$

respectively. Note that using the spin-polarized counterpart of the exchange hole from spin-unpolarized version can be evaluated using the spin-scaling relation,

$$\rho_x[\rho_\uparrow, \rho_\downarrow] = \frac{\rho_\uparrow}{\rho} \rho_x[2\rho_\uparrow] + \frac{\rho_\downarrow}{\rho} \rho_x[2\rho_\downarrow]. \tag{4.7}$$

In the LC scheme, Eq.(4.5) is used to construct the SR part of the RS hybrid functional and the LR HF is given by,

$$E_x^{LR} = -\frac{1}{2} \sum_\sigma \sum_i^{occ} \sum_j^{occ} \int \int \psi_{i\sigma}(\mathbf{r}_1)\psi_{j\sigma}^*(\mathbf{r}_2) \frac{erf(\mu r_{12})}{r_{12}} \psi_{j\sigma}(\mathbf{r_1})\psi_{i\sigma}(\mathbf{r}_2) d^3r_1 \, d^3r_2 , \tag{4.8}$$

where ψ's are the spin-dependent molecular orbitals. The first and most obvious step towards the development of the SR semilocal functional having the following form,

$$E_x^{SR} = -\frac{1}{2} \int \rho(\mathbf{r})\epsilon_x^{unif}(\mathbf{r})\left\{1 - \frac{8}{3}a\left(\sqrt{\pi} \, erf(\frac{1}{2a}) + (2a - 4a^3)e^{-\frac{1}{4a^2}} - 3a + 4a^3\right)\right\} d^3r . \tag{4.9}$$

It is based on LDA exchange hole, where $a = \frac{\mu}{2k_F}$. However, this scheme does not incorporate the inhomogeneity of the system due to the absence of gradient-dependent terms.

Later, Iikura-Tsuneda-Yanai-Hirao (ITYH) [338] incorporate the gradient dependent term inside this scheme through the momentum vector $k_F \to k^{GGA}$, where k^{GGA} is the GGA exchange energy functional induced modified inhomogeneous wave vector,

$$k^{GGA} = \frac{k_F}{\sqrt{F_x^{GGA}(s)}} \, , \tag{4.10}$$

where F_x^{GGA} is the GGA enhancement factor. Using this form, the ITYH SR semilocal functional becomes,

$$E_x^{SR} \approx -\frac{1}{2} \int \rho(\mathbf{r}) \epsilon_x^{unif}(\mathbf{r}) \left\{ 1 - \frac{8}{3} a \left(\sqrt{\pi} \, erf(\frac{1}{2a}) + (2a - 4a^3) e^{-\frac{1}{4a^2}} - 3a + 4a^3 \right) \right\} F_x^{GGA} \, d^3r \, , \tag{4.11}$$

where the new $a = \frac{\mu}{2k^{GGA}}$. This simple modification in the ITHY model, when combined with B88 exchange, produces very promising results. The resultant functional based on the ITHY model is known as "coulomb attenuating method (CAM)" based functional. It combines the quality of the global hybrid B3LYP and additionally, it improves the LR correction by involving the HF exact exchange. The resultant functional is known as CAM-B3LYP [302]. Several other modifications of the CAM-B3LYP are also suggested and proposed [262, 268, 339] such as: CAM-QTP functionals [268, 339] In general, the XC functional of "CAM" type functionals is written as,

$$E_{xc}^{CAM} = [1 - (\alpha + \beta)] E_x^{DFA} + \alpha E_x^{HF} + \beta (E_x^{SR,DFA}(\mu) + E_x^{LR,HF}(\mu)) + \gamma E_c^{LYP}$$
$$+ (1 - \gamma) E_c^{VWN5} + \delta E_x^{DFA} \, , \tag{4.12}$$

where the central task of Eq.(4.12) is to construct $E_x^{SR,DFA}(\mu)$. In the "CAM" type functionals, the ITHY scheme is used to construct $E_x^{SR,DFA}(\mu)$ and the $E_x^{LR,HF}(\mu)$ is the HF LR part.

Besides the ITHY scheme, the extension of the screened Coulomb potential scheme of Heyd, Scuseria, and Ernzerhof [95, 96] has been utilized in the LC scheme to construct the LC functional based on the reverse-engineered system averaged exchange hole of PBE

functional [306, 308]. The resultant LC functional is known as LC-ωPBE which is quite a good functional for barrier heights.

4.2.1   Semilocal exchange hole based RS hybrids

In this section, we will describe the mathematical formulation of the meta-GGA level LC functionals based on the spherical averaged DME based exchange hole of Tao-Mo [35]. Though the work involving the construction of the functional [34] is not part of this thesis, yet it is necessary to understand the functional construction.Based on the DME exchange hole the semilocal SR part of the meta-GGA RS hybrid functional becomes [34],

$$
\begin{aligned}
E_x^{SR,DME} = -\int \rho \epsilon_x^{unif} \Big[\frac{1}{f^2} \Big\{ 1 &- \frac{8}{3}a\Big(\sqrt{\pi}erf(\frac{1}{2a}) + (2a - 4a^3)e^{-\frac{1}{4a^2}} - 3a + 4a^3 \Big)\Big\} \\
&+ \frac{7\mathcal{L}}{9f^4}\Big\{ 1 + 24a^2\Big((20a^2 - 64a^4)e^{-\frac{1}{4a^2}} - 3 - 36a^2 + 64a^4 + 10\sqrt{\pi}erf(\frac{1}{2a})\Big)\Big\} \\
&+ \frac{245\mathcal{M}}{54f^4}\Big\{ 1 + \frac{8}{7}a\Big((-8a + 256a^3 - 576a^5 + 3849a^7 - 122880a^9)e^{-\frac{1}{4a^2}} \\
&+ 24a^3(-35 + 224a^2 - 1440a^4 + 5120a^6) + 2\sqrt{\pi}(-2 + 60a^2)erf(\frac{1}{2a})\Big)\Big\}\Big] d^3r,
\end{aligned}
\tag{4.13}
$$

where $\epsilon_x^{unif} = \frac{9\pi\rho}{4k_f^2}$, $f = [1 + 10(70y/27) + \beta y^2]^{1/10}$, $\mathcal{L} = [3(\lambda^2 - \lambda + 1/2)(\tau - \tau^{unif} - |\nabla n|^2/72n) - (\tau - \tau^{unif}) + \frac{7}{18}(2\lambda - 1)^2\frac{|\nabla\rho|^2}{\rho}]/\tau^{unif}$, $\mathcal{M} = (2\lambda - 1)^2 \, p$, $a = \frac{\mu}{2fk_f}$, $k_f = (3\pi^2\rho)^{\frac{1}{3}}$, $\tau^{unif} = \frac{3}{10}k_f^2\rho$, $y = (2\lambda - 1)^2 \, p$ and $p = \frac{|\nabla\rho|^2}{(2k_f\rho)^2}$. The Eq.(4.13) is derived using the DME based exchange hole of TM [35] coupled with Eq.(4.5). For LR the HF exchange of Eq.(4.8) is used. The functional is named as LC-TM as it is designed using TM (only DME exchange hole) exchange hole expansion. Combining all the SR and LR parts, exchange part of LC-TM hybrid functional becomes [34],

$$
E_{xc}^{LC-TM} = E_x^{SR,DME}[\rho, \nabla\rho, \tau] + E_x^{LR,HF} \, .
\tag{4.14}
$$

The λ and β values are fixed as prescribed in the TM functional [35] i.e., $\lambda = 0.6866$ and $\beta = 79.873$. This completes the exchange part of the LC-TM functional. For the

correlation, the LYP [36] correlation is used. However, in the original TM approach, the Tao-Perdew-Staravarov-Scuseria (TPSS) [84] based correlation is used.

Note that use of TPSS correlation with the present proposed exchange the MAE of AE6 molecules becomes 12.27 kcal/mol, 11.45 kcal/mol, 10.91 kcal/mol, 10.60 kcal/mol with $\mu = 0.30$ bohr^{-1}, $\mu = 0.33$ bohr^{-1}, $\mu = 0.35$ bohr^{-1} and $\mu = 0.40$ bohr^{-1} respectively. Therefore, with LC-TM exchange and LYP correlation, the proposed LR corrected RS functional becomes,

$$E_{xc}^{LC-TMLYP} = E_{xc}^{LC-TM}[\rho, \nabla\rho, \tau] + E_x^{LR,HF} + E_c^{LYP} \,. \qquad (4.15)$$

Concerning the range-separation parameter, it will be fixed in the next section.

In this chapter, we focus on the MESI related problems of LC-TMLYP along with the BLYP, B3LYP, LC-BLYP, CAM-B3LYP, rCAM-B3LYP, CAM-QTP00, CAM-QTP01 functionals.

4.2.2   Fixing the range-separation parameter (μ)

It is well known that in RS hybrid functional theory, it is customary to tune the RS parameter related to the properties of the system. In thermochemistry, one always chooses atomization energies (AE6) and barrier heights (BH6) [340] because those represents the whole thermochemical test set related to the atomization energies and barrier height. In this case, also, we fix the LC-TMLYP μ value by tuning it with respect to the AE6 test set [341]. Here, the AE6 geometries are taken from [342–344]. In Fig. 4.1, the MAE of the LC-TMLYP functional is plotted for different μ values which results $\mu = 0.28$ bohr^{-1} for the present functional.

In Table 4.1, the values of different RS parameters for the exchange and correlation are also presented. In Table 4.2, the MAE of AE6 molecules for BLYP, B3LYP, LC-BLYP, CAM-B3LYP, rCAM-B3LYP, CAM-QTP00, and CAM-QTP01 functionals along with LC-TMLYP are summarized. From the results of the Table 4.2, it is evident that LC-TMLYP is a promising candidate for AE6.
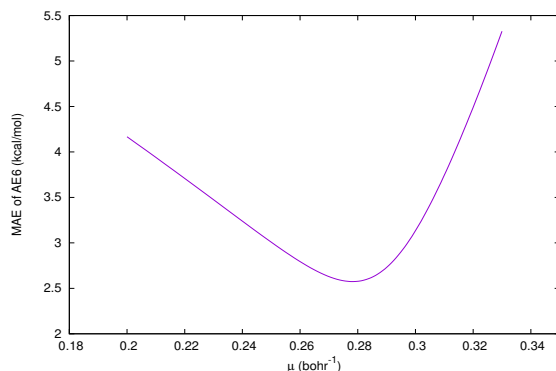
Figure 4.1: Variation of the MAE of the AE6 set for LC-TMLYP with different values of μ.

Table 4.1: Different parameters used in the considered functionals. The μ parameter is in bohr^{-1} unit.

Name	Exchange				Correlation
	α	β	μ	δ	γ
CAM-B3LYP	0.19	0.46	0.33	0.0	0.81
rCAM-B3LYP	0.18352	0.94979	0.33	0.13590	1.0
LC-BLYP	0.0	1.0	0.33	0.0	1.0
CAM-QTP00	0.54	0.37	0.29	0.0	0.80
CAM-QTP01	0.23	0.77	0.31	0.0	0.80
LC-TMLYP	0.0	1.0	0.28	0.0	1.0

4.2.3 Understanding one, many-electron Self-Interaction error, and fractional occupation related problems in DFT

As the present chapter deals with the MESI related problems of the LC-TMLYP functional, a clear understanding of the one-electron and many-electron self-interaction error (SIE) is necessary. In DFT, SIE is one of the foremost problems that hinder the accuracy level of DFT. To understand the SIE problem, the most commonly used example is the potential energy of H_2^+ for which the density functional approximations (DFA) show unphysical results. As H_2^+ molecule has one-electron, in the large separation of two atoms, each atom should share half of the electron whose description is beyond the limit of commonly used DFA. Lets us start with the one-electron self-interaction problem. The one-electron SIE can be understood as the non-vanishing of the Hartree and XC energy

Table 4.2: AE6 atomization energies (in kcal/mol) as obtained using different functionals. The reference CCSD(T) values are taken from ref. [34]

Molecules	BLYP	LC-BLYP	B3LYP	CAM-B3LYP	rCAM-B3LYP	CAM-QTP00	CAM-QTP01	LC-TMLYP	CCSD(T)
SiH_4	317.17	324.91	323.36	325.02	324.52	329.12	328.13	323.28	324.59
SiO	194.51	202.58	187.16	188.00	189.09	172.39	189.67	187.3	192.36
S_2	35.42	106.92	102.8	99.99	97.41	91.99	100.43	97.33	103.11
C_3H_4	700.95	726.97	702.28	704.72	704.86	691.57	713.27	701.81	701.36
$C_2H_2O_2$	641.41	672.89	631.93	635.46	637.98	604.59	644.34	632.98	632.36
C_4H_8	1130.45	1184.92	1141.80	1150.42	1154.76	1141.74	1169.15	1145.09	1145.23
MAE	16.92	20.03	1.92	3.26	4.61	12.78	9.45	2.23	–

functional for one electron system. Now, in the HF theory framework one can write

$$J[\rho_i] + E_{xc}[\rho_i, 0] = 0 . \tag{4.16}$$

In DFA, the XC only partially cancel the Hartree energy. Therefore, a spurious self-interaction error remains. Now, splitting the E_{xc} into exchange and correlation parts, Eq.(4.16) reduced to,

$$
\begin{aligned}
J[\rho_i] + E_x[\rho_i, 0] &= 0 , \\
E_c[\rho_i, 0] &= 0 .
\end{aligned}
\tag{4.17}
$$

The above one-electron self-interaction free conditions for exchange and correlation are not fully satisfied by the LSDA, GGA, and meta-GGA functionals. But the meta-GGA functionals satisfy the self-interaction free correlation condition.

Concerning the "many-electron self-interaction (MESI) error", it is most commonly used in modern density functional theory [48, 144, 260–271]. In fact, the MESI error is considered as a generalization of one-electron SIE. Generally speaking, the MESI error is also a SIE but occurs in the many-electron systems. There is no compact definition of the MESI in DFT community. However, the one-electron SIE which is conventionally defined through the definition of Eq.(4.16) is very difficult to quantify in case of many electrons. In earlier reported work [48, 144, 260–271], the MESI error is quantified as the inability of describing the straight line behavior in case of fractional particle (occupation) number.

Therefore, the MESI error is related to systems, where the electron number (N) of the system can fluctuate between integers. Perdew et. al. [48] showing that in exact DFT, one can obtain the exact straight line with derivative discontinuity (Δ_{xc}) showing at each integer number. The straight line in the case of the molecular system actually indicates that the HOMO and LUMO energies of fluctuating electron system should remain constant at orbital energies of highest orbital energy ($-\epsilon_H$) and lowest orbital energy ($-\epsilon_L$). But this is not the case for DFA. This is due to the delocalization of the highest occupied (or lowest unoccupied) electron. The MESI problem hinders various chemical processes especially in describing the transition states of the reactions barriers. It has been observed that DFA are delocalized (or convex in nature) while the HF is highly localized (concave in nature). As a solution to the delocalization and localization problems within DFA and HF, it has been suggested to mix the DFA with HF. This results to several global and RS hybrids, which mix the HF exchange with density functional exchange either globally or in the RS scheme.

The terminology fractional occupation number (q) is often encountered in DFT. In principle, the MESI error of a functional can be understood based on the fractional occupation number of a system. The example we discussed in this section (dissociation of H_2^+ molecule) to encapsulate the SIE problem is also related to the fractional occupation number. Thus, changing the frontier orbital occupation fractionally one can study the MESI problem. However, before going into the formal example of a system, lets first understand the fractional occupation number from the perspective of Janak's theorem [57]. According to this theorem,

$$\frac{\partial E}{\partial n_{i,\sigma}} = \epsilon_{i,\sigma} \ , \tag{4.18}$$

where $\epsilon_{i,\sigma}$ is the ith energy eigenvalue. A more general form of Janak's theorem has been adopted using generalized Kohn-Sham scheme (GKS) [56], where it is shown that for a fixed configuration (potential), the energy becomes stationary with respect to the potential. Hence, only the the fractional change ($\delta n_{i=f} = q$) of the frontier level occupation $n_{i=f}$ physically important i.e.,

$$\frac{\partial E_v}{\partial N} = \left(\frac{\partial E_v}{\partial n_{i=f}} \right)_v = \epsilon_{i=f,\sigma} \ , \tag{4.19}$$

where $n_f = n_{LUMO}$ if one fill up the lowest unoccupied orbital ($q = \delta N > 0$) and $n_f = n_{HOMO}$ if one remove particles from the highest occupied orbital ($q < 0$). Upon using the above expression, the total energy becomes,

$$E(N_0 + q) = (1 - q)E(N_0) + qE(N_0 + 1) \quad 0 \leq q \leq 1 \tag{4.20}$$

and

$$E(N_0 + q) = (1 + q)E(N_0) - qE(N_0 - 1) \quad -1 \leq q \leq 0 \,, \tag{4.21}$$

where Eq.(4.20) and Eq.(4.21) corresponds to addition and removal of the fraction of particle 'q' respectively. This expression will be used in the next section to calculate the energies of the fractionally occupied systems. It has been shown that the exact density functional is piecewise linear in between two integer [48]. But in reality, the DFA fails to achieve the piece-wise linearity and predict wrong energy for fractional occupation due to lack of non-locality. Whereas, the HF exact exchange is highly localized due to the lack of correlation.

4.2.4 Performance of LC-TMLYP in MESI related problems

Computational Setup: All the computational results are obtained using the NWChem [99] code with Gaussian-type basis set. Regarding the details of the basis set, it is defined more explicitly in the results and discussions section for different calculations along with the test sets. Our test cases includes (i) fractional occupation number related problem of C atom, (ii) dissociation curve of H_2^+, and H_2 molecules, and (iii) fractional occupation number and the dissociation limit of LiF molecule.

4.2.4.1 Functional performance for atom with fractional occupation

Firstly, we consider the performance of XC functionals on the fractional occupation number in atoms. To encapsulate the fractional occupation number problem, C atom is considered as an example. The behavior of different functionals is demonstrated in Fig. 4.2. Here, we vary the particle number of the highest occupied level fractionally in steps of
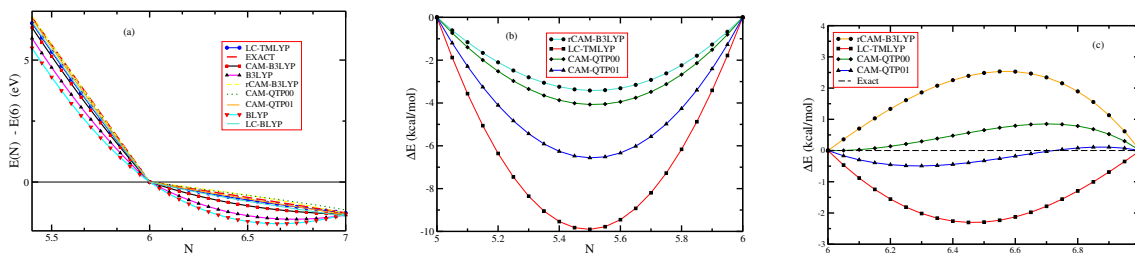
Figure 4.2: (a) The deviation of different functionals from exact straight line behavior in case of C atom. In Fig. (b) $-1 \leq q \leq 0$ and (c) $0 \leq q \leq 1$ the deviation of considered functionals are shown from the exact behavior.

0.05 ($= q$=fractional particle number). The exact straight lines corresponds to the experimental ionization potential (IP) energy (In between $5 \leq N < 6$) and electron affinity (EA) (In between $6 < N \leq 7$).

In our demonstration, BLYP is the only semilocal functional. Being a semilocal functional BLYP functional includes inherent delocalization error which shows the piecewise convexity during the change in the fractional particle number. But, this piecewise convexity becomes close to the exact upon mixing the fraction of HF. Therefore, we observe an error minimization in the performance of the rCAM-B3LYP, LC-TMLYP, LC-BLYP, CAM-QTP00 and CAM-QTP01 functionals. The LC-BLYP also shows significant improvement in the fractional particle number curve compared to the BLYP. It is noticeable that the CAM-B3LYP also shows significant improvement compared to the B3LYP. Further improvement in the fractional occupation curve is obtained with rCAM-B3LYP, CAM-QTP00, and CAM-QTP01 functionals because all these functionals are further improved to to reduce the delocalization error of CAM-BLYP. However, in this case of the meta-GGA RS hybrid LC-TMLYPit is quite close to the exact straight in the range $6 < N \leq 7$. In this region, CAM-QTP00, and CAM-QTP01 perform better than rCAM-B3LYP which is slightly localized. In Fig. 4.2b and Fig. 4.2c we plotted the behavior of the different functionals for the fractional occupation number of the C atom. Here, the
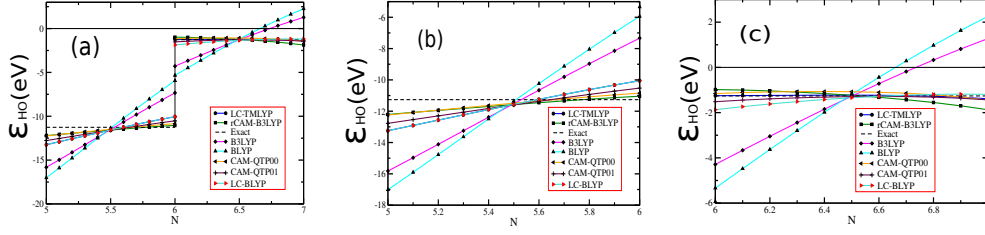
Figure 4.3: Shown is the highest occupied energy of C atom as a function of electron number N. Exact ε_{HO} is obtained from -IP and -EA. The $6-311++(3df, 3pd)$ basis set is used.

ΔE is calculated using the following expression,

$$\begin{aligned} \Delta E_{q \ni [0,1]} &= E(N_0 + q) - [(1-q)E(N_0) + qE(N_0 + 1)] , \\ \Delta E_{q \ni [-1,0]} &= E(N_0 + q) - [(1+q)E(N_0) - qE(N_0 - 1)] . \end{aligned}$$

(4.22)

In Fig. 4.2b and Fig. 4.2c we plot only those functionals which are close to the exact straight line behavior.

In Fig. 4.4, the nature of the highest occupied orbital energy (ε_{HO}) of C atom is shown with the occupation number variation. Form there it is obvious that the BLYP and B3LYP are not stable for C^- because these functionals show positive ε_{HO} value.

4.2.4.2 Dissociation energy curve of H_2^+ and H_2

Getting exact behavior of the dissociation energy curve of H_2^+ and H_2 is also a challenge of the semilocal DFT. But mixing the HF exchange with DFA improves the dissociation curve. The RS hybrid functionals show improvement for the H_2^+ molecule dissociation curve compared to the global hybrids. In the large distance of separation of the H_2^+ molecule ($R = 10$ Å), fractional occupation electron in each part exists (0.5), which can not be described within the semilocal density functionals. As shown in Fig. 4.4a, the semilocal BLYP deviates most from the HF dissociation curve, while from B3LYP we observe improvement over BLYP. But, the most interesting improvement is observed for
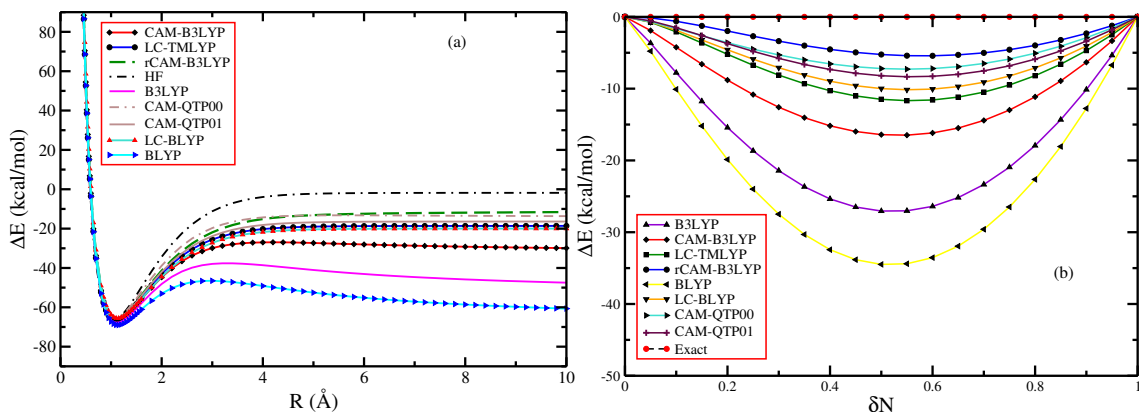
Figure 4.4: (a) Dissociation limit of the H_2^+ molecule and (b) deviation from its of exact behavior for H atom.

the RS hybrid functionals.

To predict the accuracy of functionals, in Fig. 4.4b we also calculate the energy deviation of the different functionals for the fractional occupation number of H atom using the formula,

$$\Delta E = E(N + q) - [(1 - q)E(N) + qE(N + 1)] . \tag{4.23}$$

From Fig. 4.4b, it is observed that the proposed LC-TMLYP shows improvement over other LR corrected hybrid functionals.

4.2.4.3   Fractional occupation number related problem for molecules

To quantify the functional performance for the fractional occupation number related problem for molecules we consider the dissociation energy curve of the LiF molecule. The dissociation energies in this case is measured by using the formula $\Delta E = Li^{+q} + F^{-q} - (Li + F)$, where q is the fractional electron flows from Li to F atom during the dissociation.

In Fig. 4.5, the performance considered functional are shown. Interestingly the semilocal functional show quite a good performance for the integer particle number deviate more for fractional occupation number because of the MESI error. However, the improved performance is observed in the case of RS hybrid functional.
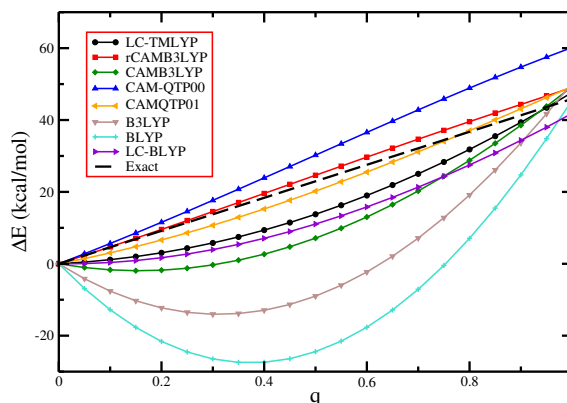
Figure 4.5: The dissociation limit of LiF molecule is shown for fractional occupation number.

4.2.4.4　Performance in thermochemistry

The thermochemical accuracy of the LC-TMLYP is measured with the Minnesota 2.0 data set [195] except for the atomization energies. The atomization energies are performed using the G$2/148$ molecular test set [342–344] where the geometries are optimized at the MP2 level theory. The present study is done using following thermochemical test sets: (i) Energies of 17 atoms (H$-$Cl) (AE17) [195], (ii) Atomization energies of 6 molecules (AE6) [195, 340], (iii) Atomization energy of 148 molecules (G$2 - 148$) (iv) $21 -$ ionization potentials (IP21) [195, 291, 297, 350–352], (v) 13 electron affinities (EA13) [195, 291, 297, 352], (vi) 8 proton affinities (PA8) [195, 353], (vii) 12 alkyl bond dissociation energies (ABDE12) [87, 195, 351, 354], (viii) 7 hydrocarbon chemistry (HC7) [160, 195], (ix) 13 thermochemistry of π systems (πTC13) [87, 195], (x) isomerization energies of 7 molecules [195, 355], (xi) HTBH38 - 38 hydrogen transfers barrier heights [195, 351, 356–358], (xii) NHTBH38 - 38 non-hydrogen transfers barrier heights [195, 351, 356–358], and (xiii) DC9 - 9 difficult cases [195]. All the calculations are performed using the $6 - 311 + +(3df, 3pd)$ basis set except for atoms and molecules having He as an element. In that case, aug-cc-pVQZ basis set is used because the $6 - 311 + +(3df, 3pd)$ basis set is not available for He. We summarize the results of all the functionals in Table 4.3.

Table 4.3 shows that the CAM-B3LYP performs well for atomic energies (AE17). However, we observe quite a good performance from LC-TMLYP functional also. For the atomization energies of the AE6 set, B3LYP performs quite well, but impressive performance is observed for the LC-TMLYP which shows the least MAE. It is also noticed that the rCAM-B3LYP and QTP functionals deviate more than LC-TMLYP functional. Considering other test set, LC-TMLYP is quite a good performer for the ionization poten-

Table 4.3: Performance of different methods for the different thermochemical test sets. The MAE (in kcal/mol) is shown here. All the calculations are performed in the NWChem code with the $6-311++G(3df, 3pd)$ basis set.

Method	BLYP	LC-BLYP	B3LYP[a]	CAM-B3LYP[b]	rCAM-B3LYP	CAM-QTP00	CAM-QTP01	LC-TMLYP
AE17	9.86	**81.25**	17.39	**7.65**	17.77	13.48	20.65	8.08
AE6	16.92	**20.03**	**1.92**	3.26	4.61	12.78	9.45	2.23
G2-148	10.94	**23.20**	4.31	4.33	5.41	14.16	9.89	**3.51**
IsoL6	**3.65**	**1.82**	2.54	2.03	2.27	2.03	2.03	2.18
IP21	4.38	7.39	5.29	4.56	9.08	**9.30**	8.74	**3.86**
EA13	2.56	2.56	2.22	1.96	**1.85**	**3.74**	1.93	2.82
PA8	1.62	**4.77**	**1.10**	1.37	2.79	1.54	2.42	1.16
ABDE12	11.51	3.04	9.67	6.63	3.41	7.77	**2.52**	**13.14**
HC7	**26.56**	10.33	15.93	**5.35**	8.77	9.16	9.58	8.81
πTC13	5.77	1.95	**5.77**	3.40	**1.39**	5.28	**1.79**	4.43
(N)HTBH76	**8.38**	5.39	5.79	2.99	**2.39**	2.97	2.85	2.66
DC9	27.07	**52.93**	20.81	**9.53**	16.98	30.33	23.35	14.44

[a] IP21, EA13, PA8, πTC13 and HC7 results of B3LYP are taken from ref. [38]
[b] All results except AE6 of CAM-B3LYP are taken from ref. [34]

the rCAM-B3LYP performs in a superior way compared to other functionals. For reaction barrier heights (hydrogen and non-hydrogen), the rCAM-B3LYP shows quite a impressive performance. Note that in this case the LC-TMLYP performs better than B3LYP and CAM-B3LYP which indicating the good features of the LC-TMLYP for both the atomization energies and barrier heights. Lastly, for the DC9 test set also we observe good performance from LC-TMLYP functional.

4.3   Screened Meta-GGA Hybrid Functional

The aim of this section is to construct a screened hybrid functional using the meta-GGA semilocal exchange hole and employing Hartree-Fock exchange in the SR along with LR semilocal functional. The motivation of the present construction is the same as that is proposed in the HSE06 functional but the meta-GGA level. To construct the present functional, we use the semilcal exchange hole of Tao-Mo functional [35] and its underlying construction which is used in the LR corrected functional as described in the previous section. The present functional form includes both the DME based localized exchange hole [35] and fourth-order gradient approximation [35]. To do so, we employ the slowly varying fourth order gradient approximation through the uniform electron gas exchange hole. The physical basis of the present construction will be described in the next section. This method is a pathway to construct a screened hybrid functional in the meta-GGA level for the condensed-matter systems which will be discussed in chapter 5.

4.3.1   Methods

We start with the general scheme for constructing the screened hybrid XC functional. Using the HF exact exchange (E_x^{HF}) the hybrid functionals are defined as,

$$E_{xc}^{hybrid} = aE_x^{HF} + (1-a)E_x^{SL} + E_c^{SL} , \qquad (4.24)$$

where E_x^{SL} and E_c^{SL} are the exchange and correlation energy functional in the semilocal approximation respectively. Here, a controls the HF percentage in the above functional

form. On the other hand, the screened hybrid functional based on the HSE06 functional has the following general form,

$$E_{xc} = aE_x^{HF-SR} + (1-a)E_x^{SL-SR} + E_x^{SL-LR} + E_c^{SL} \qquad (4.25)$$

which can also be written as,

$$E_{xc} = aE_x^{HF-SR} - aE_x^{SL-SR} + E_x^{SL} + E_c^{SL} . \qquad (4.26)$$

The Eq.(4.26) is obtained from Eq.(4.25), where we add the last two terms of Eq.(4.26) to construct the semilocal XC functional. The SR semilocal part of the above functional form is given by,

$$E_x^{SL-SR} = -\int \rho(\mathbf{r})\epsilon_x^{unif} \Big[wF_x^{DME-SR} + \Big\{ 1 - \frac{8}{3}\tilde{A}\Big(\sqrt{\pi}\,erf(\frac{1}{2\tilde{A}}) + (2\tilde{A} - 4\tilde{A}^3)e^{-\frac{1}{4\tilde{A}^2}} $$
$$-3\tilde{A} + 4\tilde{A}^3 \Big)\Big\}(1-w)F_x^{TM-sc} \Big] d^3r , $$
$$(4.27)$$

where, F_x^{DME-SR} is the exchange enhancement factor obtained from Eq.(4.13). In this semilocal SR, we also include the fourth-order gradient approximation through the LDA exchange hole of Eq.(4.11). However, F_x^{TM-sc} of Eq.(4.27) is originally given in ref. [35] having form,

$$F_x^{TM-sc} = \Big[1 + 10\Big\{\Big(\frac{10}{81} + \frac{50p}{729}\Big)p + \frac{146}{2025}\tilde{q}^2 - \Big(\frac{73\tilde{q}}{405}\Big)\Big[\frac{3\tau^w}{5\tau}\Big]\Big(1 - \frac{\tau^w}{\tau}\Big)\Big\}\Big]^{\frac{1}{10}} , \quad (4.28)$$

where $\epsilon_x^{unif} = \frac{3k_f}{4\pi}$ is the exchange energy per electron in the homogeneous electron gas approximation and the terms associated with the exchange enhancement factor are $f = [1 + 10(70y/27) + \beta y^2]^{1/10}$, $\mathcal{L} = [3(\lambda^2 - \lambda + 1/2)(\tau - \tau^{unif} - |\nabla\rho|^2/72n) - (\tau - \tau^{unif}) + \frac{7}{18}(2\lambda - 1)^2 \frac{|\nabla\rho|^2}{\rho}]/\tau^{unif}$, $\mathcal{M} = (2\lambda - 1)^2 p$, with $A = \frac{\mu}{2fk_f}$, $k_f = (3\pi^2\rho)^{\frac{1}{3}}$ (uniform Thomas-Fermi wave vector), $\tau^{unif} = \frac{3}{10}k_f^2\rho$ (uniform KE density), $p = \frac{|\nabla\rho|^2}{(2k_f\rho)^2}$, $y = (2\lambda - 1)^2 p$, $\tilde{A} = \frac{\mu}{2k_f}$, $\tilde{q} = \frac{3\tau}{2(3\pi^2)^{2/3}\rho^{5/3}} - \frac{9}{20} - \frac{p}{12}$, $\tau^w = |\nabla\rho|^2/8\rho$ and $w = $

$[(\tau^w/\tau)^2 + 3(\tau^w/\tau)^3]/[1 + (\tau^w/\tau)^3]^2$ (weight factor between the DME exchange energy and slowly varying density correction of TM functional). This completes the construction of the SR exchange enhancement factor.

Having discussed the semilocal SR exchange energy functional, now we focus on the correlation compatible with the newly constructed functional. For correlation part, the TPSS correlation is used [84] correlation is used. Note that the TM correlation with the present screened hybrid results to large error for the AE6. Now, regarding the parameter μ, it is fixed to 0.33 bohr^{-1}. Also, the mixing parameter, $a = 0.10$ is chosen for optimal performance of the atomization energies. The λ and β values remains the same as suggested in the case of TM functional [35], i.e., 0.6866 and 79.873. The present functional named as DME-sc-TPSSc as it is based on the DME based exchange hole coupled with slowly varying fourth-order gradient expansion (sc) and TPSS correlation.

4.3.2   Performance for atoms and molecules

The implementation of the DME-sc-TPSSc is done in the NWChem code [99] using the existing implementation of the LC-TMLYP exchange and TPSS correlation. All calculations of DME-sc-TPSSc are done self-consistently in NWChem code. The results of the DME-sc-TPSSc is also compared with the B3LYP, PBE0, TPSSh, and HSE06 functionals. Among all these functionals, the B3LYP, PBE0, and TPSSh are the global hybrids based on the B88, PBE, and TPSS semilocal exchange and compatible correlation for these exchange functionals. The HSE06 is a screened hybrid functional which uses the SR HF exchange. For the benchmark calculation we used the same test set that was considered for our previous calculation of the LC-TMLYP functional. The results are summarized in Table 4.4.

To start our analysis we consider the atomization energies of the AE6 and G2/148 test sets. The tabulated results present in Table 4.4 indicates, as usual, the B3LYP gives the smallest MAE both for the AE6 and G2 test set and it is not surprising because the B3LYP functional is accurate for the atomization energies. However, DME-sc-TPSSc is the second best functional for atomization energies benchmark with the MAE 4.008

Table 4.4: Shown is the errors (in kcal/mol) as obtained from different methods.

		B3LYP	PBE0	TPSSh	HSE06	DME-sc-TPSSc
		atomization energy (kcal/mol)				
AE6	MAE	2.7	5.8	6.3	6.7	5.7
G2/148	MAE	3.599	5.619	5.296	5.335	4.008
		ionization potential (eV)				
IP13	ME	-0.075	-0.107	-0.085	0.108	-0.010
	MAE	0.227	0.137	0.136	0.139	0.098
		electron affinity (eV)				
EA13	ME	-0.061	0.065	0.065	-0.068	0.145
	MAE	0.095	0.120	0.122	0.123	0.138
		proton affinity (eV)				
PA8	ME	-0.012	-0.052	-0.122	0.077	-0.137
	MAE	0.047	0.053	0.122	0.077	0.137
		alkyl bond dissociation energies (kcal/mol)				
ABDE12	ME	9.91	7.26	10.73	9.73	7.93
	MAE	9.91	7.26	10.73	9.73	7.93
		hydrocarbon chemistry (kcal/mol)				
HC7	ME	15.93	-5.34	5.69	0.14	2.24
	MAE	15.93	10.07	6.31	5.92	3.21
		isomerization energies (kcal/mol)				
ISOL6	ME	2.54	0.58	3.10	-1.12	2.42
	MAE	2.54	1.44	3.10	1.42	2.42
		thermochemistry of π systems (kcal/mol)				
πTC13	ME	-5.64	-5.80	-7.64	6.44	-7.93
	MAE	5.77	5.89	7.82	6.54	8.17
		barrier heights (kcal/mol)				
BH76	ME	2.81	2.12	4.88	1.46	3.55
	MAE	5.08	4.70	6.78	4.08	5.54

kcal/mol and 5.7 kcal/mol for the G2 and AE6 test set respectively. It is also noticeable that for the AE6 test set, the DME-sc-TPSSc performs better than the HSE06.

Next, the functional performance is measured for the IP, EA and PA of small molecules. We observe quite a good performance of the DME-sc-TPSSc for IP with smallest MAE
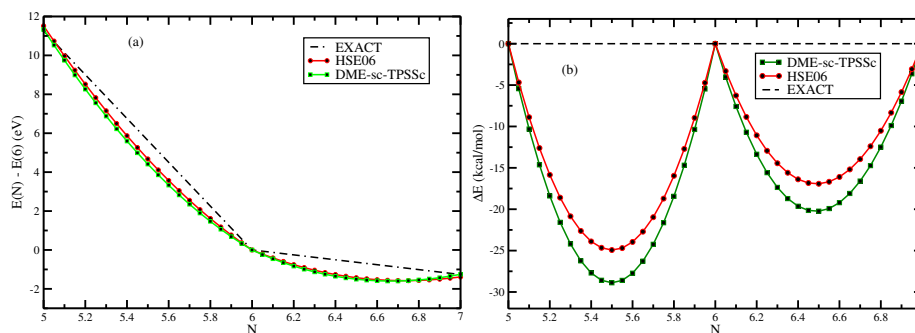
Figure 4.6: Shown are the deviation of the energy of HSE06 and DME-sc-TPSSc (a) for the fractional occupation number of C atom and (b) from the piece-wise linear extrapolation.

of 0.098 eV. Whereas, B3LYP performs well for the EA13 and PA8 test set.

For ABDE12 test set the PBE0 shows the best performance with MAE 7.268 kcal/mol. Next considering the thermochemistry of 7 hydrocarbons, the DME-sc-TPSSc outperforms other functionals with MAE 3.217 kcal/mol. For IsoL6 test set, the HSE06 achieves smallest MAE. Whereas, the DME-sc-TPSSc performs better than TPSSh meta-GGA functional. For systems with π bonds, the B3LYP achieves the smallest MAE with 5.776 kcal/mol.

As mentioned before, the accuracy of barrier heights are related to the self-interaction of the molecules in their transition states. Therefore, functionals with least MESI perform better for barrier heights. The hybrids and LR corrected hybrids show improved performance in this regard because of less MESI error. Here, we observe that the HSE06 gives the lowest MAE for the total 76 reaction barriers. The better performance of HSE06 than DME-sc-TPSSc is because the HSE06 includes more SR HF exchange in its SR part than DME-sc-TPSSc does.

Lastly, we focus on the performance of the HSE06 and DME-sc-TPSSc for the fractional electron occupation number of C atom. This example has been considered in our previous study of the LR corrected functional. In Fig. 4.6a, we have shown the deviation of the two functionals from the exact piecewise straight line behavior. The HSE06 mixes $1/4$ of the SR HF which is larger compared to the DME-sc-TPSSc SR HF mixing (10%), that is the why HSE06 performs better. This difference becomes more evident from Fig.

4.6b, where we plot in kcal/mol scale.

4.4 Conclusions

In the first part of this chapter, we investigate the performance of meta-GGA level hybrids LC-TMLYP for various MESI related problems of atoms and molecules, and tharmochemical accuracy. It has been shown that though the RS parameter of the LC-TMLYP is tuned with the AE6 molecular atomization energies, yet performs quite better for the IP, barrier heights, and MESI related problems. The interesting observation is that the LC-TMLYP performs better than CAM-B3LYP in MESI related problems by keeping the accuracy of the atomization energies. This is an interesting feature of the LC-TMLYP because in most of the functionals both the atomization energies and MESI related problems cannot be achieved simultaneously. It is evident from the rCAM-B3LYP and QTP functionals performance. The rCAM-B3LYP designed to reduce the MESI problem but it worsens the thermochemical accuracy. The QTP functionals are also not accurate for the atomization energies though those showing improvement in the MESI related problem. Strictly, speaking the LC-TMLYP gives a balanced description for both the atomization energies and the MESI related problems which is quite an interesting features of the present functional.

In the second part of the thesis, a screened meta-GGA hybrid functional (DME-sc-TPSSc) is proposed using HF exchange in the the SR and semilocal functional in the LR. The purpose of the construction is to use this scheme for the solid-state systems which have been proposed in the next chapter. The comprehensive assessment and benchmark of the present functional shows that the functional perform very promisingly.Especially, several molecular test sets. It is also shown that the HSE06 performs slightly better compared to the DME-sc-TPSSc in fractional charge prospective which is not surprising because the HSE06 mixes 25% SR HF. The promising and interesting achievement of this construction is that it will be used further to develop a screened hybrid functional in meta-GGA level for solid-state systems.

Chapter 5

Screened Meta-GGA Hybrid Functional for Solid-State Materials

This chapter will extend the method to previous chapter to construct a meta-GGA screened hybrid functional suitable for the solid-state materials. The benchmark calculations of basic solid-state properties employing the constructed exchange-correlation functional is thoroughly presented in this chapter. This chapter is based on the following research outcomes

(i) Subrata Jana, Abhilash Patra and Prasanjit Samal, J. Chem. Phys. 149, 094105 (2018).

5.1   Introduction

In chapter 3, it is discussed that the semilocal XC functionals describe most of the structural and energetic properties of solids efficiently. It is observed that different levels of semilocal approximations (L(S)DA, GGA, and meta-GGA functionals) have achieved a high level of sophistication and establish its accuracy for the electronic structure of solids. In spite of the overwhelming success, semilocal functionals struggle to predict the bandgap of solids which is one of the basic property of solids. Exemplification of the underestimation of the bandgap from semilocal functionals is described in chapter

3, where the semilocal functionals predict only 50% of the experimental bandgap. As sources of error, it is established that semilocal functionals do not contain the "derivative discontinuity" which is an essential quantity and that plays determining role in the correct prediction of the bandgaps [48, 144, 259–271]. Several resolutions and progress are made in order to better the performance of the bandgap of solids such as the DFT + U [362], the self-interaction correction method [144], the optimized effective potential (OEP) [60, 363–365], model potentials [65, 366–369], dynamical mean field theory (DMFT), DFT + DMFT [370, 371], GW approximations [372, 373] and the (screened-) hybrid functional approximations [95, 96, 245–249, 305, 335, 374–381]. But, each method has remarkable advantages and undesirable disadvantages. Among all these methods, an all-purpose formalism that can be applied for both the structural, energetic and bandgap of solids with less computational cost than accurate higher-order many-body techniques like DMFT, DFT + DMFT, GW is the screened-hybrid functional formalism. The screened-hybrid functionals designed using the short-range Hartree-Fock (HF) with the long-range semilocal functionals that keeps all the good properties of the semilocal functionals for solids and simultaneously improves the performance of the bandgap. Though the global hybrids and long-range corrected hybrids improve the bandgap performance, yet both are computationally more expensive than screened-hybrid functionals as proposed using the short-range Hartree-Fock (HF) because those methods need numbers of plane-waves to converge and long-range HF often causes a problem for metallic systems [248, 376]. Therefore, the screened-hybrid functionals can be recognized as a faster hybrid functional approach for the solids.

As discussed in chapter 4, designing (screened-)range-separated (RS) hybrid functionals requires the exchange hole which can be constructed is several ways [35, 95, 96, 314, 333, 382, 383]. Beyond the GGA exchange hole a meta-GGA exchange hole is constructed using DME technique [35] and using that hole a long-range corrected and a screened hybrid functional is also proposed in chapter 4. Taking motivation from those constructed screened hybrid functionals, in this chapter, we focus on the construction of an efficient screened meta-GGA hybrid functional for solids. In designing the present screened RS hybrid functional, we utilize the exchange hole of local density approxima-

tion to construct the long-range semilocal part. This is the possible conventional way to utilize the TM functional for RS scheme without designing its reverse-engineered exchange hole. The details of the methodology will be provided in the next section. It is noticed that this simple assumption actually performs efficiently in describing both the lattice constants and bandgaps of solids. In this chapter, we design a screened range separated hybrid functional in meta-GGA level and test the functional extensively in the plane wave pseudopotential code for the solid-state lattice constants and bandgaps using the projector-augmented-wave method.

5.2   Meta-GGA Screened Hybrid Functional for Solids

Lets start with the construction of the hybrid functional. In general, any hybrid density functional can be constructed from DFA and HF exact exchange according to the following scheme,

$$E_{xc}^{DFAh} = \alpha E_x^{HF} + (1 - \alpha) E_x^{DFA} + E_c^{DFA}. \tag{5.1}$$

Here, a fraction of HF exchange is mixed with the appropriate fraction of DFA, but no fractional mixing scheme involved in the correlation part. Thus, in the exchange only hybrid functional scheme the above equation becomes,

$$E_x^{DFAh} = \alpha E_x^{HF} + (1 - \alpha) E_x^{DFA}. \tag{5.2}$$

Now, separating the Coulomb operator in as short and long-range parts [336, 337],

$$\frac{1}{r} = w_{ee}^{SR,\mu} + w_{ee}^{LR,\mu} = \underbrace{\frac{erfc(\mu|\mathbf{r} - \mathbf{r}'|)}{|\mathbf{r} - \mathbf{r}'|}}_{SR} + \underbrace{\frac{erf(\mu|\mathbf{r} - \mathbf{r}'|)}{|\mathbf{r} - \mathbf{r}'|}}_{LR} , \tag{5.3}$$

where μ is the range-separation parameter. Using this decomposition, the exchange-only RS hybrid functional can be divided into long-range and short-range scheme utilizing the exchange hole. Now, following the proposition made by Heyd-Scuseria-Ernzerhof (HSE) [95, 96, 333], the range-separation scheme can be designed from the above hybrid

functional by splitting the exchange energy functional into the short-range and long-range part as,

$$E_{xc}^{DFAh}(\mu) = \alpha E_x^{SR-HF}(\mu) + (1-\alpha)E_x^{DFA-SR}(\mu) + E_x^{DFA-LR}(\mu) + E_c . \quad (5.4)$$

Alternatively, this can also be written as,

$$E_{xc}^{DFAh}(\mu) = \alpha E_x^{HF-SR}(\mu) - \alpha E_x^{SL-SR}(\mu) + E_x^{SL} + E_c^{SL} . \quad (5.5)$$

In the above equation, the last two parts added to the semilocal XC functional. The HF exchange used in the short-range (HF-SR) part of the above equation is given by,

$$E_x^{HF-SR}(\mu) = -\frac{1}{2}\sum_{\mathbf{k}n,\mathbf{k}'m} f_{\mathbf{k}n} f_{\mathbf{k}'m} \int \int d\mathbf{r}\, d\mathbf{r}' \frac{erfc(\mu|\mathbf{r}-\mathbf{r}'|)}{|\mathbf{r}-\mathbf{r}'|} \Psi_{\mathbf{k}n}^*(\mathbf{r})\Psi_{\mathbf{k}'m}^*(\mathbf{r}')\Psi_{\mathbf{k}n}(\mathbf{r}')\Psi_{\mathbf{k}'m}(\mathbf{r}) ,$$

$$(5.6)$$

where $\{\Psi_{\mathbf{k}n}(\mathbf{r})\}$ and $\{f_{\mathbf{k}n}\}$ are the single particle state or KS orbital.

The most difficult part of this construction is the semilocal short-range part. Construction of semilocal short-range requires the exchange hole. The reverse-engineered exchange hole is used in the construction of the popular HSE06 functional. Beyond the GGA functionals, several accurate meta-GGA level semilocal functionals are also proposed using the Kohn-Sham kinetic energy density (meta-GGA functionals) which establish their accuracy for solid-state structural and energetic properties over GGA (see chapter 3). However, not much development has been initiated in this direction of screened-meta-GGA hybrid functionals for solids. Only, recently, the TPSS [84] exchange functional is reverse-engineered to construct a meta-GGA screened hybrid functional [314]. More accurate semilocal functionals in the meta-GGA theory are developed [35] which is relevant in our present construction. Concerning the E_x^{SL}, it is given by TM semilocal exchange functional having following semilocal form,

$$E_x^{SL} = E_x^{TM} = -\int d\mathbf{r}\, \rho(\mathbf{r})\epsilon_x^{unif} F_x^{TM} = -\int d\mathbf{r}\, \rho(\mathbf{r})\epsilon_x^{SL} . \quad (5.7)$$

The semilocal short-range part is constructed by utilizing the LDA exchange hole. Using the LDA exchange hole the semilocal short-range part of the exchange energy functional becomes,

$$E_x^{SL-SR}(\mu) = -\int d\mathbf{r}\, \rho(\mathbf{r})\epsilon_x^{unif}\left\{1 - \frac{8}{3}\mathcal{A}\left(\sqrt{\pi}\, erf(\frac{1}{2\mathcal{A}}) + (2\mathcal{A} - 4\mathcal{A}^3)e^{-\frac{1}{4\mathcal{A}^2}} - 3\mathcal{A} + 4\mathcal{A}^3\right)\right\},$$

(5.8)

where $\epsilon_x^{unif} = \frac{3k_f}{4\pi}$ is the exchange energy density in the homogeneous electron gas limit and $\mathcal{A} = \frac{\mu}{2k_f}$ is involved with the RS parameter. Through $\mathcal{A}$, the screening parameter includes the semilocal short-range part. Though the other ways of including the semilocal exchange hole are proposed in chapter 4. But, in the present situation, it is found that the scheme does not perform suitably for the solid-state lattice constants and bandgap performance simultaneously. The range-separation parameter μ involving of this functional will be fixed later in this chapter.

Now, regarding the XC potential, it is combinations of semilocal XC and HF exchange potential. In DFT, the RS hybrid functionals are implemented in the generalized Kohn-Sham (gKS) formalism which contains both density and orbital information. The general expression for the potential of the exchange energy functional on Eq.(5.5) is given by,

$$v_{xc}(\mathbf{r}, \mathbf{r}') = \alpha v_x^{HF-SR}(\mathbf{r}, \mathbf{r}'; \mu) + (1 - \alpha)v_x^{SL-SR}(\mu) + v_x^{SL-LR}(\mu) + v_c^{SL}.$$

(5.9)

Alternatively, this can also be written as,

$$v_{xc}(\mathbf{r}, \mathbf{r}') = \alpha v_x^{HF-SR}(\mathbf{r}, \mathbf{r}'; \mu) - \alpha v_x^{SL-SR}(\mu) + v_x^{SL} + v_c^{SL},$$

(5.10)

where the semilocal short-range (SL-SR) and semilocal long-range (SL-LR) parts are added to the semilocal exchange-correlation functional which in our present case is the TM functional. Here, the parameter, α controls the amount of HF exchange mixing with the semilocal exchange functional and μ is the range separated parameter. The $\alpha = 0$

value corresponds to pure semilocal formalism. Unlike the pure semilocal functional, the potential obtained from Eq.(5.10) is now non-local. Here, the RS parameter μ is included in the HF exact exchange through the following equation,

$$v_x^{HF-SR}(\mathbf{r},\mathbf{r}';\mu) = -\sum_{\mathbf{k}'m} f_{\mathbf{k}'m}\Psi_{\mathbf{k}'m}(\mathbf{r})\frac{erfc(\mu|\mathbf{r}-\mathbf{r}'|)}{|\mathbf{r}-\mathbf{r}'|}\Psi_{\mathbf{k}'m}^*(\mathbf{r}') \,, \qquad (5.11)$$

where Ψ_is are single-particle electronic orbitals or Bloch states. This is obtained from Eq.(5.6). Except screened HF exchange, other unknown potentials of Eq.(5.10) are the screened potential ($v_x^{SL-SR}(\mu)$) and the semilocal potential (v_x^{SL}). In meta-GGA level theory (implemented in the gKS formalism) the exchange potential is obtained not only by taking the derivative with respect of density and gradient of density of the exchange energy functional but also the partial derivative to KS kinetic energy density is also required. Therefore, in the gKS formalism, the general form of the semilocal exchange potential is expressed as,

$$v_x^{SL(-SR)}(\mathbf{r})\Psi_i(\mathbf{r}) = \underbrace{\left[\frac{\partial(\rho(\mathbf{r})\epsilon_x^{SL(-SR)}(\mathbf{r}))}{\partial\rho(\mathbf{r})} - \nabla\frac{\partial(\rho(\mathbf{r})\epsilon_x^{SL(-SR)}(\mathbf{r}))}{\partial\nabla\rho(\mathbf{r})}\right]}_{v_x^{GGA}}\Psi_i(\mathbf{r})$$
$$\underbrace{-\frac{1}{2}\nabla\left(\frac{\partial(\rho\epsilon_x^{SL(-SR)}(\mathbf{r}))}{\partial\tau(\mathbf{r})}\right)\nabla\Psi_i(\mathbf{r}) - \frac{1}{2}\frac{\partial(\rho(\mathbf{r})\epsilon_x^{SL(-SR)}(\mathbf{r}))}{\partial\tau(\mathbf{r})}\vec{\nabla}^2\Psi_i(\mathbf{r})}_{v_x^\tau} \,,$$

$$(5.12)$$

where $\epsilon_x^{SL(-SR)}$ is the semilocal SR exchange energy density.

For correlation energy, the one-electron self-interaction free TPSS [84] and its modified version for TM exchange are used for the present study. It is shown in chapter 3, that the TPSS and TM correlation are giving different results for various properties of solids. Therefore, utilizing the present range-separation scheme for exchange with the TPSS and TM correlations leads to two screened RS functional which are named as: (i) SRSH-TM-TPSSc (screened RS hybrid with the TM exchange plus TPSS correlation) and (ii) SRSH-TM (screened RS hybrid with the TM exchange plus modified TPSS correlation).

5.3   Performance in Bulk Solids

5.3.1   Computational details

The newly constructed functional is implemented and tested in VASP. The implementation of the present functional is same as that is done for the TM functional as described in chapter 3.

Now, regarding the value of the range-separation parameter (μ) and mixing parameter (α) for the present functional we fix both the μ and α value as the same as used in the HSE06 functional i.e. $\alpha = 0.25$ and $\mu = 0.11$ bohr^{-1}. We found that these two values yield quite a well balanced description for both the lattice constants and bandgaps of different solids. For comparison we consider the widely used HSE06 functional. Unless otherwise stated, the default values μ and α is the same as that used in VASP recommended HSE06 calculations.

5.3.2   Lattice constants

To start with the functional performance, we first consider the lattice constant of the solids. This is one of the fundamental test that one should perform to check the robustness of the XC functional. For the benchmark calculations of SRSH-TM-TPSSc and SRSH-TM, we employ the two functionals constructed above for 47 crystalline structures. The calculation of the present functional is performed with $\Gamma-$ centered Monkhorst-Pack like $10\times10\times10$ **k** grids.

The performance of HSE06, SRSH-TM-TPSSc, and SRSH-TM are summarized in Table 5.1 and relative error is plotted in Fig. 5.1. Regarding the performance of HSE06 functional, it shows improved performance over corresponding semilocal functional PBE by mixing the fraction of HF exchange. It is well known that the PBE functional has an inherent tendency to overestimate the lattice constants which also streams into the performance of the HSE06 functional performance. However, an improved version of the HSE06 is proposed based on the PBEsol which is known as the HSEsol functional [249].

Table 5.1: Shown is the calculated lattice parameters a_0 (in Å) of different solids using different approximations. Reference values are taken from ref. [179, 245]. In last two rows we also show the error statistics.

Solids	HSE06	%	SRSH-TM-TPSSc	%	SRSH-TM	%	Expt.
C (A2)	3.548	-0.53	3.550	-0.48	3.545	-0.62	3.567
Si (A2)	5.432	0.04	5.420	-0.18	5.408	-0.40	5.430
Ge (A2)	5.676	0.42	5.653	0.02	5.636	-0.28	5.652
SiC (B3)	4.346	-0.27	4.338	-0.46	4.332	-0.59	4.358
BN (B3)	3.597	-0.28	3.603	-0.11	3.597	-0.28	3.607
BP (B3)	4.519	-0.42	4.52	-0.40	4.509	-0.64	4.538
BAs (B3)	4.770	-0.15	4.766	-0.23	4.754	-0.48	4.777
BSb (B3)	5.216	n/a	5.202	n/a	5.188	n/a	n/a
AlP (B3)	5.470	0.18	5.461	0..02	5.448	-0.22	5.460
AlAs (B3)	5.676	0.32	5.659	0.02	5.646	-0.21	5.658
AlSb (B3)	6.151	0.24	6.130	-0.10	6.114	-0.36	6.136
$\beta-$GaN (B3)	4.521	-0.22	4.526	-0.11	4.516	-0.33	4.531
GaP (B3)	5.464	0.29	5.463	0.27	5.446	-0.03	5.448
GaAs (B3)	5.667	0.34	5.653	0.09	5.635	-0.23	5.648
GaSb (B3)	6.099	0.05	6.075	-0.34	6.055	-0.67	6.096
InP (B3)	5.921	0.94	5.923	0.68	5.903	0.63	5.866
InAs (B3)	6.108	0.89	6.095	0.68	6.075	0.34	6.054
InSb (B3)	6.516	0.57	6.496	0.26	6.473	-0.09	6.479
ZnS (B3)	5.419	0.18	5.436	0.50	5.412	0.05	5.409
ZnSe (B3)	5.693	0.44	5.699	0.55	5.676	0.14	5.668
ZnTe (B3)	6.135	0.75	6.129	0.65	6.099	0.16	6.089
CdS (B3)	5.880	1.06	5.924	1.82	5.893	1.29	5.818
CdSe (B3)	6.133	1.34	6.164	1.85	6.133	1.34	6.052
CdTe (B3)	6.543	0.97	6.568	1.36	6.533	0.81	6.480
MgO (B1)	4.197	-0.24	4.195	-0.28	4.187	-0.47	4.207
MgS (B3)	5.652	8.65	5.647	8.55	5.632	8.27	5.622
MgSe (B1)	5.454	1.00	5.462	1.15	5.411	0.76	5.400
MgTe (B3)	6.452	0.50	6.446	0.40	6.424	0.06	6.420
CaS (B1)	5.698	0.16	5.722	0.58	5.699	0.17	5.689
CaSe (B1)	5.938	0.37	5.966	0.84	5.939	0.38	5.916
CaTe (B1)	6.369	0.33	6.404	0.88	6.369	0.33	6.348
SrS (B1)	6.034	0.73	6.071	1.35	6.046	0.93	5.990
SrSe (B1)	6.268	0.54	6.302	1.09	6.275	0.66	6.234
SrTe (B1)	6.684	0.66	6.721	1.22	6.688	0.72	6.640
BaS (B1)	6.432	0.67	6.487	1.53	6.454	1.02	6.389
BaSe (B1)	6.656	0.92	6.707	1.70	6.673	1.18	6.595
BaTe (B1)	7.057	0.71	7.115	1.54	7.075	0.97	7.007
Ag (A1)	4.146	1.89	4.151	2.02	4.135	1.62	4.069
Al (A1)	4.020	-0.30	3.980	-1.29	3.979	-1.31	4.032
Cu (A1)	3.637	0.94	3.573	-0.83	3.573	-0.83	3.603
Pd (A1)	3.904	0.59	3.923	1.08	3.909	0.72	3.881
K (A3)	5.32	1.82	5.297	1.38	5.273	0.92	5.225
Li (A3)	3.466	-0.32	3.439	-1.09	3.440	-1.06	3.477
LiCl (B1)	5.116	0.19	5.100	-0.12	5.076	-0.59	5.106
LiF (B1)	4.015	0.12	3.973	-0.92	3.968	-1.05	4.010
NaCl (B1)	5.613	0.32	5.556	-0.70	5.540	-0.98	5.595
NaF (B1)	4.576	-0.71	4.513	-2.08	4.507	-2.21	4.609
ME (Å)	0.024	—	0.024	—	0.004	—	—
MAE (Å)	0.030	—	0.042	—	0.032	—	—
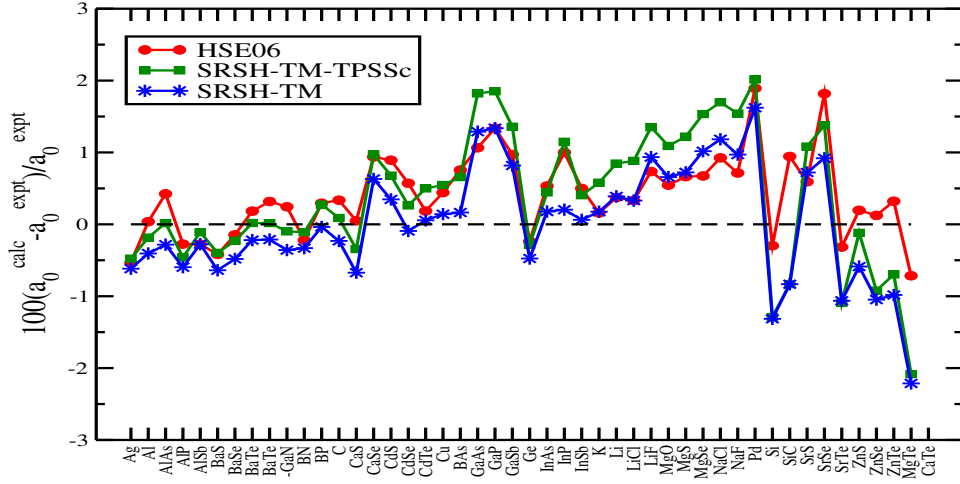
Figure 5.1: Percentage error in lattice constants of all considered solids of Table 5.1.

Overall, we obtain MAE 0.030Å from the HSE06 functional.

Now, regarding the performance of newly constructed SRSH-TM-TPSSc and SRSH-TM, the SRSH-TM-TPSSc overestimates the lattice constants of most of the solids compared to that obtained with the SRSH-TM functional. This is due to the use of the TPSS correlation. The TM correlation satisfies more exact constraints than TPSS correlation when combined with the TM exchange. The same trend is also following in the performance of SRSH-TM-TPSSc and SRSH-TM functionals. It is observed that HF exchange with TM-TPSS functional overestimates the lattice constants more and gives the MAE of 0.042 Å. However, the screened hybrid functional proposed using the TM correlation with HF exchange improves its performance over SRSH-TM-TPSSc.

5.3.3   Bandgaps

The accurate prediction of the bandgap is achievable within the hybrid density functional scheme due to the cancellation of the delocalization and localization errors arising from semilocal and HF exchange. The screened hybrid functional keep all the good properties of its base semilocal functional intact and additionally, improve the bandgap performance corresponding to its semilocal nature. As the present scheme is on the hybrid interface. Therefore, improvement in the performance of SRSH-TM-TPSSc and SRSH-TM is ob-

served than its semilocal TMTPSS and TM functionals (for TMTPSS and TM functional results see chapter 3). Note that the meta-GGA functionals implemented in framework of gKS incorporate some amount of the derivative discontinuity. Therefore, within meta-GGA screened hybrids the improvement in bandgap comes from both the semilocal formalism and mixing of HF exchange.

Table 5.2: Band gaps using different functionals calculated at the experimental lattice constants. The experimental references are taken from ref. [369].

Solids	Geometry(Å)	HSE06	%	SRSH-TM-TPSSc	%	SRSH-TM	%	Expt.
MgO(A1)	4.207	6.49	-17.11	6.84	-12.64	6.71	-14.30	7.83
BaS (A1)	6.389	3.06	-21.13	3.16	-18.55	3.09	-20.36	3.88
BaSe (A1)	6.595	2.76	-22.90	2.91	-18.99	2.83	-20.94	3.58
BaTe (A1)	7.007	2.27	-26.29	2.45	-20.45	2.38	-22.72	3.08
ScN (A1)	4.500	0.86	-4.44	1.07	18.88	1.02	13.33	0.9
AgCl (A1)	5.546	2.43	-25.23	2.73	-16.00	2.66	-18.15	3.25
AgBr (A1)	5.772	2.14	-21.03	2.59	-4.42	2.50	-7.74	2.71
C (A2)	3.567	5.29	-3.81	5.45	-0.90	5.36	-2.54	5.5
Si (A2)	5.430	1.17	0.00	1.41	20.51	1.30	11.11	1.17
Ge (A2)	5.430	0.82	10.81	1.04	40.54	1.01	36.48	0.74
SiC (A3)	4.358	2.35	-2.89	2.53	4.54	2.44	0.82	2.42
BN (A3)	3.616	5.90	-7.23	6.19	-2.67	6.07	-4.55	6.36
BP (A3)	4.538	2.01	-4.76	2.19	4.28	2.10	0.00	2.1
BAs (A3)	4.777	1.87	28.08	1.98	35.61	1.91	30.82	1.46
AlN (A3)	4.342	4.72	-3.67	4.95	1.02	4.84	-1.22	4.9
AlP (A3)	5.463	2.34	-6.40	2.62	4.80	2.51	0.40	2.5
AlAs (A3)	5.661	2.15	-4.03	2.40	7.62	2.29	2.69	2.23
AlSb (A3)	6.136	1.81	6.50	1.99	17.75	1.90	12.42	1.69
GaN (A3)	3.180	3.17	-3.35	3.18	-3.04	3.13	-4.57	3.28
GaP (A3)	5.451	2.29	-2.55	2.40	2.12	2.33	-0.85	2.35
GaAs (A3)	5.648	1.44	-5.26	1.88	23.68	1.83	20.39	1.52
InP (A3)	5.869	1.52	7.04	1.82	28.16	1.77	24.64	1.42
InAs (A3)	6.058	0.53	26.19	0.92	119.04	0.88	109.52	0.42
InSb (A3)	6.479	0.53	120.83	0.99	312.50	0.96	300.00	0.24
MgTe (A3)	6.420	3.38	-6.11	3.80	5.55	3.70	2.77	3.6
CuCl (A3)	5.501	2.28	-32.94	2.37	-30.29	2.31	-32.05	3.4
CuBr (A3)	5.820	2.08	-32.24	2.31	-24.75	2.24	-27.03	3.07
CuI (A3)	6.063	2.59	-16.98	2.91	-6.73	2.83	-9.29	3.12
ZnS (A3)	5.409	3.32	-13.54	3.61	-5.98	3.52	-8.33	3.84
ZnSe (A3)	5.668	2.41	-14.53	2.82	0.00	2.74	-2.83	2.82
AgI (A3)	6.499	2.57	-11.68	2.84	-2.40	2.78	-4.46	2.91
CdS (A3)	5.818	2.19	-12.40	2.45	-2.40	2.37	-5.20	2.5
CdSe (A3)	6.052	1.59	-14.05	1.96	5.94	1.89	2.16	1.85
CdTe (A3)	6.480	1.55	-3.72	2.01	24.84	1.94	20.49	1.61
ME (eV)		-0.306	–	-0.044	–	-0.121	–	–
MAE (eV)		0.371	–	0.329	–	0.331	–	–

The benchmark calculations of the screened hybrid functionals for the bandgap assessment are performed with the same set of semiconductors as it is done for the TM functional in chapter 3. Our present test set consists of 34 semiconductors and the performance of all the screened functionals are done self-consistently.In Table 5.2 we summarized all the functionals performance along with the experimental bandgaps values.
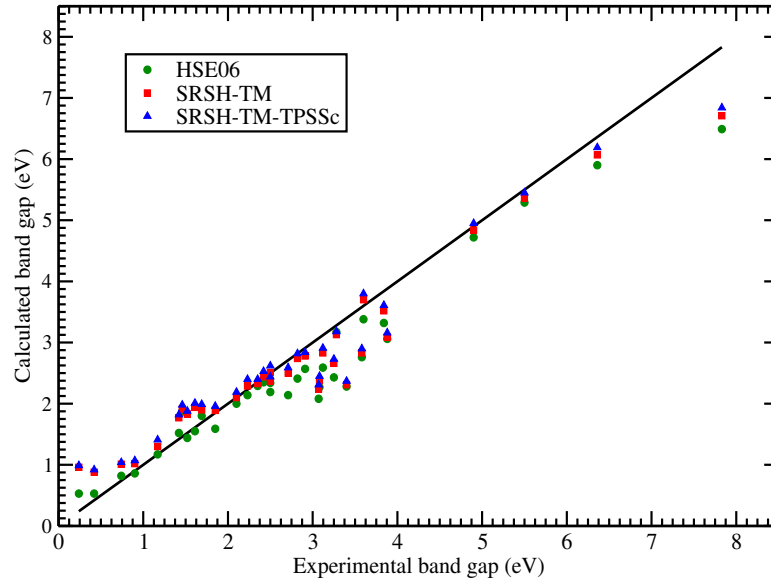
Figure 5.2: Experimental versus calculated bandgaps of all the solids using different functionals presented in Table 5.2.

The experimemtal versus calculated band gaps are also plotted in Fig. 5.2. From Table 5.2, we observe that all the screened hybrid functionals perform better compared to its base semilocal functional due to the inclusion of HF exchange. It is well known that the screened hybrids which mix HF exchange, improve the bandgap of of narrow and intermediate solids (up to $\sim$ 7eV). For large bandgap, those functionals show underestimation. This tendency is observed in the performance of the HSE06 functional. Regarding the performance of meta-GGA screened RS hybrids: SRSH-TM-TPSSc and SRSH-TM, it is observed that the bandgap is more enhanced than HSE06 value for all the materials which is not surprising because, in the semilocal level, meta-GGA improve the bandgap over GGA. It is observed that screened meta-GGA hybrids: SRSH-TM-TPSSc and SRSH-TM are showing improvement in many cases, particularly for which HSE06 shows underestimation in the bandgaps.

Regarding the overall comparison of all the considered functionals, HSE06 and SRSH-TM perform quite well. It is observed that for ScN, Si, Ge, SiC, GaP, InP, InAs, InSb, and CdTe solids the HSE06 performs quite accurately. The bandgaps obtained from SRSH-TM are also matching very closely with that of HSE06. However, we observe overestimation in the performance of bandgaps of the SRSH-TM-TPSSc for these solids. Overall,

the performance of the SRSH-TM is quite satisfactory over HSE06 for the bandgaps of several semiconductors. Interestingly, we also observe that a few bandgaps reported using TPSS based screened hybrid functionals in reference [314] is also comparable with the bandgap of SRSH-TM in Table 5.2 which is very motivating because the present functional form is very simple corresponding to the proposition made in [314].

5.3.4   Atomization energies of AE6 molecules

Though the SRSH-TM functional shows very qualitative performance yet question remains on its performance in describing the molecular atomization energies. It is well known that for molecular properties the HSE06 performs well. To estimate the functional performance, we consider the atomization energies of the AE6 tests. In VASP code all molecular calculations are performed $15 \times 15 \times 15$ simulation box and $1 \times 1 \times 1$ $\Gamma-$ centered $\mathbf{k}$ point. It is noteworthy to mention that the aspherical corrections to the electrostatic energy contribution are properly taken into account through the keyword LASPH =.TRUE.

The results of the atomization energies of the AE6 molecules for the hybrids SRSH-TM, HSE06 together with LDA, GGA (PBE, PBEsol) and meta-GGA (TPSS, TMTPSS, and TM) semilocal functionals are summarized in Table 5.3. From the results, it is obvious that both the SRSH-TM and SRSH-TM-TPSSc functionals fail badly in this case. The lowest MAE is obtained with HSE06. Though average performance is observed with SRSH-TM, the SRSH-TM-TPSSc functional shows massive overestimation. The SRSH-TM functional is is quite good in predicting the atomization energies of SiH_4, S_2, C_3H_4 and C_4H_4, but shows underestimation the atomization energies for SiO and $C_2H_2O_2$. The lack of quality performance from these functionals can be explained from the view point of its construction. This is because here we utilize only the LDA exchange hole to construct the functional instead of full reverse-engineered exchange hole.

Table 5.3: AE6 atomization energies (in kcal/mol) as obtained from different approximations.

	L(S)DA	PBE [178]	PBEsol [178]	TPSS [178]	TMTPSS [35]	TM [35]	HSE06	SRSH-TM-TPSSc	SRSH-TM	Expt. [178]
SiH_4	342.2	313.2	323.2	333.7	332.9	316.1	315.6	387.8	339.6	322.8
SiO	219.9	195.8	204.6	186.9	186.2	187.5	182.0	226.7	166.6	192.7
S_2	131.9	115.4	123.9	109.8	108.7	111.2	108.1	172.2	97.4	102.8
C_3H_4	794.3	720.9	749.0	707.5	705.6	703.4	708.9	759.2	692.5	705.1
$C_2H_2O_2$	742.7	662.6	694.8	633.4	636.4	640.0	631.4	681.4	594.2	634.0
C_4H_8	1293.2	1167.1	1217.4	1154.8	1155.1	1146.8	1158.3	1240.8	1148.1	1149.4
MAE (kcal/mol)	70.1	14.6	34.3	5.3	5.2	5.1	6.4	60.2	17.0	–

5.3.5   Conclusions

In this chapter, screened meta-GGA hybrid functionals (SRSH-TM-TPSSc and SRSH-TM) are proposed. The performance of both the functionals are tested for solid-state the lattice constants and bandgaps. The results are compared with the popular GGA functional HSE06. The results obtained from SRSH-TM-TPSSc and SRSH-TM is found to be very interesting.

From the perspective of lattice constants, the overall performance of SRSH-TM is quite impressive. It has been observed that the HSE06 shows bit overestimation in lattice constants which is modified by the present screened meta-GGA functional. Also, the SRSH-TM performs better than SRSH-TM-TPSSc for all properties. This is because of the TM correlation which satisfies more exact constraints than SRSH-TM-TPSSc.

Concerning the construction point of view, the functional form is very simple. Only the LDA based exchange hole is employed in the short-range of the semilocal exchange together with HF short-range exchange. The performance of SRSH-TM for lattice constants and bandgaps indicates that it could be a good competitor of HSE06. Especially, we found that the HSE06 has the tendency to underestimate the bandgaps which get improved by the meta-GGA level screened functionals. Though in a few cases SRSH-TM overestimates the bandgap more compare to experimental values, yet overall performance of SRSH-TM is quite well.

The present screened hybrid functional based on TM semilocal functional keeps all the good properties of the TM functional intact and additionally, it improves the performance of TM for bandgap of solids. In between the two meta-GGA screen functionals, the SRSH-TM performs in a more balanced way than SRSH-TM-TPSSc for both lattice constants and bandgaps.

Lastly, we conclude, although the atomization energies are obtained from both the functionals are not so impressive but still it can be considered as a good meta-GGA screened hybrid functional for solids. The main advantage of the present SRSH-TM functional is that it mixes HF exchange which enables the TM functional to perform in a more satisfactory way for the solid-state bandgaps.

Chapter 6

Studies of Two-Dimensional Quantum Systems

In this chapter, we study the two-dimensional quantum dot systems by constructing the meta-GGA level exchange functional in low-dimension. The behavior of the different meta-GGA ingredients is also discussed for a model two dimensional system. This chapter is based on the following research outcomes

(i) Subrata Jana and Prasanjit Samal, J. Phys. Chem. A 121, 4804 (2017).

(ii) Subrata Jana, Abhilash Patra and Prasanjit Samal, Physica E 97, 268-276 (2018).

(iii) Subrata Jana and Prasanjit Samal, J. Chem. Phys. 148, 024111 (2018).

6.1 Introduction

So far, we have applied the density functional formalism for the electronic structure calculations in three-dimensional bulk systems. A wide range of density functional approximations with varying capabilities is developed and applied to accurately describe various phenomena in three dimensions (3D). This is shown elaborately in previous chapters. However, nowadays the theoretical aspects of the cutting edge research in low dimensions materials such as quantum dots, and quantum Hall systems are also gained momentum and

keenly attracted the attention [384, 385]. Going from 3D to 2D is a problem related to the dimensional crossover because in all these systems the motion of electrons is restricted in one direction. The generalized-gradient approximations (GGA) of exchange-correlation (XC) functionals as developed for 3D diverge when applied to (quasi-)2D to strong 2D limit [386, 387]. However, meta-GGA functionals and exact exchange show promising nature for (quasi-)2D systems [170, 386]. It is also shown in reference [386] that the exchange hole based on semilocal functionals also shows divergence nature at the strict 2D limit. While the behavior of the exact exchange remains finite. However, the problem of dimensional crossover can also be solved by developing GGA and meta-GGA functionals that obey (quasi-)2D limit when applied to 2D systems [388, 389].

The paradigm model system to understand the 2D phenomena is the two-dimensional electron gas (2DEG). From the limitations and promising nature of GGA, meta-GGA, and the exact exchange functionals for (quasi-)2D systems, it is clearly evident that one needs to construct the 2D functionals for describing the 2DEG. However, several many-electron theories are already developed to understand and predict the basic phenomena related to the 2DEG. The obvious first step towards such an attempt is the Hartree-Fock theory. To reduce the computational cost and include the correlation effect, density functional theory with local and semilocal approximations of exchange and correlation are also developed during the last decade or so on [39–41, 390–408].

The search for promising as well as accurate semilocal XC functionals to describe the systems based on two-dimensional homogeneous electron gas (2D-HEG) is a challenging task. Unlike 3D, there is not much development initiated in this direction. However, the attempt towards the development of XC functionals for such systems is parallel to that in 3D. The lowest rung of the 2D XC functional is the 2D local density approximation (2D-LDA) [390] which is developed based on 2D-HEG. One rung higher to the 2D-LDA, i.e., 2D generalized gradient approximations (2D-GGA) [395] are also developed. The state of art of this chapter is to climb higher rung of the 2D-GGA by exploring the behavior of KS-KE density and using it to construct a non-empirical meta-GGA level functional. We will begin this chapter discussing the behavior of the KS-KE for a model 2D system (2D quantum harmonic oscillator). Then we will apply the constructed local and semilocal

functionals on various quantum dots systems to assessed and validate our formalism.

Based on the knowledge of the construction of the KS-KE, in this chapter we also propose a meta-GGA semilocal functional using the density matrix expansion technique. Assessment of the proposed functional for model systems showing its remarkable accuracy over previous proposed LDA and GGA based semilocal functionals.

6.2   Formal Properties of 2D Functionals

We start by discussing the formal exact constraint as applied for the functional development in 2D. This is necessary as it is used further to develop the semilocal functional in 2D. However, like the 3D exchange functional, all the properties related to the 2DEG have a 3D analog.

6.2.1   Uniform coordinate scaling

Wavefunction : For a coordinate scaling parameter $\gamma \, (> 0)$, the 2D wavefunction scaled uniformly as,

$$\Psi_\gamma(\mathbf{r}_1, ... \mathbf{r}_N) = \gamma^N \Psi_\gamma(\gamma \mathbf{r}_1, ... \gamma \mathbf{r}_N) \, , \tag{6.1}$$

where both the scaled and unscaled Ψ satisfy the normalization condition i.e.,

$$\langle \Psi_\gamma | \Psi_\gamma \rangle = \langle \Psi | \Psi \rangle = 1 \, . \tag{6.2}$$

Density: The density corresponding to the scaled wavefunction becomes,

$$\rho_\gamma(\mathbf{r}) = \gamma^2 \rho(\gamma \mathbf{r}) \, , \tag{6.3}$$

which satisfies the electronic number conserving criteria

$$\int \rho_\gamma(\mathbf{r}) \, d^2r = \int \rho(\gamma \mathbf{r}) \, d^2(\gamma r) = N \, , \tag{6.4}$$

where $\gamma > 1$ resulting to higher density, whereas, $\gamma < 1$ for smaller density.

Hartree energy: In 2D, the Hartree energy is given by

$$E_H = \frac{1}{2} \int d^2(r) \int d^2(r') \frac{\rho(\mathbf{r})\rho(\mathbf{r'})}{|\mathbf{r} - \mathbf{r'}|} \ . \tag{6.5}$$

Upon applying scaling relation it reduces to

$$
\begin{aligned}
E_H &= \gamma \frac{1}{2} \int d^2(\gamma r) \int d^2(\gamma r') \frac{\rho(\gamma\mathbf{r})\rho(\gamma\mathbf{r'})}{|\gamma\mathbf{r} - \gamma\mathbf{r'}|} \ , \\
&= \gamma E_H[\rho]
\end{aligned}
\tag{6.6}
$$

Kinetic energy: Because of the involvement of $\sum_{i=1,2} \frac{d^2}{dx_i^2}$, the scaling relation of the expectation value of kinetic energy operator is obtained in a straightforward manner as,

$$\langle \Psi_\gamma | \hat{T} | \Psi_\gamma \rangle = \gamma^2 \langle \Psi | \hat{T} | \Psi \rangle \ . \tag{6.7}$$

Following this, one can also obtain the scaling relation of the non-interaction or KS kinetic energy. The scaling relation of the KS kinetic energy becomes,

$$T_s[\rho_\gamma] = \gamma^2 T_s[\rho] \ . \tag{6.8}$$

Exchange energy: The scaling relation of exchange energy functional in 2D can be derived from the constraint search formalism. This is analogous to the 3D constraint search counterpart. The exchange energy functional in constraint search formalism is written as,

$$E_x[\rho] = \langle \Phi_\rho^{min} | \hat{V}_{ee} | \Phi_\rho^{min} \rangle - E_H[\rho] \ . \tag{6.9}$$

Now, under uniform density scaling the exchange energy becomes,

$$E_x[\rho_\gamma] = \langle \Phi_{\rho_\gamma}^{min} | \hat{V}_{ee} | \Phi_{\rho_\gamma}^{min} \rangle - E_H[\rho_\gamma] \ . \tag{6.10}$$

Again, upon applying the scaling relation of E_H the scaling relation of exchange energy is obtained as,

$$E_x[\rho_\gamma] = \gamma E_x[\rho].\tag{6.11}$$

Correlation energy: Analogous to the 3D, the correlation energy in 2D does not follow any simple scaling rule.

6.2.2   Spin scaling relation

The spin scaling relations enable one to convert a density functional into spin-density functional. In principle, one has to develop only the spin-unpolarized functional. Using the spin scaling relation it can be easily generalized to spin-polarization form. It is noteworthy to mention that the spin scaling relation in 2D and 3D are equivalent.

To express the spin scaling relation of different energy functional, we start with the KS kinetic energy. Expressing the KS KE as the sum of the spin-up and spin-down contributions, we obtain:

$$T_s[\rho_\downarrow, \rho_\uparrow] = T_s[\rho_\uparrow, 0] + T_s[0, \rho_\downarrow, 0].\tag{6.12}$$

For spin-unpolarized system it becomes,

$$T_s[\rho] = T_s[\rho/2, 0] + T_s[0, \rho/2] = 2T_s[\rho/2, 0] \ ,\tag{6.13}$$

where $\rho = \rho_\uparrow + \rho_\downarrow$. The spin-polarization form of the above equation can be easily obtained upon using the spin-scaling relation of the density i.e., $\rho = 2\rho_\uparrow$ and $\rho = 2\rho_\downarrow$. Applying spin-scaling relation, the KS kinetic energy becomes,

$$
\begin{aligned}
T_s[2\rho_\uparrow] &= 2T_s[\rho_\uparrow, 0] \\
T_s[2\rho_\downarrow] &= 2T_s[0, \rho_\downarrow] \ ,
\end{aligned}
\tag{6.14}
$$

which upon using Eq.(6.12) becomes,

$$T_s[\rho_\downarrow, \rho_\uparrow] = \frac{1}{2}T_s[2\rho_\uparrow] + \frac{1}{2}T_s[2\rho_\downarrow] \ .\tag{6.15}$$

Similarly, one can obtain the spin-scaling relation for the exchange energy functional as,

$$E_x[\rho_\downarrow, \rho_\uparrow] = \frac{1}{2}E_x[2\rho_\uparrow] + \frac{1}{2}E_x[2\rho_\downarrow] \ . \tag{6.16}$$

Regarding the correlation energy functional, it comes from the combination of parallel and anti-parallel spin contributions. Therefore, no simple spin scaling relation is applicable for correlation.

6.2.3   Other miscellaneous properties

Exchange energy for one and two electron systems: For the one-electron systems, the exchange and correlation energies become,

$$E_x[\rho] = -U[\rho]$$
$$E_c[\rho] = 0 \ . \tag{6.17}$$

For two electron systems,

$$E_x[\rho] = -\frac{1}{2}U[\rho] \ . \tag{6.18}$$

Exact conditions on XC hole: The XC hole becomes an important concept in the development of functionals in 2D. The XC energy is nothing but the electrostatic interaction between the electron located at $\vec{r}$ and the XC hole at $\vec{r} + \vec{u}$ surrounding it. Just like 3D, the XC hole obeys important normalization condition: $\int \rho_{xc}(\vec{r}, \vec{r} + \vec{u}) \, d^2u = -1$. The exchange and correlation hole in 2D obeys the same rule as 3D. The exact properties of the XC hole in 2D are discussed in detail in this chapter. Another important feature of the exchange hole in the exact small u expansion, which will be discussed later in this chapter.

6.3   Development of GGA Functionals in 2D

We start with the density functional ground state energy of the quantum mechanical many-particle system in 2D

$$E[\rho] = T_s[\rho] + E_H[\rho] + E_{xc}[\rho] + \int v(\mathbf{r})\rho(\mathbf{r})d^2r \; , \tag{6.19}$$

where all the energy notations have their usual meaning. Similar to the 3D, in this case also, The XC energy functional (E_{xc}) can be decomposed as the exchange and correlation parts such that $E_{xc}[\rho] = E_x[\rho] + E_c[\rho]$. This is because the exchange and correlation obey different properties and scaling rules. However, several approximations for the exchange energy functional exists for two-dimensional system. The most promising one is the exchange energy functional as obtained from the Taylor series expansion of the exchange hole. In this section, we discuss the details of the gradient approximations for exchange derived from the Taylor series expansion of the exchange hole. Further, this technique will be used to construct the modified GGA for 2D.

Similar to the $3D$, in $2D$ case also the spin-unpolarized exchange energy functional in terms of the exchange hole is defined as,

$$E_x[\rho] = \frac{1}{2} \int d^2r \int d^2u \frac{\rho(\mathbf{r})\rho_x(\mathbf{r}, \mathbf{r} + \mathbf{u})}{u} \; . \tag{6.20}$$

The exchange hole appearing in Eq.(6.20) is associated with the 1st order reduced density matrix,

$$\rho_x(\mathbf{r}, \mathbf{r} + \mathbf{u}) = -\frac{|\Gamma(\mathbf{r}, \mathbf{r} + \mathbf{u})|^2}{2\rho(\mathbf{r})} \; , \tag{6.21}$$

where $\Gamma(\mathbf{r}, \mathbf{r} + \mathbf{u}) = 2\sum_i^{occ} \psi_i^*(\mathbf{r})\psi_i(\mathbf{r} + \mathbf{u})$, and ψ_i are the occupied KS orbitals. The exchange hole obeys two important properties: (i) the normalization sum rule $\int \rho_x(\mathbf{r}, \mathbf{r} + \mathbf{u}) \, d^2u = -1$ and (ii) the negativity constraint $\rho_x(\mathbf{r}, \mathbf{r} + \mathbf{u}) \leq 0$. In $2D$, the exchange energy E_x involves the cylindrical average of the exchange hole $\langle \rho_x(\mathbf{r}, \mathbf{r} + \mathbf{u}) \rangle$ over the

direction of **u**, i.e.

$$\langle \rho_x(\mathbf{r}, \mathbf{r} + \mathbf{u}) \rangle = \int \frac{d\Omega_u}{2\pi} \rho_x(\mathbf{r}, \mathbf{r} + \mathbf{u}) \, . \tag{6.22}$$

Upon using the spin-scaling relation exchange energy becomes,

$$E_x[\rho_\uparrow, \rho_\downarrow] = \frac{1}{2} E_x[2\rho_\uparrow] + \frac{1}{2} E_x[2\rho_\downarrow] \, . \tag{6.23}$$

From the discussion above it is clear that knowing the cylindrical averaged exchange hole one can construct the exchange energy functional. Regarding the GGA for 2D, it can be constructed in several ways: (i) using the Taylor series expansion of exchange hole or (ii) using the asymptotic properties related to the exchange potential or exchange energy or (iii) by imposing relevant physical constraints. The 2D GGA proposed by Pittalis et.al. [395] and Jana et. al. [41] is obtained using the small and large-gradient expansions of the exchange hole. However, the GGA exchange functional as developed in the reference [41, 395] is obtained by utilizing the asymptotic properties related to the exchange potential or exchange energy.

6.3.1   Taylor expansion of exchange hole

Pittalis et. al. [395] proposed the first ever 2D GGA functional by extending the idea of Becke's construction. In their construction, the spin-polarization form the exchange energy functional (Eq.(6.20)) is written as,

$$E_x[\rho_\sigma] = -\pi \sum_{\sigma=\uparrow,\downarrow} \int d^2 r \rho_\sigma(\mathbf{r}) \int d^2 u \langle \rho_{x,\sigma}(\mathbf{r}, \mathbf{r} + \mathbf{u}) \rangle \, . \tag{6.24}$$

Now, the Taylor expansion of $\langle \rho_{x,\sigma}(\mathbf{r}, \mathbf{r} + \mathbf{u}) \rangle$ up to the second order of **u** i.e., term upto $\mathbf{u}^2$ gives

$$\langle \rho_{x,\sigma}(\mathbf{r}, \mathbf{r} + \mathbf{u}) \rangle = \rho_\sigma(\mathbf{r}) + \frac{1}{4} \left[\nabla^2 \rho_\sigma(\mathbf{r}) - 2\tau_\sigma(\mathbf{r}) + \frac{1}{2} \frac{|\nabla \rho_\sigma(\mathbf{r})|^2}{\rho_\sigma} + 2 \frac{\vec{j}_{p,\sigma}^2(\mathbf{r})}{\rho_\sigma(\mathbf{r})} \right] u^2 + \dots, \tag{6.25}$$

where, $\tau = \sum_i^{occ} |\vec{\nabla}\psi_{i,\sigma}|^2$ and $\vec{j}_{p,\sigma}$ are the KS kinetic energy density and paramagnetic current density respectively. However, this model failed to achieve the homogeneous electron gas limit of the exchange hole and can not be applied directly to the exchange energy expressing. To use this expansion to construct the exchange energy functional, Pittalis et. al. [395] made the same argument as Becke's in 3D. They consider that the 2D homogeneous electron gas (2D-HEG) is a good reference system to model the exchange hole in the small density-gradient limit (SGL). Incorporating the SGL limit, the exchange hole becomes,

$$
\langle \rho_{x,\sigma}(\mathbf{r},\mathbf{r+u}) \rangle = \begin{cases} [1 + a_\sigma(\mathbf{r})u^2 + b_\sigma(\mathbf{r})u^4 + \ldots] \langle \rho_{x,\sigma}^{2DHEG}(\mathbf{r},\mathbf{r+u}) \rangle, & \text{if } k_{F,\sigma}u < z \\ \langle \rho_{x,\sigma}^{2DHEG}(\mathbf{r},\mathbf{r+u}) \rangle, & \text{if } k_{F,\sigma}u \geq z. \end{cases}
$$

$$(6.26)$$

where $\langle \rho_{x,\sigma}^{2DHEG}(\mathbf{r},\mathbf{r+u}) \rangle = \frac{4J_1^2(k_{F,\sigma}u)}{k_{F,\sigma}^2 u^2}\rho_\sigma(\mathbf{r})$ (J_1 is the first order Bessel function and $k_F = (4\pi\rho_\sigma)^{\frac{1}{2}}$ be the Thomas-Fermi wave-vector in 2D) is the exchange-hole functional in 2D-HEG limit and z is the first root of the first order Bessel function J_1 which needs to be evaluated numerically. Now, keeping the terms in the polynomial of Eq.(6.26) up to u^4 and comparing it with the Taylor expanded cylindrical averaged exchange hole expression of Eq.(6.25), the coefficients $a_\sigma(\mathbf{r})$ and $b_\sigma(\mathbf{r})$ is obtained as,

$$
a_\sigma(\mathbf{r}) = \frac{1}{4\rho_\sigma}\left[\frac{2}{3}\nabla^2\rho_\sigma + \frac{1}{2}\frac{|\vec{\nabla}\rho_\sigma|^2}{\rho_\sigma}\right].
$$

$$(6.27)$$

The coefficient b is determined upon using the normalization sum rule to the cylindrical averaged exchange hole and it is given by,

$$
b_\sigma(\mathbf{r}) = -4\pi\frac{I(1)}{I(3)}\rho_\sigma(\mathbf{r})a_\sigma(\mathbf{r}),
$$

$$(6.28)$$

where $I(m)$ is associated with the Bessel function via $I(m) = \int_0^z dy J_1^2(y)$. For slowly varying density limit the semi-classical approximation of kinetic energy density [409] can be considered as a good reference system and upon substituting it, the SGL of exchange

energy functional becomes,

$$E_{x,\sigma}^{\text{SGL}} = -\frac{5}{48\sqrt{\pi}} \left[\frac{I(0)I(3) - I(1)I(2)}{I(3)} \right] \int \frac{|\nabla\rho_\sigma(\mathbf{r})|^2}{\rho_\sigma^{3/2}(\mathbf{r})} \, d^2r \ . \tag{6.29}$$

Having established the SGL of the exchange energy, we now concentrate on the large density-gradient limit (LGL) of it. Regarding the LGL, Pittalis et. al. [395] prescribed that the density gradient term dominates over the rest of the terms in the exchange hole expression. Also, to ensure the convergence criteria of cylindrical averaged exchange hole a Gaussian function is introduced within it. Thus, according to the formalism prescribed by Pittalis et. al. [395], the cylindrical averaged exchange hole in the LGL becomes,

$$\langle \rho_{x,\sigma}(\mathbf{r}, \mathbf{r} + \mathbf{u}) \rangle \approx \left[\frac{1}{8} \frac{|\nabla\rho_\sigma(\mathbf{r})|^2}{\rho_\sigma(\mathbf{r})} u^2 \right] F(\alpha_\sigma(\mathbf{r})u) \ , \tag{6.30}$$

where the Gaussian function $F(y) = e^{-y^2}$ and the parameter α_σ are determined from the normalization of the exchange hole. This leads to the LGL of exchange energy i.e.,

$$E_{x,\sigma}^{\text{LGL}} = -\frac{\pi^{1/4}}{2^{3/2}} G(2) G^{-3/4}(3) \int d^2r \frac{|\nabla\rho_\sigma(\mathbf{r})|^{1/2}}{\rho_\sigma^{3/4}(\mathbf{r})} \ , \tag{6.31}$$

where the function $G(m)$ is determined as,

$$G(m) = \int_0^\infty dy \, y^m e^{-y^2}. \tag{6.32}$$

Finally, incorporating the SGL and LGL of the spin-polarized exchange energy functional and interpolating between these two limits, Pittalis et. al. [395] constructed the exchange energy functional as

$$E_x^{\text{2D-GGA}}[\rho_\sigma, \nabla\rho_\sigma] = E_x^{\text{LDA}}[\rho_\sigma] - \beta \sum_{\sigma=\uparrow,\downarrow} \int d^2r \frac{|\nabla\rho_\sigma(\mathbf{r})|^2}{\rho_\sigma^{3/2}(\mathbf{r}) \left[1 + \gamma \frac{|\nabla\rho_\sigma(\mathbf{r})|^2}{\rho_\sigma^3(\mathbf{r})} \right]^{3/4}} \ , \tag{6.33}$$

where

$$E_x^{\text{2D-LDA}}[\rho_\sigma] = -\frac{8}{3\sqrt{\pi}} \int d^2r \rho_\sigma^{3/2}(\mathbf{r}) \tag{6.34}$$

is the 2D-LDA exchange energy obtained from the homogeneous electron gas limit. The values of the parameter β and γ are obtained by fitting the exchange energy of the parabolic quantum dots which becomes $\beta = 0.003317$ and $\gamma = 0.008323$ respectively.

6.3.2 Modified GGA exchange energy functional

In this section we construct a modified form of 2D-GGA functional. In 3D, the inhomogeneity is included in the GGA approximation through the reduced density gradient. Analogous to that, in 2D, we construct a exchange energy functional by incorporating the reduced density gradient ($s = \frac{|\nabla \rho_\sigma(\mathbf{r})|^2}{2k_F\rho}$). The forms of 3D and 2D reduced density gradient is similar. However, the only difference is that in 3D, $s \sim \rho^{5/3}$ and in 2D, it becomes $s \sim \rho^{3/2}$. The power of ρ in the reduced density gradient can also be derived from dimensional analysis. Now, motivated by the construction of the enhancement factor in 3D GGA functional, we construct a form of 2D-GGA enhancement factor by utilizing the cylindrical average exchange hole model described in the previous section. Once the spin-unpolarized form of the 2D-GGA is constructed, it can be easily transformed into its spin-polarized form. This is one of the most captivating features of describing any GGA as a functional of its reduced density gradient.

Analogous to 3D, in 2D also, one can write

$$E_x^{GGA}[\rho] = \int d^2r \; A_x \rho(\mathbf{r})^{3/2} F_x[s] \; , \tag{6.35}$$

where $A_x = \frac{4(2\pi)^{1/2}}{3\pi}$ and $s = \frac{|\vec{\nabla}\rho|}{2(2\pi)^{1/2}\rho^{3/2}}$ is the reduced density gradient. Again, using the SGL and LGL of the 2D exchange enhancement factor. Regarding the SGL of F_x, it is obtained to be

$$F_x^{SGL} \;\; = \;\; 1 + \mu^{SGL}s^2 \; , \tag{6.36}$$

where the small gradient expansion coefficient μ^{SGL} of the enhancement factor is nothing but $\mu^{SGL} = \frac{2\pi^{3/2}}{4^{3/2}\sqrt{\pi}}\left[\frac{I(0)I(3)-I(1)I(2)}{I(3)}\right]$. The value of μ^{SGL} is obtained using the same procedure as described in the previous section but in the spin-unpolarized form.

Regarding the LGL of the exchange enhancement factor, it is obtained as,

$$F_x^{LGL} \;=\; 1 + \mu^{LGL} s^{\frac{1}{2}} \;, \tag{6.37}$$

where $\mu^{LGL} = \left(\frac{\pi}{4}\right)^{\frac{1}{4}} \frac{\kappa^{LGL}}{A_x}$ with the parameter $\kappa^{LGL} = 0.35078$.

Here, we observe that the SGL and LGL expansion of the enhancement factor F_x shows its dependency on s^2 and $s^{\frac{1}{2}}$ respectively. Combination these two limit we propose the following form of the exchange enhancement factor,

$$F_x^{2D-MODGGA}(s) = 1 + \mu \frac{s \log(g)}{1 + \beta s^{\frac{1}{2}} \log(g) + (1 - e^{-cs^2})} \;, \tag{6.38}$$

where $g = s + \sqrt{1 + s^2}$. This enhancement factor correctly obeys the large and small gradient limit of the exchange enhancement factor. But, the parameters are different from previously obtained it's SGL and LGL values. Regarding the parameters μ, β and c, these are obtained by using the LGL of the enhancement factor and by considering the physically relevant 2D systems like few-electrons parabolic quantum dots. This is done to improve the flexibility of the newly proposed functional. In Fig. 6.1, we compare the newly constructed 2D-MODGGA (2D modified GGA) enhancement factor with two other GGA level functionals, 2D-GGA [395] and 2D-B88 [403]. As shown in Fig. 6.1, the 2D-MODGGA enhancement factor increases monotonically unlike 2D-GGA and 2D-B88 enhancement factors.

6.3.3   Comparison shopping for the gradient-corrected 2D functionals

We employ the 2D-MODGGA functional for the model systems using the 2D suite code OCTOPUS [105]. The OCTOPUS [105] code performs the solution of the KS equation in 2D grid by solving the equation,

$$[-\frac{1}{2}\nabla^2 + v_{KS}(\mathbf{r})]\psi_i(\mathbf{r}) = \varepsilon_i \psi_i(\mathbf{r}), \tag{6.39}$$
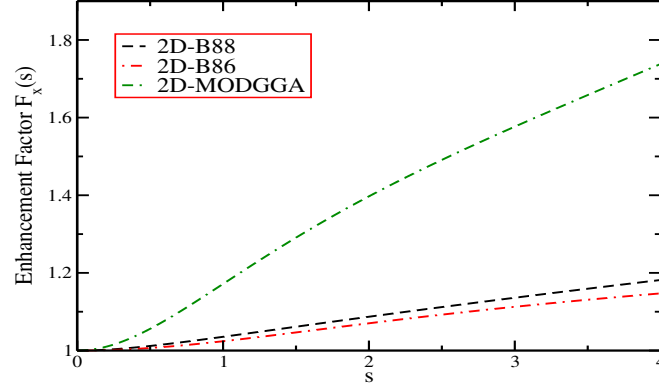
Figure 6.1: Shown is the exchange enhancement factors for F_x^{MODGGA}. For comparison the exchange enhancement factor of 2D-B88 and 2D-B86 are also shown.

Table 6.1: Shown are the exchange energies (in a.u.) as obtained from different functional for parabolic quantum dot with different confinement strengths. The error statistics (mean absolute error (MAPE)), Δ is also reported in the last row.

N	ω	$-E_x^{2D-KLI}$	$-E_x^{2D-LDA}$	$-E_x^{2D-B86}$	$-E_x^{2D-B88}$	$-E_x^{2D-MODGGA}$
2	1/6	0.380	0.337	0.368	0.364	0.378
2	0.25	0.485	0.431	0.470	0.464	0.482
2	0.50	0.729	0.649	0.707	0.699	0.723
2	1.00	1.083	0.967	1.051	1.039	1.070
2	1.50	1.358	1.214	1.319	1.304	1.361
2	2.50	1.797	1.610	1.748	1.728	1.756
2	3.50	2.157	1.934	2.097	2.074	2.089
6	$1/1.89^2$	1.735	1.642	1.719	1.775	1.735
6	0.25	1.618	1.531	1.603	1.594	1.619
6	0.42168	2.229	2.110	2.206	2.241	2.228
6	0.50	2.470	2.339	2.444	2.431	2.469
6	1.00	3.732	3.537	3.690	3.742	3.727
6	1.50	4.726	4.482	4.672	4.648	4.716
6	2.50	6.331	6.008	6.258	6.226	6.305
6	3.50	7.651	7.264	7.562	7.525	7.605
12	0.50	5.431	5.257	5.406	5.387	5.434
12	1.00	8.275	8.013	8.230	8.311	8.275
12	1.50	10.535	10.206	10.476	10.444	10.518
12	2.50	14.204	13.765	14.122	14.080	14.149
12	3.50	17.237	16.709	17.136	17.086	17.129
20	0.50	9.765	9.553	9.746	9.722	9.780
20	1.00	14.957	14.638	14.919	15.029	14.970
20	1.50	19.108	18.704	19.053	19.188	19.113
20	2.50	25.875	25.334	25.796	25.973	25.853
20	3.50	31.491	30.837	31.392	31.603	31.429
Δ (MAPE)			5.70	1.70	3.90	0.48

where ψ_i are the KS orbitals. The KS potential $v_{KS}(\mathbf{r})$ is given by $v_{KS}(\mathbf{r}) = v_H(r) + v_{xc}(\mathbf{r}) + v_{ext}(\mathbf{r})$. Here, the external potential is either $v_{ext}(r) = \frac{1}{2}\omega^2 r^2$ or $-V_0 e^{-\omega^2 r^2}$. To test the functional performance, we choose the parabolic quantum dot potential ($v_{ext}(r) = \frac{1}{2}\omega^2 r^2$) with $N = 2$ and confinement strength $\omega = 1/6, 0.25$ and 0.50. In our calculation we use the orbital and density of the exact exchange (within Krieger-Li-Iafrate (KLI)

Table 6.2: Shown are the exchange energies (in atomic units) of Gaussian quantum dot ($v_{ext} = -V_0 e^{-\omega^2 r^2}$) system with different confinement strength as obtained with different approximations. The mean absolute error (MAPE), Δ is also reported in the last row.

V_0	N	ω^2	$-E_x^{2D-KLI}$	$-E_x^{2D-LDA}$	$-E_x^{2D-B86}$	$-E_x^{2D-B88}$	$-E_x^{2D-MODGGA}$
10	2	0.25	1.573	1.405	1.529	1.557	1.543
10	2	1/6	1.427	1.274	1.386	1.412	1.403
10	2	0.50	1.839	1.643	1.788	1.821	1.793
40	6	0.1	6.525	6.194	6.450	6.533	6.495
40	6	0.25	8.255	7.840	8.160	8.263	8.192
40	6	1/6	7.454	7.076	7.367	7.461	7.407
40	20	0.1	25.387	24.871	25.311	25.490	25.355
40	20	1/6	28.692	28.122	28.611	28.815	28.635
40	20	0.25	31.348	30.736	31.263	31.490	31.268
40	30	0.1	39.548	38.985	39.493	39.722	39.500
40	30	1/6	44.156	43.546	44.099	44.363	44.076
Δ (MAPE)				5.09	1.18	0.50	0.80

approximation [410]) as the reference input for our functional. Upon comparing the exact exchange results within Krieger-Li-Iafrate (KLI) approximation [410], the values of the μ, β and c are obtained to be $0.84089\,\mu^{LGL}$, 0.248 and 0.1 respectively. This choice of values are quite realistic as using these parameters we observe that the mean percentage error of the overall test set gets reduced. In Table 6.1 we summarize the results as obtained using different level of approximations. Our comparison functional includes 2D-LDA, 2D-B88 [403] and 2D-B86 [395]. From Table 6.1 it is evident that 2D-MODGGA reduces the error significantly compared to the existing GGA functionals.

Next, the testing of the functional is carried out for Gaussian quantum dots and the results are given in Table 6.2. To obtain the bound states for large particle numbers, one needs large $-V_0$ value. Therefore, we restrict our present study for a few electron numbers and considerably large potential depth. From Table 6.2 it is evident that the 2D-B88 works well in the low-density profile but deviates from exact exchange values as the electron number increases. In this perspective, the 2D-B86 and 2D-MODGGA give overall good results for the whole test set. 2D-MODGGA reduces the error present in 2D-B86 through its improved form.

6.4 Inclusion of the Kohn-Sham Kinetic Energy Density: Importance and Behavior

So far all the methods we discussed are based on HEG and GGA. As, one step forward, it is always interesting to include the KS-KE into the functional ingredient. But, before going into the formal derivation of the first-ever KS kinetic energy density-dependent functional [39], it is crucial to explore the role of KS kinetic energy density for 2D. Note that the KS kinetic energy density is an importance quantity which is used to construct the electron localization factor (ELF) [405]. In this section, we will explore the behavior of the KS-KE using the two-dimensional isotropic quantum harmonic oscillator as a model system. The behavior of KS-KE is studied thoroughly in 3D [411, 412] ,but the same is not explored in 2D. In this chapter, However, KS-KE density behaves similar to the its 3D counterpart for the asymptotic region of the finite 2D systems.

To study rigorously the nature of the KS-KE density in 2D, we begin by considering the single-electron non-interacting eigenstates of 2D isotropic harmonic oscillator.This system is very useful to gain better physical insight of the behavior of the KS-KE density τ^{KS} in 2D. In this section, our focus will remains on two important domains: $\mathbf{r} \to 0$ and $\mathbf{r} \to \infty$. To do this, we start with the Fock-Darwin equation of 2D quantum Harmonic oscillator [384] with eigenfunctions

$$\Psi_{nl}(\mathbf{r}, \phi) = \frac{e^{il\phi}}{\sqrt{2\pi}}\sqrt{\frac{n!}{(n+|l|)!}}e^{-\frac{r^2}{4}}\left(\frac{r}{\sqrt{2}}\right)^{|l|}L_n^{|l|}\left(\frac{r^2}{2}\right) = f_{nl}(\mathbf{r})e^{-\frac{r^2}{4}}e^{il\phi}, \quad (6.40)$$

where

$$f_{nl} = \frac{1}{\sqrt{2\pi}}\sqrt{\frac{n!}{(n+|l|)!}}\left(\frac{r}{\sqrt{2}}\right)^{|l|}L_n^{|l|}\left(\frac{r^2}{2}\right) \quad (6.41)$$

is the radial function connected with the associated Laguerre polynomials,

$$L_n^{|l|}(x) = \sum_{m=0}^{n}(-1)^m\frac{(n+|l|)!}{(n-m)!\,(|l|+m)!\,m!}\,x^m\,, \quad (6.42)$$

where $n(= 0, 1, 2.....)$ and $l(= 0, \pm1, \pm2....)$ are radial and orbital quantum numbers respectively. The corresponding densities are also given by

$$\rho_{nl}(\mathbf{r}) = |\Psi_{nl}(\mathbf{r}, \phi)|^2 = [f_{nl}(\mathbf{r})]^2 e^{-r^2/2}. \tag{6.43}$$

Now, expressing the the KS-KE density in terms of the polynomial function we obtain,

$$\tau_{nl}^{KS} = \frac{1}{2}|\nabla\Psi_{nl}(\mathbf{r}, \phi)|^2 = \frac{1}{2}\Big[\frac{df_{nl}}{dr} - \frac{1}{2}rf_{nl}\Big]^2 e^{-r^2/2} + \frac{l^2\rho_{nl}}{2r^2} . \tag{6.44}$$

The 1st term on the right side of Eq.(6.44) is the VW-KE density which is obtained by using Eq.(6.43) into $\tau^{VW} = \frac{|\vec{\nabla}\rho|^2}{8\rho}$. Therefore, resultant Eq.(6.44) becomes,

$$\tau_{nl}^{KS} = \tau^{VW}[\rho_{nl}] + \frac{l^2\rho_{nl}(\mathbf{r})}{2r^2} . \tag{6.45}$$

The Eq.(6.45) is the paramount equation of this section and it will be used to explore the behavior of KS-KE density. Using Eq.(6.45), KS-KE density becomes

$$\tau^{KS} = \sum_{nl} \tau_{nl}^{KS}. \tag{6.46}$$

Note that in general $\tau^{VW}[\rho] \neq \sum_{nl}\tau^{VW}[\rho_{nl}]$.

6.4.1   r $\rightarrow$ 0 behavior of 2D KS-KE density

In this subsection, we discuss elaborately discuss the behavior of 2D KS-KE density at **r** $\rightarrow$ **0**. To do so we start with the different orbitals contribution as follows: (i) From the Fock-Darwin equation the density corresponding to s $(l = 0)$ becomes

$$\rho_{n0}(\mathbf{r}) = [f_{n0}(\mathbf{r})]^2 e^{-r^2/2}, \tag{6.47}$$

where

$$f_{n0}(\mathbf{r}) \;=\; \frac{1}{\sqrt{2\pi}} L_n^0\left(\frac{r^2}{2}\right) = \frac{1}{\sqrt{2\pi}}\left[1 - \frac{1}{2}nr^2 + \frac{1}{16}n(n-1)r^4 - \dots\dots\right]. \quad (6.48)$$

Thus, in $\mathbf{r} \to 0$ limit, the $\rho_{n0}(\mathbf{r})$, KS-KE and VW-KE density becomes,

$$\rho_{n0}(r \to 0) = \frac{1}{2\pi}\left[1 - \frac{1}{2}(2n+1)r^2 + \frac{1}{8}(3n^2 + 3n + 1)r^4 ..\right]. \quad (6.49)$$

and

$$\tau_{n0}^{KS}(r \to 0) = \tau_{n0}^{VW}(r \to 0) \;=\; \frac{1}{16\pi}\left[(2n+1)^2 r^2 - \frac{1}{2}(4n^3 + 6n^2 + 4n + 1)r^4 ..\right] \quad (6.50)$$

In principle, if only s orbital is occupied then $\rho_{n0}(0) = \frac{1}{2\pi}$ but we obtain vanishing KS-KE and VW-KE densities.

(ii) Now, if the p $(l = 1)$ shell is occupied, then

$$\rho_{n1}(\mathbf{r}) = [f_{n1}(\mathbf{r})]^2 e^{-r^2/2}, \quad (6.51)$$

where

$$\begin{aligned}
f_{n1}(\mathbf{r}) &= \frac{1}{\sqrt{2\pi}}\frac{1}{\sqrt{n+1}}\frac{r}{\sqrt{2}}L_n^1\left(\frac{r^2}{2}\right)\\
&= \frac{1}{\sqrt{2\pi}}\frac{1}{\sqrt{n+1}}\frac{r}{\sqrt{2}}\left[(n+1) - \frac{1}{4}n(n+1)r^2 + \frac{1}{48}(n+1)n(n-1)r^4 - \dots\dots\right].
\end{aligned} \quad (6.52)$$

So, in the limit $\mathbf{r} \to 0$ the density expression of Eq.(6.51) becomes,

$$\rho_{n1}(\mathbf{r} \to 0) = \frac{1}{2\pi}\left[\frac{1}{2}(n+1)r^2 - \frac{1}{4}(n+1)^2 r^4 + \dots\right]. \quad (6.53)$$

Similarly, for $l = 0$ and $\mathbf{r} \to 0$ cases also,

$$\tau_{n1}^{KS}(r \to 0) = \frac{1}{4\pi}[(n+1) - (n+1)^2 r^2 + ...]$$

(6.54)

and

$$\tau_{n1}^{VW}(r \to 0) = \frac{1}{8\pi}\left[(n+1) - \frac{3}{2}(n+1)^2 r^2 + ...\right].$$

(6.55)

Therefore, no cusp condition is observed in the case of p $(l = 1)$. But interestingly, we observe the ratio of KS-KE to that of VW-KE density for $l = 1$ becomes,

$$\frac{\tau_{n1}^{KS}(\mathbf{r} \to 0)}{\tau_{n1}^{VW}(\mathbf{r} \to 0)} = 2.$$

(6.56)

In 3D, the similar condition is also observed but the corresponding ratio becomes 3 [412].

In a more general way, the above conditions can also be written as, For $l = 0$:

$$\tau_{n0}^{KS}(\mathbf{r} \to 0) = \tau^{VW}[\rho_{n0}](\mathbf{r} \to 0) = 0,$$

(6.57)

$l = 1$:

$$\tau_{n1}^{KS}(\mathbf{r} \to 0) = \tau^{VW}[\rho_{n1}](\mathbf{r} \to 0) + \frac{1}{2}A_{n1},$$

(6.58)

and
$l = 2$:

$$\tau_{n2}^{KS}(\mathbf{r} \to 0) = \tau^{VW}[\rho_{n2}](\mathbf{r} \to 0),$$

(6.59)

where A_{nl} is associated with the Laguerre polynomials.

Note that in a compact notation form Eq.(6.57) to Eq.(6.59) can also be written as ,

$$
\tau_{nl}^{KS}(\mathbf{r} \to 0) = \begin{cases} 0 & l = 0 \\ \frac{1}{2}A_{n1} + \frac{1}{2}A_{n1} = 2\tau^{VW}[\rho_{n1}](\mathbf{r} \to 0) & l = 1 \\ 0 & l \geq 2, \end{cases} \tag{6.60}
$$

where the following factor is used:

$$
\tau^{VW}[\rho_{n1}](\mathbf{r} \to 0) = \frac{1}{8}\frac{(2A_{n1}r)^2}{A_{n1}r^2} = \frac{1}{2}A_{n1} . \tag{6.61}
$$

So, Eq.(6.60) also confirms the validity of Eq.(6.56). Now, Eq.(6.60) together with Eq.(6.47) results in,

$$
\tau^{KS}(\mathbf{r} \to 0) = \sum_{nl} \tau_{nl}^{KS}(\mathbf{r} \to 0) = \sum_{n} 2\tau^{VW}[\rho_{n1}](\mathbf{r} \to 0) \tag{6.62}
$$

From the above analysis one can conclude that the $l = 1$ orbital is important for the VW-KE density at $\mathbf{r} \to 0$. The show the validity of the resultant mathematical expression of Eq.(6.62) we also plot the ratio τ^{VW}/τ^{KS} for the parabolic quantum dot systems with $N = 6$ electrons (shown in Fig. 6.2). From this figure it is evident that the presence of s orbital, the above mentioned ratio becomes zero near origin and it keeps increasing as r increases, which clearly indicates the inclusion of p orbital. Whereas, both τ^{unif} and $\tau^{VW} + \alpha\,\tau^{unif}$ start from finite value at $r \to 0$. Here, we consider the slowly varying approximation of $\alpha = \frac{\tau^{KS} - \tau^{VW}}{\tau^{unif}} \approx 1 - 2p + \frac{8}{3}q$ and $\tau^{unif} = \pi\rho^2/2$. This is because s electron density has finite value at $r \to 0$. All these numerical evidence actually establish the validity of our theoretical framework.

6.4.2 $\mathbf{r} \to \infty$ behavior of 2D KS-KE density

To show the behavior of 2D KS-KE density in $\mathbf{r} \to \infty$ we consider the contributes of the outermost valence shells only. We characterize the quantum numbers of the outermost valence shells as $n \to n'$, $l \to l'$ and density corresponding to those orbitals as $\rho \to \rho'$.
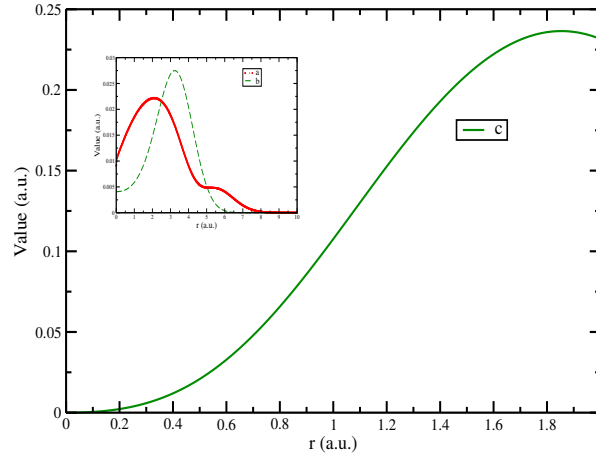
Figure 6.2: Shown are near origin behavior (for $N = 6$ electron) of (a) $\tau^{\sigma-VW} + \alpha^\sigma \tau^{\sigma-unif}$ (where, $\alpha = 1 - 2p + \frac{8}{3}q$ is the meta-GGA ingredient defined in the slowly varying density limit), (b) $\tau^{\sigma-unif}$ and (c) $\tau^{\sigma-VW}/\tau^{\sigma-KS}$. Here we have shown near origin behavior of $\tau^{\sigma-VW}/\tau^{\sigma-KS}$.

Form Eq.(6.45) the difference of the KS-KE density and the VW KE deinsity is given by,

$$\tau' = \tau^{KS} - \tau^{VW} \rightarrow_{\mathbf{r}\to\infty} \tau^{KS}_{n'l'} - \tau^{VW}_{n'l'} = \frac{l'^2 \rho'_{n'l'}}{2r^2}. \tag{6.63}$$

Note that for $l' = 0$ type outer shell $\tau^{KS} \to \tau^{VW}$. However, for $l' \neq 0$, there are other orbital contribution also. To make this point more evident we also plot the differences of the KS-KE density from its VW-KE density and the same is shown in Fig. 6.3. From Fig. 6.3 we observe that $\tau^{KS} \to \tau^{VW}$ (as $\mathbf{r} \to \infty$).

6.5   Meta-GGA Functional in 2D

Based on the development so far, in this section, we now develop a meta-GGA level functional in 2D. Regarding the functional development in 2D, so far all the development for the 2D functionals are done upto the level of LDA [390] and GGA [39–41, 390–408]. As discussed before, the GGA functional is proposed by Pittalis et. al. [395] is
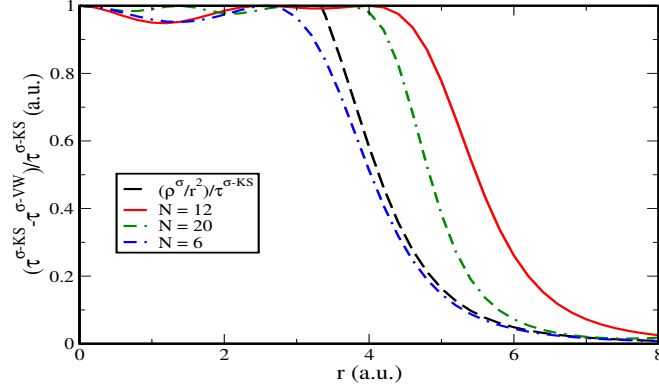
Figure 6.3: Shown is the deviation of the exact KS-KE density from the VW KE density for N = 6 ($\omega = 0.25$), N = 12 ($\omega = 1/1.89^2$) and N = 20 ($\omega = 0.50$). For comparison $\frac{\rho^\sigma(\mathbf{r})/r^2}{\tau^{\sigma-KS}}$ for N = 6 ($\omega = 0.25$) is also shown.

based on the Taylor series expansion of the exchange hole. However, in chapter 3 we have shown that the exchange hole can be constructed in several ways like using Taylor series expansion, real space cutoff procedure, or the density matrix expansion (DME) technique. It is noteworthy the the most advance technique is the DME expansion. The exchange hole based on the DME expansion technique shows its correct behavior not only for the small separation, but also do converge for large separation. In this section we will construct a 2D exchange hole and the corresponding functional based on the DME expansion technique. We will benchmark our functional to the model systems like parabolic and Gaussian quantum dots.

6.5.1 Exchange hole and energy under generalized coordinate transformation

Under general coordinate transformation (see APPENDIX B for the details) i.e. $(\vec{r}_1, \vec{r}_2) \rightarrow (\vec{r}^\lambda, u)$, where $\vec{r}^\lambda = \lambda \vec{r}_1 + (1-\lambda)\vec{r}_2$, the exchange energy functional of Eq.(6.20) becomes,

$$E_x = \frac{1}{2} \int d^2 r^\lambda \rho(\vec{r}^\lambda) \int \frac{\rho^t_{x2D}(\vec{r}^\lambda, u)}{u} \, d^2 u \, , \tag{6.64}$$

where the generalized coordinate transformed exchange hole ρ_{x2D}^t is given by

$$\rho_x^t = -\frac{|\Gamma_1^t(\vec{r}^\lambda - (1-\lambda)\vec{u}, \vec{r}^\lambda + \lambda\vec{u})|^2}{2\rho(\vec{r})} \ . \tag{6.65}$$

Γ_1^t is 1st order reduced density matrix. The parameter, λ is the coordinate transformed parameter and can take values $1/2 \to 1$ (or, $0 \to 1/2$). Note that $\lambda = 1$ and $\lambda = \frac{1}{2}$ correspond to the conventional and on top exchange holes [234]. Now, using the Taylor series expansion the transformed single particle KS density matrix around $u = 0$ becomes

$$
\begin{aligned}
\Gamma_1^t(\mathbf{r}, \mathbf{r} + \mathbf{u}) &= e^{\mathbf{u}.[-(1-\lambda)\vec{\nabla}_1 + \lambda\vec{\nabla}_2]} \Gamma_1^t(\mathbf{r}, \mathbf{u})|_{\mathbf{u}=0} \\
&= e^{\mathbf{u}.[-(1-\lambda)\vec{\nabla}_1 + \lambda\vec{\nabla}_2]} \Big[\sum_i^{occ} \Psi_i^*(\mathbf{r}^\lambda - (1-\lambda)\mathbf{u})\Psi_i(\mathbf{r}^\lambda + \lambda\mathbf{u})| \Big]_{\mathbf{u}=0} \\
&= e^{\mathbf{u}.[-(1-\lambda)\vec{\nabla}_1 + \lambda\vec{\nabla}_2]} \sum_i^{occ} \Psi_i^*(\mathbf{r}^\lambda)\Psi_i(\mathbf{r}^\lambda) \\
&= [1 + u[-(1-\lambda)\vec{\nabla}_1 + \lambda\vec{\nabla}_2]cos\theta + u^2[-(1-\lambda)\vec{\nabla}_1\lambda\vec{\nabla}_2]^2 cos^2\theta] \\
&\qquad\qquad \sum_i^{occ} \Psi_i^*(\mathbf{r}^\lambda)\Psi_i(\mathbf{r}^\lambda) \ , \tag{6.66}
\end{aligned}
$$

where $\vec{\nabla}_1$ and $\vec{\nabla}_2$ are the gradient operators which are acting on Ψ_i^* and Ψ_i respectively. The exchange energy functional for 2D can be constructed from the cylindrical average of the exchange hole $\langle \rho_x(\vec{r}, \vec{r} + \vec{u})\rangle_{cyl}$ over the direction of $\vec{u}$ i.e.

$$\langle \rho_x(\vec{r}, \vec{r} + \vec{u})\rangle_{cyl} = \int \rho_x(\vec{r}, \vec{r} + \vec{u}) \frac{d\Omega_u}{2\pi} \ . \tag{6.67}$$

Applying this method the and doing the Taylor series expansion results the correct small u expansion of the coordinate transformed exchange hole as,

$$\langle \rho_x^t \rangle = -\frac{\rho(\vec{r})}{2} - \frac{1}{4}\Big[\Big(\lambda^2 - \lambda + \frac{1}{2}\Big)\nabla^2\rho(\vec{r}) - 2\tau + \frac{1}{4}\Big(2\lambda - 1\Big)^2 \frac{|\vec{\nabla}\rho(\vec{r})|^2}{\rho(\vec{r})} \Big]u^2 \ . \tag{6.68}$$

Note that the above expansion recovered the correct small 'u' expansion in 2D [395] upon considering $\lambda = 1$. The Eq.(6.68) is more general than the proposed one in ref. [395].

6.5.2 A new form semilocal exchange hole and the functional

Here we employ the DME technique by satisfying three important criteria of the exchange hole. The underlying exchange hole rightly obtain: (i) the uniform electron gas limit of the exchange hole, (ii) correct small 'u' expansion upon considering terms upto u^2, and (iii) the large u-limit (i.e. 0 to ∞ integral limit of u) do converge for the direct implementation of this exchange hole in the exchange energy functional. To achieve this goal we consider following plane wave expansion in terms of the Bessel and Hypergeometric functions

$$e^{\frac{kucos\phi y}{k}} = \mathcal{A} + \mathcal{B} , \tag{6.69}$$

where

$$\begin{aligned}
\mathcal{A} &= \frac{2}{ku} \sum_{n=0}^{\infty} (-1)^n (2n+1) J_{2n+1}(ku) C_{2n}^1 \left(-i \frac{ycos\phi}{k} \right) \\
\mathcal{B} &= \frac{2}{ku^2} \sum_{n=0}^{\infty} (-1)^n (2n+1) J_{2n+1}(ku) \frac{1}{2\cos\phi} \times \frac{\partial}{\partial y} \left[C_{2n}^1 \left(-i \frac{ycos\phi}{k} \right) \right]
\end{aligned} \tag{6.70}$$

and ϕ be the azimuthal angle. The polynomials, C_{2n}^m are expressed as

$$C_{2\nu}^m(x) = (-1)^\nu \begin{pmatrix} \nu+m-1 \\ \nu \end{pmatrix} {}_2F_1(-\nu, \nu+m; \frac{1}{2}; x^2) , \tag{6.71}$$

where ${}_2F_1$ are the generalized Hypergeometric functions. J_{2n+1} are the Bessel functions, and $y = -(1-\lambda)\vec{\nabla}_1 + \lambda\vec{\nabla}_2$. Here we use the series re-summation technique along with the Gegenbauer addition theorem [413] to arrive at the above expansion (i.e. from Eq.(6.69) to Eq.(6.70)). In APPENDIX B, we derive the scheme of generalized Gegenbauer addition theorem which is used obtain Eq.(6.69). Note that using this technique the above three mentioned criteria of the exchange hole are achieved. Finally, Eq.(6.71) together with Eq.(6.69) result to the generalized coordinate transformed density matrix as,

$$\Gamma_1^t = 2\rho \frac{J_1(ku)}{ku} + \frac{6J_3(ku)}{k^3u} \mathcal{G} + \frac{24J_3(ku)}{k^3u^2} \mathcal{H} , \tag{6.72}$$

where

$$
\begin{aligned}
\mathcal{G} &= 4\cos^2\phi\{(\lambda^2 - \lambda + \frac{1}{2})\nabla^2\rho - 2\tau\} + k^2\rho \\
\mathcal{H} &= \cos\phi(2\lambda - 1)|\nabla\rho|
\end{aligned}
\tag{6.73}
$$

with $\tau = \sum_i^{occ} |\vec{\nabla}\psi_i|^2$, the KS kinetic energy density. Now, in order to make τ gauge-invariant, we modify it such that

$$
\tau \to \tilde{\tau} = \tau - 2\frac{j_p^2}{\rho},
\tag{6.74}
$$

where

$$
j_p = \frac{1}{2i}\sum_i^{occ}\{\psi_i^*(\vec{r})[\vec{\nabla}\psi_i(\vec{r})] - [\vec{\nabla}\psi_i^*(\vec{r})]\psi_i(\vec{r})\}
\tag{6.75}
$$

is the paramagnetic current density. Using the DME obtained form DME the cylindrical averaged exchange hole becomes,

$$
\langle\rho_x^t\rangle = -\frac{2J_1^2(ku)}{k^2u^2}\rho(\vec{r}) - \frac{24J_1(ku)J_3(ku)}{k^4u^2}\mathcal{L} - \frac{144J_3^2(ku)}{k^6u^4}\mathcal{M},
\tag{6.76}
$$

where

$$
\begin{aligned}
\mathcal{L} &= (\lambda^2 - \lambda + \frac{1}{2})\nabla^2\rho - 2\tau + 4\frac{j_p^2}{\rho} + \frac{1}{2}k^2\rho \\
\mathcal{M} &= (2\lambda - 1)^2\frac{|\nabla\rho|^2}{\rho}.
\end{aligned}
\tag{6.77}
$$

Note that the above mentioned expression of the exchange hole is more general than that is proposed in ref. [140]. This expression is exact for the uniform electron gas limit upon considering $k = K_F$. Note that to fulfill the normalization condition of the exchange hole we scale $k \to fk_F$, where f will be determined from the normalization of the exchange hole. Doing so we also include the inhomogeneity in the functional form which is relevant for the inhomogeneous systems. Thus considering the normalization of the exchange hole

we obtain

$$\frac{1}{f^2} + \frac{6}{f^4}y = 1 \ , \tag{6.78}$$

where $y = (2\lambda - 1)^2 p$ and $p = s^2 = \frac{|\vec{\nabla}\rho|^2}{(2k_F\rho)^2}$ is the square of the reduced density gradient (s) in 2D. Note that for slowly varying density limit, Eq.(6.78) becomes $f \approx 1 + 6y$ and in the large density gradient limit it becomes $f \to y^{\frac{1}{4}}$ [140]. To maintain the required criteria of f, we propose the following analytic form of f

$$f = [1 + 90(2\lambda - 1)^2 p + \beta(2\lambda - 1)^4 p^2]^{\frac{1}{15}} \ , \tag{6.79}$$

where the parameter λ and β will be fixed from by comparing the exact exchange results for the few-electron quantum dots systems.

Nonetheless, it is always necessary to remove the Laplacian of the density by the semi-classical approximation of the kinetic energy density. This makes the exchange energy simple and numerically more feasible. To do so we replace $\nabla^2\rho$ by,

$$\nabla^2\rho \approx 6\left[\tau - \tau_{2D}^{unif} - 2\frac{j_p^2}{\rho}\right] \ , \tag{6.80}$$

where $\tau_{2D}^{unif} = \frac{\pi\rho^2}{2}$. Using this replacement the cylindrical averaged exchange hole becomes,

$$\langle\rho_x^t\rangle = -\frac{2J_1^2(fk_Fu)}{f^2k_F^2u^2}\rho(\vec{r}) - \frac{24J_1(fk_Fu)J_3(fk_Fu)}{f^4k_F^4u^2}\mathcal{L} - \frac{144J_3^2(fk_Fu)}{f^6k_F^6u^4}\mathcal{M} \ , \tag{6.81}$$

where $\mathcal{L} = 6(\lambda^2 - \lambda + \frac{1}{2})\left[\tau - \tau_{2D}^{unif} - 2\frac{j_p^2}{\rho}\right] - 2\tau + 4\frac{j_p^2}{\rho} + \frac{1}{2}k_F^2\rho$ and $\mathcal{M} = (2\lambda - 1)^2\frac{|\nabla\rho|^2}{\rho}$. Now, the semi-local exchange energy functional in 2D can be obtained by substituting the cylindrical averaged exchange hole of Eq.(6.81) back in Eq.(6.64). This results the exchange energy expression,

$$E_x^{2D-mGGA} = -\int \rho(\vec{r})\epsilon_x^{2D-LDA}F_x^{2D-mGGA}[p, \tau, j_p] \, d^2r \ , \tag{6.82}$$

where $\epsilon_x^{2D-LDA} = \frac{4k_F}{3\pi}$ and the exchange enhancement factor $F_x^{2D-mGGA}$ is given by,

$$F_x^{2D-mGGA}[p, \tau, j_p] = \frac{1}{f} + \frac{2R}{5f^3} \tag{6.83}$$

with

$$R = 1 + \frac{128}{21}(2\lambda-1)^2 p + \frac{3\left(\lambda^2 - \lambda + \frac{1}{2}\right)\left(\tau - \tau_{2D}^{unif} - 2\frac{j_p^2}{\rho}\right) - \tau + 2\frac{j_p^2}{\rho}}{\tau_{2D}^{unif}} \; . \tag{6.84}$$

In order to visualize the behavior of the exchange enhancement factor we plot the same in Fig 6.4 for different values of the iso-orbital indicator $\alpha = \frac{\tau - \tau^W}{\tau_{2D}^{unif}}$. For comparing we also plot the 2D-B88 and 2D-GGA functional also. Unlike GGA functional the exchange enhancement factor of 2D-mGGA remains flat in the region $< 0s < 1$ and after that monotonically increases.
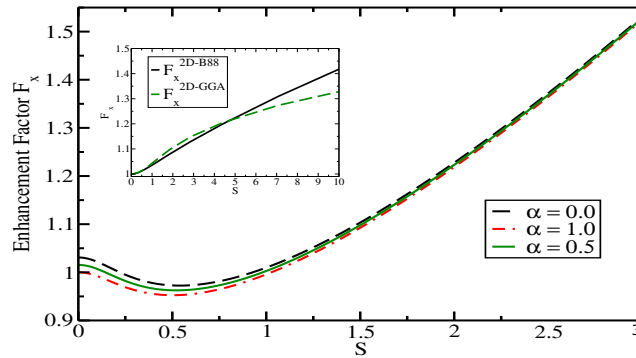
Figure 6.4: Shown is the exchange enhancement factor $F_x^{2D-mGGA}$ Eq.(6.83) (with $j_p = 0$) as a functional of s for different values of α. For comparing the enhancement factor of 2D-GGA [140] and 2D-B88 [403] are also shown in the sub-figure.

6.5.3   Performance of the 2D meta-GGA functional

To study the performance of the constructed semilocal functional we employ the functional to the $2D$ parabolic and Gaussian quantum dot systems. We fix the parameters λ and β at 0.74 and 30.0 respectively by fitting it with the exchange energies of a few-

Table 6.3: Exchange energies (in a.u.) for parabolic confined few electron quantum dots. The 1st and 2nd columns contain the number of particles and confinement strengths used for finding the parameters of the proposed functional. Results for EXX, 2D-LDA, 2D-GGA [140], 2D-B88 [403] and 2D-BR [394] are also shown for comparison with that obtained using the constructed 2D-mGGA functional. The last row contains the mean percentage error, Δ.

N	ω	$-E_x^{2D-EXX}$	$-E_x^{2D-LDA}$	$-E_x^{2D-GGA}$	$-E_x^{2D-B88}$	$-E_x^{2D-BR}$	$-E_x^{mGGA}$
2	1/6	0.380	0.337	0.368	0.364	0.375	0.386
2	0.25	0.485	0.431	0.470	0.464	0.480	0.492
2	0.50	0.729	0.649	0.707	0.699	0.722	0.735
2	1.00	1.083	0.967	1.051	1.039	1.080	1.085
2	1.50	1.358	1.214	1.319	1.304	1.354	1.354
2	2.50	1.797	1.610	1.748	1.728	1.794	1.776
2	3.50	2.157	1.934	2.097	2.074	2.020	2.113
6	$1/1.89^2$	1.735	1.642	1.719	1.749	1.775	1.736
6	0.25	1.618	1.531	1.603	1.594	1.655	1.620
6	0.42168	2.229	2.110	2.206	2.241	2.281	2.226
6	0.50	2.470	2.339	2.444	2.431	2.529	2.466
6	1.00	3.732	3.537	3.690	3.742	3.824	3.716
6	1.50	4.726	4.482	4.672	4.648	4.845	4.699
6	2.50	6.331	6.008	6.258	6.226	6.492	6.279
6	3.50	7.651	7.264	7.562	7.525	7.846	7.573
12	0.50	5.431	5.257	5.406	5.387	5.728	5.415
12	1.00	8.275	8.013	8.230	8.311	8.572	8.231
12	1.50	10.535	10.206	10.476	10.444	10.915	10.461
12	2.50	14.204	13.765	14.122	14.080	14.716	14.063
12	3.50	17.237	16.709	17.136	17.086	17.858	17.019
20	0.50	9.765	9.553	9.746	9.722	10.167	9.805
20	1.00	14.957	14.638	14.919	15.029	15.573	14.894
20	1.50	19.108	18.704	19.053	19.188	19.892	19.007
20	2.50	25.875	25.334	25.796	25.973	26.935	25.698
20	3.50	31.491	30.837	31.392	31.603	32.777	31.230
Δ(MPE)			5.7	1.7	3.9	2.8	**0.7**

Table 6.4: Exchange energies (in a.u.) for Gaussian quantum dots ($v_{ext} = -V_0 e^{-\omega^2 r^2}$) with different levels of approximation. Mean percentage error given in the last row.

V_0	N	ω^2	$-E_x^{2D-EXX}$	$-E_x^{2D-LDA}$	$-E_x^{2D-GGA}$	$-E_x^{2D-mGGA}$
10	2	0.05	1.047	0.934	1.017	1.048
10	2	0.10	1.255	1.120	1.219	1.250
10	2	0.25	1.573	1.405	1.529	1.555
10	2	1/6	1.427	1.274	1.386	1.416
10	2	0.50	1.839	1.643	1.788	1.804
40	6	0.05	5.416	5.139	5.354	5.372
40	6	0.10	6.525	6.194	6.450	6.460
40	6	0.25	8.255	7.840	8.160	8.142
40	6	1/6	7.454	7.076	7.367	7.364
Δ				8.3	2.0	**0.9**
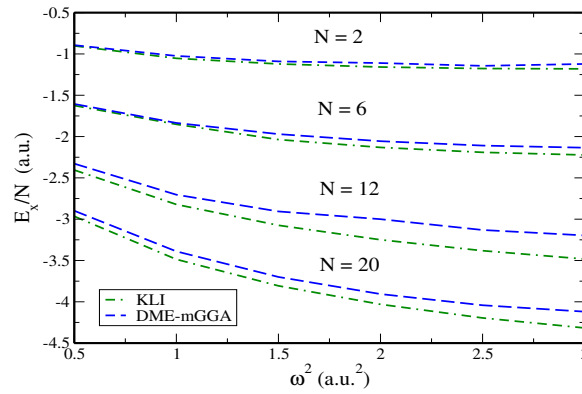
Figure 6.5: Shown in the figure, the exchange energy per electron (in a.u.) plotted versus ω^2 for a series of Gaussian quantum dots with N electrons and confinement strength ω.

electron parabolic quantum dot system. Here, all calculation is performed using the OC-TOPUS [105] code. For reference density and kinetic energy density we use the optimized effective potential (OEP) based exact exchange (EXX) within the KLI approximations [410].

Finally, in Table 6.3 the performance of the newly constructed exchange functional is summarized for the parabolic quantum dots. the obtained results of 2D-mGGA are quite superior compared to other functionals. Lastly, we employ the functional for the Gaussian quantum dots by simultaneously varying the number of electrons trapped (N), depth of the potential and confinement strength (ω). For this case, the performance is presented in Table 6.4 and plotted in Fig. 6.5. Here, also, the results are found to be in excellent agreement with KLI-EXX.

6.6   Conclusions

The main motive of this chapter is to construct the exchange energy functional to be applied for the 2D quantum systems. In principle, our developed exchange functionals can be used to describe the electronic structure of any kind of system having confined in two dimensions. In developing all these functionals, we adopt the formalism that has been used for 3D. In the first part of this chapter, we develop a modified GGA based functional using the exchange hole model by analyzing the low and high-density limits of

it. The corresponding GGA functional performs quite accurately for various quantum dot systems.

Beyond the 2D-GGA, the KS kinetic energy dependent functionals are also constructed by critically analyzing its behavior for the quantum dots systems with parabolic confinement. It is explored that the behavior of the kinetic energy density plays a crucial role in designing the KS kinetic energy dependent functionals.

The most important feature of this chapter is that we develop an exchange hole model through the density matrix expansion technique. The exchange functional constructed here is meta-GGA level. This is the first ever attempt to construct a meta-GGA level semilocal functional by explicitly designing its underlying exchange hole. The proposed exchange hole recovers correctly all the necessary importance features. The constructed exchange energy function also showing its accuracy for various $2D$ quantum dot systems. The functional is not only physically appealing but also practically useful as it opens the path for constructing exchange correlation functionals in two dimensions analog to Jacob's ladder in three dimensions.

Chapter 7

Conclusions and Outlook

7.1   Summary

In this thesis, we assessed and developed meta-GGA level semilocal and hybrid functionals for the atoms, molecules, and solid-state systems in three and two-dimensions. The developed meta-GGA functionals are studied within the framework of the projector augmented plane wave. Also, fractional occupation related problems have been assessed from the long-range corrected meta-GGA functional. Screened meta-GGA hybrid functional is also developed using short-range Hartree-Fock for the atoms, molecular and solid-state systems. Finally, quantum dot systems are studied by developing accurate meta-GGA semilocal functionals via the first-principles approach.

The most important conclusions which can be drawn from our development, and benchmarking study of the electronic properties of the molecular, bulk and lower-dimensional systems are summarized as follows:

- The developed and benchmarking calculations of the meta-generalized gradient approximations (meta-GGA) show that the accurate prediction of the structural and energetic properties of the solids can be achievable beyond the generalized gradient approximations (GGA). In this thesis, we emphasize on this fact by testing and compairing the most advanced meta-GGA functionals. Our benchmark calculations show that the meta-GGA functionals developed by satisfying more exact

constraints "qualitatively" improves most of the solid-state performances. The most interesting features of the thesis are that we have done a comparative study of the two most advanced meta-GGAs like strongly constrained and appropriately normed (SCAN) and Tao-Mo (TM) semilocal functionals within the plane wave basis set. Benchmark calculations indicate that the two functionals accurately predict most of the solid-state properties. The TM functional accurately predicts the lattice constants of the solids over other contemporary functionals. This is quite an interesting feature of the TM functionals because several other properties depend on the accuracy of the lattice constants. However, our assessment of the semilocal functionals for the transition metals show different trends as we found that the Perdew-Burke-Ernzerhof (PBE) GGA performs better than advanced meta-GGA.

- As an effort to construct meta-GGA level long-range range-separated hybrid functional, we develop a hybrid by tuning the range-separation parameter and tested the performance of the functional for thermochemical accuracy and problems related to the fractional occupation number. We observe that using meta-GGA level long-range corrected hybrids the properties related to the fractional occupation number can be improved without hindering the thermochemical accuracy. On the next level of our construction, we also propose a meta-GGA screened hybrid functional using the short-range Hartree-Fock and long-range semilocal XC functional. The fact that the performance of the proposed screened hybrid functional for the molecular systems further motivate us to use the functional for studying solid-state materials.

- Hence, we utilize the proposed meta-GGA screened hybrid functional in the solid-state study by combining the TM functional with the LDA exchange hole in the short-range semilocal part instead of constructing the full reverse engineered exchange hole. Implementation and benchmark calculations of the proposed functional in the plane wave pseudopotential code generates both the lattice constants and bandgap of solids quite satisfactorily. The screened hybrid functional keeps all the good properties of the TM functional intact, besides improvement in the bandgap of solids is observed. The present proposition can be considered as one

step ahead of the popularly used Heyd-Scuseria-Ernzerhof (HSE) functional by utilizing the Kohn-Sham kinetic energy density in screened meta-GGA functional rung.

- Lastly, we construct an accurate meta-GGA exchange functional for the two-dimensional quantum dots systems. Our developed method is in parallel to that proposed in three dimensional for the TM functional. To do so, we first construct an exchange hole by satisfying all the exact constraints of the hole and utilize that exchange hole for the construction of the exchange energy functional in two dimensions. Results obtained from the proposed meta-GGA functional showing its accuracy over all the previously proposed GGA based functionals. In principle, the presently constructed exchange functional can also be used to describe the properties related to any kind of confined systems in two-dimensional.

7.2   Future prospects

- The assessment and benchmark performance of the recently developed and most advanced semilocal functionals in the plane wave pseudopotential code will surely help the user to choose a particular functional for performing the solid-state calculations. Also, our recent studies focus on the improvement of the TM functional by developing compatible correlation energy such that the functional performance becomes free from correlation energy anomaly. Performance of the functional in surface energy, work function, and adsorption energies is also forming part of our ongoing research projects.

- The hybrid functionals we proposed for the molecular and solid-state calculations can be further extended for the time-dependent density functional calculations. The generalized dielectric dependent meta-GGA hybrid functional for solids can also be developed based on these present propositions. More extensive study and development of a screened meta-GGA functionals for both the molecular and solid-state materials will be the subject of work we will carry beyond this thesis.

- The formalism we developed for the two-dimensional quantum system is a subject of our future work to apply extensively on a larger set of quantum dots and practical usefullness of the developed functional will be provided.

Appendix A

Supplementary Materials for Chapter 4

Table A.1: Total energies of atoms (hatrees) computed using aug-cc-pVQZ basis set. The accurate reference values of each atomic systems are taken from ref. [195].

Atom	Accurate	B3LYP	PBE0	TPSSh	HSE06	DME-sc-TPSSc
H	-0.500	-0.502	-0.501	-0.500	-0.503	-0.499
He	-2.904	-2.915	-2.895	-2.908	-2.902	-2.910
Li	-7.478	-7.492	-7.466	-7.487	-7.475	-7.490
Be	-14.667	-14.672	-14.636	-14.670	-14.647	-14.674
B	-24.654	-24.664	-24.619	-24.666	-24.632	-24.670
C	-37.845	-37.860	-37.806	-37.863	-37.821	-37.863
N	-54.589	-54.605	-54.545	-54.611	-54.562	-54.605
O	-75.067	-75.099	-75.021	-75.102	-75.040	-75.092
F	-99.734	-99.773	-99.679	-99.769	-99.700	-99.748
Ne	-128.938	-128.977	-128.868	-128.968	-128.890	-128.937
Na	-162.255	-162.298	-162.182	-162.288	-162.205	-162.253
Mg	-200.053	-200.098	-199.967	-200.082	-199.992	-200.042
Al	-242.346	-242.393	-242.254	-242.379	-242.280	-242.327
Si	-289.359	-289.399	-289.256	-289.391	-289.283	-289.327
P	-341.259	-341.288	-341.143	-341.287	-341.171	-341.212
S	-398.110	-398.142	-397.983	-398.139	-398.013	-398.053
Cl	-460.148	-460.178	-460.009	-460.175	-460.039	-460.074
MAE		0.026	0.063	0.022	0.044	0.021

Table A.2: Atomization energies of the G2 test set computed using aug-cc-pVQZ basis set. All quantities are in kcal/mol.

Molecule	Name	CCSD(T)	B3LYP	PBE0	TPSSh	HSE06	DME-sc-TPSSc
$AlCl_3$	Aluminum trichloride	313.454	293.202	304.142	302.176	298.920	314.406
AlF_3	Aluminum trifluoride	432.192	415.208	411.605	412.195	406.825	415.663
BCl_3	Boron trichloride	323.172	312.892	328.359	318.887	321.741	328.278
BF_3	Boron trifluoride	469.403	464.873	466.460	459.390	459.986	459.737
BeH	Berilium monohydride	50.789	58.113	55.985	50.197	55.948	59.035
CCl_4	Tetrachloromethane	313.633	294.972	317.493	305.412	307.687	322.960
CF_4	Tetrafluoromethane	478.081	468.906	478.858	468.327	468.783	473.488
CH	Methylidyne radical	83.869	85.561	83.008	86.609	83.623	86.746
CH_2Cl_2	Dichloromethane	370.105	363.661	372.625	370.492	366.442	375.302
CH_2F_2	Difluoromethane	436.843	435.229	436.739	437.229	430.501	437.080
CH_2O_2	Formic acid	500.306	498.830	500.369	493.422	493.313	491.616
CH_2O	Formaldehyde	373.210	373.530	372.150	371.701	368.032	370.714
CH_2	Singlet carbene	180.619	181.028	176.432	180.619	175.233	180.033
CH_2	Triplet carbene	189.742	192.264	193.716	198.372	192.235	195.453
CH_3Cl	Chloromethane	394.518	392.717	395.368	397.937	390.766	398.126
CH_3	Methyl radical	306.590	310.204	308.517	313.852	306.314	310.930
CH_3O	Hydroxymethyl radical	408.552	411.164	410.924	410.911	405.986	406.028
CH_3O	Methoxy radical	398.894	403.937	403.132	405.078	398.573	400.955
CH_3S	Methylthio radical	381.246	382.346	384.332	386.415	379.841	381.979
CH_4	Methane	418.872	421.224	417.861	424.748	414.689	421.096
CH_4O	Methanol	511.829	511.982	510.089	511.973	504.388	507.297
CH_4S	Thiomethanol	473.495	471.634	472.869	477.136	467.419	475.058
$CHCl_3$	Trichloromethane	343.726	331.733	347.317	340.229	339.399	350.778
CHF_3	Trifluromethane	458.777	453.630	459.068	454.456	450.947	456.693
CHO	Formyl radical	278.282	280.381	280.297	278.037	276.853	277.268
CN	Cyano radical	180.065	178.840	178.247	175.409	175.927	178.971
CNH	Hydrogen cyanide	311.523	312.502	310.083	307.926	306.936	311.384
CNH_3O_2	Methyl nitrite	597.491	598.763	599.394	597.417	589.594	600.172
CNH_3O_2	Nitromethane	599.632	602.577	604.904	600.381	595.005	602.773
CNH_5	Methylamine	580.082	584.793	581.720	585.121	575.592	581.165
C_2Cl_4	Tetrachloroethylene	469.319	451.178	479.107	462.009	466.800	479.017
C_2F_4	Tetrafluroethylene	587.668	584.157	596.684	583.310	584.511	588.466
C_2H	Ethynyl radical	263.659	262.757	266.490	262.267	263.119	261.660
C_2H_2	Acetylene	402.763	403.153	404.139	401.988	399.953	402.015
$C_2H_2O_2$	Glyoxal	632.360	630.604	634.689	625.389	625.829	625.606
C_2H_2O	Ketene	530.603	533.813	537.741	531.309	531.043	530.538
C_2H_3Cl	Vinyl Chloride	541.516	539.705	546.643	544.055	539.583	545.584
C_2H_3	Vinyl radical	443.495	447.689	449.933	450.301	445.269	447.579
$C2H_3F$	Vinyl fluoride	571.223	572.586	575.603	574.272	568.497	573.267
C_2H_3O	Carbonyl methane	579.876	582.681	586.206	582.575	579.056	579.508
C_2H_3OCl	Acetyl chloride	666.141	663.119	672.060	665.272	662.502	667.383
C_2H_3OF	Acetyl fluoride	704.174	702.790	708.625	702.189	698.904	701.127
C_2H_4	Ethylene	561.341	563.715	564.026	566.248	558.549	563.460
$C_2H_4O_2$	Acetic acid	800.868	798.778	804.219	795.331	793.291	792.064
$C_2H_4O_2$	Methyl formate	784.033	782.802	786.502	781.639	775.770	779.339
C_2H_4O	Acetaldehyde	675.005	675.749	678.197	675.912	670.265	672.746
C_2H_4O	Oxirane	648.827	648.389	654.618	653.490	646.021	650.030
C_2H_4S	Thiirane	623.588	619.677	629.933	628.913	621.384	627.489
C_2H_5Cl	Ethyl chloride	690.032	687.116	693.581	694.724	685.145	693.489
C_2H_5	Ethyl radical	601.427	605.718	607.585	611.654	601.652	606.016
C_2H_5O	Ethoxy radical	695.120	695.919	698.855	699.301	690.471	693.688
C_2H_6	Ethane	710.204	712.113	712.371	718.143	705.519	712.034
C_2H_6O	Dimethyl ether	796.040	796.596	797.168	800.651	787.769	795.623
C_2H_6O	Ethanol	808.220	807.325	809.175	809.495	799.634	803.327
C_2H_6OS	Dimethyl sulfoxide	854.413	845.880	852.485	852.760	840.628	850.025
C_2H_6S	Dimethyl sulfide	766.299	763.395	768.400	772.005	759.221	768.416
C_2H_6S	Thioethanol	767.393	764.115	769.258	772.090	759.960	768.727
C_2N_2	Cyanogen	498.280	501.221	502.594	492.144	496.098	500.305

Table A.3: Atomization energies of the G2 test set computed using aug-cc-pVQZ basis set. All quantities are in kcal/mol.

Molecule	Name	CCSD(T)	B3LYP	PBE0	TPSSh	HSE06	DME-sc-TPSSc
C_2NF_3	Trifluroacetonitril	639.494	633.221	643.356	628.465	631.486	636.709
C_2NH_3	Acetonitrile	613.275	615.730	617.186	613.745	610.351	614.196
C_2NH_5	Aziridine	717.130	720.420	726.284	725.154	717.109	722.287
C_2NH_5O	Acetamide	864.915	868.547	872.338	865.155	861.016	862.778
C_2NH_7	Dimethylamine	867.075	871.340	871.603	874.967	861.670	870.369
C_2NH_7	Ethaylamine	875.261	878.751	879.523	881.377	869.545	876.087
C_3H_4	Allene	699.982	704.981	709.655	706.774	701.792	704.232
C_3H_4	Cyclopropene	678.007	679.304	689.130	685.124	680.583	682.053
C_3H_4	Propyne	701.358	702.843	707.787	704.337	699.904	701.435
C_3H_6	Cyclopropane	849.824	850.449	860.044	859.272	849.966	853.668
C_3H_6O	Acetone	975.379	975.183	981.651	977.443	969.802	973.123
C_3H_6	Propene	857.410	859.388	863.671	864.342	854.387	859.575
C_3H_7Cl	1-Chloropropane	983.574	979.160	989.532	989.210	977.252	986.708
C_3H_7	Isopropyl radical	897.482	901.550	907.230	909.774	897.472	902.323
C_3H_8O	Methoxyethane	1092.532	1091.878	1096.215	1098.144	1082.975	1091.623
C_3H_8O	Isopropyl alcohol	1105.317	1102.360	1108.267	1106.745	1094.719	1100.294
C_3H_8	Propane	1003.629	1004.219	1008.352	1012.632	997.659	1005.243
C_3NH_3	Acrylontrile	758.512	761.469	766.395	758.771	757.308	760.737
C_3NH_9	Trimethylamine	1156.873	1159.400	1163.365	1166.420	1149.386	1162.611
C_4H_{10}	Isobutane	1298.551	1296.761	1305.079	1307.566	1290.357	1300.143
C_4H_{10}	n-Butane	1297.126	1296.254	1304.289	1307.093	1289.745	1298.453
C_4H_4O	Furan	990.051	988.793	1006.342	992.032	991.696	990.474
C_4H_4S	Thiophene	959.884	954.121	975.908	962.274	961.478	962.981
C_4H_6	1,3-Butadiene	1007.991	1010.584	1018.587	1014.761	1006.996	1011.609
C_4H_6	2-Butyne	999.002	1001.183	1010.107	1005.471	998.529	999.708
C_4H_6	Bicyclobutane	981.134	979.529	998.760	992.053	985.475	987.505
C_4H_6	Cyclobutene	996.655	995.318	1010.303	1004.075	997.495	999.252
C_4H_6	Methylenecyclopropane	988.022	990.275	1003.777	998.218	991.407	993.245
C_4H_8	Cyclobutane	1145.231	1142.726	1157.149	1154.374	1142.893	1147.500
C_4H_8	Isobutene	1154.236	1154.729	1163.187	1162.111	1149.961	1156.481
C_4H_9	tert-Butyl radical	1194.236	1197.132	1206.877	1207.749	1193.175	1199.450
C_4NH_5	Pyrrole	1067.054	1070.436	1087.746	1073.116	1072.486	1071.863
C_5H_8	Spiropentane	1278.794	1277.914	1300.528	1292.036	1283.538	1285.290
C_5NH_5	Pyridine	1232.274	1236.854	1256.774	1238.723	1239.437	1239.671
C_6H_6	Benzene	1361.588	1362.890	1386.658	1368.504	1368.384	1366.305
Cl_2	Dichlorine	59.073	54.819	58.792	58.400	56.531	65.282
CO	Carbon monoxide	258.877	254.690	254.661	249.394	251.854	251.872
CO_2	Carbon dioxide	388.592	387.229	390.682	380.854	385.210	382.137
COF_2	Carbonyl fluoride	419.501	415.705	422.000	412.298	414.299	414.866
COS	Carbonyl sulfide	334.288	332.011	337.079	330.313	331892	334.300
CS	Carbon monosulfide	170.985	165.664	167.371	165.176	164.873	169.891
CS_2	Carbon disulphide	278.664	275.291	282.292	278.128	277.486	284.925
FCl	Chlorine monofluoride	62.572	60.189	60.176	61.917	57.899	66.998
F_2	Difluorine	38.755	36.916	34.395	39.113	32.179	44.097
F_3Cl	Chlorine trifluoride	128.346	126.029	127.172	132.329	120.509	140.060
HCl	Hydrogen Chloride	107.199	104.859	104.744	106.276	103.607	108.920
HF	Hydrogen fluoride	141.513	139.300	136.814	137.582	135.536	137.245
$HOCl$	Hypochlorus acid	165.791	162.596	162.203	161.875	158.833	164.158
HO	Hydroxyl radical	106.955	108.307	105.743	105.745	104.782	102.992
HS	Mercapto radical	87.390	87.987	86.525	88.815	85.675	86.932
H_2	Dihydrgen	109.400	110.280	104.301	112.659	104.645	111.769
H_2O_2	Hydrogen peroxide	268.655	267.134	262.887	262.457	258.456	260.590
H_2O	Water	232.565	231.099	227.101	226.927	224.867	224.026
H_2S	Hydrogen sulphide	183.298	181.640	179.444	183.955	177.571	184.373
LiF	Lithium fluoride	139.369	137.167	132.051	133.653	131.248	132.606
LiH	Lithium hydride	57.904	5/.587	52.837	58.930	53.159	58.544
Li_2	Dilithium	24.197	20.893	19.428	22.802	19.427	21.801
Na_2	Disodium	17.101	17.171	15.846	18.621	16.09	18.502

Table A.4: Atomization energies of the G2 test set computed using aug-cc-pVQZ basis set. All quantities are in kcal/mol.

Molecule	Name	CCSD(T)	B3LYP	PBE0	TPSSh	HSE06	DME-sc-TPSSc
NaCl	Sodium chloride	98.466	92.408	93.233	95.450	92.396	98.813
NF$_3$	Trifluoroamine	206.212	208.298	209.523	209.636	202.512	218.529
NH$_2$	Amino radical	181.955	188.202	183.288	186.482	181.972	185.089
NH$_3$	Ammonia	297.070	301.308	295.236	298.214	292.708	296.254
NH	Imidogen	82.787	88.145	85.303	89.103	84.877	89.148
NO$_2$	Nitrogen dioxide	227.058	232.132	232.437	228.103	227.241	231.431
NOCl	Nitrosyl chloride	191.468	192.707	191.666	191.834	187.567	200.729
NO	Nitric oxide	152.187	155.495	153.713	150.182	151.113	153.316
N$_2$	Dinitrogen	227.436	227.445	222.948	219.968	220.728	227.207
N$_2$H$_4$	Hydrazine	436.699	444.594	438.495	439.404	433.072	437.764
N$_2$O	Nitrous oxide	269.474	273.123	272.142	267.847	267.285	274.542
OCl	Monochlorine monoxide	64.532	65.219	65.919	65.888	63.520	65.014
OF$_2$	Diflourine monoxide	93.772	93.550	90.927	95.662	86.399	101.661
OS	Sulpher monoxide	125.796	124.787	124.583	123.450	121.933	122.416
O$_2$	Dioxygen	120.545	122.512	122.239	119.475	119.352	120.215
O$_2$S	Sulpher dioxide	259.766	244.873	245.509	242.371	240.056	245.441
O$_3$	Ozone	146.819	138.562	135.859	137.995	130.688	142.984
P$_2$	Diphosphorus	115.951	114.437	109.760	111.021	107.831	118.659
PF$_3$	Phosphorus trifluoride	365.156	356.327	353.282	353.311	346.720	358.472
PH$_2$	Phosphino radical	153.970	158.278	152.688	160.081	151.574	158.581
PH$_3$	Phosphane	241.475	244.201	236.754	247.599	234.807	247.906
S$_2$	Disulpher	103.112	102.127	105.408	104.785	102.947	103.256
SiCH$_6$	Methylsilane	627.656	625.703	621.001	637.227	615.352	635.468
SiCl$_4$	Silicon tetrachloride	388.483	361.134	380.051	374.291	371.568	391.150
SiF$_4$	Silicon tetrafluoride	577.546	554.321	552.458	550.756	544.495	556.948
SiH$_2$	Singlet silylene	153.678	153.585	147.022	156.112	146.174	158.040
SiH$_2$	Triplet silylene	133.260	133.158	132.205	141.321	131.164	138.881
SiH$_3$	Silyl radical	228.083	228.539	223.423	237.069	221.988	235.663
SiH$_4$	Silane	324.589	323.671	315.092	333.551	313.157	335.321
SiO	Silicon monoxide	192.359	186.596	181.364	181.082	178.994	183.946
Si$_2$H$_6$	Disilane	535.471	530.474	522.354	548.331	517.857	550.941
Si$_2$	Disilicon	73.411	69.314	71.365	72.311	69.934	72.577
MAE	–	–	3.599	5.619	5.296	5.335	4.008

Table A.5: Atomization energies (kcal/mol) of the AE6 molecules. The experimental values are taken from [195]. All calculations are done using aug-cc-pVQZ basis set.

Atom	Expt.	B3LYP	PBE0	TPSSh	HSE06	DME-sc-TPSSc
SiH$_4$	322.4	323.4	315.0	333.5	313.1	335.3
SiO	192.1	187.1	182.0	181.4	179.6	184.2
S$_2$	101.7	102.1	105.7	104.8	103.2	103.2
C$_3$H$_4$	704.8	703.2	708.1	704.6	700.2	701.6
C$_2$H$_2$O$_2$	633.4	631.4	635.8	625.9	626.9	626.0
C$_4$H$_8$	1149.0	1142.8	1157.1	1154.4	1142.9	1147.4
MAE	–	2.7	5.8	6.3	6.7	5.7

Table A.6: Ionization potential for the test set IP13 for the exchange-correlation functional shown in each column using 6-311++G(3df,3pd) basis set. The experimental values are taken from [195]. All quantities are in kcal/mol.

Molecule	Expt	B3LYP	PBE0	TPSSh	HSE06	DME-sc-TPSSc
C	259.74	266.08	265.57	264.06	265.53	261.54
S	238.34	242.89	239.89	240.79	239.84	240.35
SH	238.36	241.18	238.82	238.57	238.63	236.65
Cl	299.31	301.22	298.86	298.67	298.79	295.86
Cl_2	265.30	262.25	261.18	259.70	261.28	262.95
OH	298.90	282.93	300.57	297.69	300.63	295.58
O	313.67	326.21	319.66	321.62	320.15	322.35
O_2	278.90	289.60	286.30	284.33	286.64	280.21
P	242.80	239.30	242.78	242.66	242.63	240.83
PH	234.10	234.30	237.08	236.97	237.00	234.78
PH_2	226.30	228.72	230.75	230.67	230.70	226.05
S_2	216.00	219.88	221.19	220.20	221.07	217.66
Si	188.05	187.07	189.55	189.71	189.51	188.31
MAE	−	5.29	3.20	3.16	3.24	2.29

Table A.7: Electron affinity for the test set EA13 for the exchange-correlation functional shown in each column using 6-311++G(3df,3pd) basis set. All quantities are in kcal/mol. The experimental values are taken from [195]

Molecule	Expt	B3LYP	PBE0	TPSSh	HSE06	DME-sc-TPSSc
C	29.19	31.20	32.34	31.86	31.95	29.29
S	47.91	50.33	47.35	47.19	47.15	44.69
SH	53.84	53.50	51.30	51.03	51.03	51.99
Cl	84.24	84.65	82.51	82.24	82.09	83.81
Cl_2	55.60	64.43	59.21	60.46	59.93	53.72
OH	42.30	40.54	35.34	35.26	35.16	34.69
O	33.77	36.84	30.48	29.85	30.46	25.97
O_2	10.80	11.37	4.72	6.69	5.29	3.65
P	16.92	21.50	17.55	18.02	17.57	17.88
PH	23.20	24.96	21.83	21.51	21.69	19.77
PH_2	29.40	28.48	26.31	25.86	26.04	26.26
S_2	38.50	38.15	35.99	35.86	36.10	33.33
Si	32.33	30.44	33.13	32.34	32.92	31.14
MAE	−	2.22	2.79	2.85	2.87	3.37

Table A.8: Proton affinities for the test set PA8 for the exchange-correlation functional shown in each column using 6-311++G(3df,3pd) basis set. All quantities are in kcal/mol. The experimental values are taken from [195]

Molecule	Expt	B3LYP	PBE0	TPSSh	HSE06	DME-sc-TPSSc
NH_3	211.90	210.99	212.64	213.74	213.10	214.42
H_2O	171.80	170.84	172.48	173.04	172.88	172.95
C_2H_2	156.60	158.67	161.07	162.92	161.51	161.97
SiH_4	156.50	157.53	156.61	159.03	157.65	159.43
PH_3	193.10	193.28	192.97	196.17	193.81	198.39
H_2S	173.70	174.92	175.07	176.88	175.85	177.77
HCl	137.10	138.15	139.15	140.39	139.48	140.84
H_2	105.90	104.53	106.35	108.14	106.62	106.46
MAE	−	1.10	1.25	2.84	1.79	3.20

Table A.9: FORWARD barrier heights of hydrogen transfer reactions for the HTBH38 test set for the exchange-correlation functional shown in each column using aug-cc-pVQZ basis set. All quantities are in kcal/mol. The experimental values are taken from [195]

	Molecule	Expt	B3LYP	PBE0	TPSSh	HSE06	DME-sc-TPSSc
1.	H + HCl → H$_2$+ Cl	5.70	-1.00	2.72	-3.63	2.66	1.06
2.	OH + H$_2$ → H$_2$O + H	4.90	0.72	0.18	0.41	1.56	0.99
3.	CH$_3$ + H$_2$ → CH$_4$ + H	12.10	8.78	6.94	8.00	8.23	8.93
4.	OH + CH$_4$ →H$_2$O + CH$_3$	6.50	2.27	2.01	1.70	3.28	3.62
5.	H + H$_2$ → H$_2$ + H	9.60	4.28	5.66	1.16	6.09	2.04
6.	OH + NH$_3$ → H$_2$O + NH$_2$	3.00	-2.26	-1.86	-3.63	-0.59	-2.33
7.	HCl + CH$_3$ → CH$_4$ + Cl	1.70	-1.42	-2.26	-2.30	-1.24	3.44
8.	OH + C$_2$H$_6$ → H$_2$O + C$_2$H$_5$	3.20	-0.68	-0.80	-1.26	0.44	0.27
9.	F + H$_2$ → HF + H	1.42	-5.69	-4.54	-5.78	-3.52	-6.08
10.	O + CH$_4$ → OH + CH$_3$	13.47	7.32	7.76	7.94	8.83	11.26
11.	H + PH$_3$ → H$_2$ + PH$_2$	3.10	-1.06	0.38	-4.15	0.65	-0.35
12.	H + HO → H$_2$ + O	10.50	4.10	7.11	-0.13	7.27	0.08
13.	H + H$_2$S → H$_2$ + HS	3.50	-0.59	1.05	-3.76	1.33	0.52
14	O + HCl →OH + Cl	9.57	1.13	2.44	1.22	3.56	7.49
15.	CH$_3$ + NH$_2$ → CH$_4$ + NH	8.00	6.26	5.23	4.52	6.37	6.51
16.	C$_2$H$_5$ + NH$_2$ →C$_2$H$_6$ + NH	7.50	8.83	7.14	6.45	8.28	7.80
17.	NH$_2$ + C$_2$H$_6$ → NH$_3$ + C$_2$H$_5$	10.40	8.89	7.48	8.33	8.82	9.97
18.	NH$_2$ + CH$_4$ → NH$_3$ + CH$_3$	14.50	11.41	10.05	10.86	11.36	12.91
19.	s-trans cis-C$_5$H$_8$ → s-trans cis-C$_5$H$_8$	38.40	38.81	35.59	36.20	36.71	37.77
	MAE	–	4.20	3.39	5.52	3.07	3.43

Table A.10: BACKWARD barrier heights of hydrogen transfer reactions for the HTBH38 test set for the exchange-correlation functional shown in each column using aug-cc-pVQZ basis set. All quantities are in kcal/mol. The experimental values are taken from [195]

	Molecule	Expt	B3LYP	PBE0	TPSSh	HSE06	DME-sc-TPSSc
1.	H + HCl → H$_2$+ Cl	7.86	3.41	2.38	2.76	3.72	3.94
2.	OH + H$_2$ → H$_2$O + H	21.20	7.91	17.23	8.94	17.08	10.24
3.	CH$_3$ + H$_2$ → CH$_4$ + H	15.30	5.77	11.88	6.23	11.94	7.30
4.	OH + CH$_4$ → H$_2$O + CH$_3$	19.60	5.50	14.12	12.00	15.08	14.49
5.	H + H$_2$ → H$_2$ + H	9.60	5.31	5.66	1.16	6.09	2.04
6.	OH + NH$_3$ → H$_2$O + NH$_2$	12.70	5.25	7.61	5.83	8.81	7.54
7.	HCl + CH$_3$ → CH$_4$ + Cl	7.06	2.30	2.34	2.32	3.53	4.69
8.	OH + C$_2$H$_6$ → H$_2$O + C$_2$H$_5$	19.90	4.10	15.89	13.46	16.78	15.31
9.	F + H$_2$ → HF + H	33.40	10.02	28.03	19.13	27.51	19.35
10.	O + CH$_4$ → OH + CH$_3$	7.90	3.29	4.19	2.75	5.27	4.06
11.	H + PH$_3$ → H$_2$ + PH$_2$	23.20	0.07	20.68	20.95	22.04	22.06
12.	H + HO → H$_2$ + O	12.87	6.77	5.73	6.81	7.11	8.92
13.	H + H$_2$S → H$_2$ + HS	16.76	0.72	12.53	13.75	14.09	14.86
14	O + HCl → OH + Cl	9.36	4.76	3.48	0.67	4.78	1.54
15.	CH$_3$ + NH$_2$ → CH$_4$ + NH	22.40	5.16	16.59	18.06	17.64	20.75
16.	C$_2$H$_5$ + NH$_2$ → C$_2$H$_6$ + NH	18.30	3.60	13.90	15.56	15.02	17.87
17.	NH$_2$ + C$_2$H$_6$ →NH$_3$ + C$_2$H$_5$	17.40	1.72	14.71	13.59	15.75	15.13
18.	NH$_2$ + CH$_4$ → NH$_3$ + CH$_3$	17.80	4.26	12.69	11.69	13.75	13.89
19.	s-trans cis-C$_5$H$_8$ → s-trans cis-C$_5$H$_8$	38.40	0.41	35.59	36.20	36.71	37.77
	MAE	–	4.23	4.50	6.26	3.58	4.69

Table A.11: FORWARD barrier heights of non-hydrogen transfer reactions for the NHTBH38/04 test set for the exchange-correlation functional shown in each column using aug-cc-pVQZ basis set. All quantities are in kcal/mol. The experimental values are taken from [195].

	Molecule	Expt	B3LYP	PBE0	TPSSh	HSE06	DME-sc-TPSSc
1.	H + N$_2$O $\rightarrow$ OH + N$_2$	17.13	11.39	13.93	9.41	14.42	11.06
2.	H + HF $\rightarrow$ HF + H	42.18	30.91	33.64	29.08	34.21	32.18
3.	H + ClH $\rightarrow$ HCl + H	18.00	12.75	13.69	9.06	14.25	14.84
4.	H + FCH$_3$ $\rightarrow$ HF + CH$_3$	30.38	21.58	25.48	19.72	25.57	22.35
5.	H + F$_2$ $\rightarrow$ HF + F	2.27	43.76	47.59	40.31	47.74	44.30
6.	CH$_3$ + FCl $\rightarrow$ CH$_3$F + Cl	6.75	-1.05	1.47	-1.61	1.82	2.80
7.	F- + CH$_3$F $\rightarrow$ FCH$_3$ + F-	-0.34	-2.21	-1.01	-4.67	-0.22	-5.09
8.	F-...CH$_3$F $\rightarrow$ FCH$_3$...F-	13.38	10.46	11.90	8.19	12.09	8.88
9.	Cl- + CH$_3$Cl $\rightarrow$ ClCH$_3$ + Cl-	3.10	-0.30	1.10	-2.77	1.48	-3.35
10.	Cl-...CH$_3$Cl $\rightarrow$ ClCH$_3$...Cl-	13.41	9.12	11.14	7.21	11.09	7.65
11.	F- + CH$_3$Cl $\rightarrow$ FCH$_3$ + Cl-	-12.54	-14.73	-13.73	-17.25	-13.08	-18.46
12.	F-...CH$_3$Cl $\rightarrow$ FCH$_3$...Cl-	3.44	0.48	1.78	-1.23	1.81	-1.08
13.	OH- + CH$_3$F $\rightarrow$ HOCH$_3$ + F-	-2.44	-4.00	-3.29	-6.56	-2.52	-6.53
14	OH-...CH$_3$F $\rightarrow$ HOCH$_3$...F-	10.96	8.16	9.21	5.64	9.38	6.62
15.	H + N$_2$ $\rightarrow$ HN$_2$	14.36	7.51	8.53	4.10	9.09	6.23
16.	H + CO $\rightarrow$ HCO	3.17	-0.63	0.24	-4.27	0.67	-2.56
17.	H + C$_2$H$_4$ $\rightarrow$ CH$_3$CH$_2$	1.72	-0.18	0.67	-3.93	1.06	-3.58
18.	CH$_3$ + C$_2$H$_4$ $\rightarrow$ CH$_3$CH$_2$CH$_2$	6.85	6.05	4.12	4.16	5.24	4.72
19.	HCN $\rightarrow$ CNH	48.07	47.39	46.30	47.41	46.55	47.49
	MAE	–	6.12	5.14	8.10	4.75	7.12

Table A.12: BACKWARD barrier heights of non-hydrogen transfer reactions for the NHTBH38/04 test set for the exchange-correlation functional shown in each column using aug-cc-pVQZ basis set. All quantities are in kcal/mol. The experimental values are taken from [195].

	Molecule	Expt	B3LYP	PBE0	TPSSh	HSE06	DME-sc-TPSSc
1.	H + N$_2$O $\rightarrow$ OH + N$_2$	82.27	73.12	69.18	66.70	71.42	66.37
2.	H + HF $\rightarrow$ HF + H	42.18	30.91	33.64	29.08	34.21	32.18
3.	H + ClH $\rightarrow$ HCl + H	18.00	12.75	13.69	9.06	14.25	14.84
4.	H + FCH$_3$ $\rightarrow$ HF + CH$_3$	57.02	48.61	49.82	45.83	51.06	47.17
5.	H + F$_2$ $\rightarrow$ HF + F	105.80	145.94	149.45	138.61	150.61	137.39
6.	CH$_3$ + FCl $\rightarrow$ CH$_3$F + Cl	59.16	51.06	53.51	47.81	53.81	48.25
7.	F- + CH$_3$F $\rightarrow$ FCH$_3$ + F-	-0.34	-2.21	-1.01	-4.67	-0.22	-5.09
8.	F-...CH$_3$F $\rightarrow$ FCH$_3$...F-	13.38	10.46	11.90	8.19	12.09	8.88
9.	Cl- + CH$_3$Cl $\rightarrow$ ClCH$_3$ + Cl-	3.10	-0.30	1.10	-2.77	1.48	-3.35
10.	Cl-...CH$_3$Cl $\rightarrow$ ClCH$_3$...Cl-	13.41	9.12	11.14	7.21	11.09	7.65
11.	F- + CH$_3$Cl $\rightarrow$ FCH$_3$ + Cl-	20.11	18.42	19.68	16.76	20.16	16.70
12.	F-...CH$_3$Cl $\rightarrow$ FCH$_3$...Cl-	29.42	26.42	28.19	25.01	28.26	25.86
13.	OH- + CH$_3$F $\rightarrow$ HOCH$_3$ + F-	17.66	15.91	17.63	12.70	18.35	12.33
14	OH-...CH$_3$F $\rightarrow$ HOCH$_3$...F-	47.20	45.08	48.73	42.72	48.29	41.24
15.	H + N$_2$ $\rightarrow$ HN$_2$	10.61	10.76	11.54	9.40	11.43	8.01
16.	H + CO $\rightarrow$ HCO	22.68	24.54	25.38	23.98	25.19	22.44
17.	H + C$_2$H$_4$ $\rightarrow$ CH$_3$CH$_2$	41.75	41.80	44.19	41.46	44.14	38.96
18.	CH$_3$ + C$_2$H$_4$ $\rightarrow$ CH$_3$CH$_2$CH$_2$	32.97	29.48	34.49	29.86	33.60	29.08
19.	HCN $\rightarrow$ CNH	32.82	33.52	32.68	32.73	32.81	31.83
	MAE:		5.76	5.25	7.24	4.91	6.92

Table A.13: Thermochemistry of π system for the πTC13 test set for functional shown in each column. All quantities are in kcal/mol. The 6-311++G(3df,3pd) basis set is used. The experimental values are taken from [195].

Molecule	Expt	B3LYP	PBE0	TPSSh	HSE06	DME-sc-TPSSc
E2-E1	-1.40	-2.23	-2.20	-2.58	-1.99	-2.99
E4-E3	-8.80	-2.40	-2.98	-1.38	-2.84	-0.57
E6-E5	-14.30	-5.54	-6.41	-3.93	-6.04	-2.68
P-2	167.81	168.54	170.77	172.06	171.29	172.13
P-4	193.45	198.54	198.25	200.96	199.21	201.24
P-6	209.68	216.32	215.73	218.84	216.79	230.76
P-8	219.67	227.62	226.90	230.31	228.01	239.01
P-10	225.95	235.68	234.83	238.44	236.04	217.41
SB-2	214.46	215.37	216.54	217.24	216.97	231.60
SB-4	226.15	229.77	230.63	231.63	231.15	241.36
SB-6	233.44	239.46	240.09	241.38	240.69	248.29
SB-8	238.16	246.22	246.69	248.23	247.38	248.29
SB-10	240.97	251.29	251.61	253.41	252.42	253.54
MAE	–	5.77	5.89	7.82	6.54	8.17

Table A.14: Alkyl Bond Dissociation Energies for the ABDE12 test set for functional shown in each column. All quantities are in kcal/mol. The aug-cc-pVQZ basis set is used. The experimental values are taken from [195].

Molecule	Expt	B3LYP	PBE0	TPSSh	HSE06	DME-sc-TPSSc
C_2H_6	97.39	91.71	95.29	90.41	92.85	90.17
iPr-CH_3	95.00	84.99	89.16	83.90	86.46	86.79
C_2H_6O	89.79	82.33	85.30	81.57	82.71	83.49
iPr-OCH_3	91.51	79.68	83.07	78.90	80.16	83.65
Et-H	108.92	106.34	104.71	106.45	103.80	105.98
Et-CH_3	95.89	88.27	92.13	87.08	89.61	88.22
Et-OCH_3	95.26	82.09	85.23	81.27	82.55	84.38
Et-OH	100.29	93.34	95.88	92.10	93.25	94.27
tBu-H	103.86	99.59	98.08	99.76	97.10	100.71
tBu-CH_3	93.67	81.64	86.19	80.68	83.24	85.75
tBu-OCH_3	89.27	75.87	79.64	75.26	76.41	82.07
tBu-OH	115.02	90.95	93.92	89.60	90.92	95.13
MAE		9.91	7.26	10.73	9.73	7.93

Table A.15: Isomerization Energies for the IsoL6 test set for functional shown in each column. All quantities are in kcal/mol. The 6-311++G(3df,3pd) basis set is used. The experimental values are taken from [195].

Molecule	Expt	B3LYP	PBE0	TPSSh	HSE06	DME-sc-TPSSc
10-	6.82	2.72	5.85	2.50	5.31	2.64
13-	33.52	30.24	31.47	28.68	31.34	29.21
14-	5.30	3.96	5.75	3.40	5.14	3.42
20-	4.66	4.28	5.13	4.25	5.04	3.19
3-	9.77	7.39	11.40	8.22	10.27	8.39
9-	21.66	17.97	18.68	16.15	17.96	20.41
MAE		2.54	1.44	3.10	1.42	2.42

Table A.16: Reaction Energies for the HC7 test set for functional shown in each column. All quantities are in kcal/mol. The 6-311++G(3df,3pd) basis set is used. The experimental values are taken from [195].

Molecule	Expt	B3LYP	PBE0	TPSSh	HSE06	DME-sc-TPSSc
E22 - E1	14.34	0.12	24.43	16.50	20.58	16.44
E31 - E1	25.02	2.67	33.42	21.35	28.22	20.98
$(CH_3)_3CC(CH_3)_3 \rightarrow$ n-C_8H_18	1.90	-7.86	-4.54	-5.80	-6.45	3.21
n-C_6H_14 + 4 $CH_4 \rightarrow 5C_2H_6$	9.81	4.64	5.85	4.36	5.15	9.11
n-C_8H_18 + 6 $CH_4 \rightarrow 7C_2H_6$	14.84	6.86	8.67	6.44	7.63	13.64
adamantane $\rightarrow$ 3 C_2H_4 + 2 C_2H_2	193.99	164.78	215.80	185.27	201.95	187.98
biclo[2.2.2]octane $\rightarrow$ 3 C_2H_4 + C_2H_2	127.22	104.36	140.87	119.13	131.04	120.04
MAE		15.93	10.07	6.31	5.92	3.21

Appendix B

Supplementary Materials for Chapter 6

B.1 Generalized Coordinate Transformation in 2D

The spherically averaged exchange hole density is related to the 1st order reduced density matrix (DM) as,

$$\langle \rho_{x\sigma}(\vec{r}, \vec{r} + \vec{u}) \rangle = -\frac{\langle |\Gamma_{1\sigma}(\vec{r}, \vec{r} + \vec{u})|^2 \rangle}{\rho_\sigma(\vec{r})} \ . \tag{B.1}$$

The 1st order reduced DM in related to the KS orbitals as,

$$\Gamma_{1\sigma}(\vec{r}, \vec{r} + \vec{u}) = \sum_i^{\sigma \ occ} \Psi_{i\sigma}^*(\vec{r}) \Psi_{i\sigma}(\vec{r} + \vec{u}) \ . \tag{B.2}$$

However, one can relate the reduced DM and its cylindrical averged as,

$$\langle |\Gamma_{1\sigma}(\vec{r}, \vec{r} + \vec{u})| \rangle = \frac{1}{2\pi} \int \Gamma_{1\sigma}(\vec{r}, \vec{r} + \vec{u}) \, d\Omega_u \ . \tag{B.3}$$

Now, we introduce the novel technique of density matrix expansion proposed by Tao et. al. [234]. This is based on a general linear coordinate transformation from $(\vec{r}, \vec{r} + \vec{u}) \rightarrow (\vec{r_1}, \vec{r_2})$. Lets consider the matrix transformation,

$$\begin{pmatrix} \vec{r} \\ \vec{r} + \vec{u} \end{pmatrix} = \begin{pmatrix} a & b \\ c & d \end{pmatrix} \cdot \begin{pmatrix} \vec{r_1} \\ \vec{r_2} \end{pmatrix} \ . \tag{B.4}$$

This gives a coordinate-transformed $\vec{r} = r_1 + (d-1)\vec{u}$ which is coupled with the condition that this coordinate transformation make Jacobian of transformation unity, where Jacobian of transformation $\mathcal{J}$ is defined as,

$$\mathcal{J} = \begin{pmatrix} a & b \\ c & d \end{pmatrix} . \tag{B.5}$$

Under the general coordinate transformation, the exchange energy remains invariant i.e.,

$$E_x = -\frac{1}{4} \int d^2r \int d^2u \frac{|\Gamma(\vec{r}, \vec{r} + \vec{u})|^2}{u} , \tag{B.6}$$

where

$$\begin{aligned} \vec{r} &= a\vec{r}_1 + b\vec{r}_2 \\ \vec{r} + \vec{u} &= c\vec{r}_1 + d\vec{r}_2 \end{aligned} \tag{B.7}$$

Using this fact the Eq(B.6) becomes,

$$E_x = \frac{1}{4} \int d^2r_1 \int d^2r_2 \frac{|\Gamma_1^t(a\vec{r}_1 + b\vec{r}_2, c\vec{r}_1 + d\vec{r}_2)|^2}{|(d-b)\vec{r}_2 - (a-c)\vec{r}_1|} |\mathcal{J}|^3 . \tag{B.8}$$

Now, in proper coordinate transformation, $\mathcal{J} = 1$, which implies $ad - bc = 1$. Therefore, u transforms as,

$$\vec{u} = (c-a)\vec{r}_1 + (d-b)\vec{r}_2 . \tag{B.9}$$

All these conditions implies that

$$\begin{aligned} d - b &= 1 \\ a + d &= 2 \\ c + d &= 1 . \end{aligned} \tag{B.10}$$

Using all these the exchange energy expression of Eq.(B.8) becomes,

$$
\begin{aligned}
E_x &= \frac{1}{4} \int d^2 r_1 \int d^2 r_2 \frac{|\Gamma_1^t(a\vec{r}_1 + b\vec{r}_2, c\vec{r}_1 + d\vec{r}_2)|^2}{|(d-b)\vec{r}_2 - (a-c)\vec{r}_1|} |\mathcal{J}|^3 \\
&= \frac{1}{2} \int d^2 r_1 \int d^2 r_2 \frac{\rho_x^t(\vec{r}_1, \vec{r}_2)\rho(\vec{r}_1)}{|\vec{r}_2 - \vec{r}_1|}
\end{aligned}
\tag{B.11}
$$

where,

$$
\rho_x^t(\vec{r}_1, \vec{r}_2) = -\frac{|J|^3 |\vec{r}_2 - \vec{r}_1|}{|(d-b)\vec{r}_2 - (a-c)\vec{r}_1|} \times \frac{|\Gamma_1^t(a\vec{r}_1 + b\vec{r}_2, c\vec{r}_1 + d\vec{r}_2)|^2}{2\rho(\vec{r}_1)} .
\tag{B.12}
$$

This is the coordintate transformed exchange-hole. Upon simplifying this becomes,

$$
\begin{aligned}
\rho_x^t(\vec{r}_1, \vec{r}_2) &= -\frac{|\Gamma_1^t(\vec{r}_1 + [d-1]\vec{u}, \vec{r}_1 + d\vec{u})|^2}{2\rho(\vec{r}_1)} \\
&= \rho_x(\vec{r}_1 + [d-1]\vec{u}, \vec{r}_1 + [d-1]\vec{u} + \vec{u})\frac{\rho(\vec{r}_1 + [d-1]\vec{u})}{\rho(\vec{r}_1)} .
\end{aligned}
\tag{B.13}
$$

The on-top ($\vec{u} = 0$) exchange hole density is just $\rho_x^t(\vec{r}_1, \vec{r}_1) = \rho_x(\vec{r}_1, \vec{r}_1) = -\frac{\rho}{2}$. In the above expression, $d = 1$ corresponds to the similarity transformation that make the exchange hole unaltered. Whereas, $d = 1$ corresponds to the exchange energy density that decay asymptotically ($-\frac{1}{2}\frac{1}{r}$). But, for other values of d, the corresponding exchange energy density decays exponentially. Therefore, makes it more localized near the reference point. To exemplify the asymptotic and expontial decay of exchange energy density, we start with the exchange energy density under generalized coordinate transformation. The ground state of single electron wavefunction for the 2D quantum harmonic oscillator is given by,

$$
\psi_\sigma(\mathbf{r}) = \frac{\alpha}{\sqrt{\pi}} exp\left[-\frac{\alpha^2 r^2}{2} \right] .
\tag{B.14}
$$

and the corresponding exchange energy density for 2D QHO as,

$$
\epsilon_{x\sigma}(\mathbf{r}) = -\frac{|\alpha|}{2}\sqrt{\pi} exp\left[-\frac{\alpha^2 r^2}{2} \right] I_0\left(\frac{\alpha^2 r^2}{2} \right) .
\tag{B.15}
$$

Now, under generalised coordinate transformation i.e., $\mathbf{r}_d \rightarrow d\mathbf{r} + (1-d)\mathbf{r}'$, with $\mathbf{u} =$

$\mathbf{r}' - \mathbf{r}$, the spin-polarized exchange hole density for the 2D quantum harmonic oscillator becomes,

$$
\begin{aligned}
\epsilon_{x\sigma}(\mathbf{r}_d) &= -\int_0^\infty du \int_0^{2\pi} d\phi \frac{|\alpha|}{2}\sqrt{\pi} exp\Big[-\frac{\alpha^2}{2}\Big\{\mathbf{r}_d^2 + (1-d)^2 u^2 - 2(1-d)\mathbf{r}_d u cos\phi\Big\}\Big] \\
&\quad I_0\Big[\frac{\alpha^2}{2}(\mathbf{r}_d^2 + (1-d)^2 u^2 - 2(1-d)\mathbf{r}_d u cos\phi)\Big] .
\end{aligned}
\tag{B.16}
$$

As, $r_d \to \infty$, the corresponding exchange hole density behaves as,

$$
\lim_{\mathbf{r}_d \to \infty} \epsilon_x^\sigma(\mathbf{r}_d) \approx -\frac{exp^{-2(1-d)\alpha^2 r_d}}{r_d} .
\tag{B.17}
$$

Thus, the correct asymptotic behavior of exchange energy functional achieved only for $d = 1$. For other values of d, the exchange energy shows exponential decay. On the other hand, we observe faster decay of exchange energy density at $d = 0.5$ compared to $d = 1$. This makes the exchange hole more localized around the reference point.

B.2 Exchange Hole Under Generalized Coordinate Transformation

The property of exchange hole under generalized coordinate transformation is of great interest as the exchange energy can be evaluated directly from the cylindrically averaged exchange hole density. Before discussing the effect of generalized coordinate transformation, we consider the Becke's exchange hole expansion in 3D and its generalization in 2D by Pittalis et.al. [395] The gradient expansion of cylindrically averaged exchange hole in 2D is obtained using Taylor series expansion as

$$
\begin{aligned}
< \rho_{x2D}(\vec{r}, \vec{u}) >_{cyl} &= < e^{\vec{u}.\vec{\nabla}} \sum_i^{occ} \Psi_i^*(\vec{r})\Psi_i(\vec{r}+\vec{u})|_{\vec{u}=0} >_{cyl} \\
&= -\frac{\rho(\vec{r})}{2} - \frac{1}{4}\Big[\frac{1}{2}\nabla^2\rho(\vec{r}) - 2\tau + \frac{1}{4}\frac{|\vec{\nabla}\rho(\vec{r})|^2}{\rho(\vec{r})}\Big]u^2 .
\end{aligned}
\tag{B.18}
$$

This is the exact expansion of cylindrically averaged exchange hole considering expansion upto u^2 in Taylor series. However, this popular expansion failed to achieve the correct uniform density exchange hole expansion. Also, it can not be used directly to the exchange energy expression due to divergency issue.

Now, we turn to discussing the effect of generalized coordinate transformation for exchange hole expansion. To do this, we consider the Taylor series expansion of the exchange hole around $u = 0$. Under the geralized coordinate transformation $\mathbf{r}$ transform into $\mathbf{r}_d \to d\mathbf{r} + (1-d)\mathbf{r}'$, with $\mathbf{u} = \mathbf{r}' - \mathbf{r}$, Using this fact and doing the Taylor series expansion and keeping the term upto u^2, we obtain the expression for cylindrical averaged exchange hole as,

$$\langle \rho_{x2D}^t \rangle = -\frac{\rho(\vec{r})}{2} - \frac{1}{4}\left[\left(d^2 - d + \frac{1}{2}\right)\nabla^2\rho(\vec{r}) - 2\tau + \frac{1}{4}\left(2d - 1\right)^2\frac{|\vec{\nabla}\rho(\vec{r})|^2}{\rho(\vec{r})}\right]u^2 \ . \quad \text{(B.19)}$$

This is the more general form than the Taylor series expansion of cylindrical averaged exchange hole in 2D because it restores the conventional cylindrically averaged exchange hole at $d = 1$. As expected, the coordinate transformation only affects the in-homogeneous terms but the homogeneous term remains invariant as the homogeneity of a system is translationally (also rotationally) invariant. All these facts has been used in chapter 6 to propose a generalised coordinate transformation based exchange hole model in 2D.

B.3 Negele and Vautherin Like Model in 2D

In chapter 6, we used the Negele and Vautherin (NV) density matrix expansion [414] to construct its 2D counterpart using more advanced technique. This model is important because it is the starting point of the series resummation of the density matrix expansion as proposed in chapter 6. However, one can construct a NV model in 2D similar to the 3D. To do so, we start with the generalized Gegenbauer addition theorem of Bessel functions which is obtained by expressing the plane wave in terms of Bessel and Hypergeometric functions. The expression of the plane waves expansion in accordance with the above

theorem is as follows,

$$e^{izcos\phi} = 2^\nu\Gamma\left(\nu\right)\sum_{m=0}^{\infty}(-1)^m(2m+\nu)\frac{J_{2m+\nu}(z)}{z^\nu}C_{2m}^\nu(icos\phi),\qquad\text{(B.20)}$$

where $J_{2m+\nu}(z)$ is the Bessel function and $C_{2m}^\nu(icos\phi)$ is associated with the generalized Hypergeometric function through

$$C_{2m}^\nu(x) = (-1)^m\begin{pmatrix} m+\nu-1 \\ m \end{pmatrix}{}_2F_1(-m,m+\nu;\frac{1}{2};x^2)\,.\qquad\text{(B.21)}$$

In the present study, the left side of Eq.(B.20) is recognized as

$$e^{iku(-icos\phi y)/u} = 2^\nu\Gamma\left(\nu\right)\sum_{m=0}^{\infty}(-1)^m(2m+\nu)\frac{J_{2m+\nu}(ku)}{(ku)^\nu}C_{2m}^\nu(-icos\phi y/u)\,.\qquad\text{(B.22)}$$

For $\nu = 1$, the reduced density matrix becomes,

$$\Gamma_1^t = 2\rho\frac{J_1(ku)}{ku} + \frac{6J_3(ku)}{k^3u}\left[4\cos^2\phi\{(d^2-d+\frac{1}{2})\nabla^2\rho\,,-2\tau\} + k^2\rho\right]\qquad\text{(B.23)}$$

By taking the cylindrical average of the above reduced density matrix it becomes,

$$\begin{aligned}\langle|\Gamma_1^t(\mathbf{r},\mathbf{r}+\mathbf{u})|^2\rangle &= \langle|\Gamma_1^t(\mathbf{r},\mathbf{r}+\mathbf{u})|\rangle^2 + O(u^4) \\ &= -\frac{\rho(\vec{r})}{2} - \frac{1}{4}\left[\left(d^2-d+\frac{1}{2}\right)\nabla^2\rho(\vec{r}) - 2\tau\right]u^2\,.\qquad\text{(B.24)}\end{aligned}$$

The Eq.(B.24) leads to the cylindrically averaged exchange hole as,

$$\langle\rho_x(r,u)\rangle_{cyl} = -\frac{2J_1^2(ku)}{k^2u^2}\rho - \frac{24J_1(ku)J_3(ku)}{k^4u^2}\{(d^2-d+\frac{1}{2})\nabla^2\rho - 2\tau + \frac{1}{2}k^2\rho\}\,.$$

$$\text{(B.25)}$$

Table B.1: Exchange energy obtain from Eq.(B.27). The NV model underestimates the exchange energy due to violation of sum rule as shown in last column of the table.

N	ω	$-E_x^{2D-EXX}$	$-E_x^{2D-LDA}$	$-E_x^{2D-NV}$
2	1.00	1.083	0.967	0.316
6	1.00	3.732	3.537	2.620
12	1.00	8.275	8.013	6.740
20	1.00	14.957	14.638	13.118

This becomes the Negele-Vautherin (NV) model in 2D upon substituting $d = \frac{1}{2}$

$$\langle \rho_x^{2D-NV}(r,u) \rangle_{cyl} = -\frac{2J_1^2(ku)}{k^2u^2}\rho - \frac{24J_1(ku)J_3(ku)}{k^4u^2}\{\frac{1}{4}\nabla^2\rho - 2\tau + \frac{1}{2}k^2\rho\}, \quad \text{(B.26)}$$

and the corresponding exchange energy is given by,

$$E_x^{2D-NV} = -\int \rho(\mathbf{r})\epsilon_x^{2D}\Big[1 + \frac{2}{5}\{\frac{\frac{1}{4}\nabla^2\rho(\mathbf{r}) - 2\tau + 2\tau^{unif}}{2\tau^{unif}}\}\Big] \quad \text{(B.27)}$$
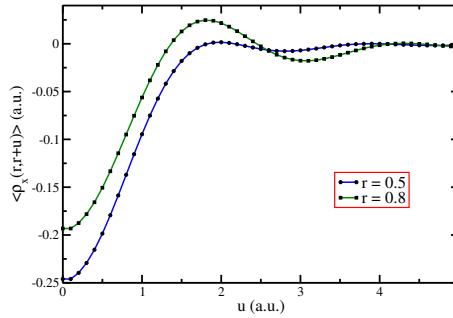
Figure B.1: Shown is the violation of the sum rule of the NV exchange hole as obtained from Eq.(B.26).

The exchange hole of NV model violets the sum rule (as shown in Fig. B.1). Therefore, underestimate the magnitude of energy (as shown in Table B.1). However, using the advanced density matrix expansion techinique of chapter 6, we recovered all the desired properties of the exchange hole.

References

[1] E. Schrödinger. "An Undulatory Theory of the Mechanics of Atoms and Molecules". In: *Phys. Rev.* 28 (6 1926), pp. 1049–1070.

[2] M. Born and R. Oppenheimer. "Zur Quantentheorie der Molekeln". In: *Annalen der Physik* 389.20 (1927), pp. 457–484.

[3] D. R. Hartree. "The Wave Mechanics of an Atom with a non-Coulomb Central Field. Part III. Term Values and Intensities in Series in Optical Spectra". In: *Mathematical Proceedings of the Cambridge Philosophical Society* 24.3 (1928), pp. 426–437.

[4] P. A. M. Dirac. "Note on Exchange Phenomena in the Thomas Atom". In: *Mathematical Proceedings of the Cambridge Philosophical Society* 26.3 (1930), pp. 376–385.

[5] V. Fock. "Näherungsmethode zur Lösung des quantenmechanischen Mehrkörperproblems". In: *Zeitschrift für Physik* 61.1 (1930), pp. 126–148.

[6] J. C. Slater. "A Simplification of the Hartree-Fock Method". In: *Phys. Rev.* 81 (3 1951), pp. 385–390.

[7] J. C. Slater. "Magnetic Effects and the Hartree-Fock Equation". In: *Phys. Rev.* 82 (4 1951), pp. 538–541.

[8] J. C. Slater. "A Generalized Self-Consistent Field Method". In: *Phys. Rev.* 91 (3 1953), pp. 528–530.

[9] L. H. Thomas. "The calculation of atomic fields". In: *Mathematical Proceedings of the Cambridge Philosophical Society* 23.5 (1927), pp. 542–548.

[10] E. Fermi. "Eine statistische Methode zur Bestimmung einiger Eigenschaften des Atoms und ihre Anwendung auf die Theorie des periodischen Systems der Elemente". In: *Zeitschrift für Physik* 48.1 (1928), pp. 73–79.

[11] P. Hohenberg and W. Kohn. "Inhomogeneous Electron Gas". In: *Phys. Rev.* 136 (3B 1964), B864–B871.

[12] W. Kohn and L. J. Sham. "Self-Consistent Equations Including Exchange and Correlation Effects". In: *Phys. Rev.* 140 (4A 1965), A1133–A1138.

[13] Eberhard Engel. *Density functional theory : an advanced course*. Berlin Heidelberg New York: Springer, 2011. ISBN: 978-3-642-14089-1.

[14] C Amador. *Density functional theory*. Berlin New York: Springer-Verlag, 1983. ISBN: 978-3-540-12721-5.

[15] Reiner Dreizler. *Density Functional Theory : an Approach to the Quantum Many-Body Problem*. Berlin, Heidelberg: Springer Berlin Heidelberg, 1990. ISBN: 978-3-642-86105-5.

[16] Eberhard Gross. *Density functional theory*. Boston, MA: Springer US Imprint Springer, 1995. ISBN: 978-1-4757-9977-4.

[17] C Fiolhais. *A primer in density functional theory*. Berlin New York: Springer, 2003. ISBN: 978-3-540-03083-6.

[18] Daniel Joubert. *Density functionals : theory and applications : proceedings of the Tenth Chris Engelbrecht Summer School in Theoretical Physics held at Meerensee, near Cape Town South Africa, 19-29- January 1997*. Berlin New York: Springer, 1998. ISBN: 978-3-540-63937-4.

[19] Stig Lundqvist. *Theory of the inhomogeneous electron gas*. New York: Plenum Press, 1983. ISBN: 978-0-306-41207-3.

[20]   R. O. Jones and O. Gunnarsson. "The density functional formalism, its applications and prospects". In: *Rev. Mod. Phys.* 61 (3 1989), pp. 689–746.

[21]   J. M. Seminario. *Modern density functional theory : a tool for chemistry*. Amsterdam New York: Elsevier, 1995. ISBN: 9780080536705.

[22]   Robert Parr. *Density-functional theory of atoms and molecules*. New York Oxford England: Oxford University Press Clarendon Press, 1989. ISBN: 978-0195092769.

[23]   Delano Chong. *Recent advances in density functional methods*. Singapore River Edge, N.J: World Scientific, 1995. ISBN: 9810231504.

[24]   John Dobson. *Electronic density functional theory : recent progress and new directions*. New York: Plenum Press, 1998. ISBN: 978-0-306-45834-7.

[25]   Narbe Mardirossian and Martin Head-Gordon. "Thirty years of density functional theory in computational chemistry: an overview and extensive assessment of 200 density functionals". In: *Molecular Physics* 115.19 (2017), pp. 2315–2372.

[26]   Axel D. Becke. "Perspective: Fifty years of density-functional theory in chemical physics". In: *The Journal of Chemical Physics* 140.18 (2014), 18A301.

[27]   Haoyu S. Yu, Shaohong L. Li, and Donald G. Truhlar. "Perspective: Kohn-Sham density functional theory descending a staircase". In: *The Journal of Chemical Physics* 145.13 (2016), p. 130901.

[28]   R. O. Jones. "Density functional theory: Its origins, rise to prominence, and future". In: *Rev. Mod. Phys.* 87 (3 2015), pp. 897–923.

[29]   Aron J. Cohen, Paula Mori-Snchez, and Weitao Yang. "Challenges for Density Functional Theory". In: *Chemical Reviews* 112.1 (2012), pp. 289–320.

[30]   Neil Qiang Su and Xin Xu. "Development of New Density Functional Approximations". In: *Annual Review of Physical Chemistry* 68.1 (2017), pp. 155–182.

[31] Eugene S. Kryachko and Eduardo V. Ludea. "Density functional theory: Foundations reviewed". In: *Physics Reports* 544.2 (2014). Density functional theory: Foundations reviewed, pp. 123 –239. ISSN: 0370-1573.

[32] W. Kohn. "Nobel Lecture: Electronic structure of matter—wave functions and density functionals". In: *Rev. Mod. Phys.* 71 (5 1999), pp. 1253–1266.

[33] Subrata Jana, Abhilash Patra, and Prasanjit Samal. "Assessing the performance of the Tao-Mo semilocal density functional in the projector-augmented-wave method". In: *The Journal of Chemical Physics* 149.4 (2018), p. 044120.

[34] Bikash Patra, Subrata Jana, and Prasanjit Samal. "Long-range corrected density functional through the density matrix expansion based semilocal exchange hole". In: *Phys. Chem. Chem. Phys.* 20 (13 2018), pp. 8991–8998.

[35] Jianmin Tao and Yuxiang Mo. "Accurate Semilocal Density Functional for Condensed-Matter Physics and Quantum Chemistry". In: *Phys. Rev. Lett.* 117 (7 2016), p. 073001.

[36] Chengteh Lee, Weitao Yang, and Robert G. Parr. "Development of the Colle-Salvetti correlation-energy formula into a functional of the electron density". In: *Phys. Rev. B* 37 (2 1988), pp. 785–789.

[37] A. D. Becke. "Density-functional exchange-energy approximation with correct asymptotic behavior". In: *Phys. Rev. A* 38 (6 1988), pp. 3098–3100.

[38] Subrata Jana and Prasanjit Samal. "A meta-GGA level screened range-separated hybrid functional by employing short range Hartree-Fock with a long range semilocal functional". In: *Phys. Chem. Chem. Phys.* 20 (13 2018), pp. 8999–9005.

[39] Subrata Jana and Prasanjit Samal. "Semilocal Exchange Energy Functional for Two-Dimensional Quantum Systems: A Step Beyond Generalized Gradient Approximations". In: *The Journal of Physical Chemistry A* 121.25 (2017), pp. 4804–4811.

[40] Subrata Jana and Prasanjit Samal. "Exploration of near the origin and the asymptotic behaviors of the Kohn-Sham kinetic energy density for two-dimensional quantum dot systems with parabolic confinement". In: *The Journal of Chemical Physics* 148.2 (2018), p. 024111.

[41] Subrata Jana, Abhilash Patra, and Prasanjit Samal. "Gradient approximated exchange energy functionals with improved performances for two-dimensional quantum dot systems". In: *Physica E: Low-dimensional Systems and Nanostructures* 97 (2018), pp. 268 –276. ISSN: 1386-9477.

[42] Mel Levy. "Universal variational functionals of electron densities, first-order density matrices, and natural spin-orbitals and solution of the v-representability problem". In: *Proceedings of the National Academy of Sciences* 76.12 (1979), pp. 6062–6065.

[43] W. Kohn. "v-Representability and Density Functional Theory". In: *Phys. Rev. Lett.* 51 (17 1983), pp. 1596–1598.

[44] Eugene S. Kryachko and Eduardo V. Ludea. "Formulation of N- and v-representable density-functional theory. I. Ground states". In: *Phys. Rev. A* 43 (5 1991), pp. 2179–2193.

[45] John M. Herbert and John E. Harriman. "N-representability and variational stability in natural orbital functional theory". In: *The Journal of Chemical Physics* 118.24 (2003), pp. 10835–10846.

[46] Paul W. Ayers and Ernest R. Davidson. "Necessary conditions for the N-representability of pair distribution functions". In: *International Journal of Quantum Chemistry* 106.7 (), pp. 1487–1498.

[47] Paul W. Ayers and Shubin Liu. "Necessary and sufficient conditions for the N-representability of density functionals". In: *Phys. Rev. A* 75 (2 2007), p. 022514.

[48] John P. Perdew et al. "Density-Functional Theory for Fractional Particle Number: Derivative Discontinuities of the Energy". In: *Phys. Rev. Lett.* 49 (23 1982), pp. 1691–1694.

[49] John P. Perdew and Mel Levy. "Physical Content of the Exact Kohn-Sham Orbital Energies: Band Gaps and Derivative Discontinuities". In: *Phys. Rev. Lett.* 51 (20 1983), pp. 1884–1887.

[50] L. J. Sham and M. Schlüter. "Density-Functional Theory of the Energy Gap". In: *Phys. Rev. Lett.* 51 (20 1983), pp. 1888–1891.

[51] Espen Sagvolden and John P. Perdew. "Discontinuity of the exchange-correlation potential: Support for assumptions used to find it". In: *Phys. Rev. A* 77 (1 2008), p. 012517.

[52] Mark E. Casida. "Correlated optimized effective-potential treatment of the derivative discontinuity and of the highest occupied Kohn-Sham eigenvalue: A Janak-type theorem for the optimized effective-potential model". In: *Phys. Rev. B* 59 (7 1999), pp. 4694–4698.

[53] Leonard Kleinman. "Significance of the highest occupied Kohn-Sham eigenvalue". In: *Phys. Rev. B* 56 (19 1997), pp. 12042–12045.

[54] John P. Perdew and Mel Levy. "Comment on "Significance of the highest occupied Kohn-Sham eigenvalue"". In: *Phys. Rev. B* 56 (24 1997), pp. 16021–16028.

[55] Weitao Yang, Aron J. Cohen, and Paula Mori-Snchez. "Derivative discontinuity, bandgap and lowest unoccupied molecular orbital in density functional theory". In: *The Journal of Chemical Physics* 136.20 (2012), p. 204111.

[56] Aron J. Cohen, Paula Mori-Sánchez, and Weitao Yang. "Insights into Current Limitations of Density Functional Theory". In: *Science* 321.5890 (2008), pp. 792–794. ISSN: 0036-8075.

[57] J. F. Janak. "Proof that $\partial E/\partial n_i = \epsilon$ in density-functional theory". In: *Phys. Rev. B* 18 (12 1978), pp. 7165–7168.

[58] A. Seidl et al. "Generalized Kohn-Sham schemes and the band-gap problem". In: *Phys. Rev. B* 53 (7 1996), pp. 3764–3774.

[59] F. Fuchs et al. "Quasiparticle band structure based on a generalized Kohn-Sham scheme". In: *Phys. Rev. B* 76 (11 2007), p. 115109.

[60] M. Städele et al. "Exact exchange Kohn-Sham formalism applied to semiconductors". In: *Phys. Rev. B* 59 (15 1999), pp. 10031–10043.

[61] M. Kuisma et al. "Kohn-Sham potential with discontinuity for band gap materials". In: *Phys. Rev. B* 82 (11 2010), p. 115106.

[62] Xiao Zheng et al. "Improving Band Gap Prediction in Density Functional Theory from Molecules to Solids". In: *Phys. Rev. Lett.* 107 (2 2011), p. 026403.

[63] Aron J. Cohen, Paula Mori-Sánchez, and Weitao Yang. "Fractional charge perspective on the band gap in density-functional theory". In: *Phys. Rev. B* 77 (11 2008), p. 115123.

[64] Paula Mori-Sánchez, Aron J. Cohen, and Weitao Yang. "Localization and Delocalization Errors in Density Functional Theory and Implications for Band-Gap Prediction". In: *Phys. Rev. Lett.* 100 (14 2008), p. 146401.

[65] R. Armiento and S. Kümmel. "Orbital Localization, Charge Transfer, and Band Gaps in Semilocal Density-Functional Theory". In: *Phys. Rev. Lett.* 111 (3 2013), p. 036402.

[66] Andreas Görling. "Exchange-correlation potentials with proper discontinuities for physically meaningful Kohn-Sham eigenvalues and band structures". In: *Phys. Rev. B* 91 (24 2015), p. 245120.

[67] Andreas Görling. "Exact treatment of exchange in Kohn-Sham band-structure schemes". In: *Phys. Rev. B* 53 (11 1996), pp. 7024–7029.

[68] Andreas Görling. "Erratum: Exact treatment of exchange in Kohn-Sham band-structure schemes [Phys. Rev. B 53, 7024 (1996)]". In: *Phys. Rev. B* 59 (15 1999), pp. 10370–10370.

[69] P. Rinke et al. "Band gap and band parameters of InN and GaN from quasiparticle energy calculations based on exact-exchange density-functional theory". In: *Applied Physics Letters* 89.16 (2006), p. 161919.

[70] T. Grabo, T. Kreibich, and E.K.U. Gross. "Optimized Effective Potential for Atoms and Molecules". In: *Molecular Engineering* 7.1 (1997), pp. 27–50. ISSN: 1572-8951.

[71] Takao Kotani. "Exact exchange-potential band-structure calculations by the LMTO-ASA method: MgO and CaO". In: *Phys. Rev. B* 50 (20 1994), pp. 14816–14821.

[72] Takao Kotani. "Erratum: Exact exchange-potential band-structure calculations by the LMTO-ASA method: MgO and CaO". In: *Phys. Rev. B* 51 (19 1995), pp. 13903–13904.

[73] Takao Kotani and Hisazumi Akai. "Exact exchange potential band-structure calculations for simple metals: Li, Na, K, Rb, and Ca". In: *Phys. Rev. B* 52 (24 1995), pp. 17153–17157.

[74] D. M. Bylander and Leonard Kleinman. "Optimized effective potentials for semiconductors". In: *Phys. Rev. B* 52 (20 1995), pp. 14566–14570.

[75] D. M. Bylander and Leonard Kleinman. "Optimized effective-potential calculations of Ge and GaAs". In: *Phys. Rev. B* 54 (11 1996), pp. 7891–7896.

[76] Jiri Klimes and Georg Kresse. "Kohn-Sham band gaps and potentials of solids from the optimised effective potential method within the random phase approximation". In: *The Journal of Chemical Physics* 140.5 (2014), p. 054516.

[77] Murray Gell-Mann and Keith A. Brueckner. "Correlation Energy of an Electron Gas at High Density". In: *Phys. Rev.* 106 (2 1957), pp. 364–368.

[78] John P. Perdew, Kieron Burke, and Matthias Ernzerhof. "Generalized Gradient Approximation Made Simple". In: *Phys. Rev. Lett.* 77 (18 1996), pp. 3865–3868.

[79] John P. Perdew et al. "Restoring the Density-Gradient Expansion for Exchange in Solids and Surfaces". In: *Phys. Rev. Lett.* 100 (13 2008), p. 136406.

[80] David C. Langreth and John P. Perdew. "Theory of nonuniform electronic systems. I. Analysis of the gradient approximation and a generalization that works". In: *Phys. Rev. B* 21 (12 1980), pp. 5469–5493.

[81] David C. Langreth and John P. Perdew. "Exchange-correlation energy of a metallic surface: Wave-vector analysis". In: *Phys. Rev. B* 15 (6 1977), pp. 2884–2901.

[82] Yue Wang and John P. Perdew. "Spin scaling of the electron-gas correlation energy in the high-density limit". In: *Phys. Rev. B* 43 (11 1991), pp. 8911–8916.

[83] John P. Perdew et al. "Accurate Density Functional with Correct Formal Properties: A Step Beyond the Generalized Gradient Approximation". In: *Phys. Rev. Lett.* 82 (12 1999), pp. 2544–2547.

[84] Jianmin Tao et al. "Climbing the Density Functional Ladder: Nonempirical Meta–Generalized Gradient Approximation Designed for Molecules and Solids". In: *Phys. Rev. Lett.* 91 (14 2003), p. 146401.

[85] John P. Perdew et al. "Workhorse Semilocal Density Functional for Condensed Matter Physics and Quantum Chemistry". In: *Phys. Rev. Lett.* 103 (2 2009), p. 026403.

[86] Jianwei Sun, Adrienn Ruzsinszky, and John P. Perdew. "Strongly Constrained and Appropriately Normed Semilocal Density Functional". In: *Phys. Rev. Lett.* 115 (3 2015), p. 036402.

[87] Yan Zhao and Donald G. Truhlar. "A new local density functional for main-group thermochemistry, transition metal bonding, thermochemical kinetics, and noncovalent interactions". In: *The Journal of Chemical Physics* 125.19 (2006), p. 194101.

[88] Jianwei Sun, Bing Xiao, and Adrienn Ruzsinszky. "Communication: Effect of the orbital-overlap dependence in the meta generalized gradient approximation". In: *The Journal of Chemical Physics* 137.5 (2012), p. 051101.

[89] Jianwei Sun et al. "Semilocal and hybrid meta-generalized gradient approximations based on the understanding of the kinetic-energy-density dependence". In: *The Journal of Chemical Physics* 138.4 (2013), p. 044113.

[90] Axel D. Becke. "A new mixing of HartreeFock and local densityfunctional theories". In: *The Journal of Chemical Physics* 98.2 (1993), pp. 1372–1377.

[91] P. J. Stephens et al. "Ab Initio Calculation of Vibrational Absorption and Circular Dichroism Spectra Using Density Functional Force Fields". In: *The Journal of Physical Chemistry* 98.45 (1994), pp. 11623–11627.

[92] Matthias Ernzerhof and Gustavo E. Scuseria. "Assessment of the PerdewBurkeErnzerhof exchange-correlation functional". In: *The Journal of Chemical Physics* 110.11 (1999), pp. 5029–5036.

[93] Viktor N. Staroverov et al. "Comparative assessment of a new nonempirical density functional: Molecules and hydrogen-bonded complexes". In: *The Journal of Chemical Physics* 119.23 (2003), pp. 12129–12137.

[94] Viktor N. Staroverov et al. "Erratum: Comparative assessment of a new nonempirical density functional: Molecules and hydrogen-bonded complexes [J. Chem. Phys. 119, 12129 (2003)]". In: *The Journal of Chemical Physics* 121.22 (2004), pp. 11507–11507.

[95] Jochen Heyd, Gustavo E. Scuseria, and Matthias Ernzerhof. "Hybrid functionals based on a screened Coulomb potential". In: *The Journal of Chemical Physics* 118.18 (2003), pp. 8207–8215.

[96] Jochen Heyd, Gustavo E. Scuseria, and Matthias Ernzerhof. "Erratum: Hybrid functionals based on a screened Coulomb potential [J. Chem. Phys. 118, 8207 (2003)]". In: *The Journal of Chemical Physics* 124.21 (2006), p. 219906.

[97] Tamar Stein et al. "Fundamental Gaps in Finite Systems from Eigenvalues of a Generalized Kohn-Sham Method". In: *Phys. Rev. Lett.* 105 (26 2010), p. 266802.

[98] John P. Perdew and Karla Schmidt. "Jacobs ladder of density functional approximations for the exchange-correlation energy". In: *AIP Conference Proceedings* 577.1 (2001), pp. 1–20.

[99] M. Valiev et al. "NWChem: A comprehensive and scalable open-source solution for large scale molecular simulations". In: *Computer Physics Communications* 181.9 (2010), pp. 1477 –1489. ISSN: 0010-4655.

[100] G. Kresse and J. Hafner. "Ab initio molecular dynamics for liquid metals". In: *Phys. Rev. B* 47 (1 1993), pp. 558–561.

[101] G. Kresse and J. Hafner. "Ab initio molecular-dynamics simulation of the liquid-metal–amorphous-semiconductor transition in germanium". In: *Phys. Rev. B* 49 (20 1994), pp. 14251–14269.

[102] G. Kresse and J. Furthmller. "Efficiency of ab-initio total energy calculations for metals and semiconductors using a plane-wave basis set". In: *Computational Materials Science* 6.1 (1996), pp. 15 –50. ISSN: 0927-0256.

[103] G. Kresse and J. Furthmüller. "Efficient iterative schemes for ab initio total-energy calculations using a plane-wave basis set". In: *Phys. Rev. B* 54 (16 1996), pp. 11169–11186.

[104] G. Kresse and D. Joubert. "From ultrasoft pseudopotentials to the projector augmented-wave method". In: *Phys. Rev. B* 59 (3 1999), pp. 1758–1775.

[105] Xavier Andrade et al. "Real-space grids and the Octopus code as tools for the development of new simulation approaches for electronic systems". In: *Phys. Chem. Chem. Phys.* 17 (47 2015), pp. 31371–31396.

[106] Yingkai Zhang and Weitao Yang. "Comment on "Generalized Gradient Approximation Made Simple"". In: *Phys. Rev. Lett.* 80 (4 1998), pp. 890–890.

[107] Zhigang Wu and R. E. Cohen. "More accurate generalized gradient approximation for solids". In: *Phys. Rev. B* 73 (23 2006), p. 235116.

[108] Gbor I. Csonka et al. "Diminished gradient dependence of density functionals: Constraint satisfaction and self-interaction correction". In: *The Journal of Chemical Physics* 126.24 (2007), p. 244107.

[109] L. Vitos et al. "Exchange energy in the local Airy gas approximation". In: *Phys. Rev. B* 62 (15 2000), pp. 10046–10050.

[110] R. Armiento and A. E. Mattsson. "Functional designed to include surface effects in self-consistent density functional theory". In: *Phys. Rev. B* 72 (8 2005), p. 085108.

[111] Yan Zhao and Donald G. Truhlar. "Construction of a generalized gradient approximation by restoring the density-gradient expansion and enforcing a tight LiebOxford bound". In: *The Journal of Chemical Physics* 128.18 (2008), p. 184109.

[112] Eduardo Fabiano, Lucian A. Constantin, and Fabio Della Sala. "Generalized gradient approximation bridging the rapidly and slowly varying density regimes: A PBE-like functional for hybrid interfaces". In: *Phys. Rev. B* 82 (11 2010), p. 113104.

[113] E. Fabiano, Lucian A. Constantin, and F. Della Sala. "Two-Dimensional Scan of the Performance of Generalized Gradient Approximations with Perdew-Burke-Ernzerhof-Like Enhancement Factor". In: *Journal of Chemical Theory and Computation* 7.11 (2011), pp. 3548–3559.

[114] Lucian A. Constantin et al. "Semiclassical atom theory applied to solid-state physics". In: *Phys. Rev. B* 93 (4 2016), p. 045126.

[115] E. Fabiano, Lucian A. Constantin, and F. Della Sala. "Testing the broad applicability of the PBEint GGA functional and its one-parameter hybrid form". In: *International Journal of Quantum Chemistry* 113.5 (), pp. 673–682.

[116] Lucian A. Constantin, E. Fabiano, and F. Della Sala. "Improving atomization energies of molecules and solids with a spin-dependent gradient correction from one-electron density analysis". In: *Phys. Rev. B* 84 (23 2011), p. 233103.

[117] Lucian A. Constantin, Adrienn Ruzsinszky, and John P. Perdew. "Exchange-correlation energy functional based on the Airy-gas reference system". In: *Phys. Rev. B* 80 (3 2009), p. 035125.

[118] E. Fabiano et al. "Assessment of the TCA functional in computational chemistry and solid-state physics". In: *Theoretical Chemistry Accounts* 134.11 (2015), p. 139.

[119] Aleksandr V. Terentjev et al. "Solid-State Testing of a Van-Der-Waals-Corrected Exchange-Correlation Functional Based on the Semiclassical Atom Theory". In: *Computation* 6.1 (2018).

[120] A. D. Becke. "Density functional calculations of molecular bond energies". In: *The Journal of Chemical Physics* 84.8 (1986), pp. 4524–4529.

[121] PETER M. W. GILL, ROSS D. ADAMSON, and JOHN A. POPLE. "Coulomb-attenuated exchange energy density functionals". In: *Molecular Physics* 88.4 (1996), pp. 1005–1009.

[122] A. D. Becke. "On the largegradient behavior of the density functional exchange energy". In: *The Journal of Chemical Physics* 85.12 (1986), pp. 7184–7187.

[123] Carlo Adamo and Vincenzo Barone. "Exchange functionals with improved long-range behavior and adiabatic connection methods without adjustable parameters: The mPW and mPW1PW models". In: *The Journal of Chemical Physics* 108.2 (1998), pp. 664–675.

[124] Ji Klime, David R Bowler, and Angelos Michaelides. "Chemical accuracy for the van der Waals density functional". In: *Journal of Physics: Condensed Matter* 22.2 (2010), p. 022201.

[125] Nicholas C. Handy and Aron J. Cohen. "A dynamical correlation functional". In: *The Journal of Chemical Physics* 116.13 (2002), pp. 5411–5418.

[126] John P. Perdew and Wang Yue. "Accurate and simple density functional for the electronic exchange energy: Generalized gradient approximation". In: *Phys. Rev. B* 33 (12 1986), pp. 8800–8802.

[127] John P. Perdew and Wang Yue. "Erratum: Accurate and simple density functional for the electronic exchange energy: Generalized gradient approximation". In: *Phys. Rev. B* 40 (5 1989), pp. 3399–3399.

[128] Yue Wang and John P. Perdew. "Correlation hole of the spin-polarized electron gas, with exact small-wave-vector and high-density scaling". In: *Phys. Rev. B* 44 (24 1991), pp. 13298–13307.

[129] John P. Perdew and Yue Wang. "Accurate and simple analytic representation of the electron-gas correlation energy". In: *Phys. Rev. B* 45 (23 1992), pp. 13244–13249.

[130] John P. Perdew et al. "Atoms, molecules, solids, and surfaces: Applications of the generalized gradient approximation for exchange and correlation". In: *Phys. Rev. B* 46 (11 1992), pp. 6671–6687.

[131]   B. Hammer, L. B. Hansen, and J. K. Nørskov. "Improved adsorption energetics within density-functional theory using revised Perdew-Burke-Ernzerhof functionals". In: *Phys. Rev. B* 59 (11 1999), pp. 7413–7421.

[132]   amonn D. Murray, Kyuho Lee, and David C. Langreth. "Investigation of Exchange Energy Density Functional Accuracy for Interacting Molecules". In: *Journal of Chemical Theory and Computation* 5.10 (2009), pp. 2754–2762.

[133]   Ying Wang et al. "Revised M06-L functional for improved accuracy on chemical reaction barrier heights, noncovalent interactions, and solid-state physics". In: *Proceedings of the National Academy of Sciences* (2017). ISSN: 0027-8424.

[134]   John P. Perdew et al. "Meta-generalized gradient approximation: Explanation of a realistic nonempirical density functional". In: *The Journal of Chemical Physics* 120.15 (2004), pp. 6898–6911.

[135]   Lucian A. Constantin, E. Fabiano, and F. Della Sala. "Meta-GGA Exchange-Correlation Functional with a Balanced Treatment of Nonlocality". In: *Journal of Chemical Theory and Computation* 9.5 (2013), pp. 2256–2263.

[136]   John P. Perdew et al. "One-parameter optimization of a nonempirical meta-generalized-gradient-approximation for the exchange-correlation energy". In: *Phys. Rev. A* 76 (4 2007), p. 042506.

[137]   Lars Goerigk and Stefan Grimme. "A General Database for Main Group Thermochemistry, Kinetics, and Noncovalent Interactions Assessment of Common and Reparameterized (meta-)GGA Density Functionals". In: *Journal of Chemical Theory and Computation* 6.1 (2010), pp. 107–126.

[138]   Pierre-Franois Loos. "Exchange functionals based on finite uniform electron gases". In: *The Journal of Chemical Physics* 146.11 (2017), p. 114108.

[139]   Stefan Kurth, John P. Perdew, and Peter Blaha. "Molecular and solid-state tests of density functional approximations: LSD, GGAs, and meta-GGAs". In: *International Journal of Quantum Chemistry* 75.45 (), pp. 889–909.

[140]   A. D. Becke and M. R. Roussel. "Exchange holes in inhomogeneous systems: A coordinate-space model". In: *Phys. Rev. A* 39 (8 1989), pp. 3761–3767.

[141]   Adrienn Ruzsinszky et al. "A meta-GGA Made Free of the Order of Limits Anomaly". In: *Journal of Chemical Theory and Computation* 8.6 (2012), pp. 2078–2087.

[142]   S. H. Vosko, L. Wilk, and M. Nusair. "Accurate spin-dependent electron liquid correlation energies for local spin density calculations: a critical analysis". In: *Canadian Journal of Physics* 58.8 (1980), pp. 1200–1211.

[143]   Emil Proynov and Jing Kong. "Analytic form of the correlation energy of the uniform electron gas". In: *Phys. Rev. A* 79 (1 2009), p. 014103.

[144]   J. P. Perdew and Alex Zunger. "Self-interaction correction to density-functional approximations for many-electron systems". In: *Phys. Rev. B* 23 (10 1981), pp. 5048–5079.

[145]   E. Wigner. "Effects of the electron interaction on the energy levels of electrons in metals". In: *Trans. Faraday Soc.* 34 (0 1938), pp. 678–685.

[146]   Phillip A. Stewart and Peter M. W. Gill. "Becke-Wigner : a simple but powerful density functional". In: *J. Chem. Soc., Faraday Trans.* 91 (24 1995), pp. 4337–4341.

[147]   John P. Perdew. "Density-functional approximation for the correlation energy of the inhomogeneous electron gas". In: *Phys. Rev. B* 33 (12 1986), pp. 8822–8824.

[148]   Lucian A. Constantin, Eduardo Fabiano, and Fabio Della Sala. "Semilocal dynamical correlation with increased localization". In: *Phys. Rev. B* 86 (3 2012), p. 035130.

[149]   Axel D. Becke. "Densityfunctional thermochemistry. IV. A new dynamical corre-
        lation functional and implications for exactexchange mixing". In: *The Journal of
        Chemical Physics* 104.3 (1996), pp. 1040–1046.

[150]   Emil Proynov and Jing Kong. "Improved meta-GGA Correlation Functional of
        the Lap Family". In: *Journal of Chemical Theory and Computation* 3.3 (2007),
        pp. 746–754.

[151]   Jess Wellendorff et al. "Density functionals for surface science: Exchange-correlation
        model development with Bayesian error estimation". In: *Phys. Rev. B* 85 (23
        2012), p. 235149.

[152]   Takao Tsuneda, Toshihisa Suzumura, and Kimihiko Hirao. "A new one-parameter
        progressive Colle-Salvetti-type correlation functional". In: *The Journal of Chem-
        ical Physics* 110.22 (1999), pp. 10664–10678.

[153]   Haoyu S. Yu et al. "Nonseparable exchangecorrelation functional for molecules,
        including homogeneous catalysis involving transition metals". In: *Phys. Chem.
        Chem. Phys.* 17 (18 2015), pp. 12146–12160.

[154]   Fred A. Hamprecht et al. "Development and assessment of new exchange-correlation
        functionals". In: *The Journal of Chemical Physics* 109.15 (1998), pp. 6264–6271.

[155]   A. Daniel Boese et al. "New generalized gradient approximation functionals". In:
        The Journal of Chemical Physics 112.4 (2000), pp. 1670–1678.

[156]   A. Daniel Boese and Nicholas C. Handy. "A new parametrization of exchangecor-
        relation generalized gradient approximation functionals". In: *The Journal of Chem-
        ical Physics* 114.13 (2001), pp. 5497–5503.

[157]   Pragya Verma and Donald G. Truhlar. "HLE16: A Local KohnSham Gradient Ap-
        proximation with Good Performance for Semiconductor Band Gaps and Molecu-
        lar Excitation Energies". In: *The Journal of Physical Chemistry Letters* 8.2 (2017),
        pp. 380–387.

[158] Thomas W. Keal and David J. Tozer. "A semiempirical generalized gradient approximation exchange-correlation functional". In: *The Journal of Chemical Physics* 121.12 (2004), pp. 5654–5660.

[159] Roberto Peverati and Donald G. Truhlar. "Exchange-Correlation Functional with Good Accuracy for Both Structural and Energetic Properties while Depending Only on the Density and Its Gradient". In: *Journal of Chemical Theory and Computation* 8.7 (2012), pp. 2310–2319.

[160] Roberto Peverati, Yan Zhao, and Donald G. Truhlar. "Generalized Gradient Approximation That Recovers the Second-Order Density-Gradient Expansion with Optimized Across-the-Board Performance". In: *The Journal of Physical Chemistry Letters* 2.16 (2011), pp. 1991–1997.

[161] Roberto Peverati and Donald G. Truhlar. "M11-L: A Local Density Functional That Provides Improved Accuracy for Electronic Structure Calculations in Chemistry and Physics". In: *The Journal of Physical Chemistry Letters* 3.1 (2012), pp. 117–124.

[162] Jess Wellendorff et al. "mBEEF: An accurate semi-local Bayesian error estimation density functional". In: *The Journal of Chemical Physics* 140.14 (2014), p. 144107.

[163] Jianwei Sun, John P. Perdew, and Adrienn Ruzsinszky. "Semilocal density functional obeying a strongly tightened bound for exchange". In: *Proceedings of the National Academy of Sciences* 112.3 (2015), pp. 685–689. ISSN: 0027-8424.

[164] Roberto Peverati and Donald G. Truhlar. "An improved and broadly accurate local approximation to the exchangecorrelation density functional: The MN12-L functional for electronic structure calculations in chemistry and physics". In: *Phys. Chem. Chem. Phys.* 14 (38 2012), pp. 13171–13174.

[165] Haoyu S. Yu, Xiao He, and Donald G. Truhlar. "MN15-L: A New Local Exchange-Correlation Functional for KohnSham Density Functional Theory with Broad Accuracy for Atoms, Molecules, and Solids". In: *Journal of Chemical Theory and Computation* 12.3 (2016), pp. 1280–1293.

[166] A. Daniel Boese and Nicholas C. Handy. "New exchange-correlation density functionals: The role of the kinetic-energy density". In: *The Journal of Chemical Physics* 116.22 (2002), pp. 9559–9569.

[167] Troy Van Voorhis and Gustavo E. Scuseria. "A novel form for the exchange-correlation energy functional". In: *The Journal of Chemical Physics* 109.2 (1998), pp. 400–410.

[168] Carlo Adamo and Vincenzo Barone. "Toward reliable density functional methods without adjustable parameters: The PBE0 model". In: *The Journal of Chemical Physics* 110.13 (1999), pp. 6158–6170.

[169] Axel D. Becke. "Density-functional thermochemistry. V. Systematic optimization of exchange-correlation functionals". In: *The Journal of Chemical Physics* 107.20 (1997), pp. 8554–8560.

[170] Fabio Della Sala, Eduardo Fabiano, and Lucian A. Constantin. "Kinetic-energy-density dependent semilocal exchange-correlation functionals". In: *International Journal of Quantum Chemistry* 116.22 (), pp. 1641–1694.

[171] Gábor I. Csonka et al. "Assessing the performance of recent density functionals for bulk solids". In: *Phys. Rev. B* 79 (15 2009), p. 155107.

[172] Fabien Tran, Julia Stelzl, and Peter Blaha. "Rungs 1 to 4 of DFT Jacobs ladder: Extensive test on the lattice constant, bulk modulus, and cohesive energy of solids". In: *The Journal of Chemical Physics* 144.20 (2016), p. 204120.

[173]   Patanachai Janthon et al. "Establishing the Accuracy of Broadly Used Density Functionals in Describing Bulk Properties of Transition Metals". In: *Journal of Chemical Theory and Computation* 9.3 (2013), pp. 1631–1640.

[174]   Frédéric Labat et al. "Assessing modern GGA functionals for solids". In: *Journal of Molecular Modeling* 19.7 (2013), pp. 2791–2796. ISSN: 0948-5023.

[175]   H. Levämäki et al. "Quasi-non-uniform gradient-level exchange-correlation approximation for metals and alloys". In: *Phys. Rev. B* 86 (20 2012), p. 201104.

[176]   Pan Hao et al. "Lattice constants from semilocal density functionals with zero-point phonon correction". In: *Phys. Rev. B* 85 (1 2012), p. 014111.

[177]   E. Fabiano, Lucian A. Constantin, and F. Della Sala. "Exchange-correlation generalized gradient approximation for gold nanostructures". In: *The Journal of Chemical Physics* 134.19 (2011), p. 194112.

[178]   Jianwei Sun et al. "Self-consistent meta-generalized gradient approximation within the projector-augmented-wave method". In: *Phys. Rev. B* 84 (3 2011), p. 035117.

[179]   Yuxiang Mo et al. "Assessment of the Tao-Mo nonempirical semilocal density functional in applications to solids and surfaces". In: *Phys. Rev. B* 95 (3 2017), p. 035118.

[180]   Hong Tang and Jianmin Tao. "Comparative study of the properties of ionic solids from density functionals". In: *Materials Research Express* 5.7 (2018), p. 076302.

[181]   Guocai Tian, Yuxiang Mo, and Jianmin Tao. "Accurate excitation energies of molecules and oligomers from a semilocal density functional". In: *The Journal of Chemical Physics* 146.23 (2017), p. 234102.

[182]   Guocai Tian, Yuxiang Mo, and Jianmin Tao. "Energetic Study of Clusters and Reaction Barrier Heights from Efficient Semilocal Density Functionals". In: *Computation* 5.2 (2017).

[183]   Yuxiang Mo, Guocai Tian, and Jianmin Tao. "Comparative study of semilocal density functionals on solids and surfaces". In: *Chemical Physics Letters* 682 (2017), pp. 38 –42. ISSN: 0009-2614.

[184]   Joachim Paier. "Hybrid Density Functionals Applied to Complex Solid Catalysts: Successes, Limitations, and Prospects". In: *Catalysis Letters* 146.5 (2016), pp. 861–885. ISSN: 1572-879X.

[185]   Philipp Haas et al. "Construction of an optimal GGA functional for molecules and solids". In: *Phys. Rev. B* 83 (20 2011), p. 205117.

[186]   Guo-Xu Zhang et al. "Performance of various density-functional approximations for cohesive properties of 64 bulk solids". In: *New Journal of Physics* 20.6 (2018), p. 063020.

[187]   L Delczeg et al. "Density functional study of vacancies and surfaces in metals". In: *Journal of Physics: Condensed Matter* 23.4 (2011), p. 045006.

[188]   Jianmin Tao, John P. Perdew, and Adrienn Ruzsinszky. "Long-range van der Waals attraction and alkali-metal lattice constants". In: *Phys. Rev. B* 81 (23 2010), p. 233102.

[189]   Mitsuru Kodera, Tatsuya Shishidou, and Tamio Oguchi. "Spin-Polarized AM05 Functional for 3d-Transition Metals". In: *Journal of the Physical Society of Japan* 79.7 (2010), p. 074713.

[190]   Philipp Haas et al. "Insight into the performance of GGA functionals for solid-state calculations". In: *Phys. Rev. B* 80 (19 2009), p. 195109.

[191]   Philipp Haas, Fabien Tran, and Peter Blaha. "Calculation of the lattice constant of solids with semilocal functionals". In: *Phys. Rev. B* 79 (8 2009), p. 085104.

[192]   Fabien Tran et al. "Performance on molecules, surfaces, and solids of the Wu-Cohen GGA exchange-correlation energy functional". In: *Phys. Rev. B* 75 (11 2007), p. 115131.

[193]   Nicholas E. Singh-Miller and Nicola Marzari. "Surface energies, work functions, and surface relaxations of low-index metallic surfaces from first principles". In: *Phys. Rev. B* 80 (23 2009), p. 235407.

[194]   Christopher J. Cramer and Donald G. Truhlar. "Density functional theory for transition metals and transition metal chemistry". In: *Phys. Chem. Chem. Phys.* 11 (46 2009), pp. 10757–10816.

[195]   Roberto Peverati and Donald G. Truhlar. "Quest for a universal density functional: the accuracy of density functionals across a broad spectrum of databases in chemistry and physics". In: *Philosophical Transactions of the Royal Society of London A: Mathematical, Physical and Engineering Sciences* 372.2011 (2014). ISSN: 1364-503X.

[196]   Chandra Shahi, Jianwei Sun, and John P. Perdew. "Accurate critical pressures for structural phase transitions of group IV, III-V, and II-VI compounds from the SCAN density functional". In: *Phys. Rev. B* 97 (9 2018), p. 094111.

[197]   Abhirup Patra et al. "Properties of real metallic surfaces: Effects of density functional semilocality and van der Waals nonlocality". In: *Proceedings of the National Academy of Sciences* (2017). ISSN: 0027-8424.

[198]   Yubo Zhang et al. "Comparative first-principles studies of prototypical ferroelectric materials by LDA, GGA, and SCAN meta-GGA". In: *Phys. Rev. B* 96 (3 2017), p. 035143.

[199]   Haowei Peng and John P. Perdew. "Rehabilitation of the Perdew-Burke-Ernzerhof generalized gradient approximation for layered materials". In: *Phys. Rev. B* 95 (8 2017), p. 081105.

[200]   Michael G. Medvedev et al. "Density functional theory is straying from the path toward the exact functional". In: *Science* 355.6320 (2017), pp. 49–52. ISSN: 0036-8075.

[201] Haowei Peng et al. "Versatile van der Waals Density Functional Based on a Meta-Generalized Gradient Approximation". In: *Phys. Rev. X* 6 (4 2016), p. 041005.

[202] Jianwei Sun et al. "Accurate first-principles structures and energies of diversely bonded systems from an efficient density functional". In: *Nature Chemistry* 8 (2016), p. 831.

[203] Daniil A. Kitchaev et al. "Energetics of MnO_2 polymorphs in density functional theory". In: *Phys. Rev. B* 93 (4 2016), p. 045132.

[204] Bing Xiao et al. "Testing the Jacob's ladder of density functionals for electronic structure and magnetism of rutile VO_2". In: *Phys. Rev. B* 90 (8 2014), p. 085134.

[205] Bing Xiao et al. "Testing density functionals for structural phase transitions of solids under pressure: Si, SiO_2, and Zr". In: *Phys. Rev. B* 88 (18 2013), p. 184103.

[206] Yuan Fang et al. "Ice phases under ambient and high pressure: Insights from density functional theory". In: *Phys. Rev. B* 87 (21 2013), p. 214101.

[207] Pan Hao et al. "Performance of meta-GGA Functionals on General Main Group Thermochemistry, Kinetics, and Noncovalent Interactions". In: *Journal of Chemical Theory and Computation* 9.1 (2013), pp. 355–363.

[208] Jianwei Sun et al. "Improved lattice constants, surface energies, and CO desorption energies from a semilocal density functional". In: *Phys. Rev. B* 83 (12 2011), p. 121410.

[209] Laurids Schimka et al. "Lattice constants and cohesive energies of alkali, alkaline-earth, and transition metals: Random phase approximation and density functional theory results". In: *Phys. Rev. B* 87 (21 2013), p. 214102.

[210] Patanachai Janthon et al. "Bulk Properties of Transition Metals: A Challenge for the Design of Universal Density Functionals". In: *Journal of Chemical Theory and Computation* 10.9 (2014), pp. 3832–3839.

[211] O. Gunnarsson and B. I. Lundqvist. "Exchange and correlation in atoms, molecules, and solids by the spin-density-functional formalism". In: *Phys. Rev. B* 13 (10 1976), pp. 4274–4298.

[212] Peter Elliott et al. "Semiclassical Origins of Density Functionals". In: *Phys. Rev. Lett.* 100 (25 2008), p. 256406.

[213] Lucian A. Constantin et al. "Semiclassical Neutral Atom as a Reference System in Density Functional Theory". In: *Phys. Rev. Lett.* 106 (18 2011), p. 186406.

[214] Jianmin Tao et al. "Nonempirical density functionals investigated for jellium: Spin-polarized surfaces, spherical clusters, and bulk linear response". In: *Phys. Rev. B* 77 (24 2008), p. 245107.

[215] Lars Hedin. "New Method for Calculating the One-Particle Green's Function with Application to the Electron-Gas Problem". In: *Phys. Rev.* 139 (3A 1965), A796–A823.

[216] P. R. Antoniewicz and Leonard Kleinman. "Kohn-Sham exchange potential exact to first order in $\rho(K\rightarrow)/\rho_0$". In: *Phys. Rev. B* 31 (10 1985), pp. 6779–6781.

[217] J. A. Chevary and S. H. Vosko. "Importance of Pauli-principle restrictions for accurate numerical evaluation of the exchange-only screening function". In: *Phys. Rev. B* 42 (8 1990), pp. 5320–5323.

[218] Leonard Kleinman. "Gradient term in the Kohn-Sham exchange-correlation potential". In: *Phys. Rev. B* 10 (6 1974), pp. 2221–2225.

[219] Leonard Kleinman. "Erratum: Gradient term in the Kohn-Sham exchange-correlation potential". In: *Phys. Rev. B* 12 (8 1975), pp. 3512–3512.

[220] A. K. Rajagopal and S. Ray. "Gradient expansion in the density functional approach to an inhomogeneous electron system". In: *Phys. Rev. B* 12 (8 1975), pp. 3129–3135.

[221]   P. S. Svendsen and U. von Barth. "Gradient expansion of the exchange energy from second-order density response theory". In: *Phys. Rev. B* 54 (24 1996), pp. 17402–17413.

[222]   John P. Perdew et al. "Relevance of the Slowly Varying Electron Gas to Atoms, Molecules, and Solids". In: *Phys. Rev. Lett.* 97 (22 2006), p. 223002.

[223]   John P. Perdew, Kieron Burke, and Yue Wang. "Generalized gradient approximation for the exchange-correlation hole of a many-electron system". In: *Phys. Rev. B* 54 (23 1996), pp. 16533–16539.

[224]   SHANG-kENG MA and KEITH A. BRUECKNER. "Correlation Energy of an Electron Gas with a Slowly Varying High Density". In: *Phys. Rev.* 165 (1 1968), pp. 18–31.

[225]   D. J. W. Geldart and M. Rasolt. "Exchange and correlation energy of an inhomogeneous electron gas at metallic densities". In: *Phys. Rev. B* 13 (4 1976), pp. 1477–1488.

[226]   Mel Levy and John P. Perdew. "Tight bound and convexity constraint on the exchange-correlation-energy functional in the low-density limit, and other formal tests of generalized-gradient approximations". In: *Phys. Rev. B* 48 (16 1993), pp. 11638–11645.

[227]   Anonymous. "Erratum: Tight bound and convexity constraint on the exchange-correlation-energy functionalsin the low-density limit, and other formal tests of generalized-gradient approximations [Phys. Rev. B 48, 11638 (1993)]". In: *Phys. Rev. B* 55 (19 1997), pp. 13321–13321.

[228]   Mel Levy and John P. Perdew. "Hellmann-Feynman, virial, and scaling requisites for the exact universal density functionals. Shape of the correlation potential and diamagnetic susceptibility for atoms". In: *Phys. Rev. A* 32 (4 1985), pp. 2010–2021.

[229] G. L. Oliver and J. P. Perdew. "Spin-density gradient expansion for the kinetic energy". In: *Phys. Rev. A* 20 (2 1979), pp. 397–403.

[230] Saverio Moroni, David M. Ceperley, and Gaetano Senatore. "Static Response and Local Field Factor of the Electron Gas". In: *Phys. Rev. Lett.* 75 (4 1995), pp. 689–692.

[231] Elliott H. Lieb. "A lower bound for Coulomb energies". In: *Physics Letters A* 70.5 (1979), pp. 444 –446. ISSN: 0375-9601.

[232] Elliott H. Lieb and Stephen Oxford. "Improved lower bound on the indirect Coulomb energy". In: *International Journal of Quantum Chemistry* 19.3 (), pp. 427–439.

[233] C. D. Hu and David C. Langreth. "Beyond the random-phase approximation in nonlocal-density-functional theory". In: *Phys. Rev. B* 33 (2 1986), pp. 943–959.

[234] Jianmin Tao, Michael Springborg, and John P. Perdew. "Properties of the exchange hole under an appropriate coordinate transformation". In: *The Journal of Chemical Physics* 119.13 (2003), pp. 6457–6464.

[235] Michael Springborg. "Localizing the exchange hole". In: *Chemical Physics Letters* 308.1 (1999), pp. 83 –90. ISSN: 0009-2614.

[236] A. D. Becke. "HartreeFock exchange energy of an inhomogeneous electron gas". In: *International Journal of Quantum Chemistry* 23.6 (), pp. 1915–1922.

[237] F. D. Murnaghan. "The Compressibility of Media under Extreme Pressures". In: *Proceedings of the National Academy of Sciences* 30.9 (1944), pp. 244–247. ISSN: 0027-8424.

[238] Alim B. Alchagirov et al. "Energy and pressure versus volume: Equations of state motivated by the stabilized jellium model". In: *Phys. Rev. B* 63 (22 2001), p. 224115.

[239] W. B. Holzapfel. "Equations of state for solids under strong compression". In: *High Pressure Research* 16.2 (1998), pp. 81–126.

[240] Alim B. Alchagirov et al. "Reply to "Comment on 'Energy and pressure versus volume: Equations of state motivated by the stabilized jellium model' "". In: *Phys. Rev. B* 67 (2 2003), p. 026103.

[241] Francis Birch. "Finite Elastic Strain of Cubic Crystals". In: *Phys. Rev.* 71 (11 1947), pp. 809–824.

[242] V. Wang et al. "Structural, electronic, and optical properties of GaInO3: A hybrid density functional study". In: *Journal of Applied Physics* 115.4 (2014), p. 043708.

[243] Hendrik J. Monkhorst and James D. Pack. "Special points for Brillouin-zone integrations". In: *Phys. Rev. B* 13 (12 1976), pp. 5188–5192.

[244] Peter E. Blöchl, O. Jepsen, and O. K. Andersen. "Improved tetrahedron method for Brillouin-zone integrations". In: *Phys. Rev. B* 49 (23 1994), pp. 16223–16233.

[245] Jochen Heyd et al. "Energy band gaps and lattice parameters evaluated with the Heyd-Scuseria-Ernzerhof screened hybrid functional". In: *The Journal of Chemical Physics* 123.17 (2005), p. 174101.

[246] J. Paier et al. "Screened hybrid density functionals applied to solids". In: *The Journal of Chemical Physics* 124.15 (2006), p. 154709.

[247] J. Paier et al. "Erratum: Screened hybrid density functionals applied to solids [J. Chem. Phys. 124, 154709 (2006)]". In: *The Journal of Chemical Physics* 125.24 (2006), p. 249901.

[248] M Marsman et al. "Hybrid functionals applied to extended systems". In: *Journal of Physics: Condensed Matter* 20.6 (2008), p. 064201.

[249] Laurids Schimka, Judith Harl, and Georg Kresse. "Improved hybrid functional for solids: The HSEsol functional". In: *The Journal of Chemical Physics* 134.2 (2011), p. 024116.

[250] E A Owen and D Madoc Jones. "Effect of Grain Size on the Crystal Structure of Cobalt". In: *Proceedings of the Physical Society. Section B* 67.6 (1954), p. 456.

[251] S. Shallcross et al. "An ab initio effective Hamiltonian for magnetism including longitudinal spin fluctuations". In: *Phys. Rev. B* 72 (10 2005), p. 104437.

[252] Yaakov Kraftmakher. "Equilibrium vacancies and thermophysical properties of metals". In: *Physics Reports* 299.2 (1998), pp. 79 –188. ISSN: 0370-1573.

[253] H. (Ed.) Ullmaier. *Atomic Defects in Metals / Atomare Fehlstellen in Metallen (Landolt-Brnstein: Numerical Data and Functional Relationships in Science and Technology - New Series)*. Springer, 1991. ISBN: 354051435X.

[254] Thomas R. Mattsson and Ann E. Mattsson. "Calculating the vacancy formation energy in metals: Pt, Pd, and Mo". In: *Phys. Rev. B* 66 (21 2002), p. 214110.

[255] T. Korhonen, M. J. Puska, and R. M. Nieminen. "Vacancy-formation energies for fcc and bcc transition metals". In: *Phys. Rev. B* 51 (15 1995), pp. 9526–9532.

[256] Bharat Medasani et al. "Vacancy formation energies in metals: A comparison of MetaGGA with LDA and GGA exchangecorrelation functionals". In: *Computational Materials Science* 101 (2015), pp. 96 –107. ISSN: 0927-0256.

[257] Yuxiang Mo et al. "Performance of a nonempirical density functional on molecules and hydrogen-bonded complexes". In: *The Journal of Chemical Physics* 145.23 (2016), p. 234306.

[258] Jianwei Sun et al. "Density Functionals that Recognize Covalent, Metallic, and Weak Bonds". In: *Phys. Rev. Lett.* 111 (10 2013), p. 106401.

[259] John P. Perdew et al. "Density functional with full exact exchange, balanced nonlocality of correlation, and constraint satisfaction". In: *Phys. Rev. A* 78 (5 2008), p. 052513.

[260] John P. Perdew et al. "Nonlocality of the density functional for exchange and correlation: Physical origins and chemical consequences". In: *The Journal of Chemical Physics* 108.4 (1998), pp. 1522–1531.

[261] Oleg A. Vydrov, Gustavo E. Scuseria, and John P. Perdew. "Tests of functionals for systems with fractional electron number". In: *The Journal of Chemical Physics* 126.15 (2007), p. 154109.

[262] Aron J. Cohen, Paula Mori-Snchez, and Weitao Yang. "Development of exchange-correlation functionals with minimal many-electron self-interaction error". In: *The Journal of Chemical Physics* 126.19 (2007), p. 191109.

[263] Adrienn Ruzsinszky et al. "Spurious fractional charge on dissociated atoms: Pervasive and resilient self-interaction error of common density functionals". In: *The Journal of Chemical Physics* 125.19 (2006), p. 194112.

[264] Mark R. Pederson, Adrienn Ruzsinszky, and John P. Perdew. "Communication: Self-interaction correction with unitary invariance in density functional theory". In: *The Journal of Chemical Physics* 140.12 (2014), p. 121103.

[265] D. Hofmann et al. "Using complex degrees of freedom in the Kohn-Sham self-interaction correction". In: *Phys. Rev. A* 85 (6 2012), p. 062514.

[266] Mark R. Pederson, Richard A. Heaton, and Chun C. Lin. "Densityfunctional theory with selfinteraction correction: Application to the lithium moleculea)". In: *The Journal of Chemical Physics* 82.6 (1985), pp. 2688–2699.

[267] Adrienn Ruzsinszky et al. "Density functionals that are one- and two- are not always many-electron self-interaction-free, as shown for H2+, He2+, LiH+, and Ne2+". In: *The Journal of Chemical Physics* 126.10 (2007), p. 104102.

[268] Duminda S. Ranasinghe et al. "Does the ionization potential condition employed in QTP functionals mitigate the self-interaction error?" In: *The Journal of Chemical Physics* 146.3 (2017), p. 034102.

[269] Junwei Lucas Bao, Laura Gagliardi, and Donald G. Truhlar. "Self-Interaction Error in Density Functional Theory: An Appraisal". In: *The Journal of Physical Chemistry Letters* 9.9 (2018), pp. 2353–2358.

[270] Oleg A. Vydrov and Gustavo E. Scuseria. "Effect of the PerdewZunger self-interaction correction on the thermochemical performance of approximate density functionals". In: *The Journal of Chemical Physics* 121.17 (2004), pp. 8187–8193.

[271] Paula Mori-Snchez, Aron J. Cohen, and Weitao Yang. "Many-electron self-interaction error in approximate density functionals". In: *The Journal of Chemical Physics* 125.20 (2006), p. 201102.

[272] Axel D. Becke. "Densityfunctional thermochemistry. I. The effect of the exchangeonly gradient correction". In: *The Journal of Chemical Physics* 96.3 (1992), pp. 2155–2160.

[273] Axel D. Becke. "Densityfunctional thermochemistry. II. The effect of the PerdewWang generalizedgradient correlation correction". In: *The Journal of Chemical Physics* 97.12 (1992), pp. 9173–9177.

[274] Axel D. Becke. "Densityfunctional thermochemistry. III. The role of exact exchange". In: *The Journal of Chemical Physics* 98.7 (1993), pp. 5648–5652.

[275] C. Adamo and V. Barone. "Toward reliable adiabatic connection models free from adjustable parameters". In: *Chemical Physics Letters* 274.1 (1997), pp. 242 –250. ISSN: 0009-2614.

[276] Yihan Shao, Martin Head-Gordon, and Anna I. Krylov. "The spinflip approach within time-dependent density functional theory: Theory and applications to diradicals". In: *The Journal of Chemical Physics* 118.11 (2003), pp. 4807–4818.

[277] Philip J. Wilson, Thomas J. Bradley, and David J. Tozer. "Hybrid exchange-correlation functional determined from thermochemical data and ab initio potentials". In: *The Journal of Chemical Physics* 115.20 (2001), pp. 9233–9242.

[278] Thomas W. Keal and David J. Tozer. "Semiempirical hybrid functional with improved performance in an extensive chemical assessment". In: *The Journal of Chemical Physics* 123.12 (2005), p. 121103.

[279] A. Daniel Boese and Jan M. L. Martin. "Development of density functionals for thermochemical kinetics". In: *The Journal of Chemical Physics* 121.8 (2004), pp. 3405–3416.

[280] Benjamin J. Lynch et al. "Adiabatic Connection for Kinetics". In: *The Journal of Physical Chemistry A* 104.21 (2000), pp. 4811–4815.

[281] Wee-Meng Hoe, Aron J. Cohen, and Nicholas C. Handy. "Assessment of a new local exchange functional OPTX". In: *Chemical Physics Letters* 341.3 (2001), pp. 319 –328. ISSN: 0009-2614.

[282] Stefan Grimme et al. "Consistent structures and interactions by density functional theory with small atomic orbital basis sets". In: *The Journal of Chemical Physics* 143.5 (2015), p. 054107.

[283] Yves A. Bernard, Yihan Shao, and Anna I. Krylov. "General formulation of spin-flip time-dependent density functional theory using non-collinear kernels: Theory, implementation, and benchmarks". In: *The Journal of Chemical Physics* 136.20 (2012), p. 204103.

[284] Roberto Peverati and Donald G. Truhlar. "Communication: A global hybrid generalized gradient approximation to the exchange-correlation functional that satisfies the second-order density-gradient constraint and has broad applicability in chemistry". In: *The Journal of Chemical Physics* 135.19 (2011), p. 191102.

[285] Xin Xu and William A. Goddard. "The X3LYP extended density functional for accurate descriptions of nonbond interactions, spin states, and thermochemical properties". In: *Proceedings of the National Academy of Sciences* 101.9 (2004), pp. 2673–2677. ISSN: 0027-8424.

[286] Keith W. Wiitala, Thomas R. Hoye, and Christopher J. Cramer. "Hybrid Density Functional Methods Empirically Optimized for the Computation of 13C and 1H

Chemical Shifts in Chloroform Solution". In: *Journal of Chemical Theory and Computation* 2.4 (2006), pp. 1085–1092.

[287] Yan Zhao and Donald G. Truhlar. "The M06 suite of density functionals for main group thermochemistry, thermochemical kinetics, noncovalent interactions, excited states, and transition elements: two new functionals and systematic testing of four M06-class functionals and 12 other functionals". In: *Theoretical Chemistry Accounts* 120.1 (2008), pp. 215–241. ISSN: 1432-2234.

[288] Gbor I. Csonka, John P. Perdew, and Adrienn Ruzsinszky. "Global Hybrid Functionals: A Look at the Engine under the Hood". In: *Journal of Chemical Theory and Computation* 6.12 (2010), pp. 3688–3703.

[289] Guishan Zheng et al. "Parameter Calibration of Transition-Metal Elements for the Spin-Polarized Self-Consistent-Charge Density-Functional Tight-Binding (DFTB) Method: Sc, Ti, Fe, Co, and Ni". In: *Journal of Chemical Theory and Computation* 3.4 (2007), pp. 1349–1367.

[290] Yan Zhao, Benjamin J. Lynch, and Donald G. Truhlar. "Doubly Hybrid Meta DFT: New Multi-Coefficient Correlation and Density Functional Methods for Thermochemistry and Thermochemical Kinetics". In: *The Journal of Physical Chemistry A* 108.21 (2004), pp. 4786–4791.

[291] Yan Zhao, Nathan E. Schultz, and D. G. Truhlar. "Exchange-correlation functional with broad accuracy for metallic and nonmetallic compounds, kinetics, and noncovalent interactions". In: *The Journal of Chemical Physics* 123.16 (2005), p. 161103.

[292] Yan Zhao, Nathan E. Schultz, and Donald G. Truhlar. "Design of Density Functionals by Combining the Method of Constraint Satisfaction with Parametrization for Thermochemistry, Thermochemical Kinetics, and Noncovalent Interactions". In: *Journal of Chemical Theory and Computation* 2.2 (2006), pp. 364–382.

[293] Yan Zhao and Donald G. Truhlar. "Density Functional for Spectroscopy: No Long-Range Self-Interaction Error, Good Performance for Rydberg and Charge-Transfer States, and Better Performance on Average than B3LYP for Ground States". In: *The Journal of Physical Chemistry A* 110.49 (2006), pp. 13126–13130.

[294] Haoyu S. Yu et al. "MN15: A KohnSham global-hybrid exchangecorrelation density functional with broad accuracy for multi-reference and single-reference systems and noncovalent interactions". In: *Chem. Sci.* 7 (8 2016), pp. 5032–5051.

[295] Kerwin Hui and Jeng-Da Chai. "SCAN-based hybrid and double-hybrid density functionals from models without fitted parameters". In: *The Journal of Chemical Physics* 144.4 (2016), p. 044114.

[296] Stefan Grimme. "Accurate Calculation of the Heats of Formation for Large Main Group Compounds with Spin-Component Scaled MP2 Methods". In: *The Journal of Physical Chemistry A* 109.13 (2005), pp. 3067–3077.

[297] Yan Zhao and Donald G. Truhlar. "Design of Density Functionals That Are Broadly Accurate for Thermochemistry, Thermochemical Kinetics, and Nonbonded Interactions". In: *The Journal of Physical Chemistry A* 109.25 (2005), pp. 5656–5667.

[298] Yan Zhao and Donald G. Truhlar. "Hybrid Meta Density Functional Theory Methods for Thermochemistry, Thermochemical Kinetics, and Noncovalent Interactions: The MPW1B95 and MPWB1K Models and Comparative Assessments for Hydrogen Bonding and van der Waals Interactions". In: *The Journal of Physical Chemistry A* 108.33 (2004), pp. 6908–6918.

[299] Narbe Mardirossian and Martin Head-Gordon. "B97X-V: A 10-parameter, range-separated hybrid, generalized gradient approximation density functional with non-local correlation, designed by a survival-of-the-fittest strategy". In: *Phys. Chem. Chem. Phys.* 16 (21 2014), pp. 9904–9924.

[300]   You-Sheng Lin et al. "Long-Range Corrected Hybrid Density Functionals with Improved Dispersion Corrections". In: *Journal of Chemical Theory and Computation* 9.1 (2013), pp. 263–272.

[301]   Jeng-Da Chai and Martin Head-Gordon. "Long-range corrected hybrid density functionals with damped atomatom dispersion corrections". In: *Phys. Chem. Chem. Phys.* 10 (44 2008), pp. 6615–6620.

[302]   Takeshi Yanai, David P Tew, and Nicholas C Handy. "A new hybrid exchangecorrelation functional using the Coulomb-attenuating method (CAM-B3LYP)". In: *Chemical Physics Letters* 393.1 (2004), pp. 51 –57. ISSN: 0009-2614.

[303]   Prakash Verma and Rodney J. Bartlett. "Increasing the applicability of density functional theory. IV. Consequences of ionization-potential improved exchange-correlation potentials". In: *The Journal of Chemical Physics* 140.18 (2014), 18A534.

[304]   Roberto Luiz Andrade Haiduke and Rodney J. Bartlett. "Communication: Can excitation energies be obtained from orbital energies in a correlated orbital theory?" In: *The Journal of Chemical Physics* 149.13 (2018), p. 131101.

[305]   Aliaksandr V. Krukau et al. "Influence of the exchange screening parameter on the performance of screened hybrid functionals". In: *The Journal of Chemical Physics* 125.22 (2006), p. 224106.

[306]   Thomas M. Henderson, Benjamin G. Janesko, and Gustavo E. Scuseria. "Generalized gradient approximation model exchange holes for range-separated hybrids". In: *The Journal of Chemical Physics* 128.19 (2008), p. 194105.

[307]   Oleg A. Vydrov and Troy Van Voorhis. "Nonlocal van der Waals density functional: The simpler the better". In: *The Journal of Chemical Physics* 133.24 (2010), p. 244103.

[308] Elon Weintraub, Thomas M. Henderson, and Gustavo E. Scuseria. "Long-Range-Corrected Hybrids Based on a New Model Exchange Hole". In: *Journal of Chemical Theory and Computation* 5.4 (2009), pp. 754–762.

[309] Roberto Peverati and Donald G. Truhlar. "Screened-exchange density functionals with broad accuracy for chemistry and solid-state physics". In: *Phys. Chem. Chem. Phys.* 14 (47 2012), pp. 16187–16191.

[310] Jong-Won Song et al. "Long-range corrected density functional calculations of chemical reactions: Redetermination of parameter". In: *The Journal of Chemical Physics* 126.15 (2007), p. 154105.

[311] Mary A. Rohrdanz, Katie M. Martins, and John M. Herbert. "A long-range-corrected density functional that performs well for both ground-state properties and time-dependent density functional theory excitation energies, including charge-transfer excited states". In: *The Journal of Chemical Physics* 130.5 (2009), p. 054112.

[312] Mary A. Rohrdanz and John M. Herbert. "Simultaneous benchmarking of ground- and excited-state properties with long-range-corrected density functional theory". In: *The Journal of Chemical Physics* 129.3 (2008), p. 034107.

[313] Jeng-Da Chai and Martin Head-Gordon. "Systematic optimization of long-range corrected hybrid density functionals". In: *The Journal of Chemical Physics* 128.8 (2008), p. 084106.

[314] Jianmin Tao, Ireneusz W. Bulik, and Gustavo E. Scuseria. "Semilocal exchange hole with an application to range-separated density functionals". In: *Phys. Rev. B* 95 (12 2017), p. 125115.

[315] Oleg A. Vydrov et al. "Importance of short-range versus long-range Hartree-Fock exchange for the performance of hybrid density functionals". In: *The Journal of Chemical Physics* 125.7 (2006), p. 074106.

[316] Julien Toulouse, Franois Colonna, and Andreas Savin. "Short-range exchange and correlation energy density functionals: Beyond the local-density approximation". In: *The Journal of Chemical Physics* 122.1 (2005), p. 014110.

[317] Sidi M. O. Souvi, Kamal Sharkas, and Julien Toulouse. "Double-hybrid density-functional theory with meta-generalized-gradient approximations". In: *The Journal of Chemical Physics* 140.8 (2014), p. 084107.

[318] Alexandrina Stoyanova et al. "Alternative separation of exchange and correlation energies in multi-configuration range-separated density-functional theory". In: *The Journal of Chemical Physics* 139.13 (2013), p. 134113.

[319] Julien Toulouse and Andreas Savin. "Local density approximation for long-range or for short-range energy functionals?" In: *Journal of Molecular Structure: THEOCHEM* 762.1 (2006). A Collection of Papers Dedicated to Professor Annick Goursot on the Occasion of her 60th Birthday, pp. 147 –150. ISSN: 0166-1280.

[320] Giuseppe Sansone et al. "Range-separated double-hybrid density-functional theory applied to periodic systems". In: *The Journal of Chemical Physics* 143.10 (2015), p. 102811.

[321] Cairedine Kalai and Julien Toulouse. "A general range-separated double-hybrid density-functional theory". In: *The Journal of Chemical Physics* 148.16 (2018), p. 164105.

[322] Juanita Jaramillo, Gustavo E. Scuseria, and Matthias Ernzerhof. "Local hybrid functionals". In: *The Journal of Chemical Physics* 118.3 (2003), pp. 1068–1073.

[323] Alexei V. Arbuznikov, Martin Kaupp, and Hilke Bahmann. "From local hybrid functionals to localized local hybrid potentials: Formalism and thermochemical tests". In: *The Journal of Chemical Physics* 124.20 (2006), p. 204102.

[324]   Martin Kaupp, Hilke Bahmann, and Alexei V. Arbuznikov. "Local hybrid functionals: An assessment for thermochemical kinetics". In: *The Journal of Chemical Physics* 127.19 (2007), p. 194102.

[325]   Benjamin G. Janesko and Gustavo E. Scuseria. "Local hybrid functionals based on density matrix products". In: *The Journal of Chemical Physics* 127.16 (2007), p. 164117.

[326]   Benjamin G. Janesko, Aliaksandr V. Krukau, and Gustavo E. Scuseria. "Self-consistent generalized Kohn-Sham local hybrid functionals of screened exchange: Combining local and range-separated hybridization". In: *The Journal of Chemical Physics* 129.12 (2008), p. 124110.

[327]   Alexei V. Arbuznikov and Martin Kaupp. "What can we learn from the adiabatic connection formalism about local hybrid functionals?" In: *The Journal of Chemical Physics* 128.21 (2008), p. 214107.

[328]   Alexei V. Arbuznikov and Martin Kaupp. "Local hybrid exchange-correlation functionals based on the dimensionless density gradient". In: *Chemical Physics Letters* 440.1 (2007), pp. 160 –168. ISSN: 0009-2614.

[329]   Aliaksandr V. Krukau et al. "Hybrid functionals with local range separation". In: *The Journal of Chemical Physics* 129.12 (2008), p. 124103.

[330]   Valentin V. Karasiev. "Local hybrid functionals based on exact-expression approximate exchange". In: *The Journal of Chemical Physics* 118.19 (2003), pp. 8576–8583.

[331]   Robin Haunschild et al. "Many-electron self-interaction and spin polarization errors in local hybrid density functionals". In: *The Journal of Chemical Physics* 133.13 (2010), p. 134116.

[332]   Lucian A. Constantin, John P. Perdew, and J. M. Pitarke. "Exchange-correlation hole of a generalized gradient approximation for solids and surfaces". In: *Phys. Rev. B* 79 (7 2009), p. 075126.

[333]   Matthias Ernzerhof and John P. Perdew. "Generalized gradient approximation to the angle- and system-averaged exchange hole". In: *The Journal of Chemical Physics* 109.9 (1998), pp. 3313–3320.

[334]   Jochen Heyd and Gustavo E. Scuseria. "Assessment and validation of a screened Coulomb hybrid density functional". In: *The Journal of Chemical Physics* 120.16 (2004), pp. 7274–7280.

[335]   Jochen Heyd and Gustavo E. Scuseria. "Efficient hybrid density functional calculations in solids: Assessment of the HeydScuseriaErnzerhof screened Coulomb hybrid functional". In: *The Journal of Chemical Physics* 121.3 (2004), pp. 1187–1192.

[336]   A. Savin. "On degeneracy, near-degeneracy and density functional theory". In: *Recent Developments and Applications of Modern Density Functional Theory*. Ed. by J.M. Seminario. Vol. 4. Theoretical and Computational Chemistry. Elsevier, 1996, pp. 327 –357.

[337]   Julien Toulouse, Fran çois Colonna, and Andreas Savin. "Long-range–short-range separation of the electron-electron interaction in density-functional theory". In: *Phys. Rev. A* 70 (6 2004), p. 062505.

[338]   Hisayoshi Iikura et al. "A long-range correction scheme for generalized-gradient-approximation exchange functionals". In: *The Journal of Chemical Physics* 115.8 (2001), pp. 3540–3544.

[339]   Rodney J. Bartlett, Victor F. Lotrich, and Igor V. Schweigert. "Ab initio density functional theory: The best of both worlds?" In: *The Journal of Chemical Physics* 123.6 (2005), p. 062205.

[340] Benjamin J. Lynch and Donald G. Truhlar. "Small Representative Benchmarks for Thermochemical Calculations". In: *The Journal of Physical Chemistry A* 107.42 (2003), pp. 8996–8999.

[341] Subrata Jana et al. "On the many-electron self-interaction error of the semilocal exchange hole based meta-GGA level range-separated hybrid with the B88 hybrids". In: *Chemical Physics Letters* 713 (2018), pp. 1 –9. ISSN: 0009-2614.

[342] Larry A. Curtiss et al. "Gaussian2 theory for molecular energies of first and secondrow compounds". In: *The Journal of Chemical Physics* 94.11 (1991), pp. 7221–7230.

[343] Larry A. Curtiss et al. "Assessment of Gaussian-2 and density functional theories for the computation of enthalpies of formation". In: *The Journal of Chemical Physics* 106.3 (1997), pp. 1063–1079.

[344] Larry A. Curtiss et al. "Assessment of Gaussian-2 and density functional theories for the computation of ionization potentials and electron affinities". In: *The Journal of Chemical Physics* 109.1 (1998), pp. 42–55.

[345] J. P. Perdew M. Ernzerhof K. Burke. *Recent Developments and Applications of Modern Density Functional Theory, Volume 4 (Theoretical and Computational Chemistry)*. Elsevier Science, 1996. ISBN: 0444824049.

[346] Rdiger Bauernschmitt and Reinhart Ahlrichs. "Stability analysis for solutions of the closed shell KohnSham equation". In: *The Journal of Chemical Physics* 104.22 (1996), pp. 9047–9052.

[347] M. Fuchs et al. "Describing static correlation in bond dissociation by KohnSham density functional theory". In: *The Journal of Chemical Physics* 122.9 (2005), p. 094116.

[348] Jeng-Da Chai. "Density functional theory with fractional orbital occupations". In: *The Journal of Chemical Physics* 136.15 (2012), p. 154104.

[349]   Adrienn Ruzsinszky, John P. Perdew, and Gbor I. Csonka. "Binding Energy Curves
        from Nonempirical Density Functionals. I. Covalent Bonds in Closed-Shell and
        Radical Molecules". In: *The Journal of Physical Chemistry A* 109.48 (2005),
        pp. 11006–11014.

[350]   Ruifang Li et al. "Assessment and Validation of Density Functional Approxi-
        mations for Iron Carbide and Iron Carbide Cation". In: *The Journal of Physical
        Chemistry A* 117.1 (2013), pp. 169–173.

[351]   Yan Zhao and Donald G. Truhlar. "Density Functionals for Noncovalent Inter-
        action Energies of Biological Importance". In: *Journal of Chemical Theory and
        Computation* 3.1 (2007), pp. 289–300.

[352]   Benjamin J. Lynch, Yan Zhao, and Donald G. Truhlar. "Effectiveness of Diffuse
        Basis Functions for Calculating Relative Energies by Density Functional Theory".
        In: *The Journal of Physical Chemistry A* 107.9 (2003), pp. 1384–1388.

[353]   Yan Zhao and Donald G. Truhlar. "Assessment of Density Functionals for Sys-
        tems: Energy Differences between Cumulenes and Poly-ynes; Proton Affinities,
        Bond Length Alternation, and Torsional Potentials of Conjugated Polyenes; and
        Proton Affinities of Conjugated Shiff Bases". In: *The Journal of Physical Chem-
        istry A* 110.35 (2006), pp. 10478–10486.

[354]   Ekaterina I. Izgorodina, Michelle L. Coote, and Leo Radom. "Trends in RX Bond
        Dissociation Energies (R = Me, Et, i-Pr, t-Bu; X = H, CH3, OCH3, OH, F): A Sur-
        prising Shortcoming of Density Functional Theory". In: *The Journal of Physical
        Chemistry A* 109.33 (2005), pp. 7558–7566.

[355]   Sijie Luo, Yan Zhao, and Donald G. Truhlar. "Validation of electronic structure
        methods for isomerization reactions of large organic molecules". In: *Phys. Chem.
        Chem. Phys.* 13 (30 2011), pp. 13683–13689.

[356] Amir Karton et al. "Highly Accurate First-Principles Benchmark Data Sets for the Parametrization and Validation of Density Functional and Other Approximate Methods. Derivation of a Robust, Generally Applicable, Double-Hybrid Functional for Thermochemistry and Thermochemical Kinetics". In: *The Journal of Physical Chemistry A* 112.50 (2008), pp. 12868–12886.

[357] Yan Zhao, Benjamin J. Lynch, and Donald G. Truhlar. "Multi-coefficient extrapolated density functional theory for thermochemistry and thermochemical kinetics". In: *Phys. Chem. Chem. Phys.* 7 (1 2005), pp. 43–52.

[358] Yan Zhao, Nria Gonzlez-Garca, and Donald G. Truhlar. "Benchmark Database of Barrier Heights for Heavy Atom Transfer, Nucleophilic Substitution, Association, and Unimolecular Reactions and Its Use to Test Theoretical Methods". In: *The Journal of Physical Chemistry A* 109.9 (2005), pp. 2012–2018.

[359] Yuxiang Mo, Guocai Tian, and Jianmin Tao. "Performance of a nonempirical exchange functional from density matrix expansion: comparative study with different correlations". In: *Phys. Chem. Chem. Phys.* 19 (32 2017), pp. 21707–21713.

[360] Zeng-hui Yang et al. "More realistic band gaps from meta-generalized gradient approximations: Only in a generalized Kohn-Sham scheme". In: *Phys. Rev. B* 93 (20 2016), p. 205205.

[361] John P. Perdew et al. "Understanding band gaps of solids in generalized Kohn–Sham theory". In: *Proceedings of the National Academy of Sciences* 114.11 (2017), pp. 2801–2806.

[362] Vladimir I. Anisimov, Jan Zaanen, and Ole K. Andersen. "Band theory and Mott insulators: Hubbard U instead of Stoner I". In: *Phys. Rev. B* 44 (3 1991), pp. 943–954.

[363] Takao Kotani. "Exact Exchange Potential Band-Structure Calculations by the Linear Muffin-Tin Orbital–Atomic-Sphere Approximation Method for Si, Ge, C, and MnO". In: *Phys. Rev. Lett.* 74 (15 1995), pp. 2989–2992.

[364] M. Städele et al. "Exact Kohn-Sham Exchange Potential in Semiconductors". In: *Phys. Rev. Lett.* 79 (11 1997), pp. 2089–2092.

[365] Ji Klime et al. "Singles correlation energy contributions in solids". In: *The Journal of Chemical Physics* 143.10 (2015), p. 102816.

[366] Axel D. Becke and Erin R. Johnson. "A simple effective potential for exchange". In: *The Journal of Chemical Physics* 124.22 (2006), p. 221101.

[367] Fabien Tran, Peter Blaha, and Karlheinz Schwarz. "Band gap calculations with BeckeJohnson exchange potential". In: *Journal of Physics: Condensed Matter* 19.19 (2007), p. 196208.

[368] Fabien Tran and Peter Blaha. "Accurate Band Gaps of Semiconductors and Insulators with a Semilocal Exchange-Correlation Potential". In: *Phys. Rev. Lett.* 102 (22 2009), p. 226401.

[369] Fabien Tran and Peter Blaha. "Importance of the Kinetic Energy Density for Band Gap Calculations in Solids with Density Functional Theory". In: *The Journal of Physical Chemistry A* 121.17 (2017), pp. 3318–3325.

[370] Walter Metzner and Dieter Vollhardt. "Correlated Lattice Fermions in $d = \infty$ Dimensions". In: *Phys. Rev. Lett.* 62 (3 1989), pp. 324–327.

[371] Antoine Georges and Gabriel Kotliar. "Hubbard model in infinite dimensions". In: *Phys. Rev. B* 45 (12 1992), pp. 6479–6483.

[372] M. Shishkin, M. Marsman, and G. Kresse. "Accurate Quasiparticle Spectra from Self-Consistent GW Calculations with Vertex Corrections". In: *Phys. Rev. Lett.* 99 (24 2007), p. 246403.

[373] Sergey V. Faleev, Mark van Schilfgaarde, and Takao Kotani. "All-Electron Self-Consistent GW Approximation: Application to Si, MnO, and NiO". In: *Phys. Rev. Lett.* 93 (12 2004), p. 126406.

[374] Joachim Paier, Martijn Marsman, and Georg Kresse. "Why does the B3LYP hybrid functional fail for metals?" In: *The Journal of Chemical Physics* 127.2 (2007), p. 024103.

[375] Yoon-Suk Kim et al. "Towards efficient band structure and effective mass calculations for III-V direct band-gap semiconductors". In: *Phys. Rev. B* 82 (20 2010), p. 205212.

[376] A Stroppa and G Kresse. "The shortcomings of semi-local and hybrid functionals: what we can learn from surface science studies". In: *New Journal of Physics* 10.6 (2008), p. 063020.

[377] Yoon-Suk Kim, Kerstin Hummer, and Georg Kresse. "Accurate band structures and effective masses for InP, InAs, and InSb using hybrid functionals". In: *Phys. Rev. B* 80 (3 2009), p. 035203.

[378] Kerstin Hummer, Judith Harl, and Georg Kresse. "Heyd-Scuseria-Ernzerhof hybrid functional for calculating the lattice dynamics of semiconductors". In: *Phys. Rev. B* 80 (11 2009), p. 115205.

[379] Juan E. Peralta et al. "Spin-orbit splittings and energy band gaps calculated with the Heyd-Scuseria-Ernzerhof screened hybrid functional". In: *Phys. Rev. B* 74 (7 2006), p. 073101.

[380] Edward N. Brothers et al. "Accurate solid-state band gaps via screened hybrid electronic structure calculations". In: *The Journal of Chemical Physics* 129.1 (2008), p. 011102.

[381] Subrata Jana, Abhilash Patra, and Prasanjit Samal. "Efficient lattice constants and energy bandgaps for condensed systems from a meta-GGA level screened range-separated hybrid functional". In: *The Journal of Chemical Physics* 149.9 (2018), p. 094105.

[382] Lucian A. Constantin, John P. Perdew, and Jianmin Tao. "Meta-generalized gradient approximation for the exchange-correlation hole with an application to the jellium surface energy". In: *Phys. Rev. B* 73 (20 2006), p. 205104.

[383] Lucian A. Constantin, Eduardo Fabiano, and Fabio Della Sala. "Construction of a general semilocal exchange-correlation hole model: Application to nonempirical meta-GGA functionals". In: *Phys. Rev. B* 88 (12 2013), p. 125112.

[384] L P Kouwenhoven, D G Austing, and S Tarucha. "Few-electron quantum dots". In: *Reports on Progress in Physics* 64.6 (2001), p. 701.

[385] Stephanie M. Reimann and Matti Manninen. "Electronic structure of quantum dots". In: *Rev. Mod. Phys.* 74 (4 2002), pp. 1283–1342.

[386] Yong-Hoon Kim et al. "Two-dimensional limit of exchange-correlation energy functional approximations". In: *Phys. Rev. B* 61 (8 2000), pp. 5202–5211.

[387] Aaron D. Kaplan, Kamal Wagle, and John P. Perdew. "Collapse of the electron gas from three to two dimensions in Kohn-Sham density functional theory". In: *Phys. Rev. B* 98 (8 2018), p. 085147.

[388] Lucian A. Constantin, John P. Perdew, and J. M. Pitarke. "Collapse of the Electron Gas to Two Dimensions in Density Functional Theory". In: *Phys. Rev. Lett.* 101 (1 2008), p. 016406.

[389] Lucian A. Constantin. "Dimensional crossover of the exchange-correlation energy at the semilocal level". In: *Phys. Rev. B* 78 (15 2008), p. 155106.

[390] A. K. Rajagopal and John C. Kimball. "Correlations in a two-dimensional electron system". In: *Phys. Rev. B* 15 (5 1977), pp. 2819–2825.

[391]   B. Tanatar and D. M. Ceperley. "Ground state of the two-dimensional electron gas". In: *Phys. Rev. B* 39 (8 1989), pp. 5005–5016.

[392]   Claudio Attaccalite et al. "Correlation Energy and Spin Polarization in the 2D Electron Gas". In: *Phys. Rev. Lett.* 88 (25 2002), p. 256601.

[393]   H. Saarikoski et al. "Testing of two-dimensional local approximations in the current-spin and spin-density-functional theories". In: *Phys. Rev. B* 67 (20 2003), p. 205327.

[394]   S. Pittalis et al. "Exchange-energy functionals for finite two-dimensional systems". In: *Phys. Rev. B* 76 (23 2007), p. 235314.

[395]   Stefano Pittalis et al. "Density gradients for the exchange energy of electrons in two dimensions". In: *Phys. Rev. A* 79 (1 2009), p. 012503.

[396]   S. Pittalis, E. Räsänen, and E. K. U. Gross. "Gaussian approximations for the exchange-energy functional of current-carrying states: Applications to two-dimensional systems". In: *Phys. Rev. A* 80 (3 2009), p. 032515.

[397]   S. Pittalis and E. Räsänen. "Orbital-free energy functional for electrons in two dimensions". In: *Phys. Rev. B* 80 (16 2009), p. 165112.

[398]   S. Pittalis, E. Räsänen, and C. R. Proetto. "Becke-Johnson-type exchange potential for two-dimensional systems". In: *Phys. Rev. B* 81 (11 2010), p. 115108.

[399]   E. R. "Exchange and correlation energy functionals for two-dimensional open-shell systems". In: *Physica E: Low-dimensional Systems and Nanostructures* 42.4 (2010). 18th International Conference on Electron Properties of Two-Dimensional Systems, pp. 1232 –1235. ISSN: 1386-9477.

[400]   S. Pittalis and E. Räsänen. "Laplacian-level density functionals for the exchange-correlation energy of low-dimensional nanostructures". In: *Phys. Rev. B* 82 (16 2010), p. 165123.

[401] E. Räsänen et al. "Semi-local density functional for the exchange-correlation energy of electrons in two dimensions". In: *International Journal of Quantum Chemistry* 110.12 (), pp. 2308–2314.

[402] A. Putaja et al. "Kirzhnits gradient expansion in two dimensions". In: *Phys. Rev. B* 85 (16 2012), p. 165101.

[403] J. G. Vilhena et al. "Construction of the B88 Exchange-Energy Functional in Two Dimensions". In: *Journal of Chemical Theory and Computation* 10.5 (2014), pp. 1837–1842.

[404] S. Pittalis, E. Räsänen, and M. A. L. Marques. "Local correlation functional for electrons in two dimensions". In: *Phys. Rev. B* 78 (19 2008), p. 195322.

[405] S. Pittalis et al. "Correlation energy of finite two-dimensional systems: Toward nonempirical and universal modeling". In: *Phys. Rev. B* 79 (8 2009), p. 085316.

[406] E. Räsänen, S. Pittalis, and C. R. Proetto. "Parameter-free density functional for the correlation energy in two dimensions". In: *Phys. Rev. B* 81 (19 2010), p. 195103.

[407] N. Helbig et al. "Exchange-correlation orbital functionals in current-density functional theory: Application to a quantum dot in magnetic fields". In: *Phys. Rev. B* 77 (24 2008), p. 245106.

[408] Abhilash Patra, Subrata Jana, and Prasanjit Samal. "A Parameter-Free Semilocal Exchange Energy Functional for Two-Dimensional Quantum Systems". In: *The Journal of Physical Chemistry A* 122.13 (2018), pp. 3455–3461.

[409] Matthias Brack and Brandon P. van Zyl. "Simple Analytical Particle and Kinetic Energy Densities for a Dilute Fermionic Gas in a d-Dimensional Harmonic Trap". In: *Phys. Rev. Lett.* 86 (8 2001), pp. 1574–1577.

[410] J. B. Krieger, Yan Li, and G. J. Iafrate. "Systematic approximations to the optimized effective potential: Application to orbital-density-functional theory". In: *Phys. Rev. A* 46 (9 1992), pp. 5453–5458.

[411] Fabio Della Sala, Eduardo Fabiano, and Lucian A. Constantin. "Kohn-Sham kinetic energy density in the nuclear and asymptotic regions: Deviations from the von Weizsäcker behavior and applications to density functionals". In: *Phys. Rev. B* 91 (3 2015), p. 035126.

[412] Lucian A. Constantin, Eduardo Fabiano, and Fabio Della Sala. "Kinetic and Exchange Energy Densities near the Nucleus". In: *Computation* 4.2 (2016). ISSN: 2079-3197.

[413] W. A. Al-Salam and L. Carlitz. "The Gegenbauer Addition Theorem". In: *Journal of Mathematics and Physics* 42.1-4 (), pp. 147–156.

[414] J. W. Negele and D. Vautherin. "Density-Matrix Expansion for an Effective Nuclear Hamiltonian". In: *Phys. Rev. C* 5 (5 1972), pp. 1472–1493.